WASHINGTON UNIVERSITY

SEVER INSTITUTE OF TECHNOLOGY

MODELING STUDIES

IN FIXED-BED COAL GASIFICATION

by

Amitava Bhattacharya

Prepared under the direction of Professor B. Joseph

A dissertation presented to the Sever Institute of
Washington University in partial fulfillment
of the requirements for the degree of

DOCTOR OF SCIENCE

May, 1985

Saint Louis, Missouri

WASHINGTON UNIVERSITY
SEVER INSTITUTE OF TECHNOLOGY

ABSTRACT

MODELING STUDIES

IN FIXED-BED COAL GASIFICATION

by Amitava Bhattacharya

ADVISOR: Professor B. Joseph

May, 1985

Saint Louis, Missouri

A dynamic model of a fixed bed coal gasification reactor has been developed and coded into a simulation program. The model incorporates radial and axial variations of temperature and composition within the reactor, and may also be used to simulate moving bed reactors. Results from the model have been compared with experimental data from a fixed bed unit operating at Washington University. Reasonable agreement at initial times is obtained with the temperature profiles measured in the laboratory reactor. In the past, verification of models was limited to matching flow rates and compositions of outlet gas. These variables are not very sensitive to the actual profiles inside the gasifier. This work attempts to fill this gap by matching experimental temperature data to simulation values.

Several aspects are investigated to explain the mismatch of temperature profiles at large times. This deterioration is attributed to the changing solid conversion profile with time, which depend heavily on effective reaction rates. Uncertainty in the effective reaction rates for the char + oxygen and char + steam reactions is caused by an uncertainty in the value of the mass transfer coefficient through the gas film. The effect of including axial dispersion of energy is also investigated, and is found to be marginal compared with the above effect.

TABLE OF CONTENTS

TABLE OF CONTENTS
(continued)

TABLE OF CONTENTS
(continued)

LIST OF TABLES

LIST OF FIGURES

LIST OF FIGURES
(continued)

LIST OF FIGURES
(continued)

LIST OF FIGURES
(continued)

LIST OF FIGURES
(continued)

LIST OF FIGURES
(continued)

MODELING STUDIES IN FIXED-BED COAL GASIFICATION

1. INTRODUCTION

1.1 COAL AND ITS RELEVANCE IN ENERGY

The energy system of the world, if followed from 1800 to 1970, shows the transition from a system based on wood to one based predominantly on coal, then to one based mostly on the fluid fuels, petroleum and natural gas. The picture in the US is the same, and is shown in Figure 1.1. The emergence of another major source is now apparent, with nuclear-generated power beginning to make its mark in the early 1960s. However, with the occurrence of the energy crisis in the 1970s, coal has gained predominance as a major source of energy for the future.

Even with the most optimistic forecasts for the expansion of nuclear power and the aggresive development of all other energy sources, as well as vigorous conservation, it appears that coal has a vitally important part to play in the world's energy future. At the World Energy Conference in 1977, the summation of plans indicated an increase in production of coal and related products from 2.6 billion tons of coal equivalent (TCE) in 1975 to 8.7 billion in 2020. This is an annual rate of increase of about 3%, which is similar to that obtained over the past couple of decades.

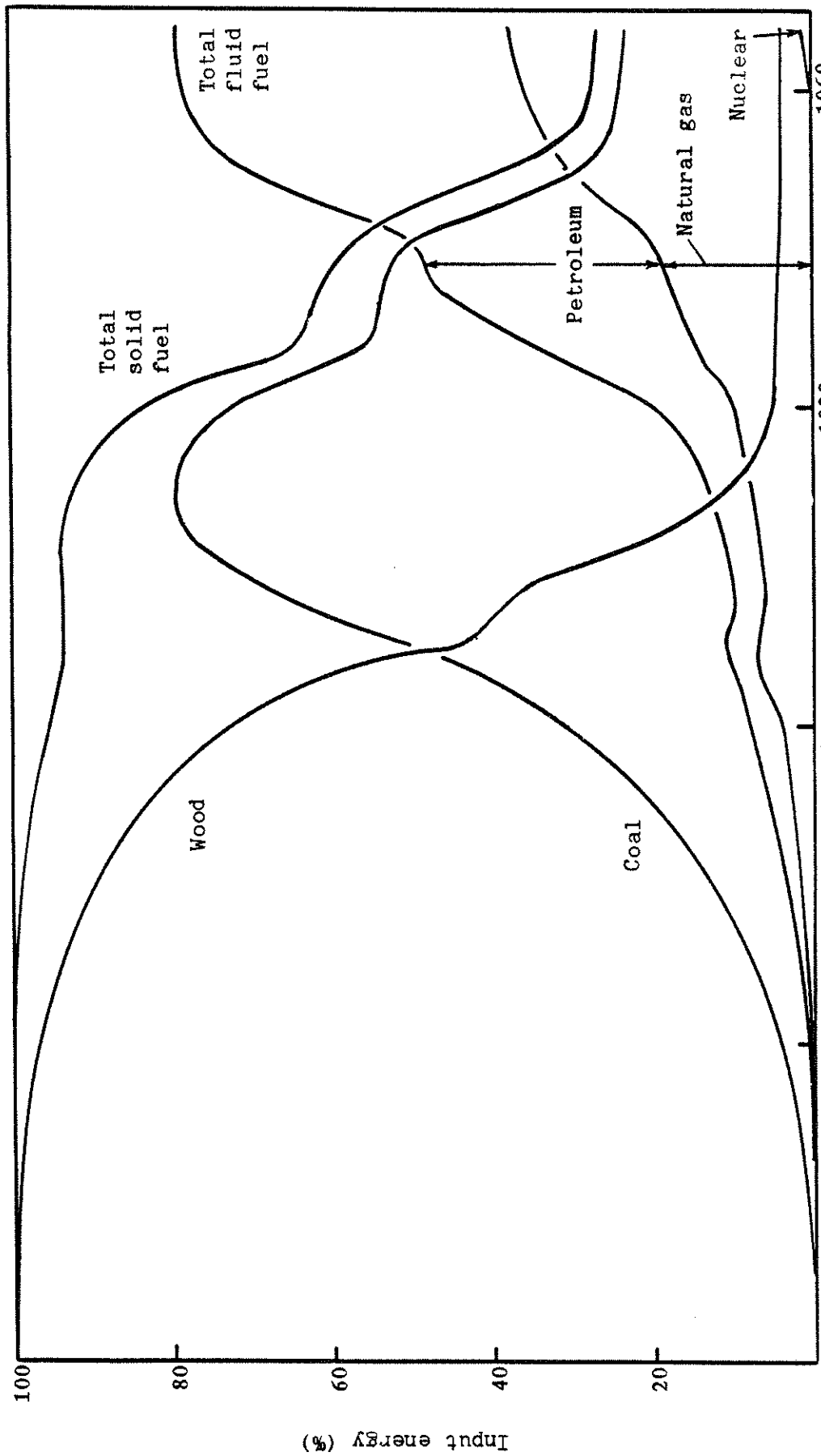

Figure 1.1 Contribution of each primary fuel to energy input. Ref (2)

The final report of the World Coal Study (WOCOL, (1)*) shows that the use of coal in industry has declined rapidly over the past two decades, and now accounts for only about 90 million TCE annually, or 9% of the total coal used by member countries of the Organization for Economic Cooperation and Development (OECD) (see Table 1.1). However, this trend is expected to be reversed, the major market growth being expected after 1985. Industries where coal use is expected to increase significantly include cement, chemicals (as fuel and feedstock), petroleum refining, and paper. Table 1.1 shows the projections for the OECD countries : Case A is a 1.75% increase in coal use per year, while Case B is a 2.5% increase.

A substantial new market for coal was projected to develop in the 1990s — as a feedstock for synthetic oil and gas plants. The total OECD market for the coal required for synthetic fuels by year 2000 was estimated to range from a low of 75 million TCE in Case A to a high of 335 million TCE (Case B) in the WOCOL study. This higher amount of coal would supply 65 large synfuel plants, each producing about 50,000 bdoe (1 bdoe is equivalent to 76 TCE per year) of synthetic oil or gas.

1.2 COAL GASIFICATION

Gaseous fuels, because of the ease with which they can be handled and their wide range of applications as heat sources and chemical feedstocks, have an important role in industrial and domestic applications. The natural gas and oil supplies of the world are not unlimited, and therefore coal gasification seems increasingly to be a major alternative for the production of gas for use as a fuel and as a chemical feedstock.

* The numbers in parenthesis in the text indicate references in the Bibliography.

TABLE 1.1

Total Coal Requirements in OECD Countries (10^6 tce)

Country/Region	TOTAL COAL[1]				
	1977	1985		2000	
		Case A	Case B	Case A	Case B
Canada	25	44	41	82	121
United States	509	655	725	1075	1700
Denmark	4.6	10.7	11.1	9.4	20.9
Finland	4.3	4.4	4.4	9	13
France	45	35	59	48	125
Germany, Fed. Rep.	102	119	126	150	175
Italy	13.5	22.3	22.9	31.5	60.5
Netherlands	4.5	10.4	10.4	23	38
Sweden	2.1	5.1	5.4	17	26
United Kingdom	109	107	115	133	179
Other Western Europe	51	61	83	135	175
Japan	79	97	102	150	224
Australia	38	65	65	141	166
Total OECD[2]	990	1235	1370	2000	3025

[1] Total includes steam plus metallurgical coal

[2] Totals are rounded

The aim of coal gasification is to convert coal into gas with little or no residue or by-products. The early part of this century saw a lot of development in this area, with the Lurgi Company of Germany being a pioneering developer.

The production of carbon monoxide and hydrogen from coal and steam is the most important reaction. However, since the reaction is endothermic, a lot of extra heat has to be supplied. This is done by having another reaction performed in parallel : that of combustion of coal with oxygen (to produce carbon monoxide and/or carbon dioxide), which is highly exothermic. Thus the product gas, which contains mainly hydrogen, carbon monoxide, and carbon dioxide, may be used as fuel or as chemical feedstock.

A third reaction — that between coal and hydrogen to produce methane — is also of significance because of the helpful effect it has on the thermal content of the product. This reaction is enhanced by high pressures, and therefore offers the possibility of increasing gasifier specific loadings if high-pressure operation is done. The Lurgi gasifier, which is the only one that operates under pressure, utilizes this aspect to advantage.

Hebden and Stroud (2) have made a fairly exhaustive classification of the available gasification processes. The four main groups are shown in Figure 1.2. The term 'fixed bed' for the setup shown in Figure 1.2(a) is inaccurate, but is in common usage because the extremities of the bed remain fixed. In this type of gasifier, lumps of coal are fed from the top while steam and oxygen are fed in countercurrent fashion through the bottom. The temperature profile in the gasifier shows a maximum, the magnitude of which is determined by the flow rates of each stream and

other operating conditions. Spent coal -- or ash -- is removed continuously from the bottom, either in molten form or in a dry state.

The second class of reactors is the fluidized bed (Figure 1.2(b)), where the coal is supplied in the form of a powder. Gas enters from the bottom, keeping the powder in a well-mixed and suspended state. As a result, the temperature and composition profiles are uniform throughout the bed. In the entrained flow gasifier (Figure 1.2(c)), pulverized coal is entrained with the gas cocurrently, and reacts in a high temperature flame. Reactions may continue downstream. Ash may be carried forward and separated from the product gas jointly with unreacted fuel. In the molten bath gasifier (Figure 1.2(d)), fuel and gas are also supplied cocurrently, the pool being of liquid ash and metal (which may be a catalyst for the carbon-steam reaction).

Fixed-bed gasifiers are by far the traditional mode and include the only commercially available high-pressure gasification process (the Lurgi process). The fluidized-bed and entrained modes have only one commercially operating example each, in the Winkler and Koppers-Totzek gasifiers respectively. Some of the operating conditions of these three processes are summarized in Table 1.2.

1.3 FIXED BED GASIFIERS

In a fixed bed gasifier, the coal enters from the top of the bed and moves down to replace that being consumed by gasification. As the coal descends, it comes in contact with hot product gases. Four different zones are formed,and are shown in Figure 1.3. When the coal reaches the combustion zone, it is finally totally consumed, leaving only ash. This ash is removed from the bottom, before which it exchanges much of its heat with the incoming colder stream of reactant

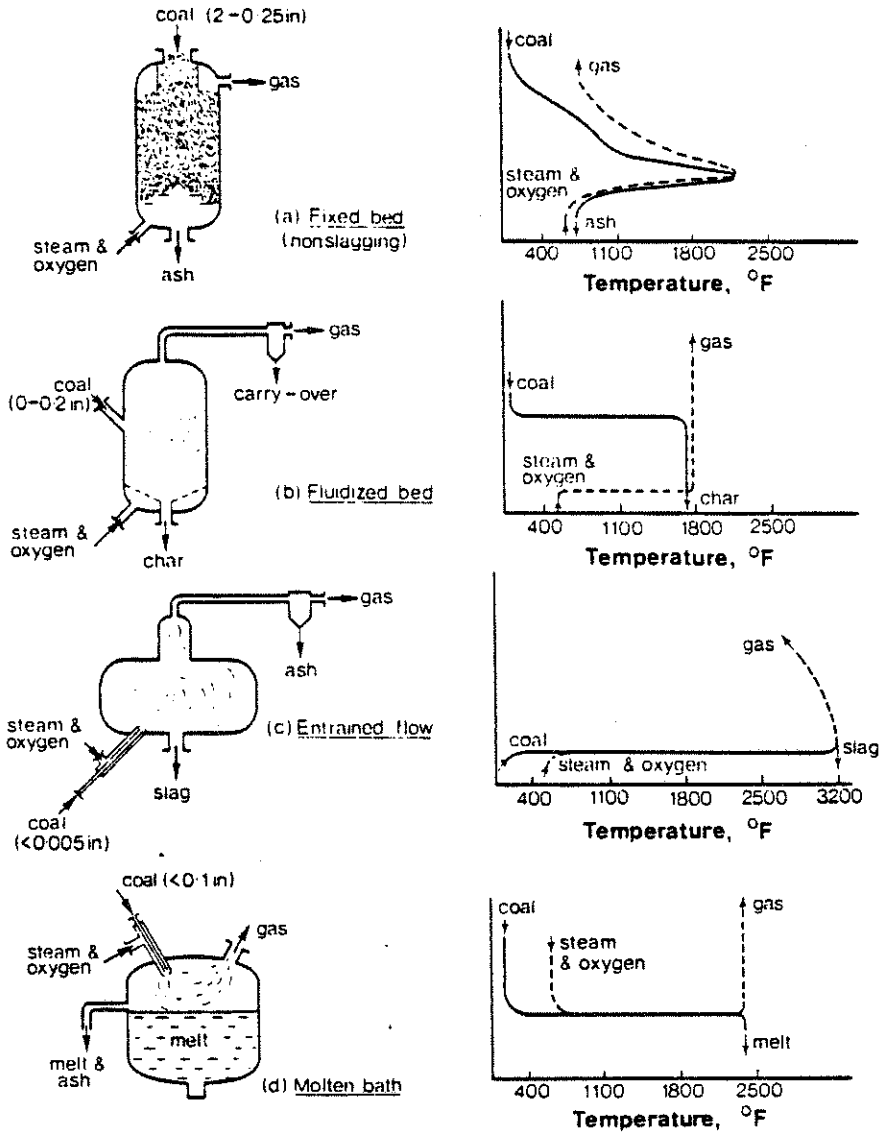

Figure 1.2 Classification of principal gasification systems (Ref (2)).

TABLE 1.2

Operating Parameters of Some Commercially Available Coal Gasification Processes (Ref (2))

	Lurgi Process	Winkler Process	Koppers-Totzek Process
Operating pressure in bar	25	1	1
Throughput in tons/hr	15	3-35	13-21
Feed coal	Mildly caking coal, coal lumps	In particular lignite, crushed coal	All coals, pulverized coal
Gasifying agent	Oxygen/steam	Oxygen/steam	Oxygen/steam
Carbon conversion (%)	99	90	90-96
Cold gas efficiency (%) (gasifier only)	75-85	75	70-77
Gas production m^3 (STP)/hour	55,000	5,000-6,000	20,000-55,000
Specific oxygen consumption in m^3 (STP)/ton coal	200-300	365	535
Specific steam consumption in tons/hour	1-1.4 (30 bar)	0.8 (low pressure steam)	0.24 (low pressure steam)
By-products	Tar, oil	Coal fines, small amounts of tar	none

gases. Another type of fixed bed gasifier — the slagging gasifier — has temperatures in the combustion zone going above the fusion temperature of ash (in excess of 1650 Kelvin). This molten ash is therefore drained off as a liquid.

The hot gaseous products rise from the reduction — or gasification — zone and come into contact with the cold incoming coal. The sensible heat content of the gases now removes most of the water and volatile matter content in the coal. These gaseous products are added to the products of combustion and gasification, and leave with the exiting gas stream.

The physical changes that coal undergoes during devolatilization are widely varying, depending upon the type of coal being used. Lignites and subbituminous coals become brittle and tend to disintegrate. High-volatile bituminous coals experience swelling and expand into dense lumps. Anthracitic coals do not cake, and maintain their original size distribution. These physical aspects are important because they may have large effects on gas flow in the gasifier. To prevent agglomeration and size segregation, mechanical stirring and agitation may be imposed.

Fixed bed systems are simple and reliable, and have a high thermal efficiency. The feed coal has to be minimally pretreated, and the product gases leave at modest temperatures. There are a number of commercial gasifiers available which fall in this category, but none that dominates the field as much as the Lurgi gasifier.

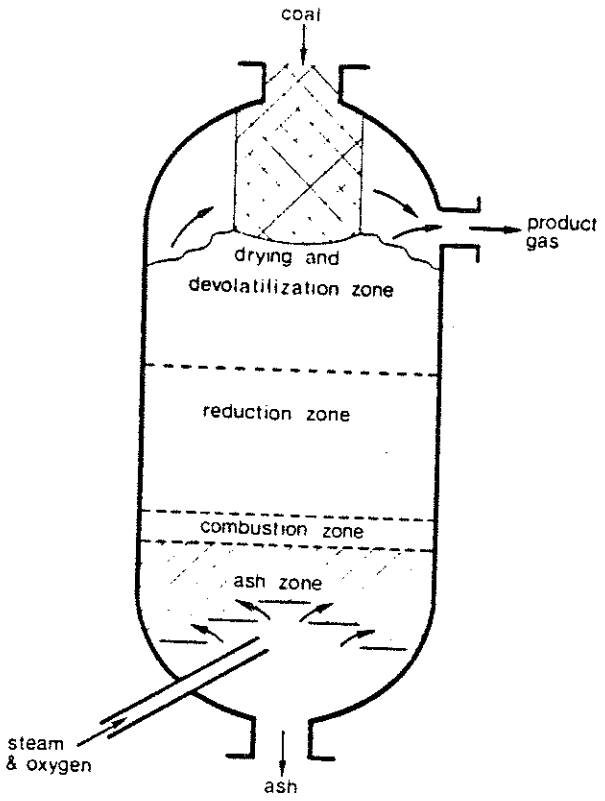

Figure 1.3 The four main zones in a nonslagging fixed bed gasifier

1.4 PAST MODELING EFFORTS

A number of models of fixed bed gasifiers have been developed in the recent past. Yoon (3) developed a steady state, homogeneous model for the Lurgi gasifier. Radial variations were accounted in that he considered two zones — an adiabatic core and a boundary layer — and wrote energy balances for each of these zones. Cho (4) and Desai (5) developed heterogeneous models for the steady state case. Their models also did not consider radial aspects. Kim (6) extended Cho's formulation to include the dynamics of a fixed bed gasifier when it went from one steady state to another because of a disturbance in one of the inputs. Yu (7) included radial effects in Yoon's formulation, and also incorporated the dynamics.

Moving bed gasifier models that have been presented until now have the disadvantage that they have not been experimentally verified under a wide range of operating conditions. Most comparisons have been for the conditions existing in the Lurgi gasifier (3) or that in the Morgantown Energy Technology Center (METC) (5). Experimental verification of the model at other conditions is therefore highly desirable.

In general, true fixed bed reactors do not exist in industry, because they can only be operated in batch mode which is highly uneconomical. Building a moving bed gasifier has its problems : namely, the coal feeding mechanism. A fixed bed gasifier is easy to build, and the model is not much different from that of a moving bed one with zero coal feed. A fixed bed reactor containing char (devolatilized coal) approximates a moving bed reactor with the coal feed cut off. Therefore, experimental and modeling studies on a fixed-bed reactor will provide results which are directly applicable to models of moving-bed reactors.

2. MATHEMATICAL MODELING OF FIXED BED GASIFIERS

2.1 INTRODUCTION

There are basically four major events that take place in a moving bed gasifier ((3), (4), (6), (7) etc.) : drying, devolatilization, gasification and combustion. Moving bed operations are generally at steady state : the events are confined to certain areas within the reactor, and thus we have the concept of zones.

The fixed bed reactor is much more difficult to model, primarily because of the fact that there is no real steady state. At best there is a pseudo-steady state, where a reaction front moves down the length of the reactor as time elapses, but does not change its' characteristics in doing so. However, some of the major events still exist : in this case therefore, they are confined to moving zones. Figures 2.1 and 2.2 give an idea of how the different events occur. Depending upon the coordinates used (spatial distance or time), the events take place in opposite order, as the figures show.

The zones, of course, are not as sharp as the two figures would indicate. There is some spread and overlap, but one can define criteria whereby some of the zones may be segregated. Combustion may be defined as that region between start of the combustion reaction (about 650 Kelvin) and the exhaustion of oxygen in the gaseous stream. This latter event corresponds closely -- but not quite exactly -- to the occurrence of a maximum in the axial temperature profile. In general, there is some oxygen left over even after the maximum, which only corresponds to the point where the system changes from being net exothermic to net endothermic.

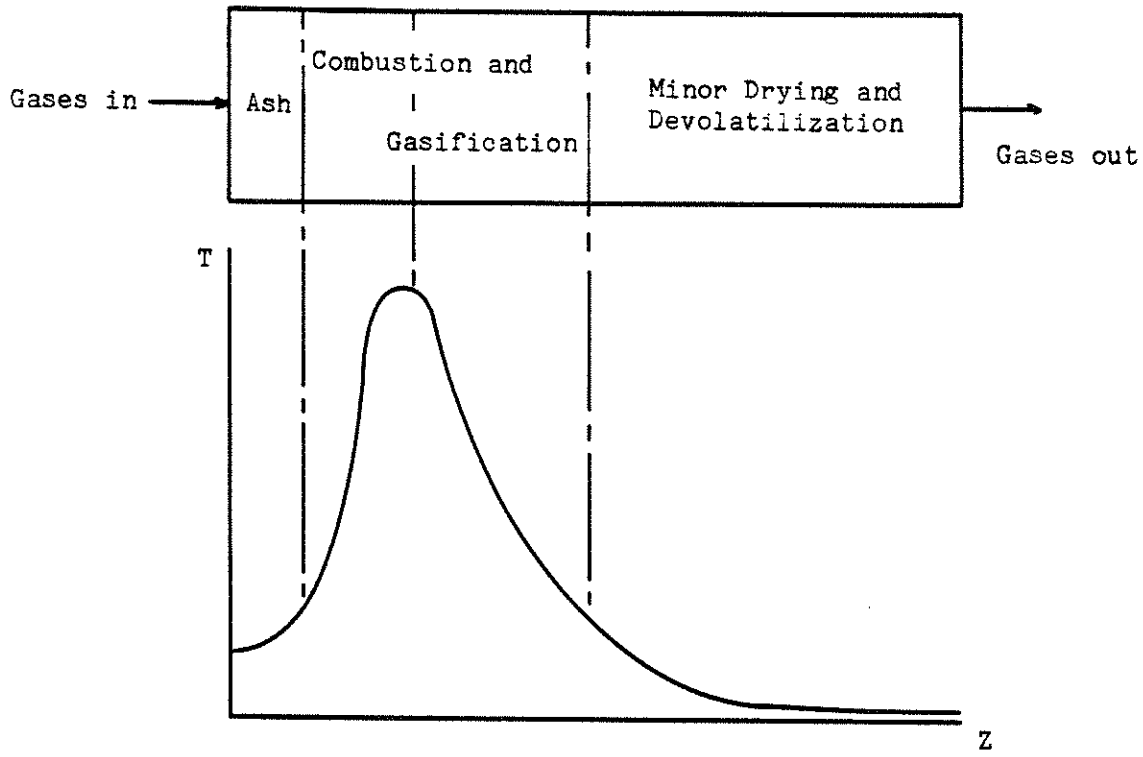

Figure 2.1 Typical temperature profile and zones in a fixed bed gasifier at a particular time

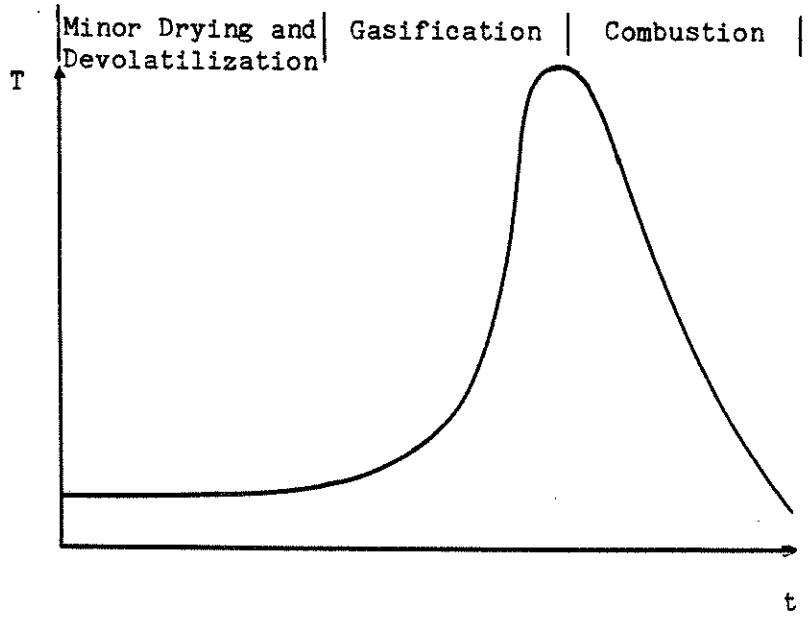

Figure 2.2 Events as a function of time at a particular axial position

Gasification starts where combustion ends, and continues until the temperature becomes low enough that the gasification reaction rates become negligible. This temperature would obviously depend on the operating pressure of the reactor. Devolatilization and drying are hard to separate, and presumably only occur in minor extents since the coal is already devolatilized.

2.2 USE OF A CHAR BED

Some moving bed simulations have been done following the model shown in Figure 2.3 ((4), (6)). Coal enters the bed, and is instantaneously changed to char with the molecular formula $CH_\alpha O_\beta$, α and β being determined by a material balance around the devolatizing/drying process. Since this char now takes part in the combustion/gasification reactions, the values of α and β have an effect on product compositions, etc.

From the discussion under Section 2.1, it is obvious that the moving bed set-up cannot be applied for a fixed bed of coal, because the α and β terms would be functions of time as well as location. Keeping track of these is too difficult a task and is not worth the effort, given the uncertainty in the knowledge of the kinetics of devolatilization and drying (Anthony and Howard(8)). One way to avoid the problem is to model a previously devolatilized bed, so that a uniform α and β may be used. Also, as discussed before, valid conclusions on the performance of moving bed reactors with coal may be drawn from simulations of fixed bed reactors with char.

2.3 KINETICS OF COMBUSTION AND GASIFICATION

There are five major reactions that occur during these two phases — four of them are heterogeneous and one is homogeneous. These are tabulated in Table 2.1. Other possible reactions — especially those

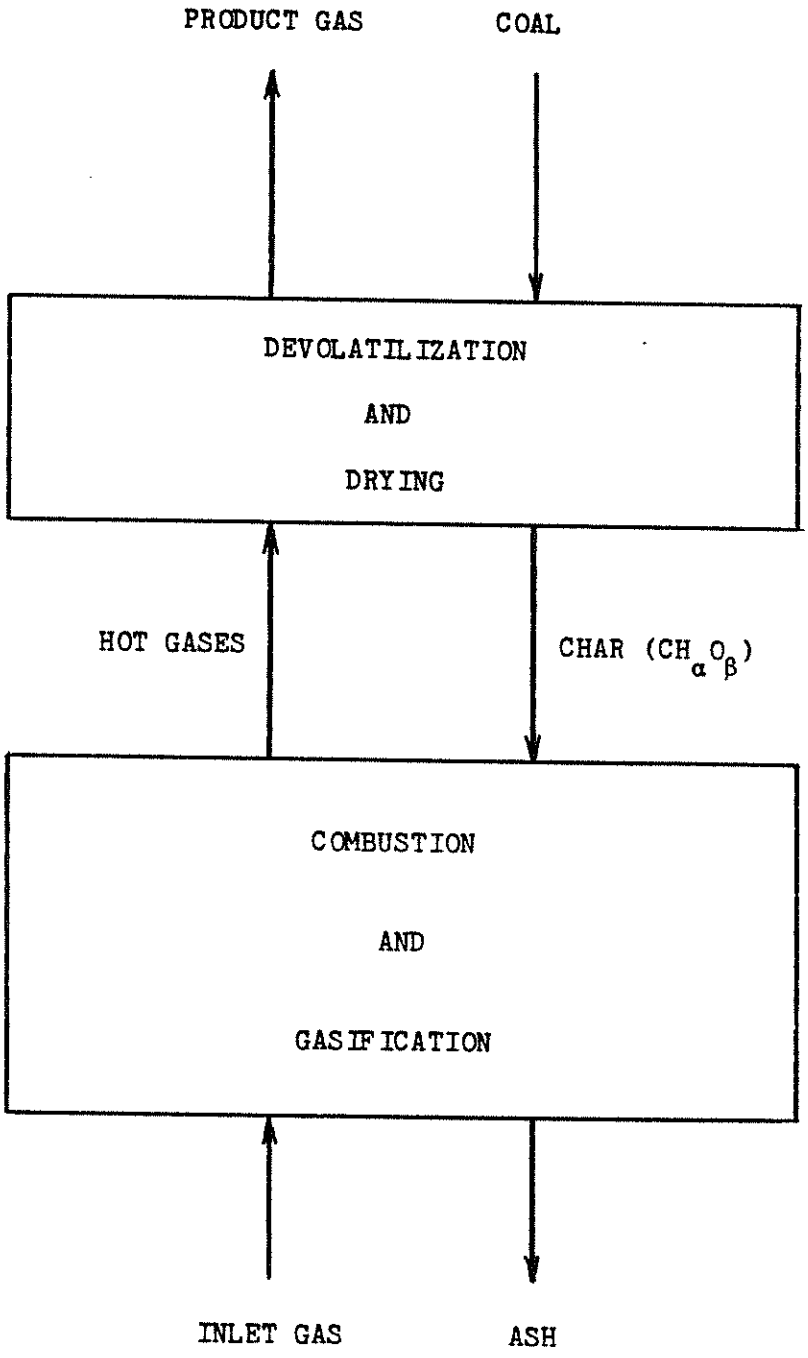

Figure 2.3 Model of a moving-bed gasifier

TABLE 2.1

Major Reactions Occurring in the Gasifier

1. $CH_\alpha O_\beta + (1-\beta)H_2O == CO + (1-\beta+\alpha/2)H_2$

2. $CH_\alpha O_\beta + CO_2 == 2CO + \beta H_2O + (\alpha/2-\beta)H_2$

3. $CH_\alpha O_\beta + (2-\alpha/2+\beta)H_2 == CH_4 + \beta H_2O$

4. $CH_\alpha O_\beta + \gamma O_2 == (2-2\gamma-\beta+\alpha/2)CO + (2\gamma+\beta-\alpha/2-1)CO_2 + (\alpha/2)H_2O$

5. $CO + H_2O == CO_2 + H_2$

Gasification : Reactions 1,2 and 3.

Combustion : Reaction 4.

Water-gas Shift : Reaction 5.

concerning sulfur and nitrogen — are ignored as they do not have a significant impact on the product gas composition. The three gasification and the water gas shift reactions are all reversible : so carbon deposition is a possibility. The molar ratio of carbon monoxide/carbon dioxide in the combustion reaction follows an Arrhenius temperature relation (Arthur (9),Rossberg (10)), with the parameters depending on the coals used and gasification rate. The stoichiometric coefficient accounts for this dependency. In this work, Rossberg's correlation is used :

$$CO/CO_2 = k^{\circ} \exp(-E/RT_g)$$

where CO/CO_2 = the molar ratio of carbon monoxide to carbon dioxide

k° = pre-exponential factor = 2512.0

E = activation energy = 41900 kJ/kmol

R = gas constant

T_g = gas temperature, in Kelvin

The char-hydrogen and char-carbon dioxide reactions are assumed to be kinetically controlled because they involve products of other reactions (water-gas shift and combustion) as reactants. The two other heterogeneous reactions are assumed to follow the shrinking core model where the rate is given by (Aris and Amundson (11)):

$$r_i = (1-\varepsilon)P_i^* \left[\frac{d_p}{6k_{g,i}} + \frac{d_p^2(1-\rho)RT_g}{12\rho D_{M,i}} + \frac{1}{\eta_i \rho^3 k_{r,i} C_c^{\circ}} \right]^{-1}$$

where ε is the void fraction of the bed, P_i^* is the effective partial pressure of reactant i and is given by

$$P^*_{H_2O} = (P_{H_2O} - P_{CO}P_{H_2}/K_s)$$

ρ is the fraction of the particle diameter which is occupied by unreacted char and is given by

$$\rho = (1 - X_c)^{1/3}$$

X_c is the local char conversion, d_p is the average particle diameter, R is the gas constant, C_c^o is the initial char concentration. $k_{r,i}$ is the intrinsic reaction rate of reaction i and is given by

$$k_{r,i} = k_{r,i}^o \exp(-E_i/RT)$$

$k_{r,i}^o$ and E_i for each of the reactions is tabulated in Table 2.2.

$k_{g,i}$ is the gas-film mass transfer coefficient, and is obtained from a j-factor correlation reported by Sen Gupta and Thodos (12):

$$k_{g,i} = \frac{2.06}{\varepsilon P} Sc^{-0.092} \left[\frac{PD_i}{d_p RT}\right]^{0.575} F_G^{0.425}$$

P is the total pressure in the reactor, Sc is the Schmidt number, D_i is the bulk phase diffusivity of species i, F_G is the total molar flux of the gas stream, $D_{M,i}$ is the effective diffusivity in the ash layer and is given by Wheeler (13) based on kinetic theory as :

$$D_{M,i} = D_i(1 - \exp(-2r\bar{V}_i/3D_i))$$

$\bar{V}_i$ is the average bulk phase velocity of gas species i and is given by

$$\bar{V}_i = 33.05*10^6*(T_g/PM_i)^{0.5}$$

M_i is the molecular weight of species i, r is the average local pore radius of the char particle and is assumed to follow a mathematical form of

$$r = C_1 \exp(C_2 X_c)$$

C_1 and C_2 are appropriate constants.

η_i is the effectiveness factor of reaction i and is given by

TABLE 2.2

Reaction parameters for Illinois and Wyoming Coal

Reaction	$k^{\circ}_{r,i}$	$E_i * 10^5$ (kJ/kmol)
Char–steam (Illinois)	$2.178 * 10^4$ (kmol/ kmol char kPa hr)	1.757
Char–steam (Wyoming)	$1.464 * 10^4$ (kmol/ kmol char kPa hr)	1.465
Char–hydrogen[1] (Illinois)	$1.465 * 10^{-4}$ (kmol/ kmol char kPa^2 hr)	0.6716
Char–hydrogen (Wyoming)	$2.931 * 10^{-4}$ (kmol/ kmol char kPa^2 hr)	0.6716
Char–oxygen (Ill. and Wyo.)	$6.360 * 10^7$ (kmol/ kmol char kPa hr)	1.130

[1] No data available in the literature

k°_r is assumed as one half of that of Wyoming coal

k°_{r,CO_2} was assumed as 0.6 k°_{r,H_2O} (Ref (3)).

$$\eta_i = \frac{1}{\phi_i}\left[\frac{1}{\tanh(3\phi_i)} - \frac{1}{3\phi_i}\right]$$

ϕ_i is given by

$$\phi_i = \frac{d_p \rho}{6}\left[\frac{k_{r,i} C_c^o}{\delta_i D_{e,i}/RT}\right]^{0.5}$$

δ_i is a stoichiometric factor, and is equal to 1 for the char-steam reaction and $1/\gamma$ for the char-oxygen reaction. $D_{e,i}$ is the effective diffusivity in the core and may be represented in an approximate sense by

$$D_{e,i} = (\theta_c/\theta_a)^2 D_{M,i}$$

θ_c and θ_a are the fractional porosity of the core and ash layer respectively. For the bulk diffusivity D_i, we can adopt a simple model based on Geankoplis (14) as :

$$D_i = (1 - y_i)\left[\sum_{j \neq i} \frac{y_j}{D_{ij}}\right]^{-1}$$

where y_i is the molar fraction of gas species i in the bulk phase, and from an empirical equation proposed by Fuller et. al.(15) :

$$D_{ij} = \frac{0.001\ T^{1.75}\left[1/M_i + 1/M_j\right]^{0.5}}{P\left[(\Sigma\nu_i)^{1/3} + (\Sigma\nu_j)^{1/3}\right]}$$

The diffusion volumes $\Sigma\nu$ are presented in Table 2.3 for the pertinent gaseous species.

All reactions are considered to be first order. The Arrhenius-type temperature dependancy factors for different coals are given in Table 2.2.

2.4 MATERIAL AND ENERGY BALANCE EQUATIONS

Axial mixing effects in both material and energy flow may be

TABLE 2.3

Values of Diffusion Volumes

for the Components Involved in

Gasification Reactions (Ref (14))

Component	
O_2	16.6
N_2	17.9
H_2O	12.7
H_2	7.7
CO	18.9
CO_2	26.9
CH_4	24.4

present because of turbulence and the presence of the solid phase, and may be accounted for by superposing an 'effective' transport mechanism on the overall transport by plug flow. However, as discussed in (7), axial dispersion is negligible according to the criteria developed by Young and Finlayson (16) unless the gas flow rate is very low. Radial dispersion of mass in the gas phase may be assumed to be negligible in comparison with the convective contributions. Radial dispersion for the energy balance may not be neglected because there is a substantial radial temperature profile, especially since non-adiabatic reactors are being considered. Additionally, since temperatures in gasifiers regularly reach very high values (about 1300 Kelvin), it would be expected that radial dispersion of heat would play a substantial role.

Under the assumption that the gas and solid phases are at the same temperature, the energy balance can be written as :

$$\frac{1}{r}\frac{\partial}{\partial r}\left[k_r r \frac{\partial T}{\partial r}\right] - \left[\sum F_i Cp_i\right]\frac{\partial T}{\partial z} - \sum R_j \sum \alpha_{ij} H_i = C_c C_{pc} \frac{\partial T}{\partial t}$$

Here α_{ij} is the stoichiometric coefficient of species i in reaction j. Gas-phase accumulation terms have also been neglected — this should not result in major inaccuracies since the residence time of gases in the reactor is of the order of a few seconds whereas the reactor operation time runs into hours.

Besides the above, one other energy balance may be written for the wall. Eigenberger (17) has shown that the effect of heat accumulation in the wall (of a tubular reactor with a highly exothermic reaction) has a considerable influence upon the transient behaviour of the reactor. Eigenberger's analysis was for disturbances imposed on reactors operating at steady state, but it is felt that for gas-solid reactors (which

are not steady since there is a moving front) having walls with high thermal capacity the effect would be not minimal. Consequently, we write the energy balance for the wall as :

$$2Rh_{eff}(T|_{r=R^-} - T_w) + 2R_o h_o(T_c - T_w) + \lambda_w(R_o - R^2)\frac{\partial^2 T}{\partial z^2}w = \rho_w C_w(R_o - R^2)\frac{\partial T}{\partial t}w$$

The solid-phase material balance equation can be written as:

$$\sum_j \alpha_{cj} R_j = \frac{\partial C}{\partial t}c$$

For the gas phase we have :

$$-\frac{\partial F}{\partial z}i + \sum_j \alpha_{ij} R_j = 0 \qquad i = 2,\ldots,m$$

There are no dispersion terms in the above, and no accumulation terms except for the solid-phase terms. Note that even though the gas phase equations have no $\frac{\partial}{\partial t}$ terms, the gas fluxes are functions of time because the reaction rates are.

The boundary conditions are:

$z = 0 \qquad F_i = F_{io} \qquad T = T_o \qquad \frac{\partial T}{\partial z}w = 0$

$z = L \qquad \frac{\partial T}{\partial z}w = 0$

$r = 0 \qquad \frac{\partial T}{\partial r} = 0 \qquad \frac{\partial F}{\partial r}i = 0 \qquad \frac{\partial C}{\partial r}c = 0$

$r = R \qquad k_r\frac{\partial T}{\partial r} = h_{eff}(T - T_w) \qquad \frac{\partial F}{\partial r}i = 0$

Initial conditions are:

$t = 0 \qquad T = T_o$

$F_i = 0$

$C_c = C_c^o$

$T_w = T_c$

The procedure used to solve this set of equations is discussed in the next chapter.

3. METHOD OF SOLUTION

3.1 NUMERICAL METHODS USED IN THE PAST

Simulation models for moving bed gasifiers have been reported before ((3),(4),(5),(6),(7)). The equations to be solved for the moving bed case were not quite the same as those for the fixed bed case — in fact, in one sense they were more difficult in that conditions at z = L had to be satisfied, thereby implying that some sort of iterative scheme had to be used.

Yoon (3) solved the steady state problem for the moving bed case. Because of the presence of steady state, he was able to reduce the number of equations in z — by utilizing C,H and O balances — so that he finally had five first order boundary value problems. This was integrated by the Runge-Kutta fifth order method, and the Fibonnaci search method for matching boundary conditions.

Desai (5), like Yoon, did not consider radial effects in his equations. He had 19 simultaneous first order non-linear ODEs which he solved using a 'Runge-Kutta with fixed length integration scheme'. To match the boundary conditions, he used a trial-and-error procedure, getting convergence 'within seven to eight iterations'. Cho (4) utilized much the same procedure as Desai with two changes : he had a heterogeneous model, and the number of gaseous species he considered were less. Because of the heterogeneous aspect, two additional iterative loops were introduced — one for solid temperatures at each axial location, and one for the gas temperature at the top of the

gasifier. A relaxation technique was utilized for each of these iterative searches, which was later changed to a Wegstein search.

Kim (6) extended this formulation to the dynamic case. By utilizing a few judicious assumptions, the same basic method was used. However, the procedure became simpler because the solid conversion profile was known at every time step, and therefore no iterations were required for the solid phase boundary condition at $z = L$.

Yu (7) included radial effects in her formulation, and therefore had to take care of the radial terms before integration in z could be done. She used orthogonal collocation on finite elements for the radial coordinate, and integrated the resulting ODEs by a fourth order Runge-Kutta method. For the dynamic case, she used exponential collocation in the infinite time domain.

Klein (18) has a survey of other previous works in this area. This includes those by Amundson and his coworkers ((19),(20),(21)), who presented models to study the solid-fuel interactions in fixed and moving beds, and considered intraparticle conduction and reactor non-adiabaticity. They solved the problem using Hankel and Laplace transforms when the heat source (due to chemical reaction) was of a certain form. Ishida and Wen (22) studied a one-dimensional problem where a single reversible noncatalytic gas-solid reaction was taking place. Amundson and Arri (23) developed a complicated model for the Lurgi gasifier in which a detailed single-particle model was incorporated, and the conduction-radiation term was included in the solid energy balance. They used an implicit finite-difference scheme to solve the set of equations.

Recently, Pirkle et. al. (24) carried out a survey comparing three methods — finite differencing, collocation on finite elements, and the method of Galerkin on finite elements — for the simulation of a fixed-bed homogeneous catalytic reactor. They considered radial dispersion in mass and energy, but no axial dispersion. Their findings show that the five-point central difference method and collocation on finite elements were equally efficient for both 'gradual reaction' and 'steep gradient' problems. The method of Galerkin on finite elements required about twice the computer time of the other two methods for 'gradual reaction' problems. For 'steep gradient' problems, the efficiency of the Galerkin method equalled that of the other two methods.

The use of Orthogonal Collocation was popularized by Villadsen and Stewart (25). In this method, the approximate solution of a differential equation is expressed as a combination of orthogonal polynomials (trial functions). The zeros of the selected orthogonal polynomials are the collocation points. Furthermore, the solution of the ODE can be expressed in terms of the values of the dependent variable at the collocation points instead of the values of the coefficients of the trial functions (Finlayson (26)). This technique in very useful in the kinds of problems that occur in chemical reactor analysis, mainly because of the fact that PDEs in r and z can be converted to ODEs in either r or z (depending on which coordinate the collocation is carried out). It is even possible to convert them to simultaneous equations in r and z, if collocation is applied to both coordinates.

Numerical comparisons of orthogonal collocation to various finite difference methods (Michael and Iordache (27)) and finite element methods (Hopkins and Wait (28)) have been published. Collocation has been

found to be superior to the Runge-Kutta fourth order method for boundary value problems and some initial value problems (Birnbaum and Lapidus (29 a,b), Villadsen and Sorensen (30)). In recent times, collocation has been used extensively in chemical reactor analysis (Young and Finlayson (31), Dixon and Cresswell (32), Sorensen et. al. (33), Finlayson (34),(35)).

In previous simulations the technique used for integrating the set of simultaneous ODEs has always been the Runge-Kutta technique. A major disadvantage with this method is the absence of error-checks, if fixed step size is chosen. For the methods which have variable step size, far too many function evaluations are required. Predictor-corrector techniques having good A-stability are good candidates for the type of system we have, where the equations are very stiff.

3.2 APPROACH USED IN THIS WORK

The system of simultaneous partial differential equations that have to be solved has three dimensions : z, r and t, and each has to be treated separately. Collocation was used for the radial dimension, and finite differencing in the time-frame so that the set of PDEs could now be rewritten as a larger set of ODEs in z. This set of equations was now numerically integrated using Gear's routine (36), which utilizes a predictor and a backward-differencing corrector. Gear's method was selected over the standard (i.e. R-K) method for reasons discussed in Appendix 10.1.

Finite differencing in time was applied to two equations -- the energy balance equation, and the solid phase mass balance :

$$\frac{1}{r}\frac{\partial}{\partial r}\left[k_r r \frac{\partial T^n}{\partial r}\right] - \left[\sum F_i Cp_i\right]\frac{\partial T^n}{\partial z} - \sum R_j^n \sum \alpha_{ij} H_i = C_c^o (1 - X^n)(1 - \varepsilon)\frac{(T^n - T^{n-1})}{\Delta t}$$

$$C_c^o\left[\frac{X^{n+1} - X^n}{\Delta t}\right] = \sum_j \alpha_{cj} R_j^n$$

These explicit equations are easy to handle, but necessarily require the time steps to be small so that stability and accuracy problems are not encountered.

Defining the dimensionless coordinates

$$\xi = z/L$$

and $$\rho = r/R$$

the equations can be written as:

$$k_r L\left[\frac{1}{R^2}\frac{\partial^2 T^n}{\partial \rho^2} + \frac{1}{R^2}\frac{\partial T^n}{\rho \partial \rho}\right] - \sum_i F_i Cp_i \frac{\partial T^n}{\partial \xi} - L\sum_j R_j^n \sum_i \alpha_{ij} H_i = LC_c^o(1-X^n)(1-\varepsilon)\frac{(T^n - T^{n-1})}{\Delta t} \tag{3.1}$$

$$C_c^o\left[\frac{X^{n+1} - X^n}{\Delta t}\right] = \sum_j \alpha_{cj} R_j^n \tag{3.2}$$

$$\frac{1}{L}\frac{\partial F^n}{\partial \xi} i = \sum_j \alpha_{ij} R_j^n \qquad i = 2,\ldots,m \tag{3.3}$$

Applying radial collocation to equation 3.1 :

$$k_r L\sum_l B_{kl} T_l^n + \frac{k_r}{R^2 \rho_k}\sum_l A_{kl} T_l^n - \left[R^2 \sum_i F_{ik} Cp_i\right]\frac{dT^n}{d\xi}k - R^2 L\sum_j R_j^n \sum_i \alpha_{ij} H_i =$$

$$C_c^o(1 - X^n)(1 - \varepsilon)\left[T_k^n \frac{-T_k^{n-1}}{\Delta t}\right] \tag{3.4}$$

Here A_{ij} and B_{ij} are the standard coefficient matrices commonly used in collocation (see (26)). The boundary condition at r = R for the energy balance can be written as :

$$\frac{k}{R} r \frac{\partial T^n}{\partial \rho}\Big|_{N+1} = - h_{eff}(T_{N+1}^n - T_w^n)$$

or,

$$k_r \sum_l A_{N+1,l} T_l^n = - h_{eff} R(T_{N+1}^n - T_w^n) \tag{3.5}$$

Equation 3.5 can be introduced into equation 3.4 to finally give :

$$k_r L \sum\left[B_{kl} + \frac{A_{kl}}{r_k} - C_{k,N+1}A_{N+1,1}\right]T_1^n + RLC_{k,N+1}h_{eff}T_w^n - R^2L\sum R_j^n\sum \alpha_{ij}H_i =$$

$$R^2\left[\sum F_{ik}Cp_i\right]\frac{dT_k^n}{d\xi} \qquad (3.6)$$

where

$$C_{k,N+1} = \left[B_{k,N+1} + A_{k,N+1}/\rho_k\right]\Big/\left[A_{N+1,N+1} \quad h_{eff}R/k_r\right]$$

Similarly, radial collocation on equation 3.3 simply yields :

$$\frac{1}{L}\frac{\partial F_{i,k}^n}{\partial x} = \sum \alpha_{ij}R_{j,k}^n \qquad \begin{matrix} k = 1,..,M \\ i = 2,..,m \end{matrix} \qquad (3.7)$$

Our system of equations have now been converted to (M+1)*N ODEs in ξ, where M is the number of gaseous species and N is the number of interior collocation points. The boundary conditions are :

$$\xi = 0, \qquad F_{ik} = F_{i0} \qquad k = 1,..,N$$

$$T_k = T_0 \qquad i = 2,..,m$$

The boundary conditions at $\rho = 0$ can be inherently satisfied by using only symmetric polynomials as trial functions :

$$T(\rho^2) = T(1) + (1 - \rho^2)\sum_i a_i P_{i-1}(\rho^2)$$

$$F_i(\rho^2) = F_i(1) + (1 - \rho^2)\sum_j a_{ij}P_{j-1}(\rho^2)$$

These polynomials are defined to be orthogonal with the condition

$$\int_0^1 W(\rho^2)P_k(\rho^2)P_m(\rho^2)\rho d\rho = 0 \qquad k \leqslant m-1$$

The boundary conditions at $\rho = 1$ yield linear equations which may be utilized to find the values of the independent variables at $\rho = 1$:

$$T_{N+1}^n = \frac{h_{eff}T_w^n/k_r - \sum A_{N+1,1}T_1^n}{A_{N+1,N+1} + h_{eff}R/k_r}$$

and

$$F_{i,N+1}^n = -\frac{\sum A_{N+1,1}F_{i,1}^n}{A_{N+1,N+1}} \qquad i = 2,..,m$$

The energy balance for the wall is treated separately from the rest

of the equations because of the second order differential term in ξ. Defining one more variable as $dT_w/d\xi$ (and thereby adding two more ODEs to the set we already have) did not work. This is because of the condition at $\xi = 1$, which implies that some sort of iteration scheme has to be utilized. This results in large amounts of computer time requirements (if convergence can be achieved at all). It was decided therefore, that finite differencing in ξ as well as in t should be done for the wall. In that case, the condition at $\xi = 1$ can be included in the formulation without any iterative search. The problem however, is in defining a small enough $\Delta\xi$ such that there is no significant loss in accuracy.

Equation 2.1 can be rewritten as :

$$\frac{\partial T}{\partial t}w = C_1(T - T_w) + C_2(T_c - T_w) + C_3\frac{\partial^2 T}{\partial \xi^2}w$$

where $$C_1 = \frac{2Rh_{eff}}{\rho_w C_w (R_o^2 - R^2)}$$

$$C_2 = \frac{2R_o h_o}{\rho_w C_w (R_o^2 - R^2)}$$

and $$C_3 = \frac{\lambda_w}{\rho_w C_w L^2}$$

Finite difference in ξ :

$$\frac{dT}{dt}w,i = C_1(T_{N+1} - T_{w,i}) + C_2(T_c - T_{w,i}) + C_3\left[\frac{T_{w,i+1} - 2T_{w,i} + T_{w,i-1}}{\Delta\xi^2}\right]$$

This can be rewritten as :

$$\frac{dT}{dt}w = \underline{\underline{A}}\underline{T}_w + \underline{B} \qquad (3.8)$$

where

$$A = \begin{vmatrix} b_1 & c_1 & & & \\ a_1 & b_2 & \ddots & & \\ & \ddots & \ddots & \ddots & \\ & & \ddots & \ddots & c_n \\ & & & a_n & b_{n+1} \end{vmatrix} \qquad B = \begin{vmatrix} C_1 T_{N+1} + C_2 T_c \\ \vdots \\ \vdots \\ \vdots \\ \vdots \end{vmatrix}$$

and the elements a, b, c are given by :

$$a_i = C_3/\Delta\xi^2 \qquad i = 1,..,n$$

$$b_i = -(C_1 + C_2 + 2C_3/\Delta\xi^2) \qquad i = 2,..,n$$

$$c_i = C_3/\Delta\xi^2 \qquad i = 1,..,n$$

$$b_1 = -(C_1 + C_2 + 2C_3/3\Delta\xi^2)$$

$$b_{n+1} = -(C_1 + C_2 + C_3/\Delta\xi^2)$$

Finite differencing equation 3.8 in t yields :

$$\frac{T_w^{n+1} - T_w^n}{\Delta t} = AT_w^{n+1} + B$$

or

$$(\underline{\underline{I}} - \underline{\underline{A}}\Delta t)\underline{T}_w^{n+1} = \underline{T}_w^n + \underline{B}\Delta t \qquad (3.9)$$

Here A is tridiagonal matrix, and therefore so is (I-AΔt). Therefore the Thomas algorithm can be used to solve this set of linear simultaneous equations.

3.3 THE ALGORITHM

The flowchart describing the solution method is given in Figure 3.1. The step-by-step procedure is as follows :

1. Read all input parameters, and the initial profiles for solid conversion and bed temperature at each collocation point, as well as the wall temperature profile.

2. Integrate the set of (M+1)*N equations in ξ (i.e. equations 3.6and 3.7) starting from the respective boundary conditions at ξ= 0, and ending at ξ = 1. This integration, as mentioned before, utilizes

Gear's routine. While the integration is being done, store the values of the independent variables at a specified set of ξ-locations.

3. Update the char-conversion and wall temperature profiles by using equations 3.2 and 3.9 respectively.

4. Repeat steps 2 and 3 in succession until some suitable criterion has been satisfied. The criterion is : either (i) achievement of steady state for a moving bed — in case a moving bed simulation is desired, or (ii) the whole bed has been converted, for a fixed bed.

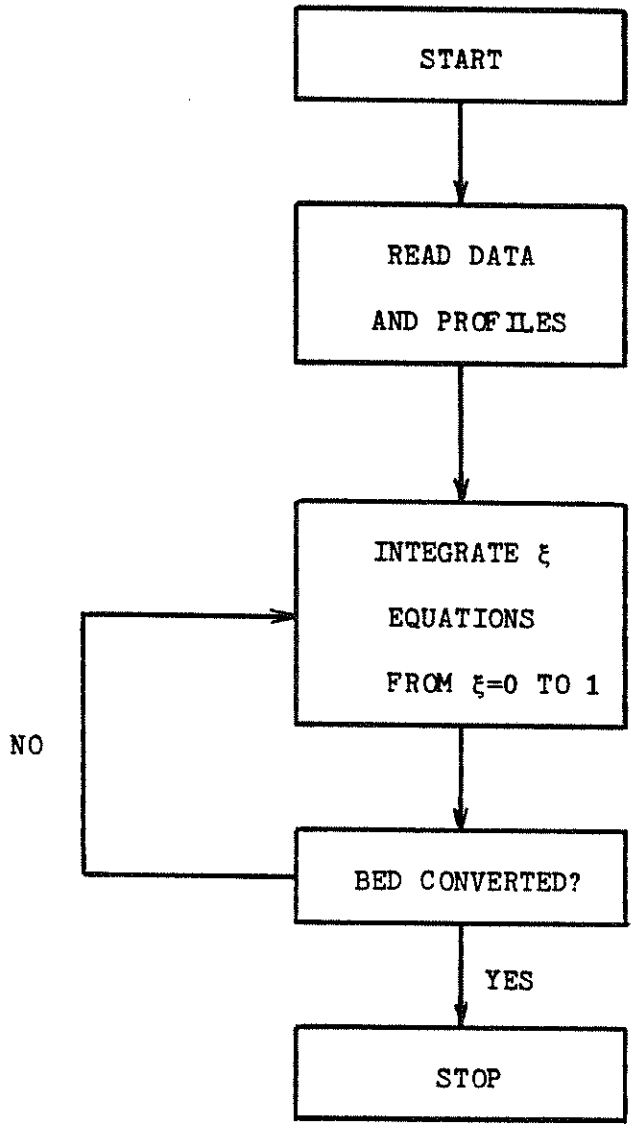

Figure 3.1 Flowchart for simulation

4. ESTIMATION OF HEAT TRANSFER PARAMETERS

4.1 DISCUSSION OF CORRELATIONS

Two parameters -- the effective thermal conductivity and the effective wall heat transfer coefficient — are required to solve the solid energy balance equation. There has been a fair amount of work done in the area of estimation of these parameters (Coberly and Marshall (37), Kwong and Smith (38), Plantz and Johnstone (39), Burnell et. al. (40), Yagii and Kunii (41)). All of these works correlate the two parameters in some way or the other to the mass flow rate of gas, the most usual variable being $d_p G/\mu$. Froment and Bischoff (42) present graphs (shown here in modified form in Figures 4.1 and 4.2) plotting most of the correlations. However, experimental data is limited to regions where $d_p G/\mu$ is greater than 30, whereas for our simulations a representative value would be 3.

Yu used the value 9.5 W/m-K for k_r for a moving bed gasifier. In a fixed bed gasifier, even though the solid phase is not in motion, one can expect a reasonably close value to that present in a moving bed reactor. However, calculation using the correlations developed by Plantz and Johnstone or Merrick (43) for example, yield the values 1.04 W/m-K and 1.10 W/m-K respectively (for the correlation of Plantz and Johnstone, $d_p G/\mu = 150$ was used). The correlations for effective wall heat transfer coefficient are even more sensitive to mass flow rates, and some of the proposed correlations (e.g., Coberly and Marshall) have very poor fits. Furthermore, the problem of low $d_p G/\mu$ values is present here too.

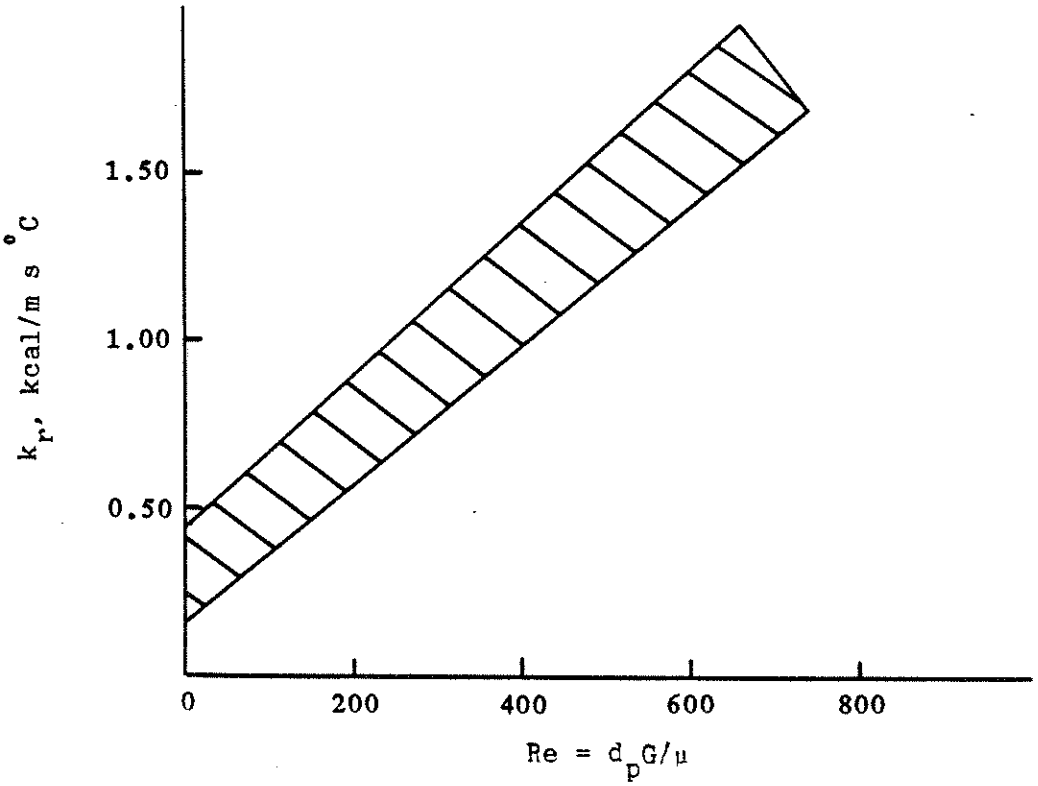

Figure 4.1 Region of uncertainty in correlations for effective thermal conductivity

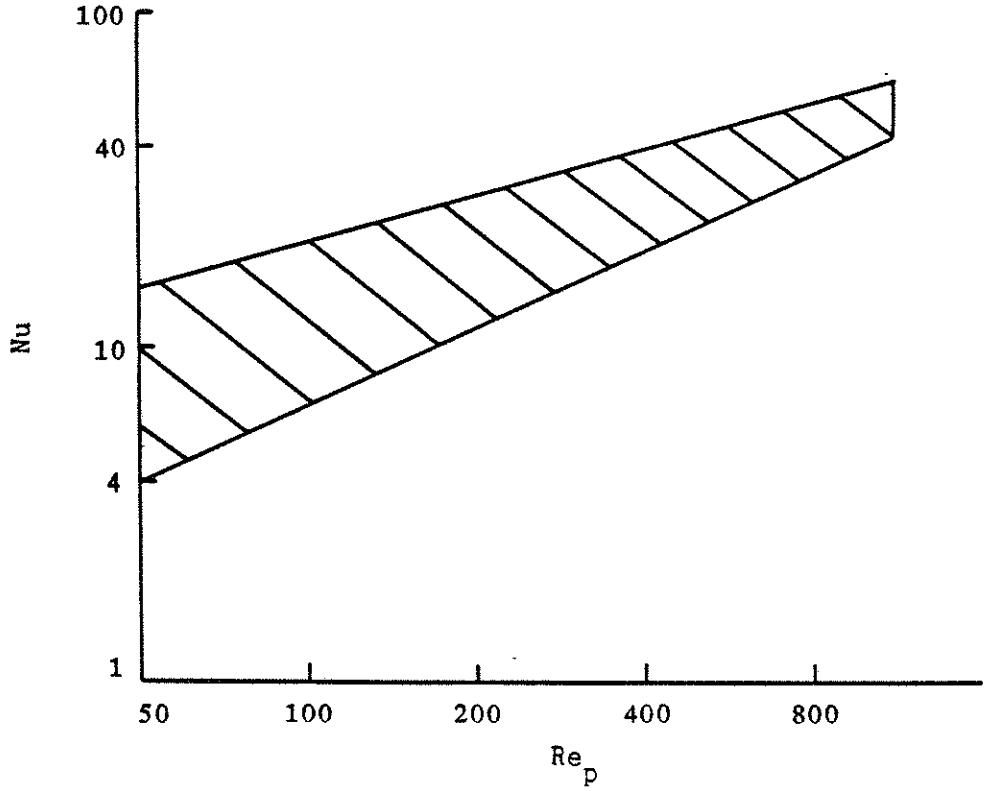

Figure 4.2 Region of uncertainty in correlations for Nusselt numbers for wall heat transfer coefficients

The values of k_r and h_{eff} have a major effect on the temperature profiles — both radially and axially. Since the correlations above do not allow for accurate or consistent predictions of these parameters, experimental determination of the parameters was carried out.

4.2 EXPERIMENTAL SETUP

The experimental setup is shown in Figure 4.3. It consists of a stainless steel vessel which is filled with char. A cold inert gas — typically nitrogen — enters from one end and exits through the other after being heated. The heat is supplied through the wall, which is surrounded by a ceramic lining in which a heating element is imbedded. Temperature profiles are measured via four thermocouples which are housed in the four thermowells labelled S,T,U and V in the figure.

The four thermowells allow the measurement of radial as well as axial temperature profiles along three radial positions in the coal bed. These three positions are chosen as the collocation points in three-point orthogonal collocation with symmetric polynomials. The fourth thermowell measures the temperature profile in the wall. The attempt in this experiment was to maintain a constant wall temperature, but as some of the results (see Table 4.1) show, this was not the case.

4.3 ANALYSIS OF DATA

To analyze the data, equations for energy balance must be written and predicted temperature profiles have to be compared with experimental ones. Assuming that physical parameters (like thermal conductivities, specific heats, etc.) retain constant values under all conditions, the energy balances at steady state for the gaseous and solid phases may be written as :

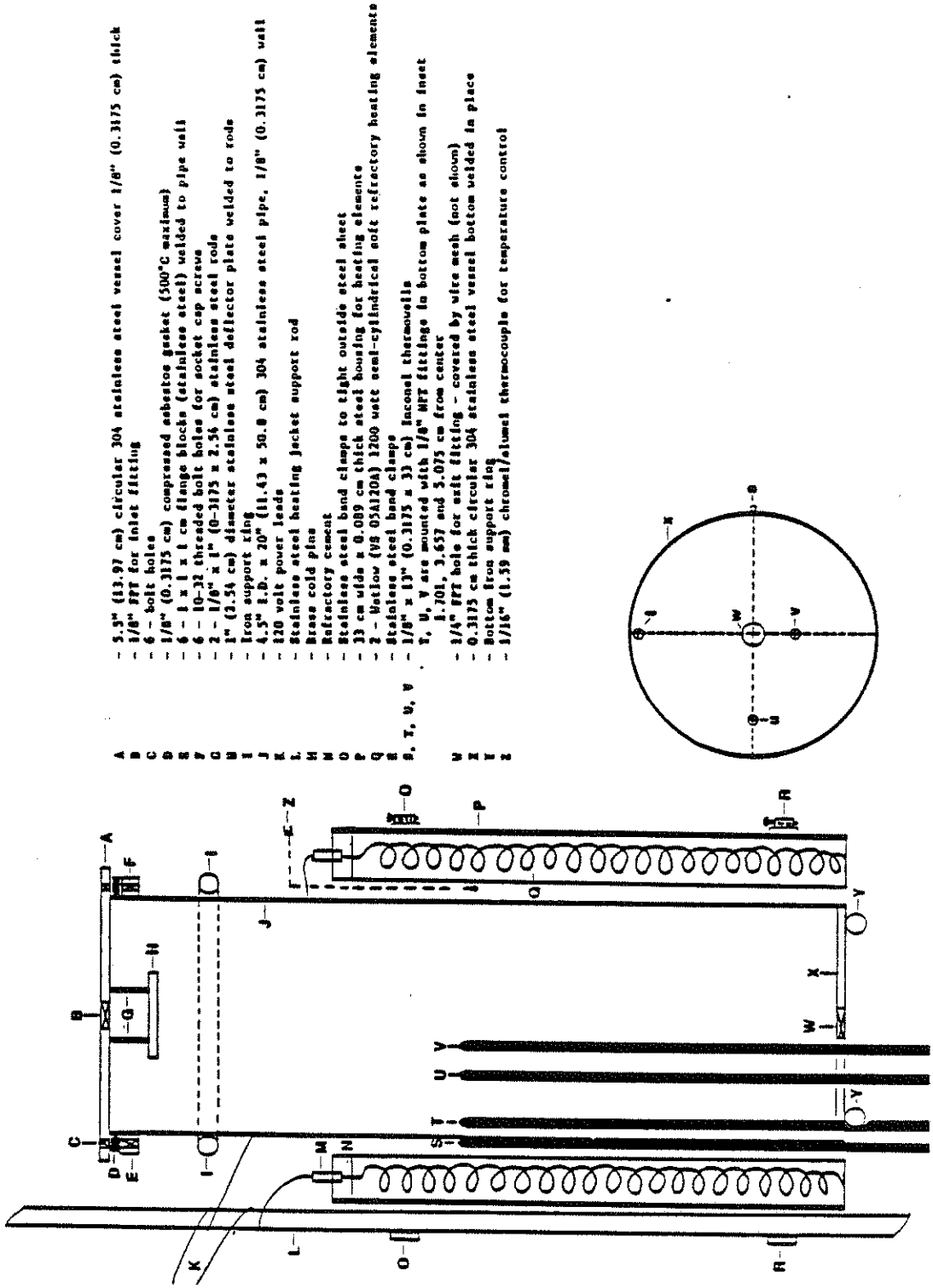

Figure 4.3 The devolatilizer

TABLE 4.1

Char Profile Results

Char Type:	Wyodac 8-20 mesh (2.362-0.833 mm)
Char Loaded:	1443.5 gms
Char Removed:	1311.0 gms
Vessel Inside Radius:	5.715 cm
Nitrogen Flowrates:	A - 1.605 m^3/hr, B - 2.166 m^3/hr (standard conditions)
Vessel Pressure:	A - 0.2393 MPa, B - 0.2807 MPa
Inlet Gas Temperature:	25°C

	RUN A				RUN B			
Depth from Top of Bed	r/R				r/R			
	Wall	0.888	0.640	0.298	Wall	0.888	0.640	0.298
4 cm	604°C	519°C	339°C	357°C	607°C	497°C	305°C	313°C
5	620	534	360	370	612	508	315	319
6	633	549	388	389	630	523	337	333
7	643	563	411	408	639	540	360	345
8	653	576	436	425	649	555	383	361
9	669	594	461	446	658	569	404	375
10	677	603	481	464	663	578	423	389

Gas phase :

$$k_{rf}\left(\frac{\partial^2 T}{\partial r^2}g + \frac{1}{r}\frac{\partial T}{\partial r}g\right) + k_{af}\frac{\partial^2 T}{\partial z^2}g - ah(T_g - T_s) = GCp\,\frac{\partial T}{\partial z}g$$

Solid phase :

$$k_{rs}\left(\frac{\partial^2 T}{\partial r^2}s + \frac{1}{r}\frac{\partial T}{\partial r}s\right) + k_{as}\frac{\partial^2 T}{\partial z^2}s + ah(T_g - T_s) = 0$$

Boundary conditions are:

(i) Symmetry:

$$r = 0 \qquad \frac{\partial T}{\partial r}g = 0$$

$$\frac{\partial T}{\partial r}s = 0$$

(ii) Heat loss to wall:

$$r = R \qquad -k_{rf}\frac{\partial T}{\partial r}g = h_{wf}(T_g - T_w)$$

$$-k_{rs}\frac{\partial T}{\partial r}s = h_{ws}(T_s - T_w)$$

(iii) Inlet conditions:

$$z = 0 \qquad -k_{af}\frac{\partial T}{\partial z}g = h_{if}(T_{in} - T_g)$$

$$-k_{as}\frac{\partial T}{\partial z}s = h_{is}(T_{in} - T_s)$$

(iv) Insulation at end of vessel:

$$z = L \qquad -k_{af}\frac{\partial T}{\partial z}g = 0$$

$$-k_{as}\frac{\partial T}{\partial z}s = 0$$

This set of equations is not easy to solve. Furthermore, it is not necessary because the experimental setup is not accurate enough that temperatures of both phases can be measured. Therefore, if the assumption of homogenity is made, we can write the energy balance as

$$k_r\left(\frac{\partial^2 T}{\partial r^2}g + \frac{1}{r}\frac{\partial T}{\partial r}g\right) + k_a\frac{\partial^2 T}{\partial z^2}g = GCp\,\frac{\partial T}{\partial z}g$$

with the boundary conditions:

$$r = 0 \qquad \frac{\partial T}{\partial r} = 0$$

$$r = R \quad -k_r \frac{\partial T}{\partial r} = h_{eff}(T - T_w)$$

$$z = 0 \quad -k_a \frac{\partial T}{\partial z} = h_i(T_{in} - T)$$

$$z = L \quad -k_a \frac{\partial T}{\partial z} = 0$$

One more simplifying assumption may be made — that of the absence of axial dispersion of heat. This is a valid assumption because the axial velocity of the gas is large, and it is expected that the convective flux term would outweigh to a large degree the axial dispersion term. The final form of the energy balance can now be written as:

$$k_r\left(\frac{\partial^2 T}{\partial r^2}g + \frac{1}{r}\frac{\partial T}{\partial r}g\right) = GCp\,\frac{\partial T}{\partial z}g$$

with the boundary conditions:

$$r = 0 \qquad \frac{\partial T}{\partial r} = 0$$

$$r = R \quad -k_r \frac{\partial T}{\partial r} = h_{eff}(T - T_w)$$

$$z = 0 \qquad T = T_{in}$$

This system of equations may be solved analytically. De Wasch and Froment (44) present the solution as :

$$\frac{T_w - T}{T_w - T_{in}} = 2\sum_{1}^{\infty} \frac{J_o(b_n r/R)e^{-ab_n^2 z}}{b_n J_1(b_n)[1 + (b_n/m)^2]}$$

where $a = k_r/GCR^2$, $m = h_{eff}R/k_r$

and b_n are the roots of

$$b_n = m[J_o(b_n)/J_1(b_n)]$$

This solution however, involves the inconvenience of evaluating b_n, and then summing an infinite series. An alternative method of solution is:

First, rewrite the equations in terms of the dimensionless variables

$$\rho = r/R,\ \xi = Z/L,\ \tau = (T-T_{in})/(T_w-T_{in})$$

as

$$\frac{\partial^2\tau}{\partial\rho^2} + \frac{1}{\rho}\frac{\partial\tau}{\partial\rho} = K_1\frac{\partial\tau}{\partial\xi} \tag{4.1}$$

with the boundary conditions

$$\rho = 0 \qquad \frac{\partial\tau}{\partial\rho} = 0$$

$$\rho = 1 \qquad \frac{\partial\tau}{\partial\rho} = K_2(1 - \tau)$$

$$z = 0 \qquad \tau = 0$$

Applying radial collocation to equation 4.1 we get:

$$\sum_{1}^{N+1} B_{ij}\tau_j + \frac{1}{\rho_i}\sum_{1}^{N+1} A_{ij}\tau_j = K_1\frac{d\tau}{d\xi}i \qquad i = 1,..,N$$

The first boundary condition is satisfied if we use symmetric polynomials of the type

$$\tau(\rho^2) = \tau(1) + (1 - \rho^2)\sum_{1}^{N} a_i P_{i-1}(\rho^2)$$

The second boundary condition yields:

$$\sum_{1}^{N+1} A_{N+1,j}\tau_j = K_2(1 - \tau_{N+1}) \tag{4.2}$$

$$\text{or,}\quad \tau_{N+1} = \frac{K_2 - \sum_{1}^{N} A_{N+1,j}\tau_j}{A_{N+1,N+1} + K_2}$$

The third boundary condition yields:

$$\text{at } \xi_i = 0,\quad \tau_i = 0 \tag{4.3}$$

Substitution of the second boundary condition into the collocated version of the energy balance gives:

$$\frac{d\underline{\tau}}{dz} = \underline{\underline{E}}\underline{\tau} + \underline{F} \tag{4.4}$$

where τ, $\underline{E}$ and $\underline{F}$ are defined by:

$$\underline{\tau} = [\tau_1, \tau_2, \tau_3 \ldots \tau_N]^T$$

$$E_{ij} = \frac{1}{K_1}\left[B_{ij} + \frac{1}{\rho_i} A_{ij} - D_i A_{N+1,j}\right] \qquad \begin{matrix} i = 1,\ldots,N \\ j = 1,\ldots,N \end{matrix}$$

$$F_i = \frac{K_2 D_i}{K_1} \qquad i = 1,\ldots,N$$

here D_i is given by

$$D_i = \frac{B_{i,N+1} + A_{i,N+1}/\rho_i}{A_{N+1,N+1} + K_2}$$

Equations 4.3 and 4.4 define an initial value problem whose solution may be written as:

$$\underline{\tau}(z) = \sum_{i}^{N} C_i \underline{G}_i e^{\lambda_i \xi} - \underline{\underline{E}}^{-1}\underline{F} \qquad (4.5)$$

here λ_i are the eigenvalues of $\underline{E}$

$\underline{G}_i$ are the corresponding eigenvectors

and C_i are given by

$$\underline{C} = \underline{\underline{G}}^{-1}(\underline{\underline{E}}^{-1}\underline{F})$$

Equation 4.5 is a simple explicit formula for the temperature at each radial collocation point as a function of ξ. Evaluation of all the coefficients, etc. need be done only once for each set of (h_{eff}, k_r, N). In our analysis, N was always chosen as 3.

This method of solution is also helpful because a non-uniform wall temperature may be easily accomodated if the wall temperature can be written as an explicit function of ξ. If we can write

$$\tau_w(\xi) = f_1 + f_2\xi + f_3\xi^2 + \ldots$$

then equation 4.2 becomes

$$\sum A_{N+1,j}\tau_j = K_2\left[f_1 + f_2\xi + f_3\xi^2 + \ldots - \tau_{N+1}\right]$$

Going through the same analysis as before, we find that the ODE to be solved is

$$\frac{d\underline{\tau}}{d\xi} = \underline{\underline{E}}\underline{\tau} + \underline{F}(\xi)$$

with $\underline{\tau}(0) = \underline{0}$

where $$F_i(\xi) = \frac{D_i K_2}{K_1} (f_1 + f_2\xi + f_3\xi^2 + \ldots)$$

Finding the homogeneous and particular solutions of the above finally yields (for the case when a linear wall temperature profile is assumed):

$$\tau(\xi) = \sum C_i \underline{G}_i \exp(\lambda_i \xi) - \underline{\underline{E}}^{-1} f_2 \xi - \underline{\underline{E}}^{-1}(\underline{\underline{E}}^{-1} f_2 + f_1)$$

where $$\underline{C} = \underline{\underline{G}}^{-1}\underline{\underline{E}}^{-1}(\underline{\underline{E}}^{-1} f_2 + f_1)$$

and $$K_1 f_1/K_2 = (f_1 D_1, f_1 D_2, f_1 D_3, \ldots)^T$$

$$K_1 f_2/K_2 = (f_2 D_1, f_2 D_2, f_2 D_3, \ldots)^T$$

Note that if we set $f_2 = 0$ and $f_1 = 1$ (i.e. constant wall temperature), the solution simplifies to the previous case.

A graphical technique was used in (37) to estimate the two parameters thom the experimental data. This technique involved the calculation of second derivatives from plots, which therefore made it very susceptible to human error. In this work, the method of De Wasch and Froment was followed, in which the sum of squares of residuals on the temperatures was minimized:

$$P = \sum_j (\tau_{exp,j} - \tau_{calc,j})^2$$

Here N is the number of radial collocation points (= 3 in this work) and NZ is the number of ξ-locations at which the temperature measurements were taken. Neither the steepest descent method nor the Fletcher-Powell method is very efficient in going to the minimum, primarily because the gradients have to be evaluated numerically. The method used was therefore the relaxation method.

The relaxation method does not involve gradients. One parameter is varied at a time, until a minimum value of P with respect to that parameter is reached. Starting from this minimum, the other parameter is varied, and so on until some suitable convergence criterion is met.

The experimental data of Table 4.1 was analyzed in this manner. The results are shown in Table 4.2. From these results we can see that as the flow rates increase, each of the two parameters increase in value. This trend has been experimentally observed by most workers. Due to the lack of sufficient data however, we are unable to present a correlation linking the gas mass flow rates with k_r and h_{eff}. The results presented here may not be very accurate because the data itself is not very accurate (for example, at low ξ, the innermost temperatures are inverted). Salam (45) discusses this subject in detail, and suggests improvements in the experimental procedure. Comparison of these results with the values used by Merrick or Yu show that the values predicted by the correlations of Merrick are more realistic.

4.4 SUGGESTIONS FOR FUTURE EXPERIMENTS

It should be noted that the experimental setup that was used to yield values for k_r and h_{eff} was not very accurate. Therefore, to get accurate parameter estimates — and there seems to be a great need for it — improvements have to be made in the experimental setup.

TABLE 4.2

Experimentally Determined Heat Transfer Parameters

	Case A	Case B
N_2 flow rate (Kgmol/hr)	0.0593	0.0823
k_r (kJ/m hr K)	2.263	2.495
h_{eff} (kJ/m^2 hr K)	235.6	274.9
P_{min}	0.0425	0.0846

The objectives of any future work should be:

(i) to evaluate k_r and h_{eff} accurately under a variety of experimental conditions. It is known that these values depend on bed to particle diameter ratio, bed porosity and uniformity of packing, velocity profile in the bed, absence (or presence) of reaction, gas mass flow rates, etc. All these variables have to be exhaustively investigated.

(ii) to evaluate the contribution of the static and dynamic portions of each parameter, since most correlations are presented in this form.

(iii)to evaluate the magnitude of effective axial conductivity and assess its importance in modeling of large scale gasifiers.

In order to accomplish the above objectives, and in order to make certain that the data base obtained is correct and useful, the parameters will have to be evaluated by several independent techniques such as from steady state and transient responses. Experiments with heat generation within the bed — by coupling a steel bar inserted in the bed with a Lepel high frequency generator — while cold gas is being fed in should alse be carried out. Provisions should be made to stop the flow and measure the transients : this should give information on the static terms which are the more important terms at low particle Reynolds numbers. Variations in static terms with coal/char type should be investigated.

Besides gas mass flow rates, other factors (eg. bed to particle diameter ratio, bed porosity and uniformity of packing, velocity profile in the bed, and absence or presence of reaction, etc.) also affect the values of the parameters of interest. Each of these aspects have to be investigated fully and exhaustive experiments carried out.

Axial conductivity measurements may be performed by measuring the axial temperature profile at steady gas flow from the bottom when the top of the bed is heated with a high intensity lamp. Using water-cooled lamps, temperatures of about 1300 Kelvin may be reached at the top of the bed, and the radial contribution to the effective axial conductivity may be examined. Velocity profiles of the exit gas may be measured, and the effect of this profile on the effective axial conductivity may be determined.

5. EXPERIMENTAL AND SIMULATION RESULTS

An experimental fixed bed gasifier was designed and built by Salam (45), and as yet, two runs have been carried out using Wyoming char. Simulation runs were also performed, with the conditions remaining the same as in the experimental runs. This chapter describes the experimental equipment, and the results (from both experiments and simulations).

5.1 EXPERIMENTAL APPROACH

This section briefly describes the process of char gasification as carried out in a bench scale fixed bed reactor which was designed and operated by Salam (45). The overall process is similar to commercial scale systems requiring similar unit operation processes. Descriptions of specific equipment can be found elsewhere (45). A summary of the process is given in Figure 5.1, and a process diagram in Figure 5.2.

The solid reactant in this process is devolatilized coal (char). The devolatilization process is carried out separately, and only char is loaded into the gasification unit. Standard analyses (proximate and ultimate) of the coal and the char can be performed, and samples are presented in Tables 5.1 and 5.2.

Three reactant gases are required as feed gas to the char gasifier. The proper preparation of this feed is essential to the process, and is also necessary if the data being measured is to have any meaning. Steam, air and/or nitrogen must be delivered accurately. A known flow rate of water is delivered to a steam generator where it is converted to steam. This steam is next mixed with known flowrates of air and/or nitrogen. This combined stream is then mixed and further heated in a

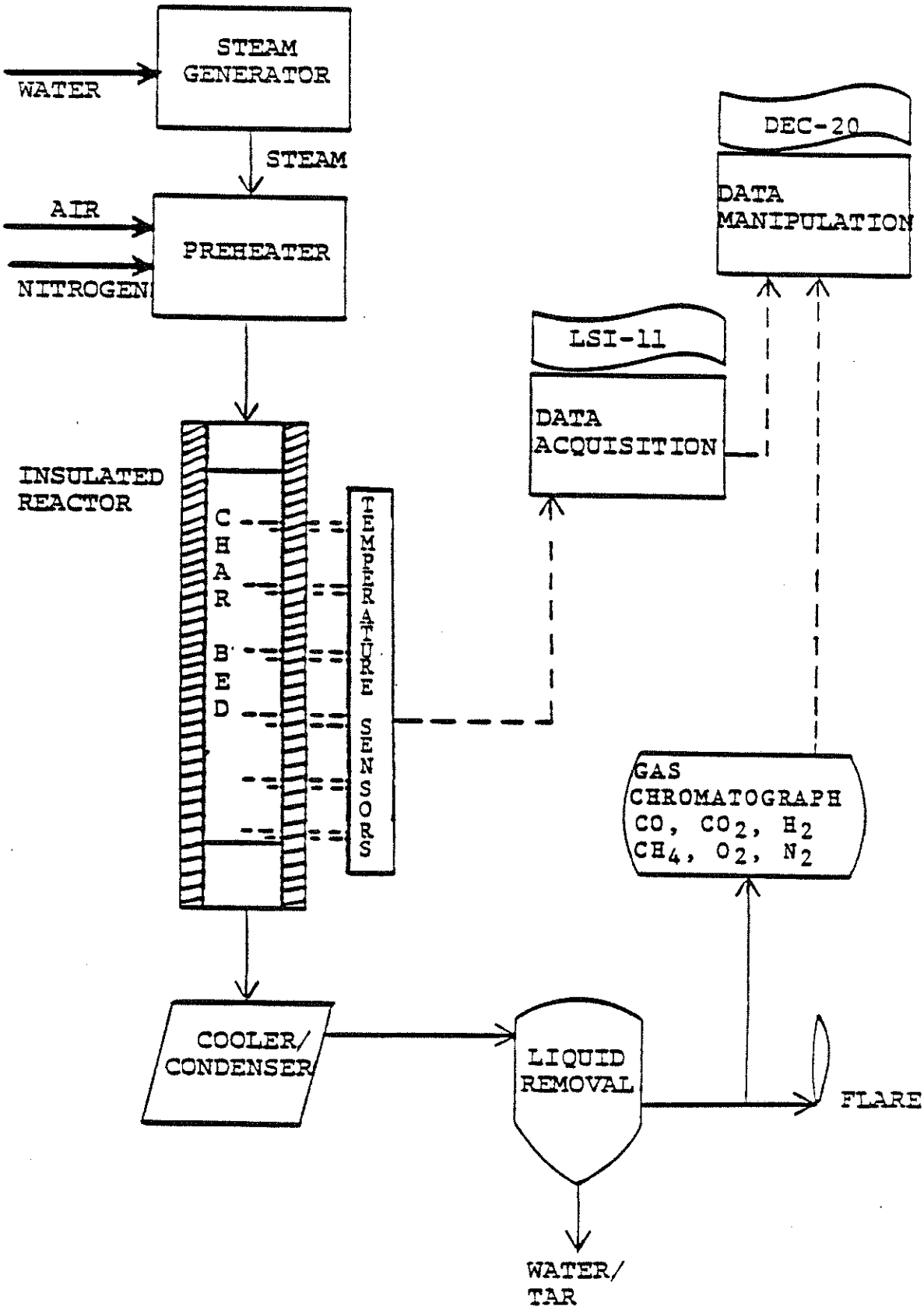

Figure 5.1 Process description (Ref (45)).

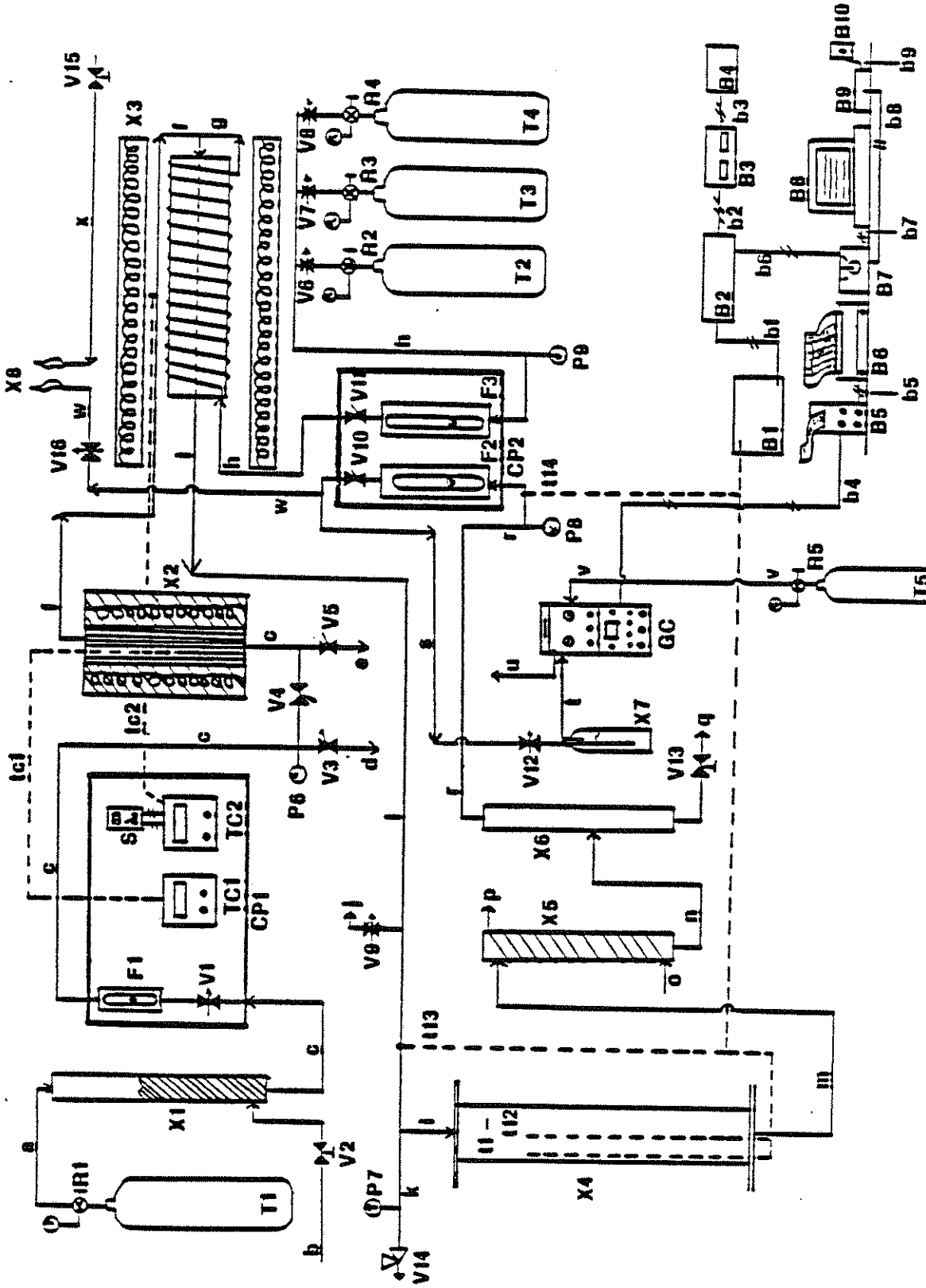

Figure 5.2 Process flow design (Ref (45)).

Legend for Figure 5.2

R1, R4 - Meco Type or Dubbl-Stage Nitrogen Regulators (with pressure gauges P1, P4)
R2, R3 - Meco Type A-8 Dubbl-Stage Air Regulators (with pressure gauges P2, P3)
R5 - Meco Type or Dubbl-Stage Helium Regulator (with pressure gauge P5)

T1, T4 - AGC size 200 compressed nitrogen cylinders
T2, T3 - AGC size 200 compressed breathing air cylinders
T5 - AGC size 300 compressed helium cylinder

V1 - Valve to control water flow from reservoir
V2 - Valve to control charging rate of reservoir
V3 - Valve to calibrate flowmeter F1
V4 - Valve to interupt water delivery to evaporator
V5 - Valve to drain evaporator
V6, V7, V8 - Valves to control gas delivery from tanks T2, T3, T4
V9 - Valve to draw gas sample of feed
V10 - Valve to pressure check system
V11 - Valve to interupt feed gas flow from T2, T3, T4
V12 - Valve to control product gas sampling flow
V13 - Valve to drain condenser
V14 - Kunkle model 264 steel relief valve with 100 psig set point
V15 - Valve to control natural gas delivery to Bunsen burner
V16 - Valve to control system back pressure

P6 - Water pressure delivery gauge (0-60 psig)
P7 - Reactor inlet gas pressure (0-60 psig)
P8 - Product gas pressure gauge (0-16 psig)
P9 - Feed gas delivery pressure (0-30 psig)

F1 - Brooks Sho-Rate (2-1355-V w/R-2-15 AA and s.s. float) flowmeter for water flowrates 0-4.96 cm^3/sec
F2 - Brooks (1110-05R2G1A w/R-6M-25-2 and s.s. RV float) flowmeter for product gas flowrates 0-3.47 m^3/hr (3.22 scfm)
F3 - Brooks (1110-05R2g1A w/R-6M-25-2 and s.s. spool float) flowmeter for feed gas flowrates 0-3.77 m^3/hr (2.22 scfm)

TC1 - Gardsmann (JF, chromel/alumel) automatic time proportioning temperature (0-600°C) controller for evaporator
TC2 - Gardsmann (JF, chromel/alumel) automatic time proportioning temperature (0-800°C) controller for preheater (or devolatilizer)
S - On/off switch for TC2 and outlet controlled by TC2

CP1 - Control panel #1
CP2 - Control panel #2

T1 - T12 - Chromel/alumel thermocouples located in gasifier
T13 - Feed gas chromel/alumel thermocouple, 1/16" diameter (1.59 mm)
T14 - Cooled product gas chromel/alumel thermocouple, 1/16" diameter
Tc1 - Evaporator thermocouple for TC1, 1/16" diameter
Tc2 - Preheater thermocouple for TC2, 1/16" diameter

X1 - 2-1/2" x 60" (6.35 x 152.4 cm) copper pipe water reservoir
X2 - Evaporator
X3 - Preheater
X4 - Gasifier
X5 - Condenser
X6 - 2-1/2" x 30" (6.35 x 76.2 cm) copper pipe separation vessel
X7 - 250 cc glass gas washing bottle (with water)
X8 - Bunsen burners

GC - Gow Mac series 500 gas chromatograph with gas sampling valve

a - 1/4" (6.35 mm) copper tubing - N_2 for pressuring water reservoir
b - 1/4" copper tubing - tap water for charging reservoir
c - 1/4" copper tubing - water deliver to evaporator
d - 1/4" Tygon tubing - calibration drain
e - 1/4" copper tubing - evaporator drain
f - 1/4" stainless steel (s.s.) tubing, insulated - carried steam from evaporator to preheater
g - hot air/N_2 line inside preheater
h - 3/8" (9.53 mm) copper tubing - N_2/air feed line
i - 3/8" s.s. tubing, insulated - hot mixed feed gas
j - 1/8" (3.18 mm) s.s. tubing, insulated - hot gas sampling line
k - 3/8" s.s. tubing, uninsulated - cold line for pressure gauge and safety valve
l - 3/8" s.s. tubing, insulated - reactor inlet line
m - 3/8" copper tubing - hot product gas line
n - 3/8" copper tubing - condensed product gas line
o - 1/4" copper tubing - condenser cooling water - in
p - 1/4" copper tubing - condenser cooling water - out
q - 3/8" copper tubing - condensate drain
r - 3/8" copper tubing - dry product gas line
s - 1/4" Tygon tubing - product gas sampling line to wash bottle
t - 1/4" Tygon tubing - washing product gas line to GC
u - 1/8" copper tubing - purged sample gas line
v - 1/8" copper tubing - Helium carrier gas line
w - 3/8" copper tubing - product gas line to Bunsen burner
x - 3/8" Tygon tubing - natural gas line to Bunsen burner

B1 - Terminal board - thermocouple extension wire to ribbon cable
B2 - LSI-11 microprocessor
B3 - Tape drives - #0) Programs #1) Data storage
B4 - 12 volt tape drive power supply
B5 - Infotronics (CRS-309) integrator
B6 - Omni-Scribe (B-5000) strip chart recorder
B7 - Switching box to set LSI-11 baud rate and configure computer lines
B8 - CRT (9600 baud) or line printer (300 baud)
B9 - Racal-Vadic (VA 3450) modem for 1200 baud data file transfer to DEC-20
B10 - Telephone jack

b1 - Thermocouple output voltages (ribbon cable)
b2 - Data to tape storage
b3 - Power line to tape drive
b4 - Gas chromatograph output
b5 - Integrator monitored, chart input
b6 - LSI-11 to switching box
b7 - Switching box to output device
b8 - Switching box to modem
b9 - Modem to DEC-20 via telephone line

TABLE 5.1

Coal Analysis

Proximate Analysis:	
As Received	
Moisture	31.87
Volatile Matter	32.46
Fixed Carbon	30.16
Ash	5.51
Heating Value (Btu/lb)	7978
Ultimate Analysis:	
Moisture-free	
Ash	8.09
Moisture- and Ash-free	
Hydrogen	5.75
Carbon	74.05
Nitrogen	1.39
Sulfur	0.53
Oxygen (by diff.)	18.28
Heating Value MAF (Btu/lb)	12,742
H/C Ratio	0.93
Ash Analysis - Wt % of Ash	
SiO_2	33.85
Al_2O_3	16.66
Fe_2O_3	5.07
TiO_2	1.03
P_2O_5	1.44
CaO	22.46
MgO	6.52
Na_2O	1.75
K_2O	0.31
SO_3	10.86

TABLE 5.2

Analyses of Produced Char

Ultimate Analysis	
% Moisture	1.15
% Carbon	81.76
% Hydrogen	1.46
% Nitrogen	0.97
% Chlorine	< 0.01
% Sulfur	0.53
% Ash	11.55
% Oxygen (by diff.)	2.58

Proximate Analysis	
% Moisture	1.15
% Ash	11.55
% Volatile Matter	8.71
% Fixed Carbon	78.59

preheater. All necessary pressures and temperatures are recorded in the preparation steps. The feed gas to the gasifier, therefore, consists of a known mixture of oxygen, steam and nitrogen at a known temperature and pressure.

The gasification vessel was carefully designed so that it could withstand the extremely high temperatures (as high as 1500-1650 Kelvin) that normally occur in coal gasification. Figure 5.3 shows the final design of the gasifier. The reactor is designed to operate as near to adiabatic conditions as possible. To minimize heat losses through the walls, a refractory lining is used. Heat losses through the ends of the vessel are limited by a layer of ceramic beads. At the top end, the beads are put in a basket which is suspended from the top. Temperature profiles in the bed are measured via thermocouples located in two thermowells in the bed (marked AA in the figure). These are the only data readings that are taken from the gasifier.

The gases produced in the gasifier must be properly treated after they exit the vessel. Several operations are done. The first of these is the cooling of the gas. This also condenses any tars, oils and water. This cold stream then flows to a separator where the liquids are removed. The saturated gas exiting the separation process is split into two parts. One part flows to a flare where it is combusted and vented. The second and smaller part is sent to a gas chromatograph where the composition of the product gas is determined.

Several major pieces of peripheral equipment are required for data acquisition. The first of these,a gas chromatograph, has already been mentioned. It is capable of accurately determining the amounts of CO,

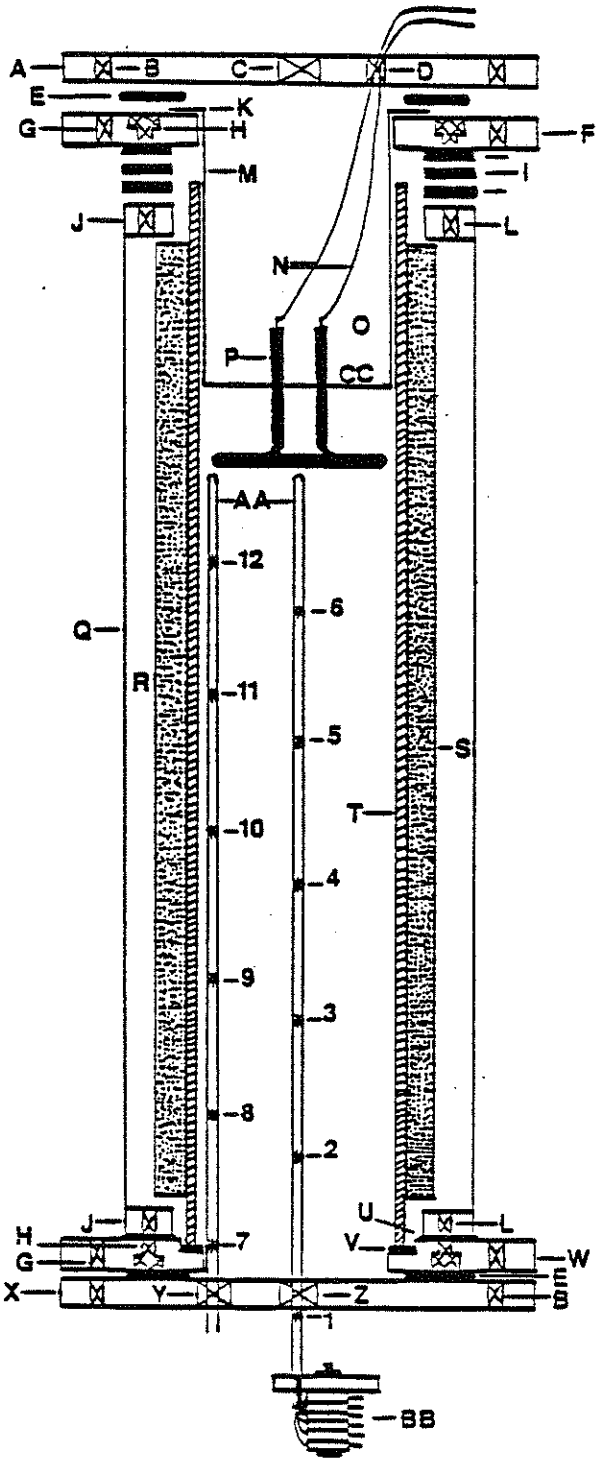

Figure 5.3 The gasifier (Ref (45)).

Legend for Figure 5.3

A - 1 cm thick x 19 cm diameter 304 stainless steel top cover
B - 6 - bolt holes
C - 1/4" FPT for stainless steel inlet fitting (centered)
D - 1/4" FPT for stainless steel ignition lead fitting (2 cm from center)
E - 1/8" (0.3175 cm) compressed asbestos (casp) gasket seals basket flange bolt holes H and cover
F - 19 O.D. x 7.75 cm I.D. steel top flange 1 cm thick
G - 6 - 1/4"-20 threaded bolt holes
H - 6 - recessed bolt holes
I - 3 - 1/8" casp gasket seals and shims top flange
J - 14.9 O.D. x 11.6 cm I.D. steel retaining flanges (1 cm thick) welded inside each end of steel shell
K - 10.8 O.D. x 7.6 cm I.D. stainless steel basket flange (0.0051 cm thick) welded to basket
L - 6 - 1/4"-20 threaded bolt holes
M - 12.7 x 10 cm stainless steel sheet (0.0051 cm thick) rolled and welded to form a 7.6 cm diameter tube for basket wall
N - Asbestos braided copper ignition leads
O - 1/2" (1.27 cm) Diamonite (95% alumina grinding media) ceramic beads
P - 1/4" x 12" (0.635 x 30.4 cm) Incoloy sheathed tubular heater bent to form 5.7 cm loop with 7 cm perpendicular legs
Q - 6" O.D. x 47.7" (15.24 x 121.2 cm) steel pipe for outside wall (0.1651 cm wall)
R - 1" x 24" x 48" (2.54 x 60.96 x 121.92 cm) Kaowool 2600 refractory blanket wraps liner twice
S - Preformed refractory sleeves (Kaowool 2600), split and slid over liner. Refractory cement fills resulting gap
T - 3-3/4" O.D. x 48" (9.525 x 121.92 cm) 304 stainless steel liner (0.3048 cm wall)
U - 1/8" casp gasket seals bottom flange
V - 1/8" casp gasket seals liner bottom
W - Bottom flange same as F with 9.75 cm shoulder 7 mm deep
X - Same as A for bottom cover
Y - 1/8" FPT for stainless steel thermowell fitting
Z - 1/4" FPT for stainless steel exit and thermowell tee fitting

AA - 3/16" O.D. (0.4762 cm) Inconel thermowells 117 and 122 cm
BB - Aluminum thermocouple plug mounting block with set screw
CC - Perforated stainless steel basket bottom (4 x 7/32" holes/inch)

Thermocouple Locations From Top of Well (Bed)

1.	113.0 cm	7.	105.1 cm
2.	91.8 cm	8.	85.7 cm
3.	71.1 cm	9.	65.7 cm
4.	51.1 cm	10.	44.4 cm
5.	29.8 cm	11.	24.3 cm
6.	11.0 cm	12.	4.8 cm

Note all thermocouples are 0.02" (0.0508 cm) diameter Inconel sheathed chromel/alumel rated at 1150°C.

CO_2, CH_4, N_2 and O_2 that are present in the gas stream. It is used in analyzing the prepared feed gas as well as the product gas. The second peripheral device is a microprocessor (LSI-11). This unit is capable of recording the temperature probe readings at a rate as fast as 17 readings per 3 seconds. These values are displayed on a CRT (or a lineprinter), and are also stored. This stored data is finally transferred via a modem to a larger computer (DEC-20), where further analysis is done.

5.2 EXPERIMENTAL RESULTS

Two complete runs were made using char in the gasifier. Several instrumentation problems were present during the first run. These problems prevented accurate measurements of the gas flow rates in and out of the gasifier. The second run performed on July 24, 1983 was more successful and is discussed here. The results of the first run can be found elsewhere (45).

Table 5.3 gives the operating conditions of the gasification run. The initial set of operating conditions for the run resulted in dangerously high temperatures, and were altered to lower the peak temperatures. The temperature profiles are plotted as a function of time in Figures 5.4 and 5.5. The thermocouple numbers refer to different axial locations in the bed : specific locations can be found in the legend for Figure 5.3. The gap in the data at 6 hours was a result of stopping the normal LSI-11 operation to save the data file (This is not a normal procedure : it was feared that an electrical storm passing the University might cause a power outage and loss of the data). Figure 5.6 shows the product gas composition as a function of time. Not shown in the figure is the trace amounts (about 0.07%) of methane produced.

TABLE 5.3

Summary of Operating Conditions

For Gasification Run 072483

Char Loaded	3645.7 gms devolatilized Wyodac char (2 mm average diameter)		
Char Composition	83.56 % Carbon 11.97 % Ash 2.33 % Oxygen 1.02 % Hydrogen 0.62 % Nitrogen 0.50 % Sulfur		
Time 0-45 min.			
INLET	Air Flowrate	1.478	m^3/hr^*
	Water Flowrate	3.48	gm/min
	O_2/H_2O	2.12	gm/gm
OUTLET	Product Gas Flowrate	2.055	m^3/hr^*
	Total Condensate	0	gm
Time 45-580min.			
INLET	Air Flowrate	1.206	m^3/hr^*
	Water Flowrate	3.48	gm/min
	O_2/H_2O	1.73	gm/gm
OUTLET	Product Gas Flowrate	2.022	m^3/hr^*
	Total Condensate	382.2	gms
Unreacted Char	697.8 gms		
Reactor Pressure	0.191 MPa		
Original Bed Length	85.7 cm		
Final Bed Length	12.0 cm		

* at 25 deg. C, 0.1013 MPa

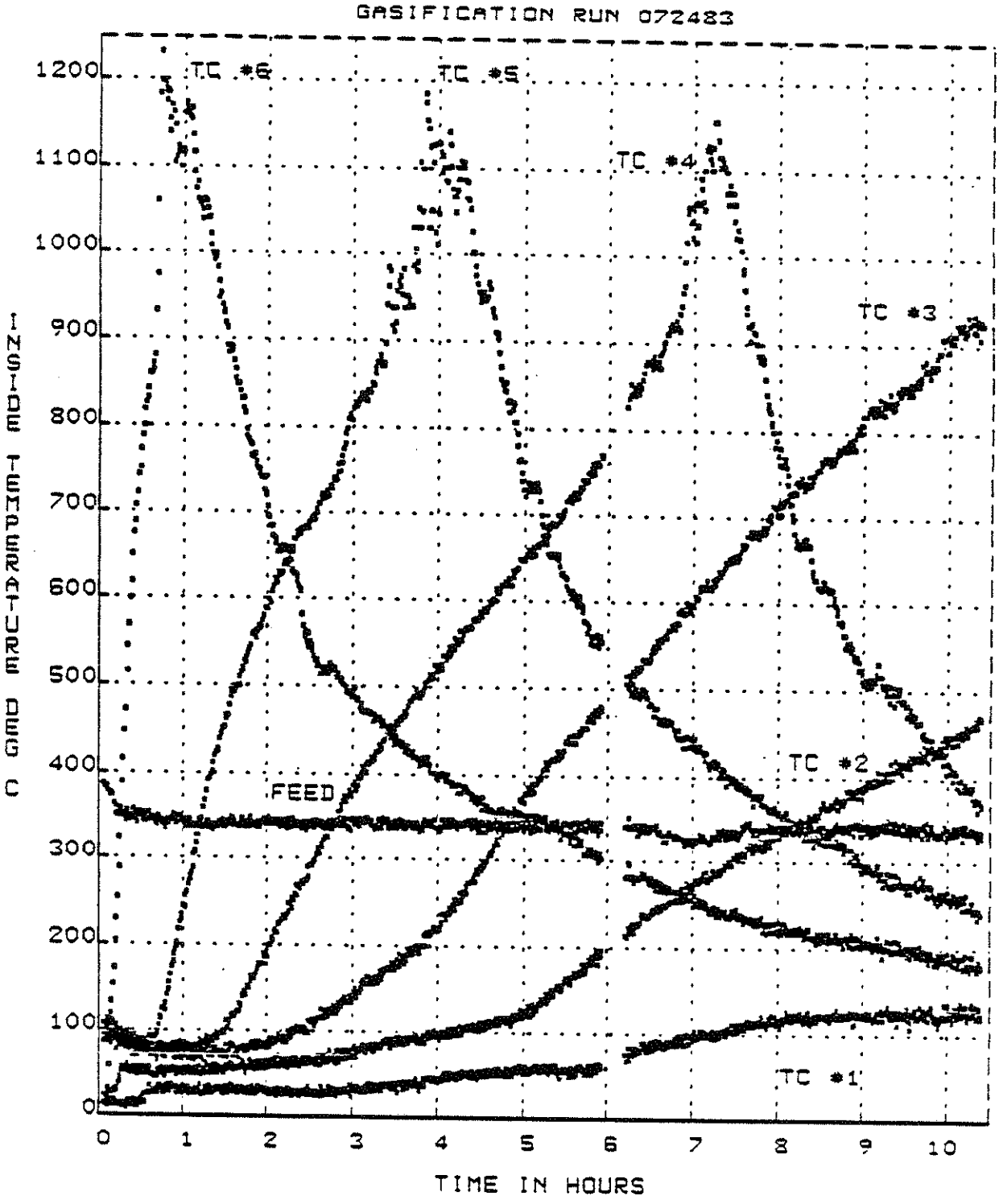

Figure 5.4 Gasification temperature profiles (TC#1 - TC#6)

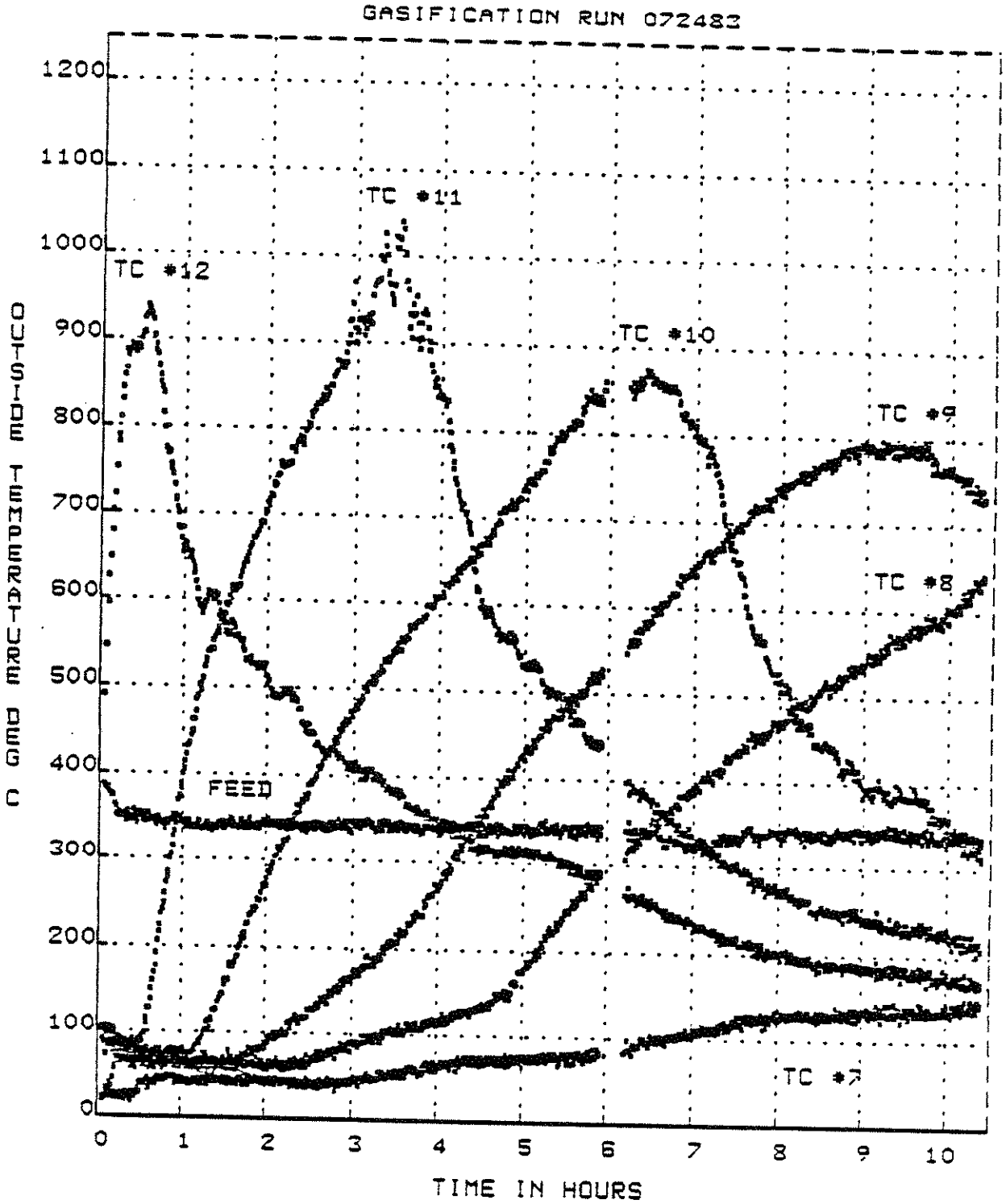

Figure 5.5 Gasification temperature profiles (TC#7 - TC#12)

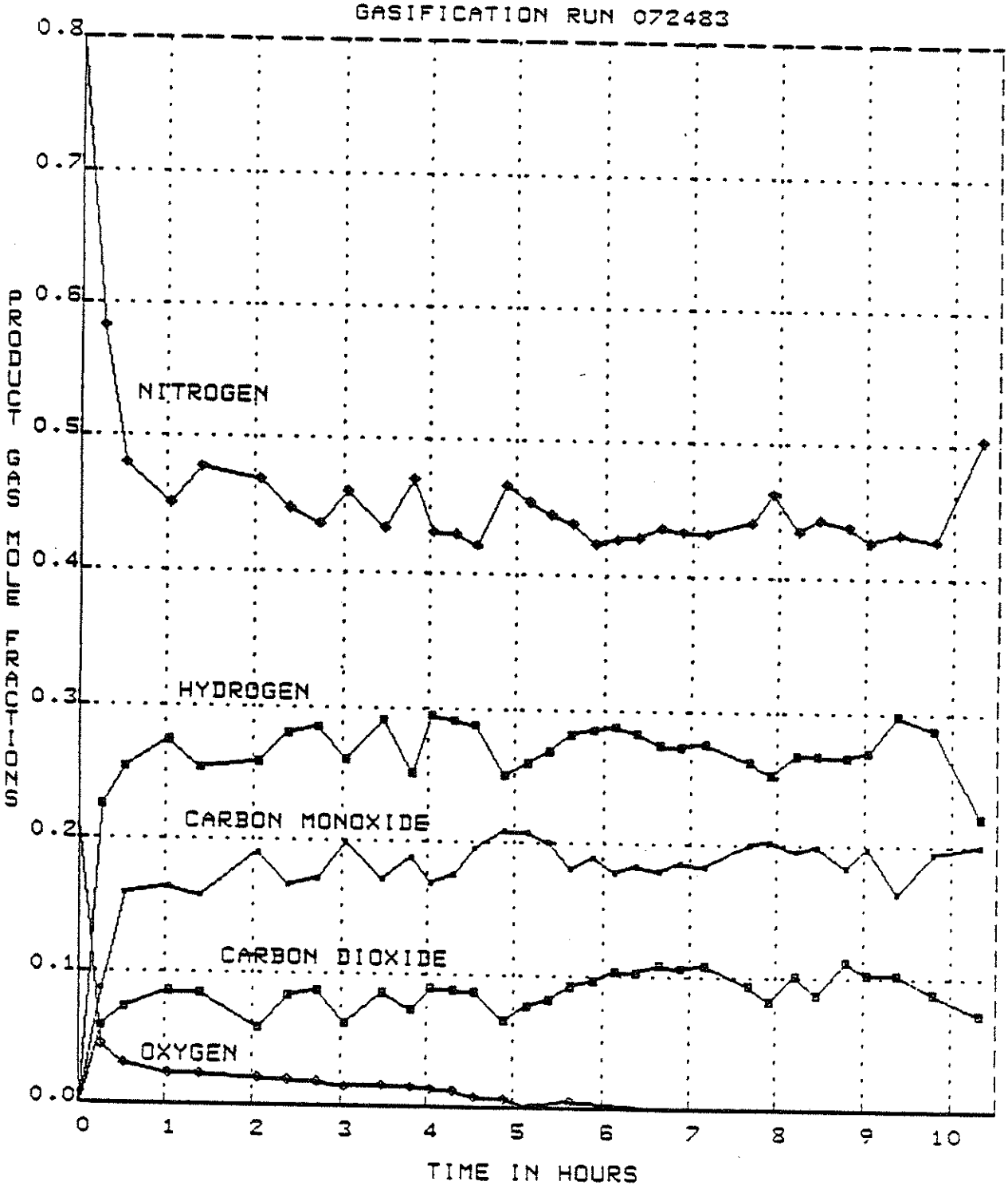

Figure 5.6 Product gas composition (H_2O - free)

Several points should be noted before an analysis of the data is done. While Figures 5.4 and 5.5 indicate a feed temperature of 350 deg. C, this is in fact the temperature of the feed as it exits the preheater. The actual inlet temperature would be much less. Thermocouple #12 (Figure 5.5) indicates that the maximum value for this temperature would be 180 deg. C. Since the other temperature readings seem to start at around 70 deg. C, it would seem that the temperature of the inlet gas as it hits the char bed is somewhere in between the two numbers.

It is also important to note that after a peak has been reached, the bed above this point collapses due to the reduction in volume when char is converted to ash (note the low ash content of the char, Table 5.2). Therefore the decreasing portions of the profiles indicate the cooling of the thermowells and the wall, and not the cooling of ash. Lastly, there are some minor fluctuations in the temperature profiles. These are felt to be caused by minor fluctuations in the water flow rate.

The product gas compositions shown in Figure 5.6 remain relatively constant during the majority of the run. Two compositions which differ from typical values are those of hydrogen and oxygen. Hydrogen percentages are almost double the typical values (which are about 15%) : these errors are caused by the gas chromatograph's poor sensitivity to hydrogen peaks. The appearance of oxygen in the exit stream was thought to be caused by bypassing of the bed (45).

5.3 SIMULATION STUDY AND RESULTS

A simulation run was performed under the operating conditions specified in Table 5.3, and this section will present the results of that study. The two parameters k_r and h_{eff} used had values of 2.4 kJ/m

hr K and 250 kJ/m^2 hr K, and N (the number of collocation points) was chosen as 2.

Figures 5.7 through 5.9 show temperature profiles at each of the collocation points and the wall at five different times (after 2,4,6,8 and 10 hours of operation), for the case when constant bed length is assumed (L=0.86 m). Each of the profiles remain the same over time (more or less), with the only difference being in the axial location at which the peaks occur. Comparison of the three profiles at a particular time (Figure 5.10) yield some interesting observations. Until Z/L = 0.09, the inlet gases cool down, since there is no reaction occurring inside the reactor, and since the wall itself is colder until that point. After that, until Z/L = 0.33, the wall (which is now hotter) heats up the gases. In this region, the temperature at the outer collocation point is higher than the temperature at the inner collocation point. There is no heat generation as yet inside the reactor, because all the char is still totally converted. At around Z/L = 0.33, the temperature at the inner collocation point reaches a high enough value (around 650 Kelvin) that the oxidation reaction becomes appreciable, and substantial heat generation occurs. Consequently, that temperature profile shoots upwards, overtaking the wall at around Z/L = 0.35. Some of the heat generated here as well as heat from the wall serves to raise the inside temperature to over 650 Kelvin, and consequently the inside temperature also shoots up and comes to a maximum — though after the outside has already reached its maximum. Note that the magnitudes of the maximum temperatures are different.

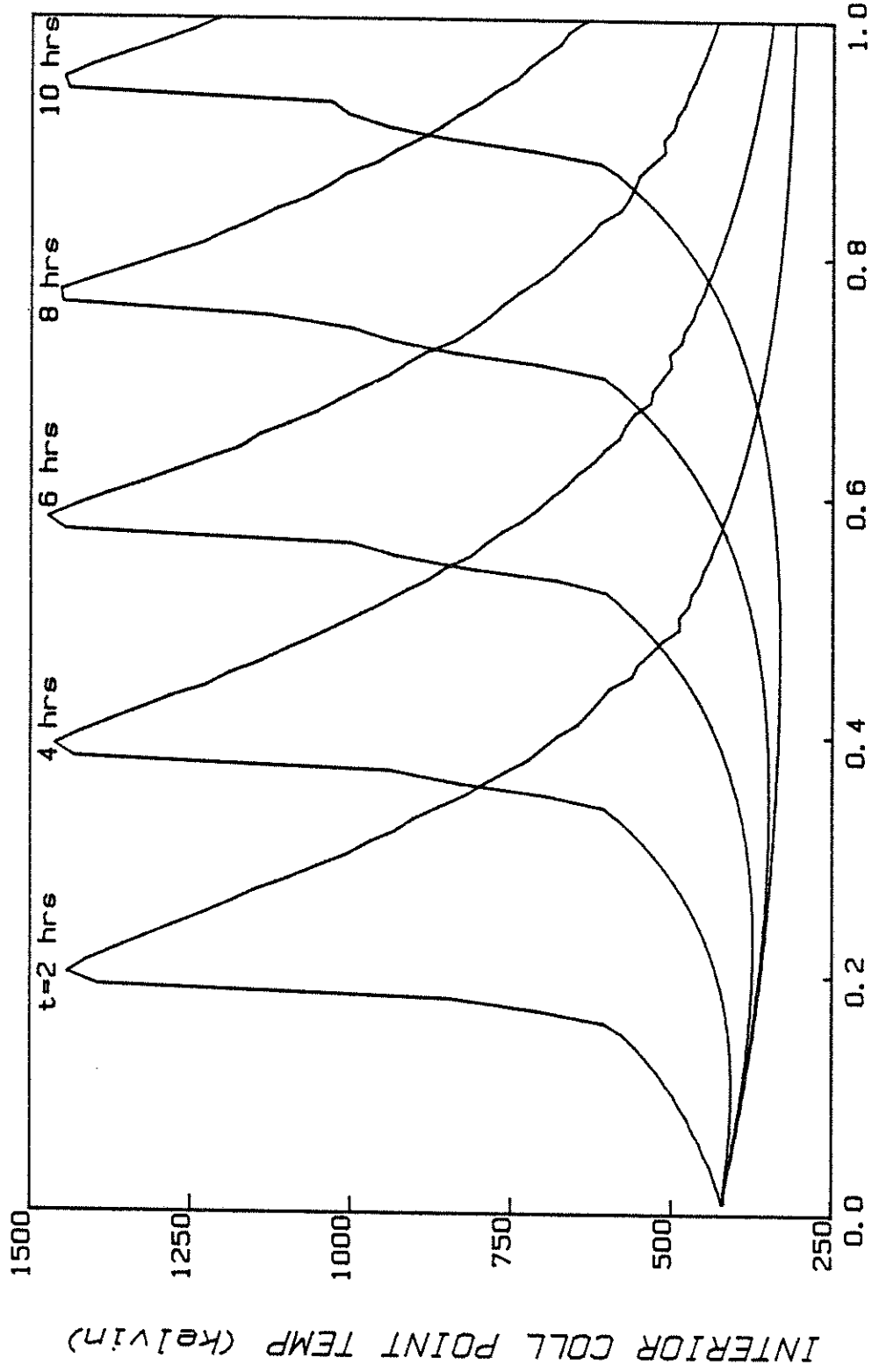

Figure 5.7 Axial temperature profiles at various times at the inner collocation point (r/R = 0.3938)

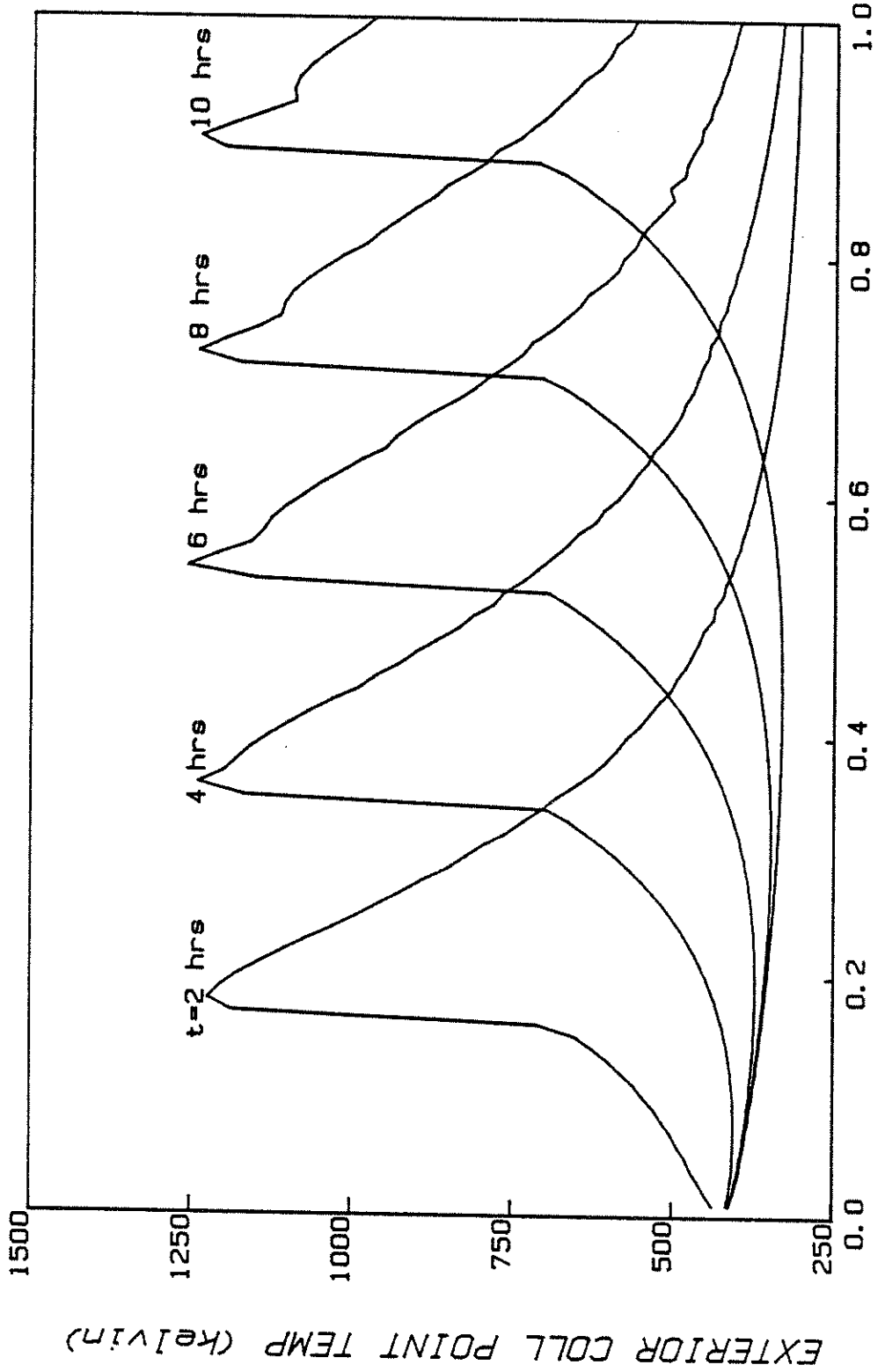

Figure 5.8 Axial temperature profiles at various times at the outer collocation point (r/R = 0.8031)

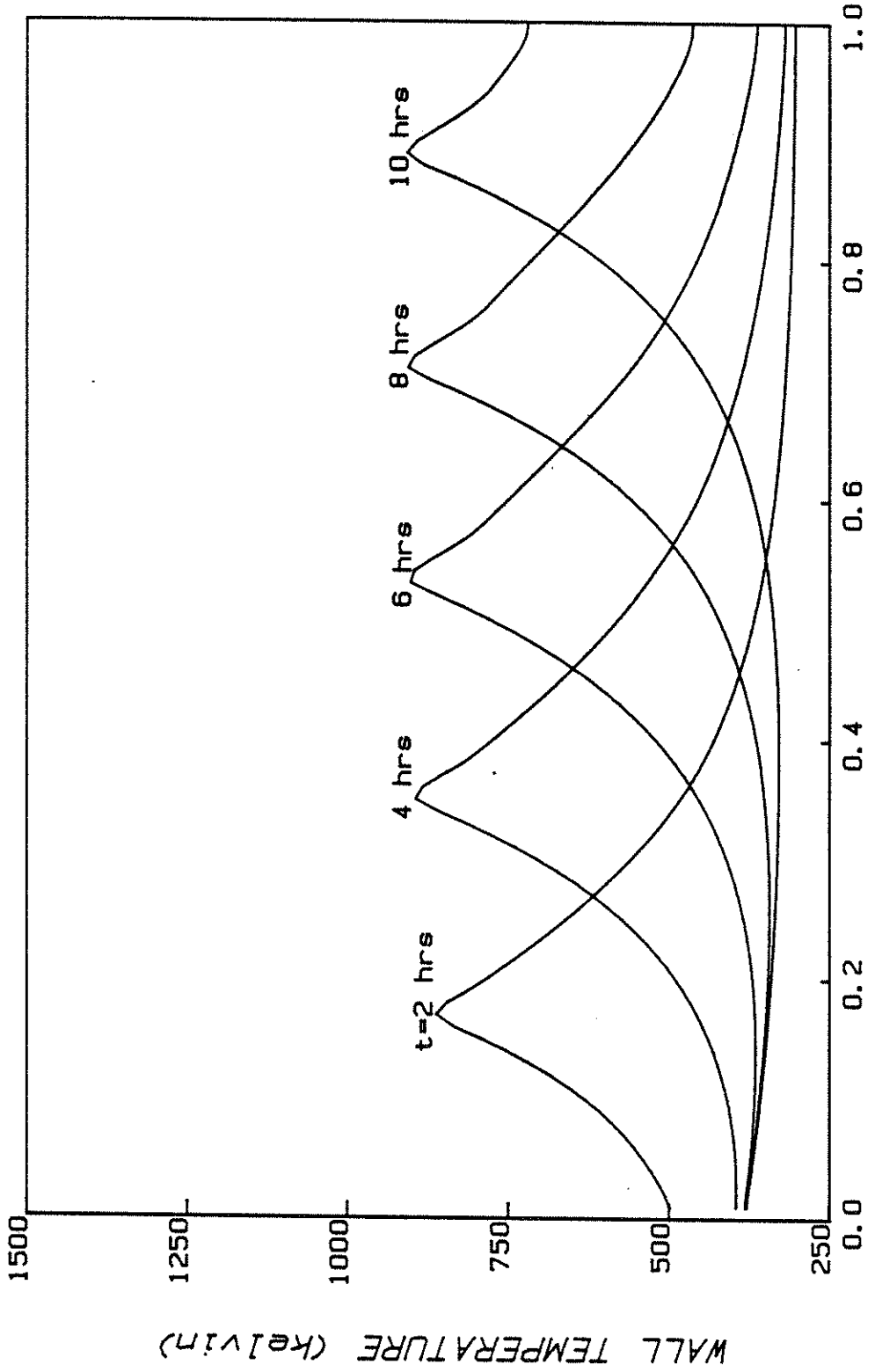

Figure 5.9 Temperature profiles at various times at the wall

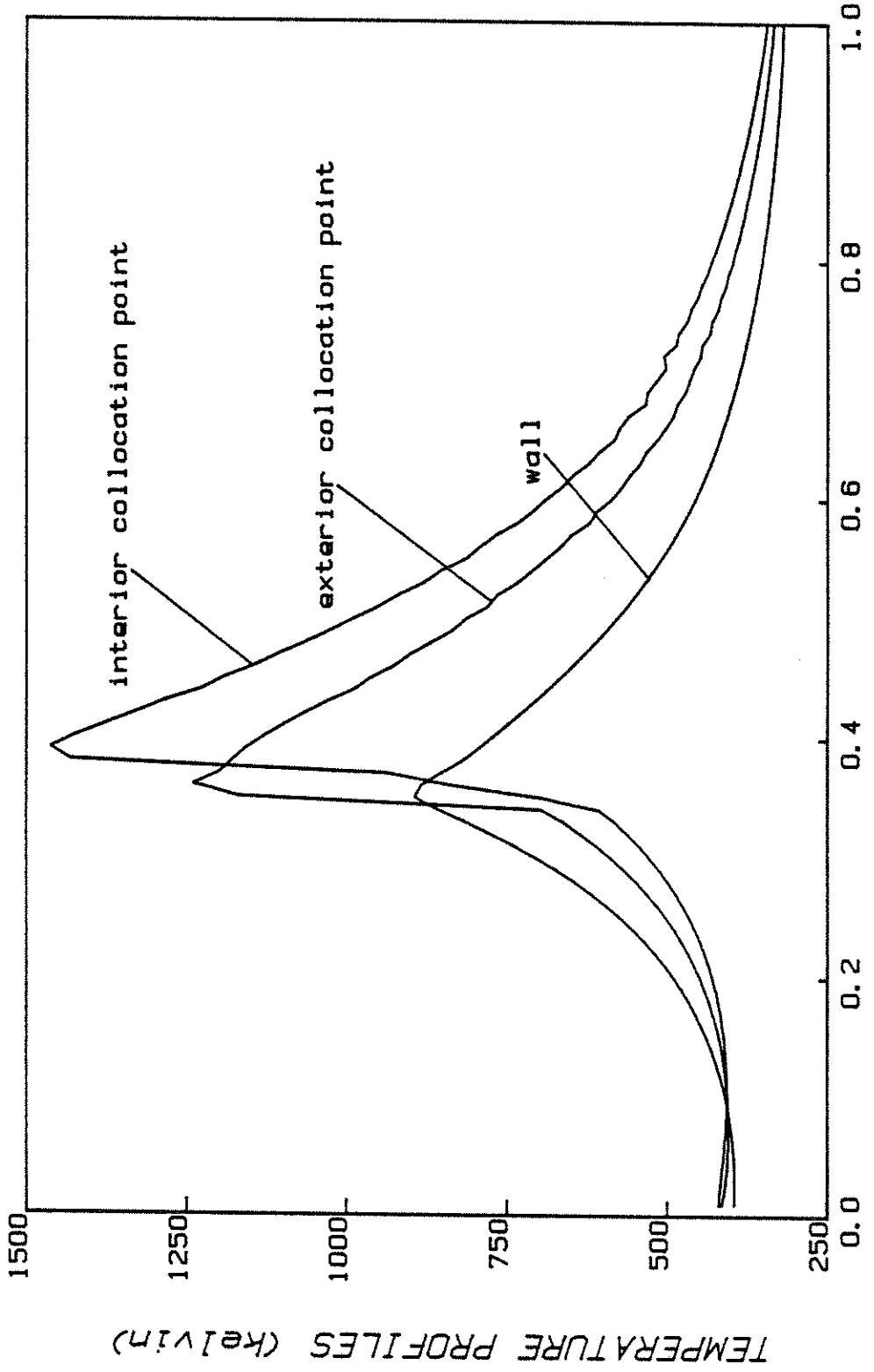

Figure 5.10 Axial temperature profiles at t = 4 hours

Figures 5.11 through 5.16 show the profiles at each collocation point of char conversion, and the various gas flux profiles. Methane flux profiles have been neglected because there is negligible yield. The char conversion profiles (Figure 5.11) shows that in the reaction zone, conversion decreases as we proceed outwards in the reactor. Moreover, the maximum temperature reached at each collocation point has a bearing on the maximum conversion possible — in Figure 5.11b, we can see that the profiles level off before total conversion. In other simulations (where the maximum temperature reached was not as high), conversion limits between 0.9 and 1.0 have been observed. Therefore, as one proceeds outwards in the reactor, the final conversion also decreases, leaving unconverted char near the wall.

The gas flux profiles are as one would expect. Near the wall, there is less steam and oxygen conversion, more carbon dioxide production, and less hydrogen and carbon monoxide production. This is mainly because temperatures are lower near the wall. The heat transferred to the wall has a large negative effect on the gasifier performance.

Comparisons between experimental data and simulation results are shown in Figures 5.17 through 5.20, and Table 5.4. Figures 5.17 and 5.18 plot the temperature profiles after one hour of operation. As we can see, the agreement is quite good. Figures 5.19 and 5.20 attempt to compare the simulation results on the same scale in which the data was taken. The agreement here was not very good, with degradation in the agreement progressively increasing as time increases. There are many reasons for this, some of which are modelling errors, and some experimental errors.

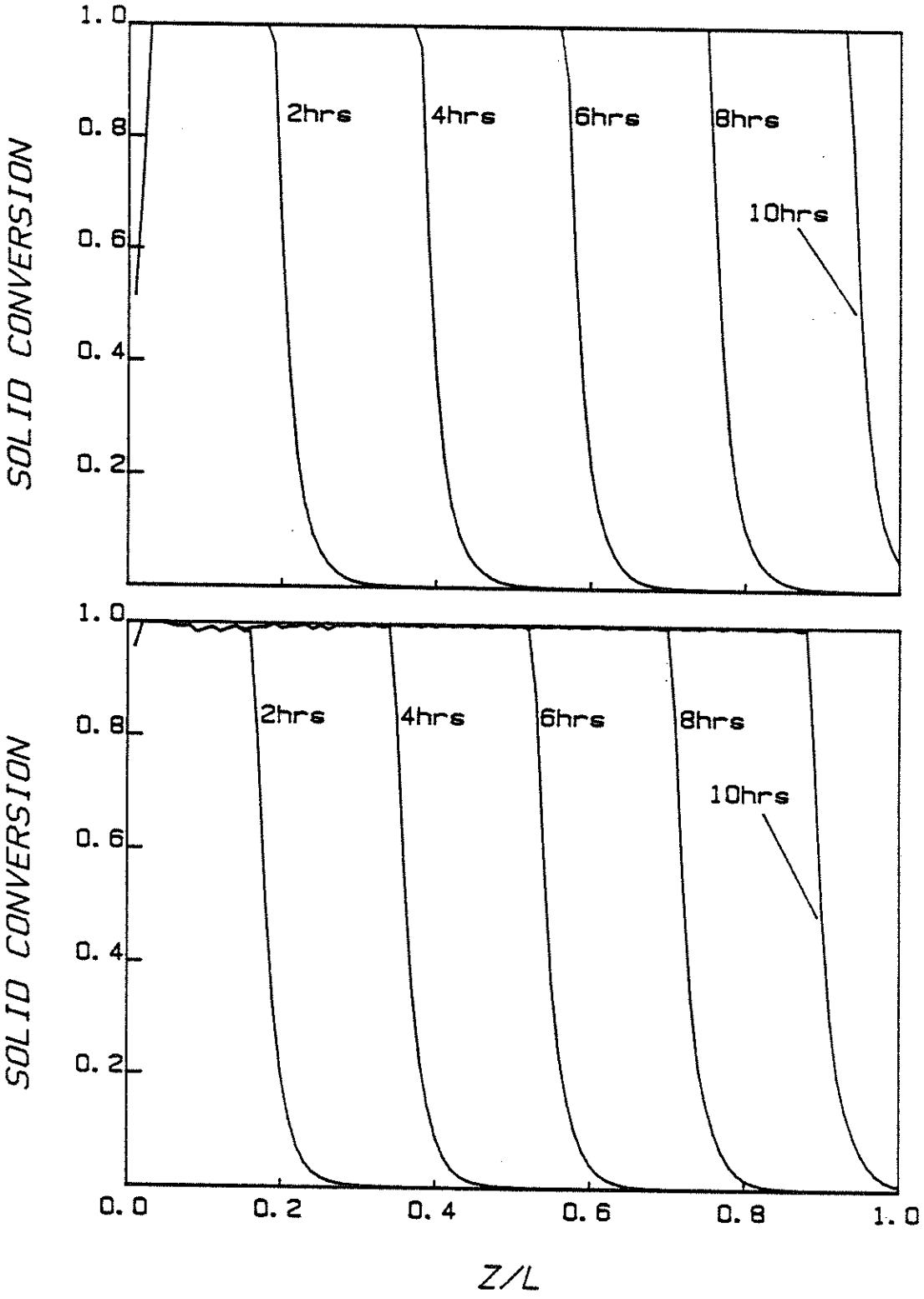

Figure 5.11 Axial profiles of solid conversion at various times (a) inner collocation point (b) outer collocation point

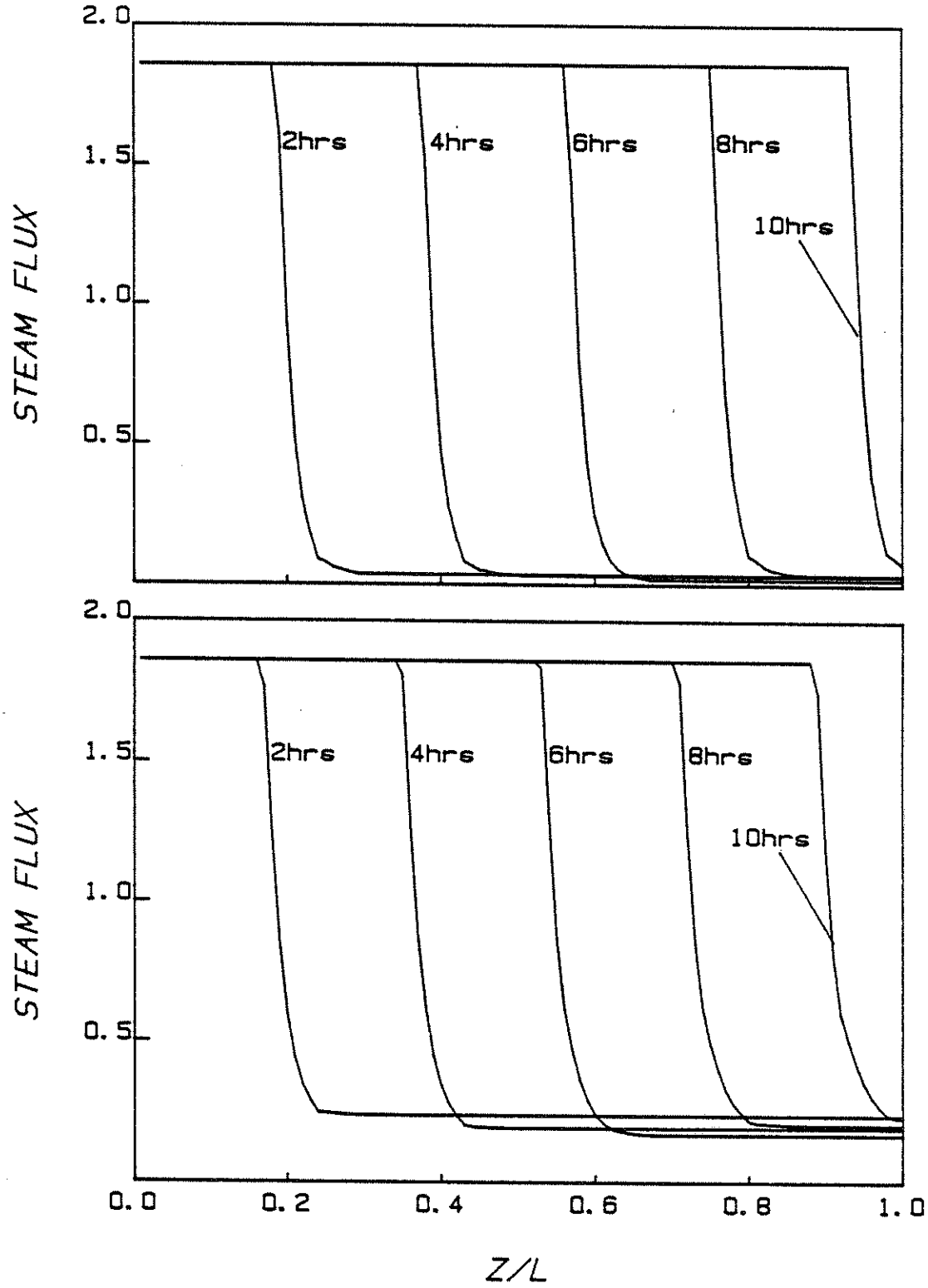

Figure 5.12 Axial steam flux (kgmol/m^2 hr) profiles at various times (a) inner collocation point (b) outer collocation point

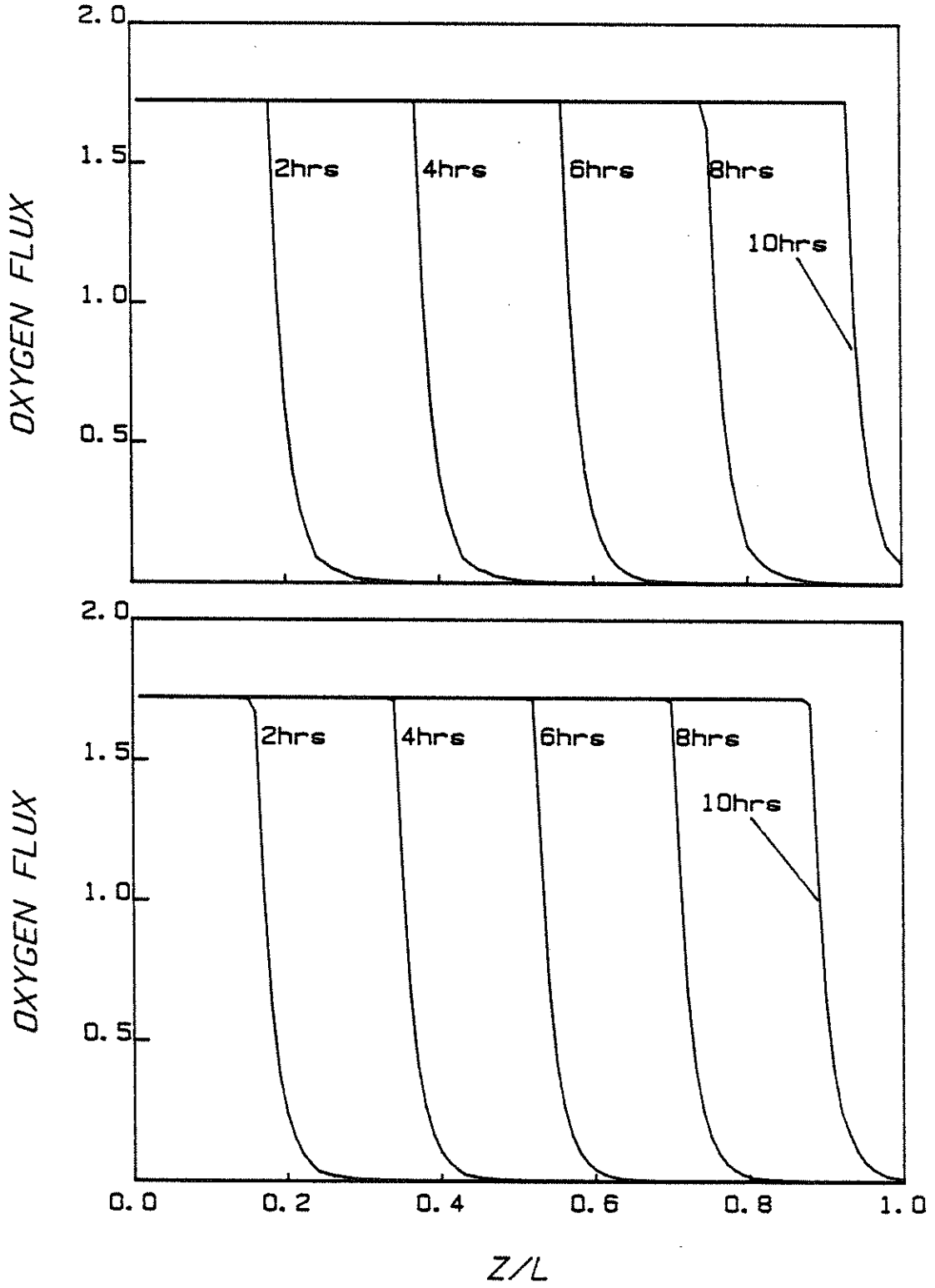

Figure 5.13 Axial oxygen flux (kgmol/m^2 hr) profiles at various times (a) inner collocation point (b) outer collocation point

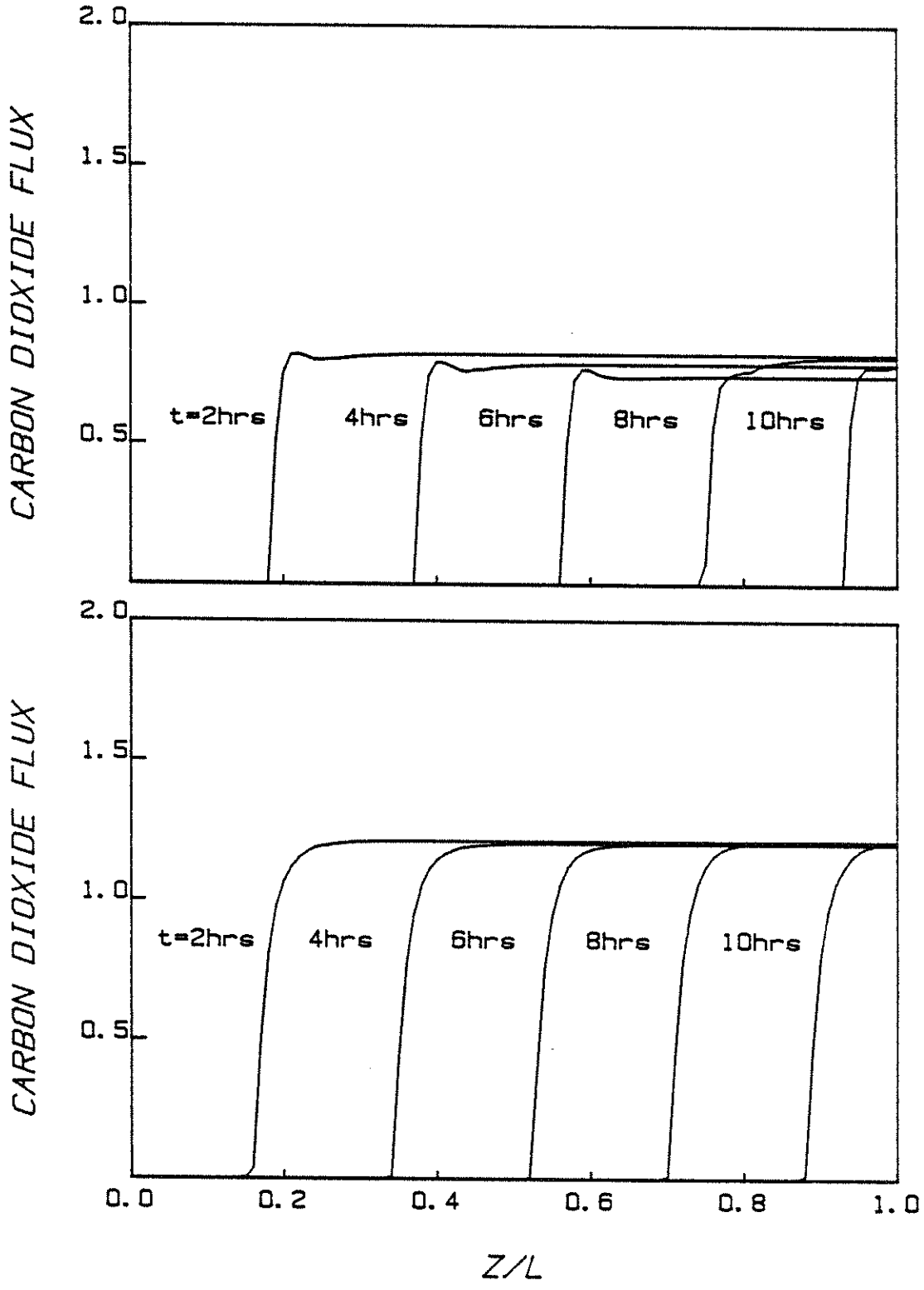

Figure 5.14 Axial CO_2 flux (kgmol/m^2 hr) profiles at various times (a) inner collocation point (b) outer collocation point

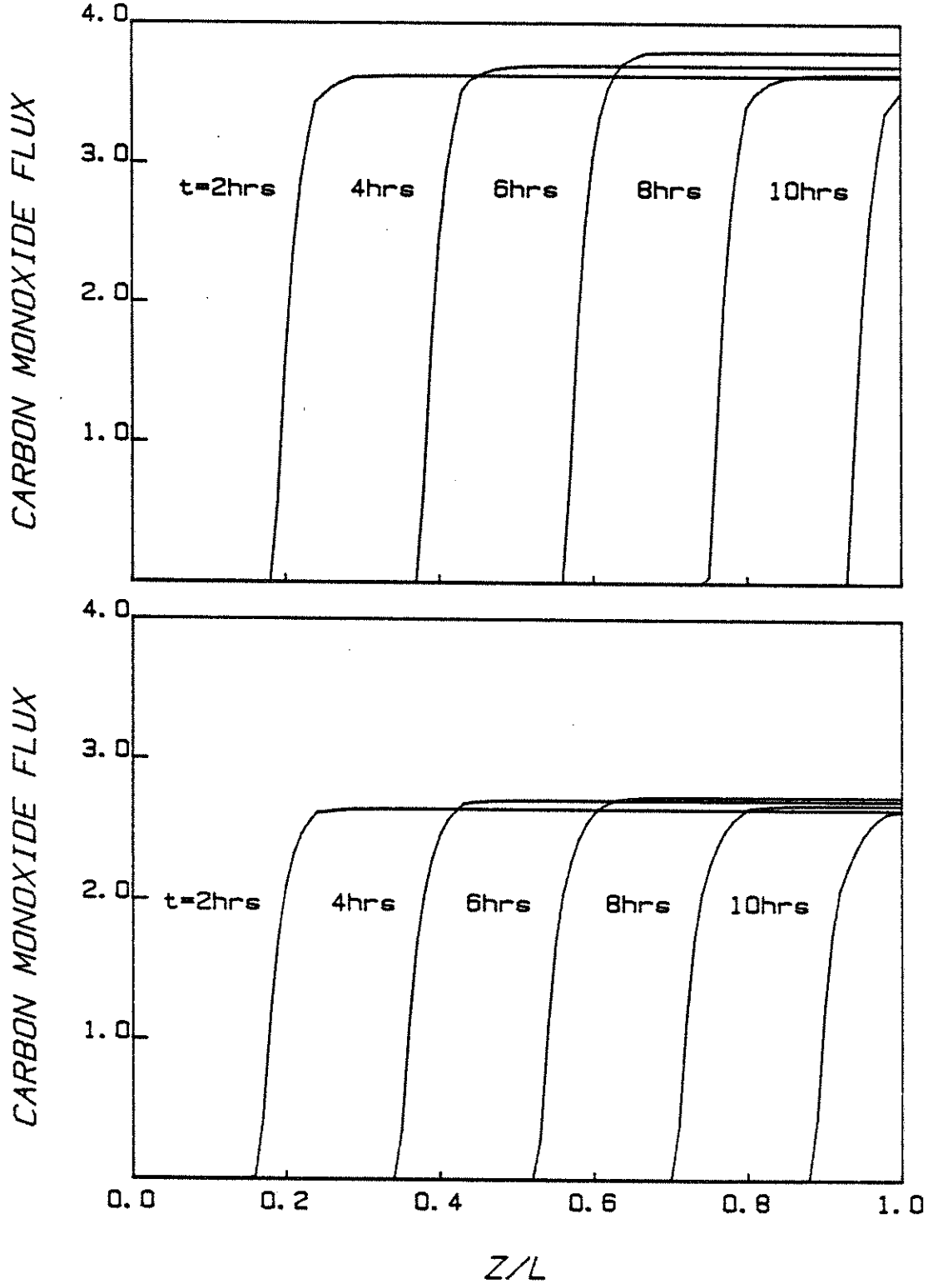

Figure 5.15 Axial CO flux (kgmol/m^2 hr) profiles at various times (a) inner collocation point (b) outer collocation point

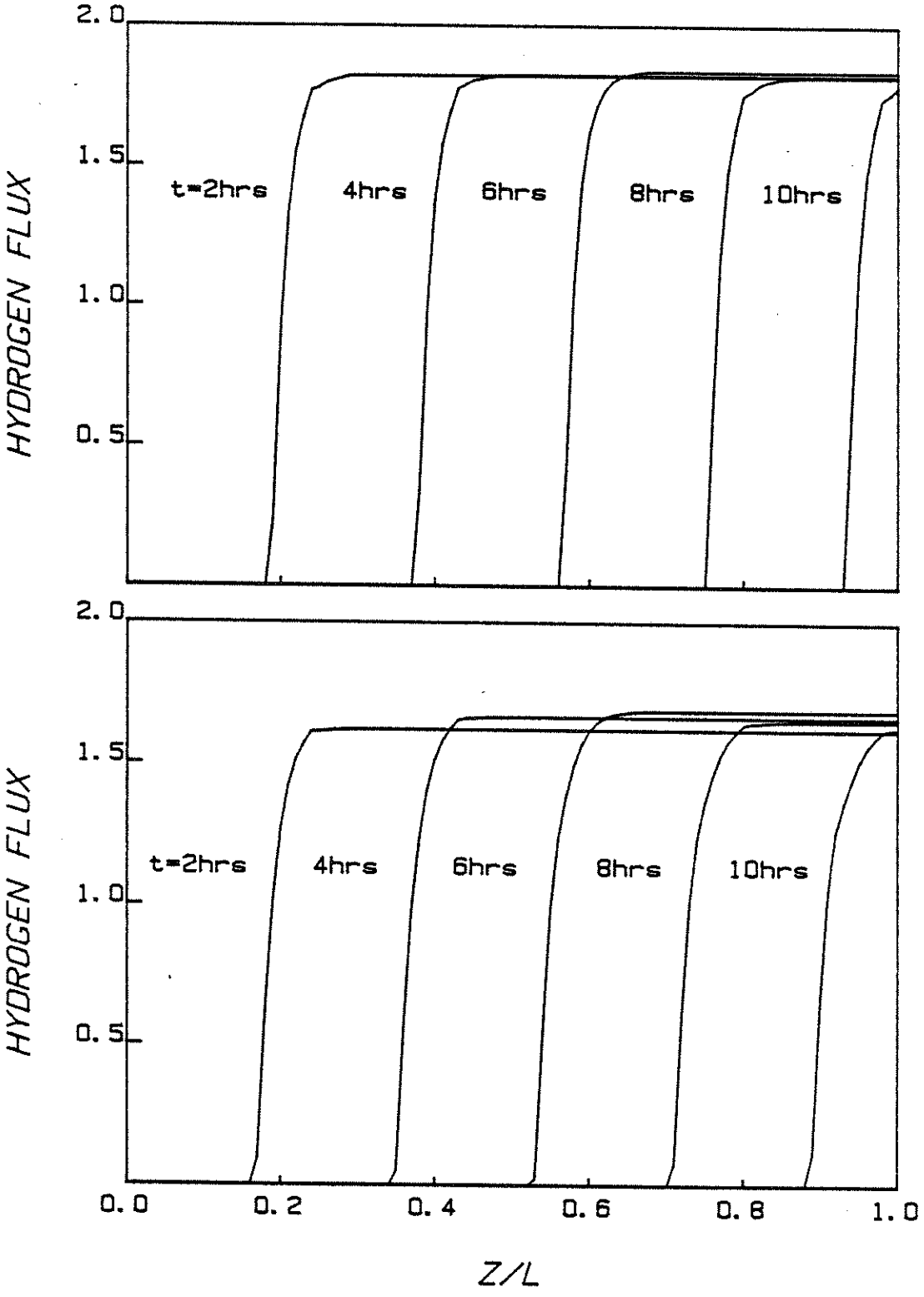

Figure 5.16 Axial H_2 flux (kgmol/m^2 hr) profiles at various times (a) inner collocation point (b) outer collocation point

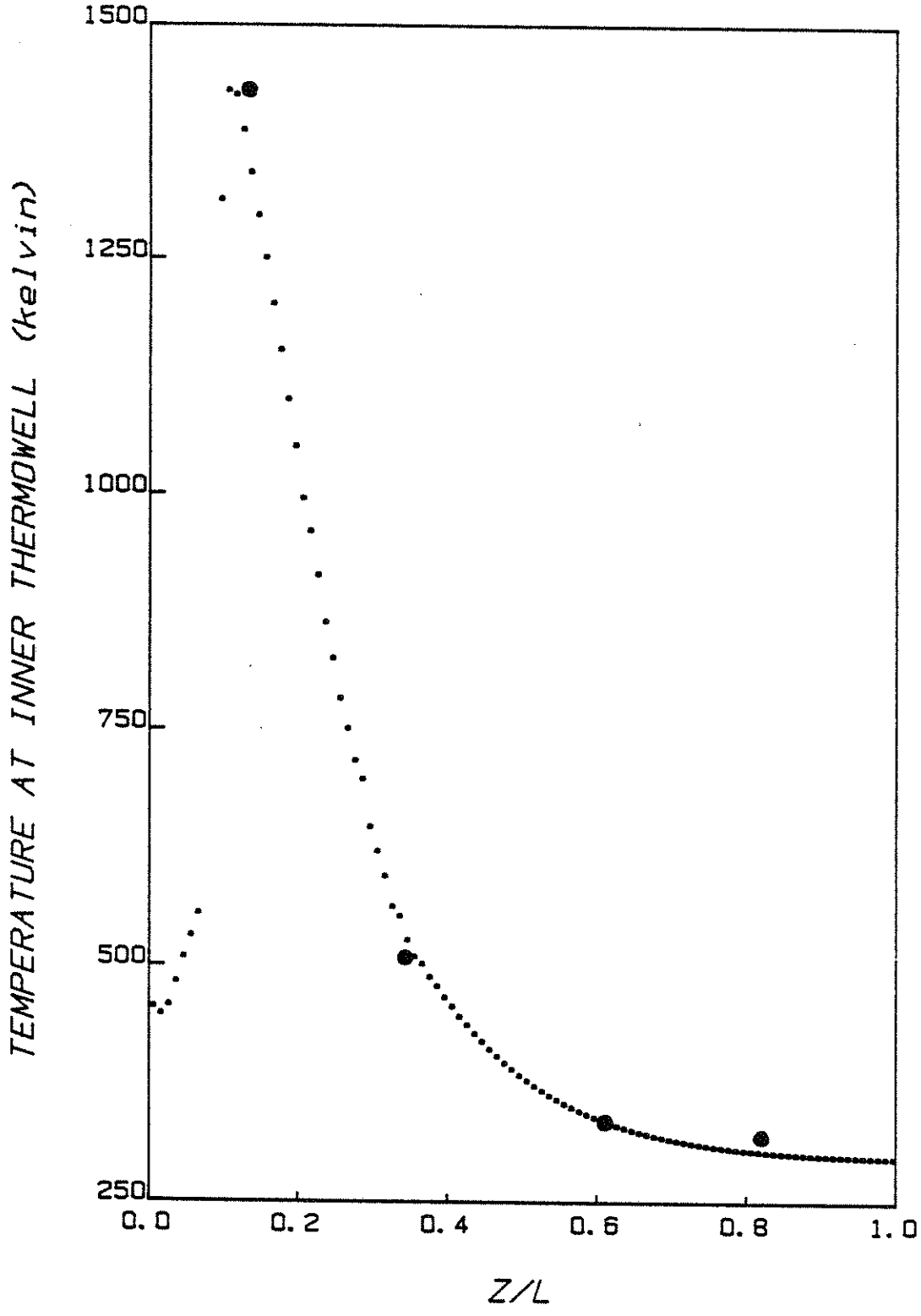

Figure 5.17 Comparison of axial temperature profiles after one hour of operation, inner thermowell location. ▪ predicted, ● measured

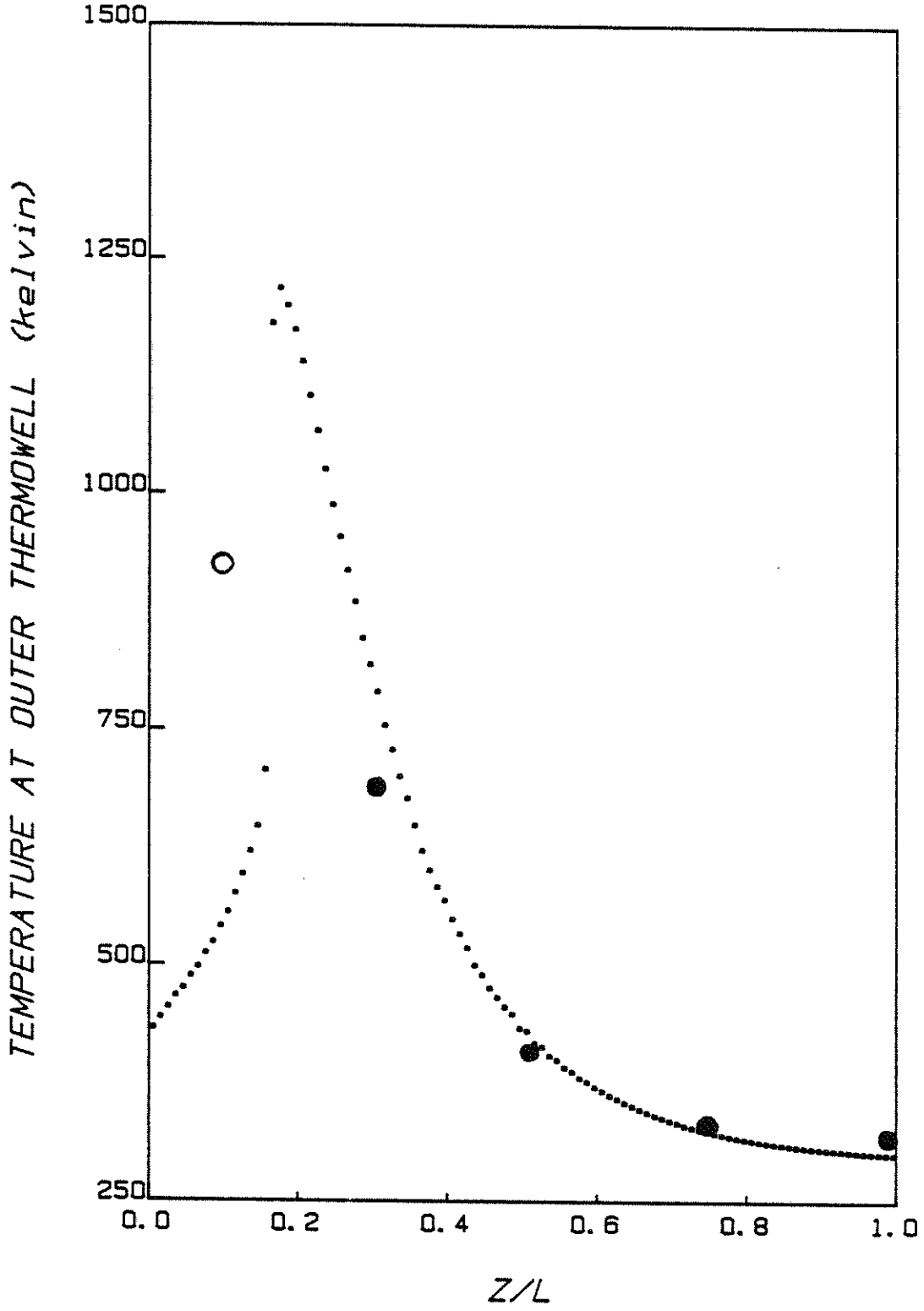

Figure 5.18 Comparison of axial temperature profiles after one hour of operation, outer thermowell location. ▪ predicted, ● measured

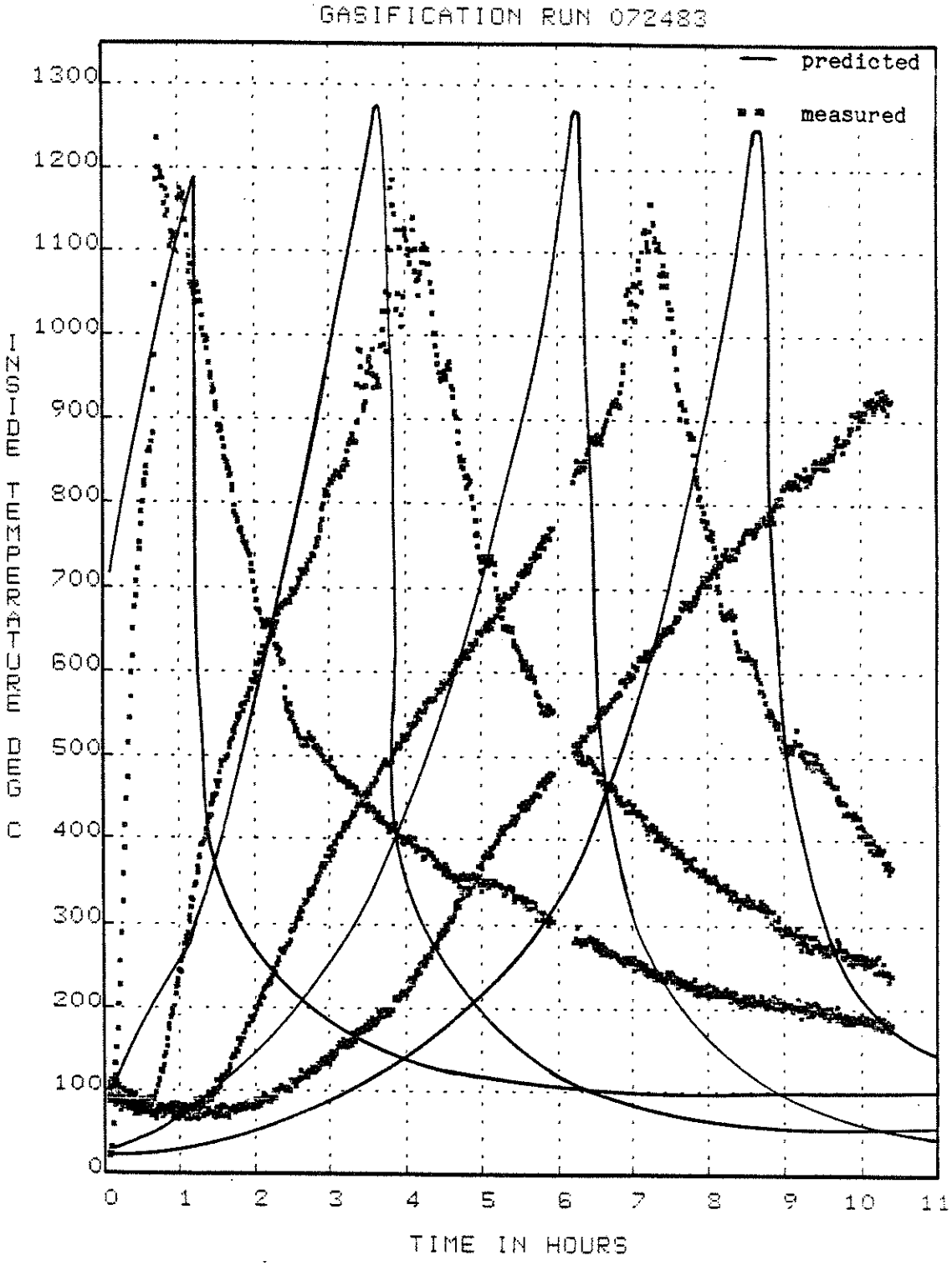

Figure 5.19 Comparison of temp. histories, inner thermowell location

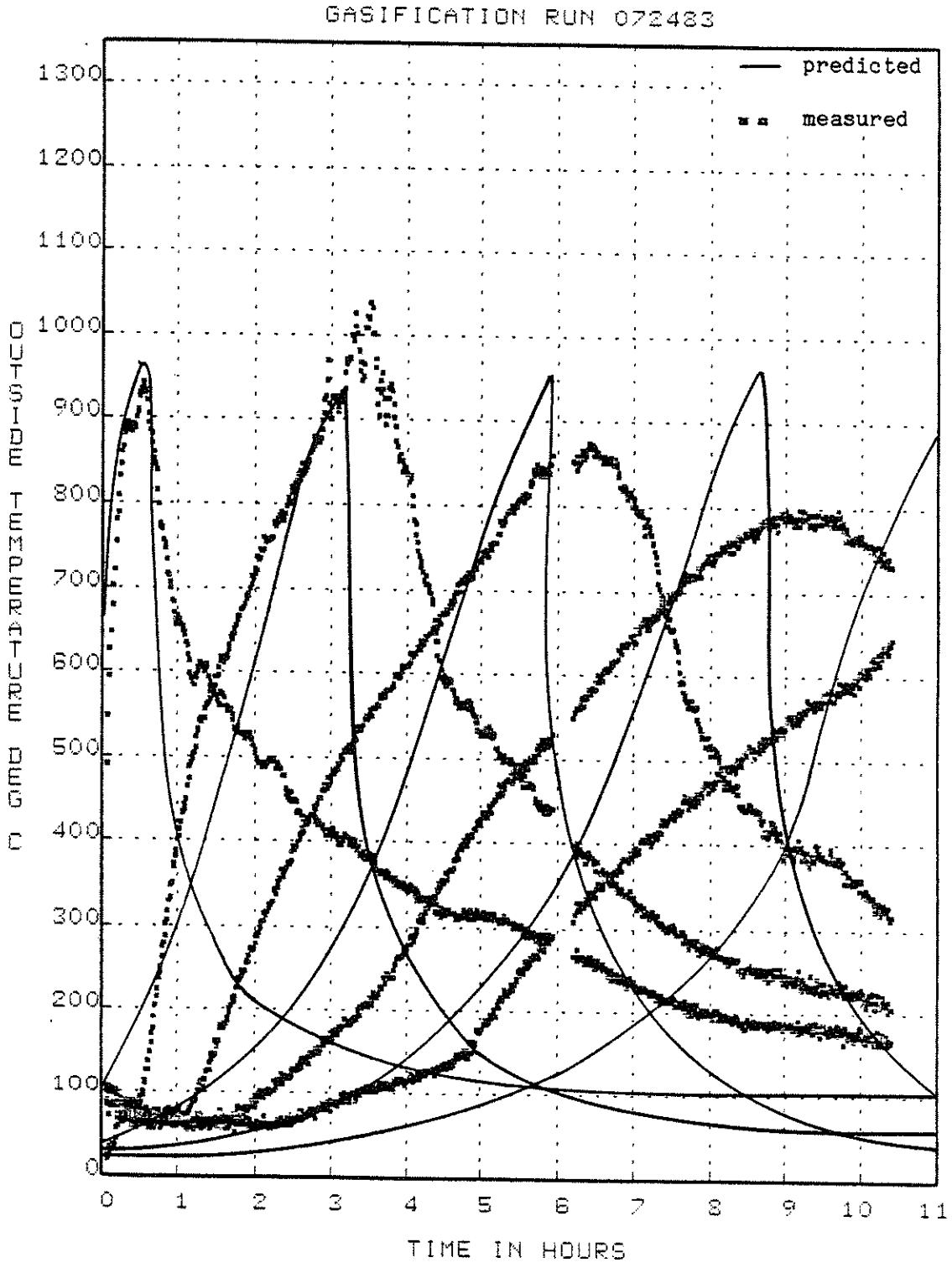

Figure 5.20 Comparison of temp. histories, outer thermowell location

TABLE 5.4

Average Composition[1] of Outlet Gas

Component	Experimental Values	Simulation Values
CH_4	0.081 (0.111)	0.005 (0.006)
O_2	0.180 (0.247)	0.004 (0.005)
H_2	27.071 (—)	13.510 (—)
CO	19.133 (26.235)	23.910 (27.645)
CO_2	9.417 (12.913)	8.350 (9.654)
N_2	44.117 (60.494)	54.210 (62.690)

[1] mol %, H_2O-free

Figures in parentheses are H_2-free.

Some of the experimental errors are discussed in (45).These include:

(i) Bypass of gas: estimated to be about 15% of entering gas.

(ii) Error in thermocouple location. Because of the difficulty in fixing the locations of the thermowells, the axial and radial locations of the thermocouples are not precisely known.

Modeling errors include :

(i) Absence of thermowell modeling. Due to conduction along the thermowell walls, some 'spreading' of the temperature readings may occur.

(ii) Incorrect modeling at a particular location after the temperature maximum has passed that location. Because of bed shrinkage, this location now lies outside the bed, and the energy balances become more complex (with radiation being an additional feature).

(iii)Non-inclusion of axial dispersion of energy: if included, this would tend to lower temperatures, and spread the profiles some more.

(iv) Incorrect kinetics of the reactions may have been assumed. An effort has been made to use simple models, but these need not be correct

This list of errors is by no means exhaustive, but is a compilation of some of the more plausible ones. Since we are most concerned here with modeling aspects, the last few sources of error are looked at more closely in the next chapter. Some of them have a greater potential of affecting the temperature profiles than the others, and are investigated. Modeling error (ii) is not thought to affect temperature profiles significantly inside the bed, and is therefore not explored.

6. MODEL IMPROVEMENTS

In Chapter 5, experimental and simulation results were presented for the gasification run of July 24, 1983. The discrepancies between experimental and simulation results were noted. This chapter explains these differences, and also describes improvements in the model. The focus here will not be towards matching the two profiles exactly: rather, qualitative arguments will be given (and investigated in some detail in most cases) to show trends that may be expected, and which are consistent with the experimental results. It is arguable that the effort spent on matching the two sets of profiles would be of doubtful value, given the low level of sophistication of the experimental setup. The object should therefore be towards only explaining the trends in the experimental data, particularly because the model is accurate at short times, when all the assumptions are valid and applicable to the larger systems for which the model is ultimately intended.

6.1 INVESTIGATIONS INTO SOME ASSUMPTIONS

For the sake of completeness, a variety of factors were investigated to see whether substantial errors could have been introduced into the model by neglecting their effects. Among these factors were the total neglect of thermowell modeling, pressure drop calculations in the bed, and radial variations of void fraction in the bed.

Pressure drops in packed beds may be estimated from the Fanning equation:

$$\frac{\Delta P}{L} g_c = - f \frac{G_M^2}{\rho d_p}$$

where the friction factor f is calculated according to the Ergun (46) relation:

$$f = \frac{1}{Re} \frac{(1-\varepsilon)}{\varepsilon^3} \left(150 + 1.75 \frac{Re}{1-\varepsilon}\right)$$

This relationship does not consider the effect of the wall, which may be important for the reactor tube to particle diameter ratios of 8:1 to 50:1. Mehta and Hawley (47) developed a modified version of the above correlation:

$$f = \left[\frac{1-\varepsilon}{\varepsilon^3}\right] \left[1 + \frac{4d_p}{6(1-\varepsilon)d_t}\right]^2 \left[\frac{150(1-\varepsilon)}{Re} + \frac{1.75}{1+4d_p/6(1-\varepsilon)d_t}\right]$$

For $d_p/d_t \ll 1$, the original Ergun equation results. To be rigorously correct however, a momentum balance must be written and solved with the energy and material balance equations. The above approximate equations yield information on whether such a rigorous treatment is required. For our run, the pressure drop for the entire bed (at startup, when the drop is the largest) works out to be 0.25 KPa (0.036 lb_f/in^2) by the Ergun relation, and 0.14 KPa (0.02 lb_f/in^2) by the Mehta and Hawley relation. Since the reactor inlet pressure is roughly 200 KPa, it seems obvious that the effect of pressure drop will be negligible on the model performance.

The radial variation of velocity profiles in packed beds has been documented by many authors (eg.Schertz and Bischoff (48), Morales et al (49)). The basic trends are as follows: near the wall, a hump in the profile appears. This deviation from the normal expectation increases with increasing flow rate, increasing nonisothermality, and increasing depth in the bed. This hump is generally thought to be caused by a variation in the radial voidage profile: i.e., near the wall of the

packed beds the voidage increases, resulting in increased flow rates. The nature of our system however, makes this information difficult to utilize. Since the bed is free to collapse as it is consumed, there is a continuous realignment of particles in the top portion of the bed. Therefore, any correlation that is applicable for truly fixed beds would not be applicable here. Moreover, taking into account the fact that the flow velocities are small, and that the region of interest is the reaction front (which is at the top of the bed at all times), it is suggested that the voidage variation has negligible effect on reactor performance.

For the sake of completeness, it was felt that the thermowells should also be modeled to see their effect on the measured temperature profiles. This effort would give an idea of the difference between measured and actual temperatures. If these turn out to be substantial, then the model equations may possibly have to be included in the gasifier model.

The energy balance for the thermowell is of the same form as that for the gasifier wall. If we make the assumption that the gas inside the well is at the same temperature as the thermowell, the equation becomes:

$$\rho_w C_w \frac{\partial T}{\partial t}_w = \frac{2h_1 r_1}{(r_2^2 - r_1^2)} (T - T_w) + k \frac{\partial^2 T}{\partial z^2}_w$$

or

$$\frac{\partial T}{\partial t}_w = C_1 (T - T_w) + C_2 \frac{\partial^2 T}{\partial \xi^2}_w$$

where

$$C_1 = \frac{2h_1 r_1}{(r_2^2 - r_1^2)\rho_w C_w}, \qquad C_2 = \frac{k}{L^2 \rho_w C_w}$$

$$\xi = z/L$$

The boundary/initial conditions for the differential equation are:

$$\xi = 0,1 \quad \frac{\partial T}{\partial \xi}w = 0 \quad ; \qquad t = 0 \qquad T_w = T_{wo}$$

After finite differencing in ξ, the equation can be written in the form:

$$\frac{d\underline{T}}{dt}w = \underline{\underline{A}}\underline{T}_w + \underline{B} \quad ; \qquad \underline{T}_w(0) = \underline{T}_{wo}$$

This set of equations may be integrated very easily by a variety of methods. If for example, finite differencing is again applied in t, a simple iterative formula results:

$$\underline{T}_w^{t+1} = \underline{\underline{D}}\underline{T}_w^t + \underline{B}^t\Delta t \qquad (6.1)$$

Here $\underline{B}$ is a function of t because it contains T (the temperature of the bed) terms, which are functions of t.

Equation 6.1 was used with the parameters specified in Table 6.1 on the simulation results presented in Chapter 5. Since the bed-thermowell heat transfer coefficient was unknown, a sensitivity analysis with respect to this coefficient was carried out. Also, a sensitivity analysis on the thermal conductivity of the thermowell material was performed. In all, a number of runs were made.

A typical result is shown in Figure 6.1. As we can see, the only substantial difference between the measured and actual temperatures in the bed are in the maximum values. This deviation decreased as the heat transfer coefficient was increased, and did not vary substantially with 10 to 20 percent changes in the thermal conductivity. The magnitude of the deviation depended on the thickness of the wells. Taking all factors into account, deviations in the maximum temperature readings amounting to 50-100 Kelvin seem entirely possible. The deviations in the temperature profiles shown in Chapter 5 (Figures 5.19 and 5.20) may

TABLE 6.1

Thermowell Parameters

Outer diameter	0.004762 m
Inner diameter	0.003262 m
Thermal conductivity	50 kJ/m hr K
Bed-well heat transfer coeff	100 kJ/m^{2}hr K
Density	8200 kg/m^3
Specific heat	0.4477 kJ/kg K

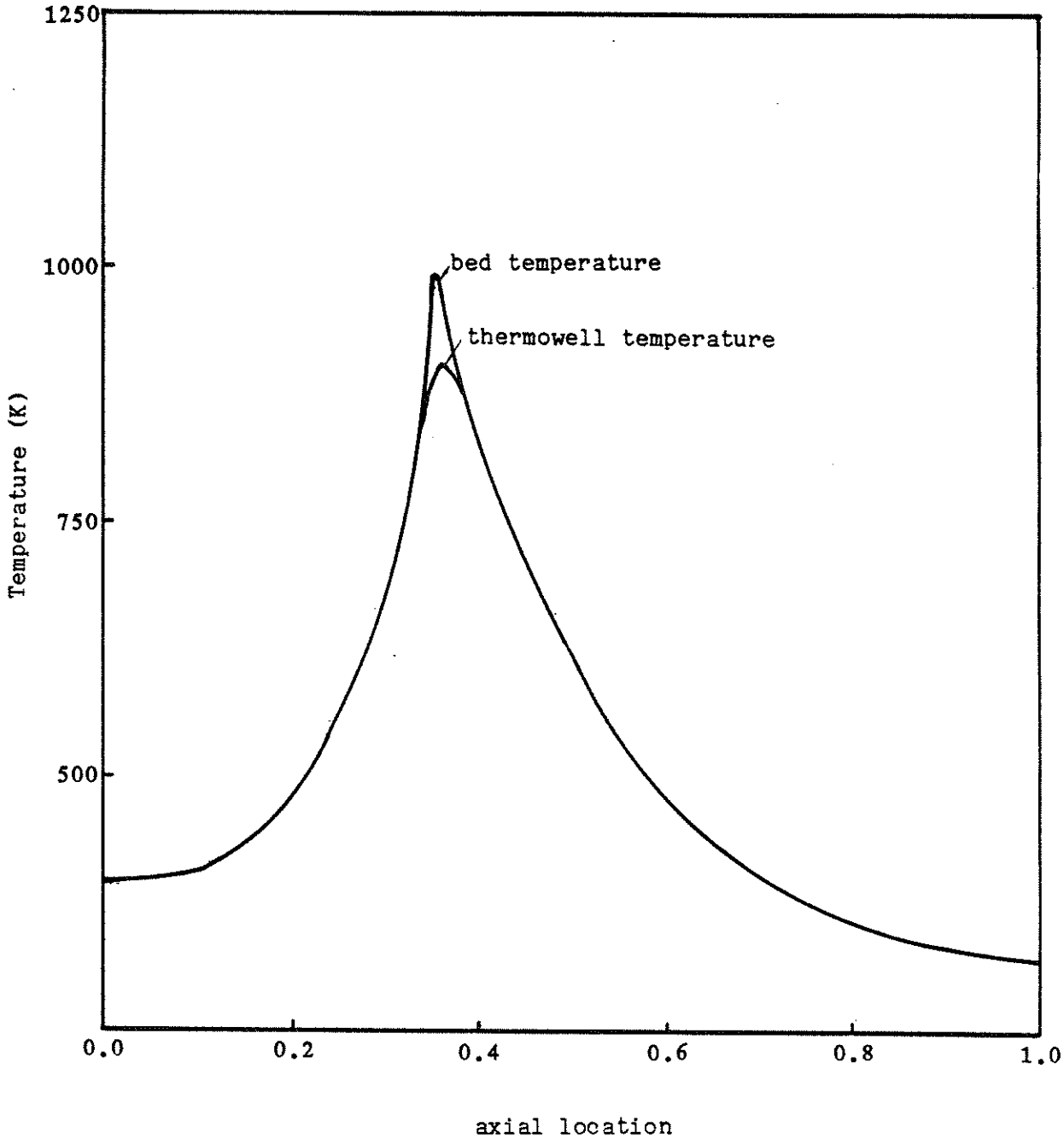

Figure 6.1 Comparison between bed and thermowell temperatures, outer thermocouple location

be affected by this: we can see that the measured maximum temperatures may be actually higher than depicted, and therefore the agreement between measured and predicted temperatures would be better.

6.2 REACTION RATE EXPRESSION

The rate expression used for the two major reactions -- the char-oxygen and the char-steam reactions -- has been developed from the shrinking core model (SCM,Figure 6.2):

$$r_i = (1-\varepsilon)P_i^*\left[\frac{d_p}{6k_{g,i}} + \frac{d_p^2(1-\rho)RT_g}{12\rho D_{M,i}} + \frac{1}{\eta_i \rho^3 k_{r,i} C_c^o}\right]^{-1}$$

The definitions for some of the terms (like ρ, η_i etc.) can be found in Chapter 2. The three terms in the denominator may be thought of as resistances to mass transfer through a gas film surrounding a char particle, diffusional resistances through the ash layer (converted coal) surrounding the unconverted core, and the intrinsic reaction rate resistance.

While this model may be approximately valid in the Lurgi gasifier and for some systems where there is no appreciable volume change in the solid phase, it is not an accurate representation of our system, where the volume change is substantial because of the low ash content of the coal. For the system at hand, it may be more reasonable to visualize a situation where the ash separates from the unreacted core, primarily because of the collapse of the bed. In this situation, there would not be a resistance due to the ash layer in the rate expression, which could be written as (3):

$$r_i = (1-\varepsilon)P_i V_c\left[\frac{d_p(1-\rho)}{6k_g} + \frac{1}{\eta_i k_{r,i} C_c^o}\right]^{-1}$$

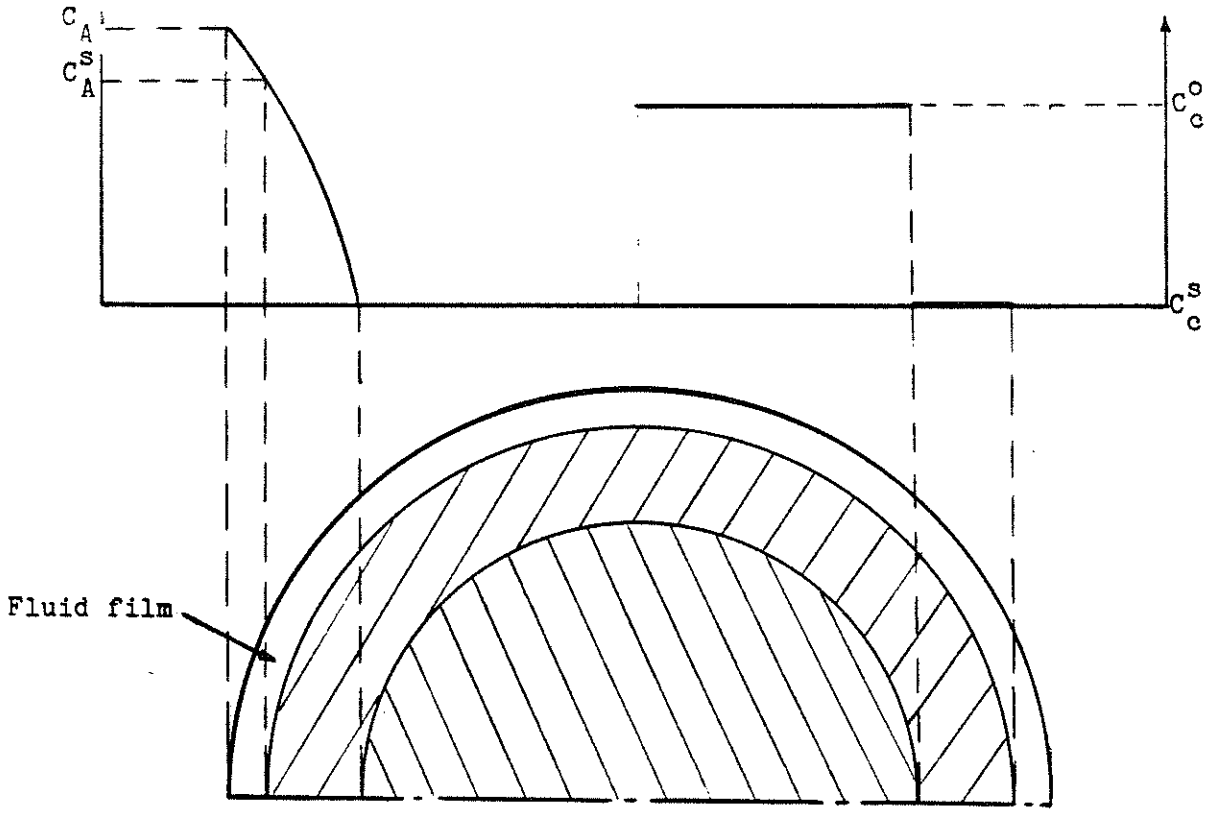

Figure 6.2 The shrinking core model

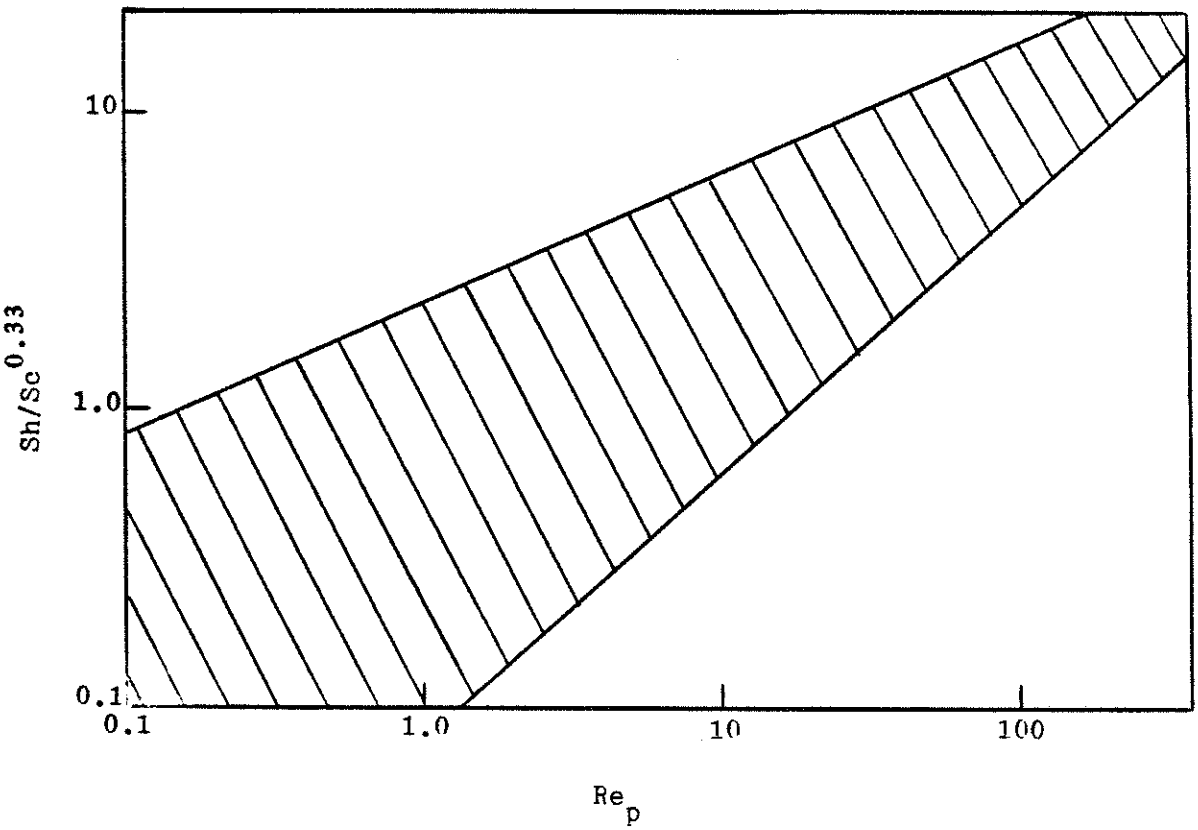

Figure 6.3 Region of uncertainty in correlations for mass transfer coefficient

Note however, that a new term V_c enters the expression which may be defined as that fraction of space occupied by the unreacted core particle.

Either expression gives rise to a difficulty. The correlation of k_g which was used in the SCM is applicable for $90 < Re < 4000$. The system at hand has $Re \sim 3.5$, caused mainly by the fact that the particle size is small (approximately 0.002 m). At this value for Re, most correlations for k_g become unreliable. Kato, Kubota and Wen (50) have addressed this problem somewhat. Figure 6.3, taken from the same reference, shows the extreme divergence of the different correlations at low values of Re, and also shows that the mass transfer coefficients in solid-gas fixed beds becomes considerably smaller than the theoretical coefficient for a single particle in a stagnant gas medium (Sh = 2.0). They proposed a new correlation, based additionally on the d_p/L ratio:

$$Sh/(Sc)^{0.33} = 0.72 \left[Re_p \left[\frac{d_p}{L}\right]^{0.6} \right]^{0.95} \qquad 0.1 \leqslant Re_p \left[\frac{d_p}{L}\right]^{0.6} \leqslant 5$$

$$Sh/(Sc)^{0.33} = 1.25 \left[Re_p \left[\frac{d_p}{L}\right]^{0.6} \right]^{0.63} \qquad 5 \leqslant Re_p \left[\frac{d_p}{L}\right]^{0.6} \leqslant 1000$$

Experimental agreement with this correlation is fairly impressive, except at the extreme values of $Re_p d_p/L$, where the data is sparse and the deviations seem to be substantial. For our system $Re_p d_p/L$ is approximately 0.09, so even this correlation is barely applicable. Comparisons between the two correlations yields numbers for k_g about 50 to 100 times as high with the ST (12) correlation as with the KKW (50) correlation. Given the uncertainty in the values for k_g, a sensitivity analysis was done. Different values for k_g were chosen around the

estimates given by the KKW correlation, and the resulting temperature profiles were matched with the actual experimental ones. After a number of trials, a value of k_g was chosen such that the minimum value of $6d_p/k_g$ was approximately 0.08 kPa m^3hr/kgmol. (As a comparison, the figures obtained from the KKW correlation are 0.12 for O_2 and 0.06 for H_2O). It should be emphasised here that this uncertainty does not exist for the larger industrial-sized gasifiers (for whom the k_g correlations are valid), and therefore this assumption has not been used in that situation. Some figures with this model corresponding to the simulation results of Chapter 5 are shown in Figures 6.4 to 6.6; the rest are given in Appendix 11.3. The profiles look the same as before. This is to be expected for a system with so high a reaction rate as the oxidation rate.

6.3 CHAR CONVERSION PROFILE

The uncertainty in k_g values discussed in Section 6.2 leads to an uncertainty in actual reaction rates for the two most important reactions in the gasifier — the char + oxygen and the char + steam reactions. This leads to another problem. Since char consumption depends very much on these reactions, and since there is no eventual steady state in the gasifier, the char conversion profile may change in form as time proceeds and not be of the same shape as shown in Figure 5.11 of Chapter 5. This fact would ultimately lead to changing temperature profiles.

A simple example of a gas-solid reactor was chosen to show these trends. Consider a hypothetical gas-solid reaction:

$$A(g) + B(s) = C(g)$$

Also consider a similar situation as in the gasifier, where reactant A enters a reactor filled with B. The reaction is exothermic, and

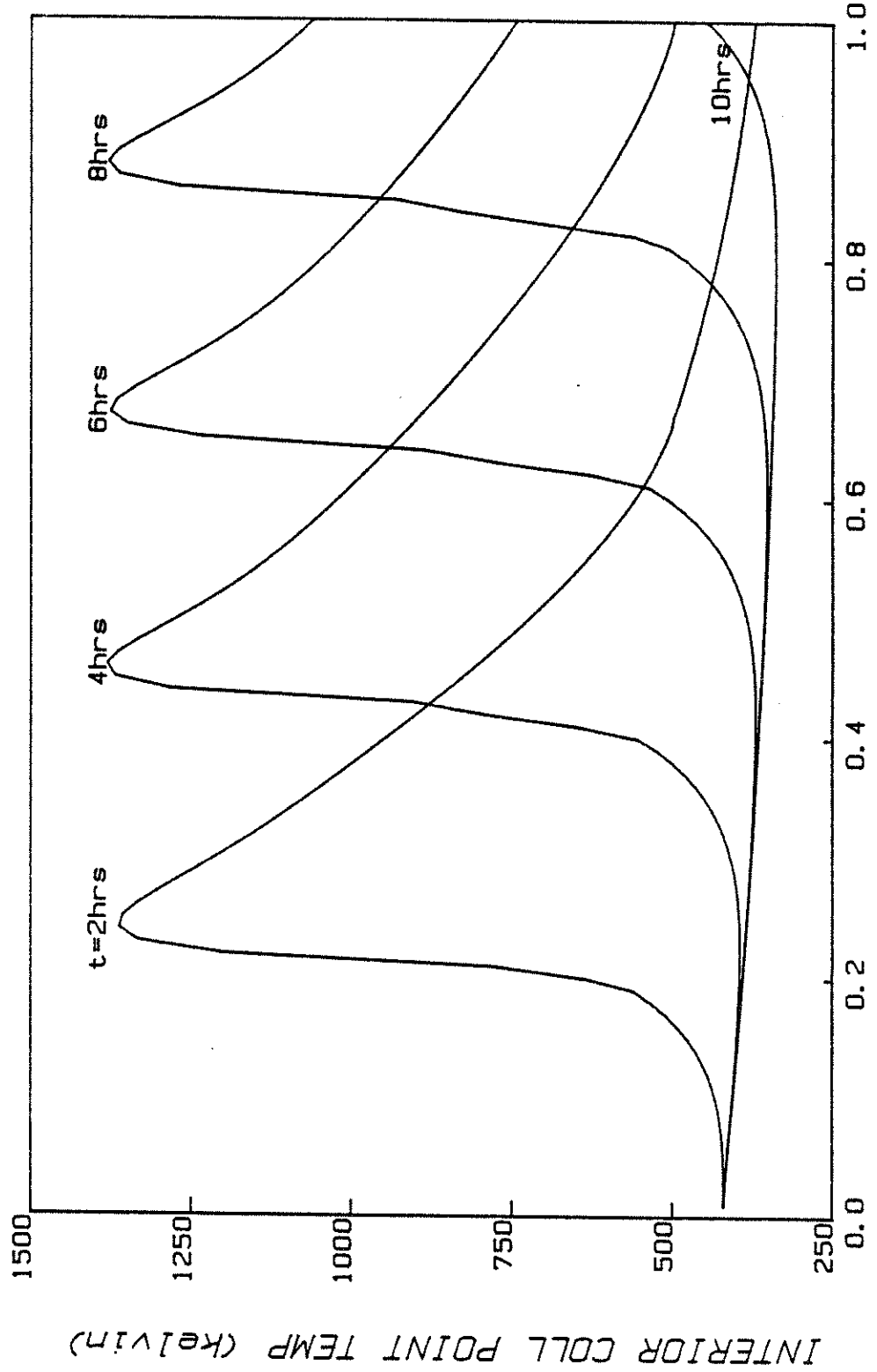

Figure 6.4 Axial temperature profiles at various times at the inner collocation point (r/R = 0.3938)

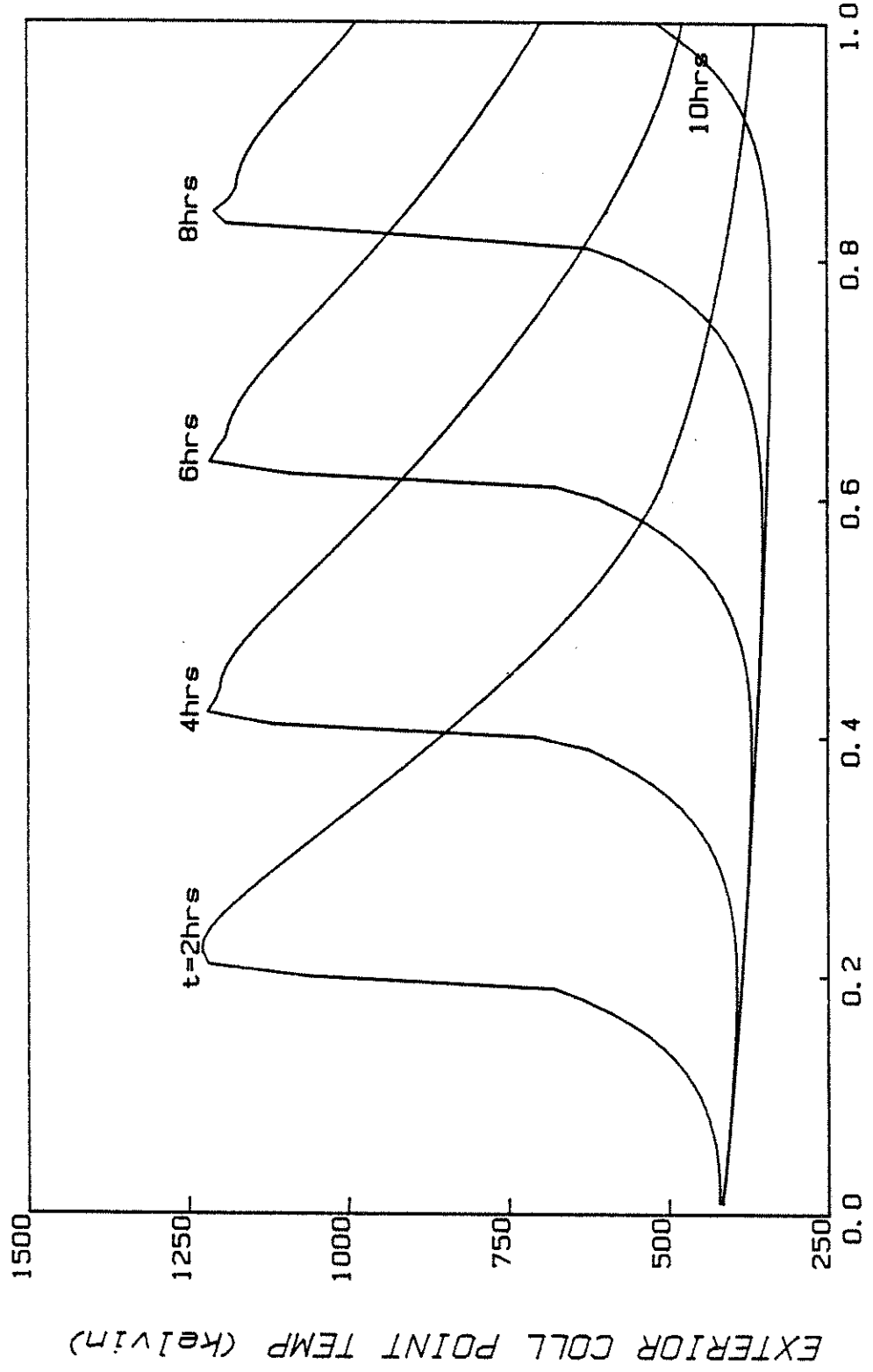

Figure 6.5 Axial temperature profiles at various times at the outer collocation point (r/R = 0.8031)

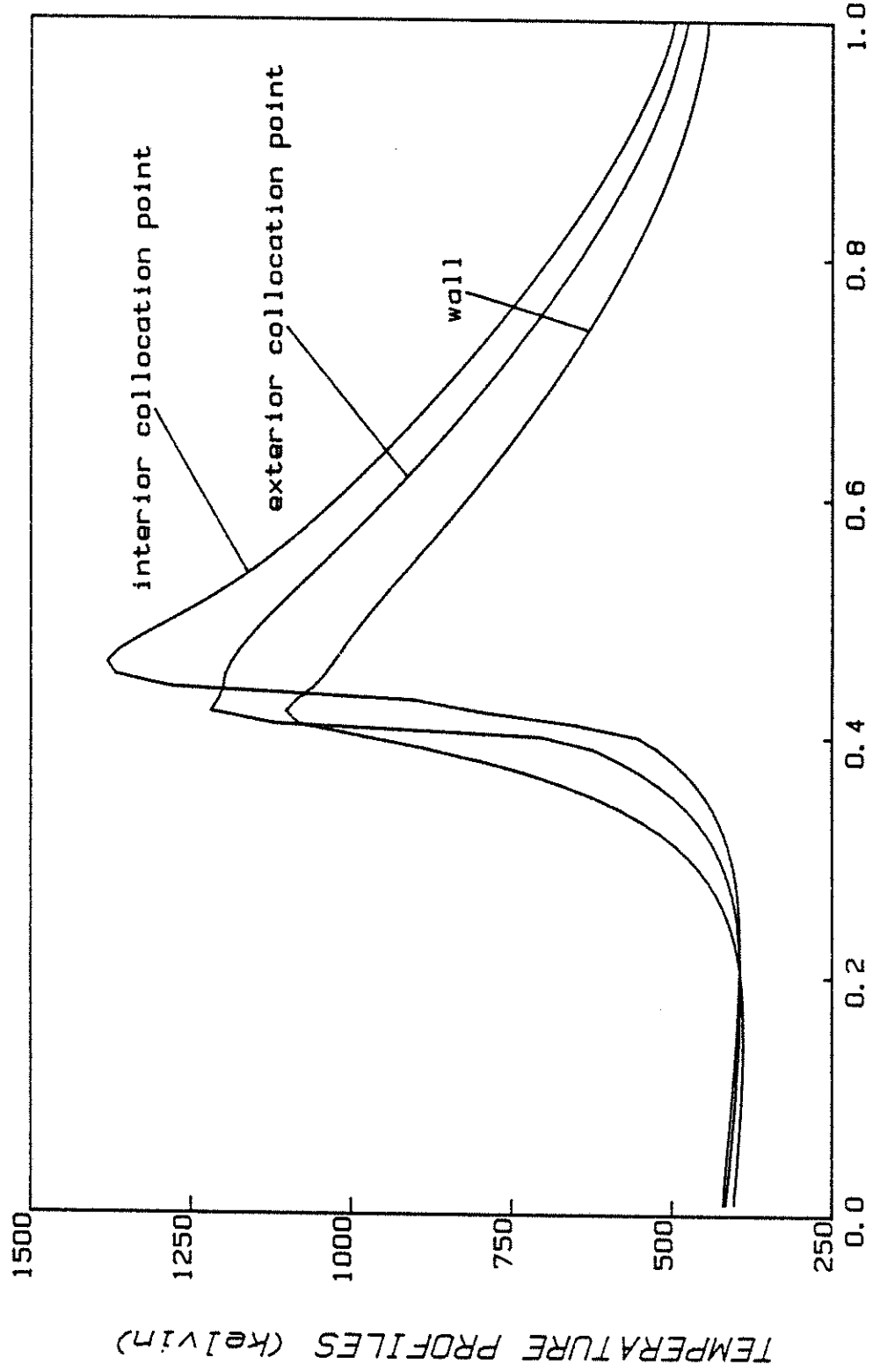

Figure 6.6 Axial temperature profiles at t = 4 hours

therefore the temperature and other profiles have the same form as in the gasifier. The assumptions made in modeling this system are the same as for the gasifier, with two additions : radial dependence is assumed absent, and the reaction rate is assumed to be controlled by the kinetics. The governing equations are :

Energy balance: $$\frac{\partial\theta}{\partial t} = -\frac{\beta\partial\theta}{L\partial z} - \gamma(\theta) + \delta r$$

Material balances:

Gas: $$\frac{\partial x}{\partial t} = -\frac{v\partial x}{L\partial z} + \mu T_o r$$

Solid: $$\frac{\partial x}{\partial t}s = \omega r$$

with $z = 0$, $\theta = 1$ and $x = 0$

$t = 0$, $x_s = 0$ and $\theta = 0$

Reaction and reactor parameters for the system are given in Table 6.2. A simple explicit Euler formula was applied to the t-coordinate, and a 4th order Runga Kutta method to z.

Results of the simulation are shown in Figures 6.7 through 6.11. Figure 6.7 shows the axial temperature profiles at various nondimensional times (t = 6000 corresponds roughly to extinction). The most significant trend in the temperature profiles is the decrease in the maximums reached as time proceeds. The reason this occurrs is apparent when the solid conversion profiles are studied (Figure 6.8). As can be seen, they change as time proceeds, and do not attain a 'pseudo steady state' form (by which we mean a profile which is of the same shape, the only change with time being in position). Therefore, the entering gas 'sees' a different solid conversion profile at different times, and therefore reacts differently. The reason the

TABLE 6.2

Reactor Parameters

α	0.0094 m^2/hr
β	0.4376 m/hr
γ	0.3970 hr^{-1}
δ	0.3333 $m^3/kgmol$
μ	0.7818 $m^3/kgmol\ K$
ω	0.018 $m^3/kgmol$
v	399 m/hr
L	0.86 m
T_o	750 K
T_w	300 K

$$r = 0.2 \exp(-3 \times 10^7 / 8314 \times T)$$

$$\theta = (T - T_w)/(T_o - T_w)$$

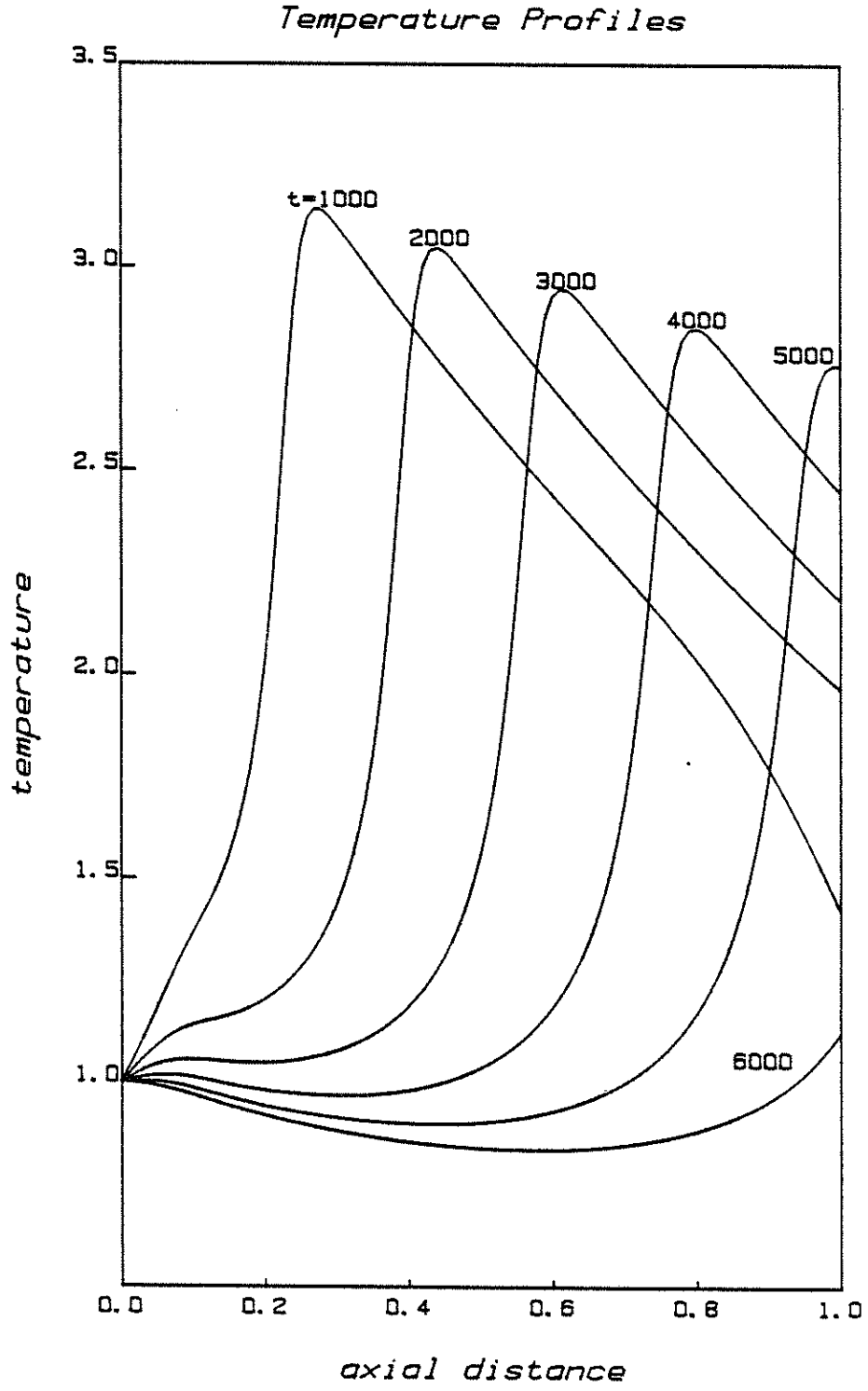

Figure 6.7 Temperature profiles at various times for system described in Table 6.2

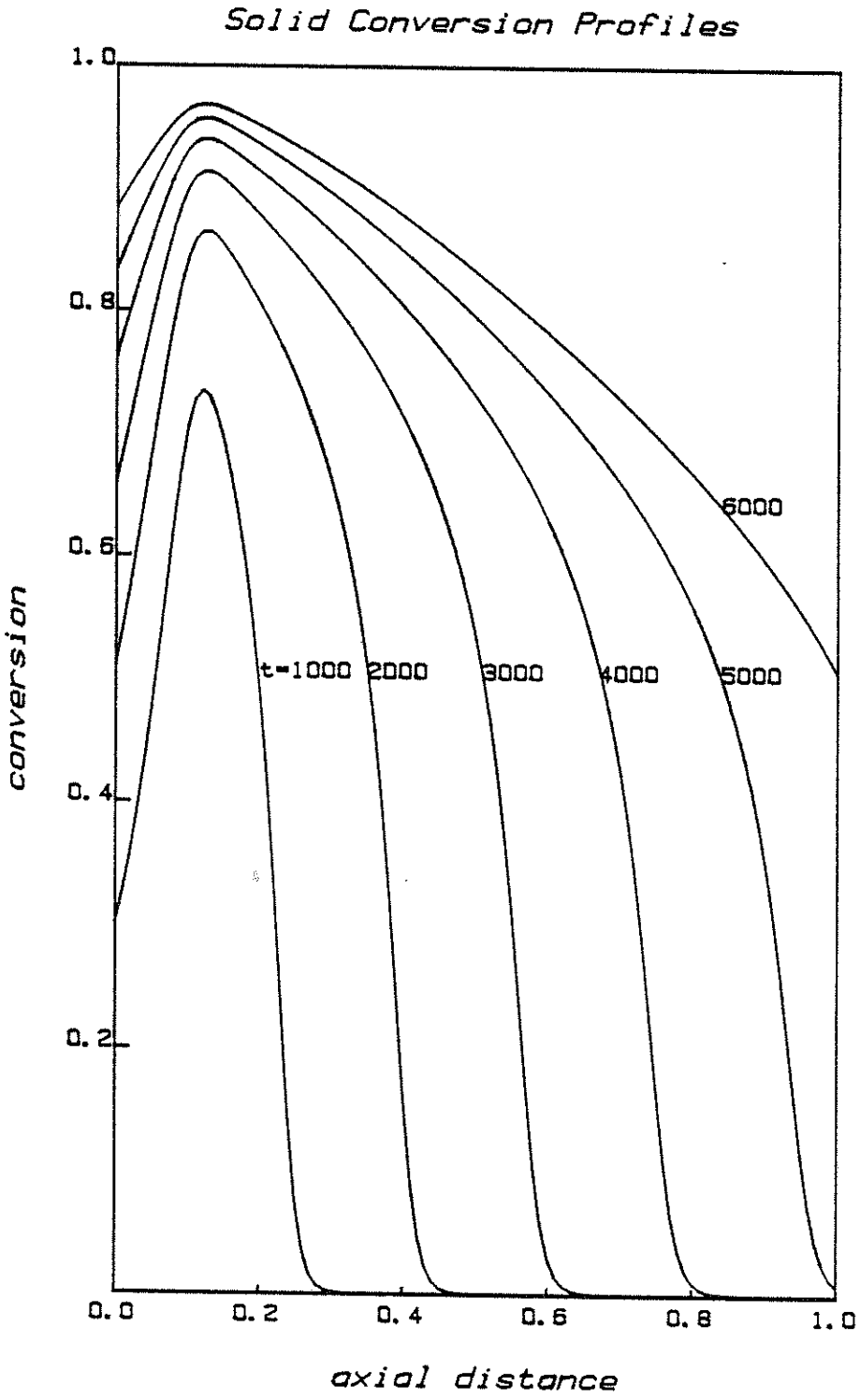

Figure 6.8 Solid conversion profiles at various times for system described in Table 6.2

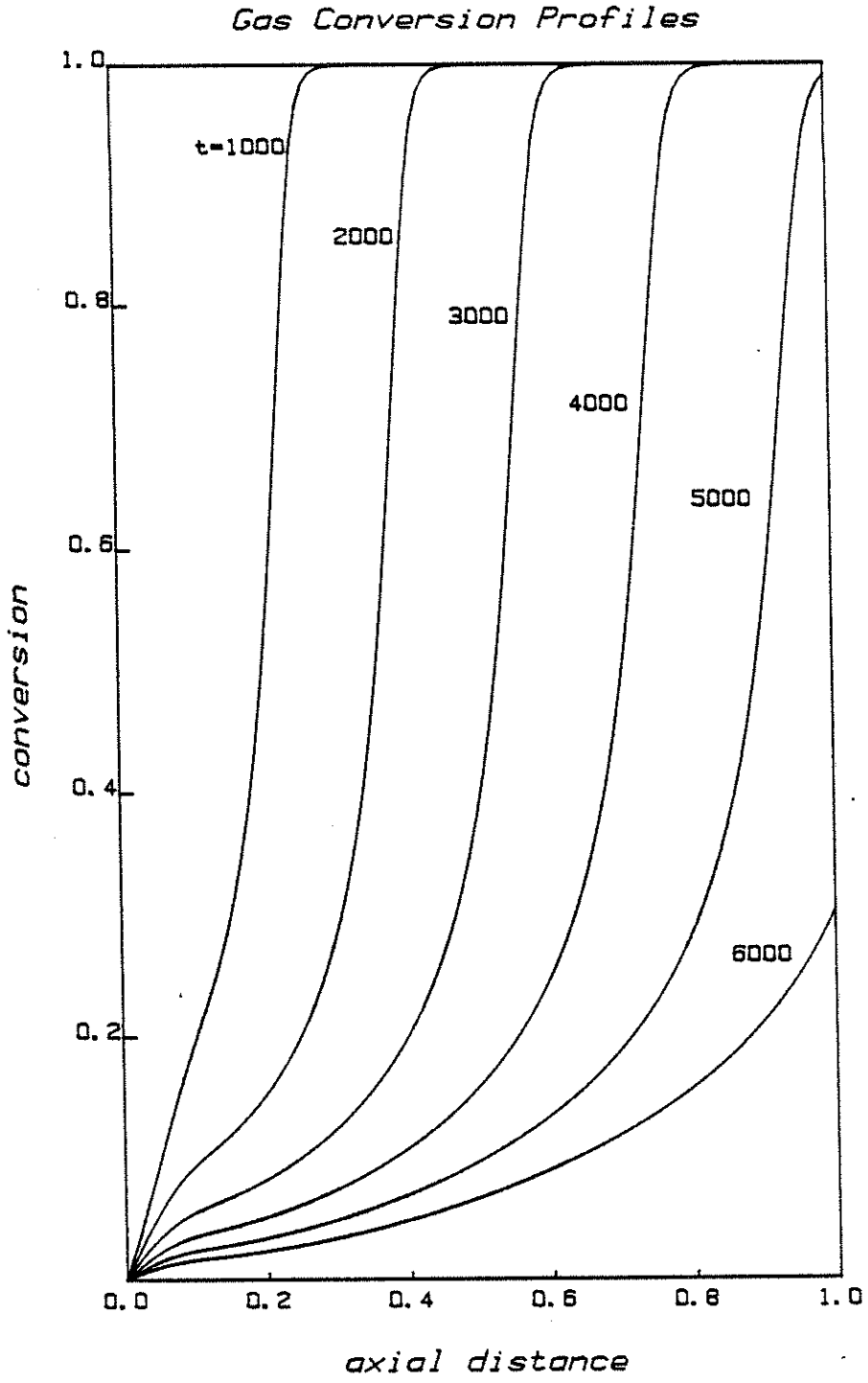

Figure 6.9 Gas conversion profiles at various times for system described in Table 6.2

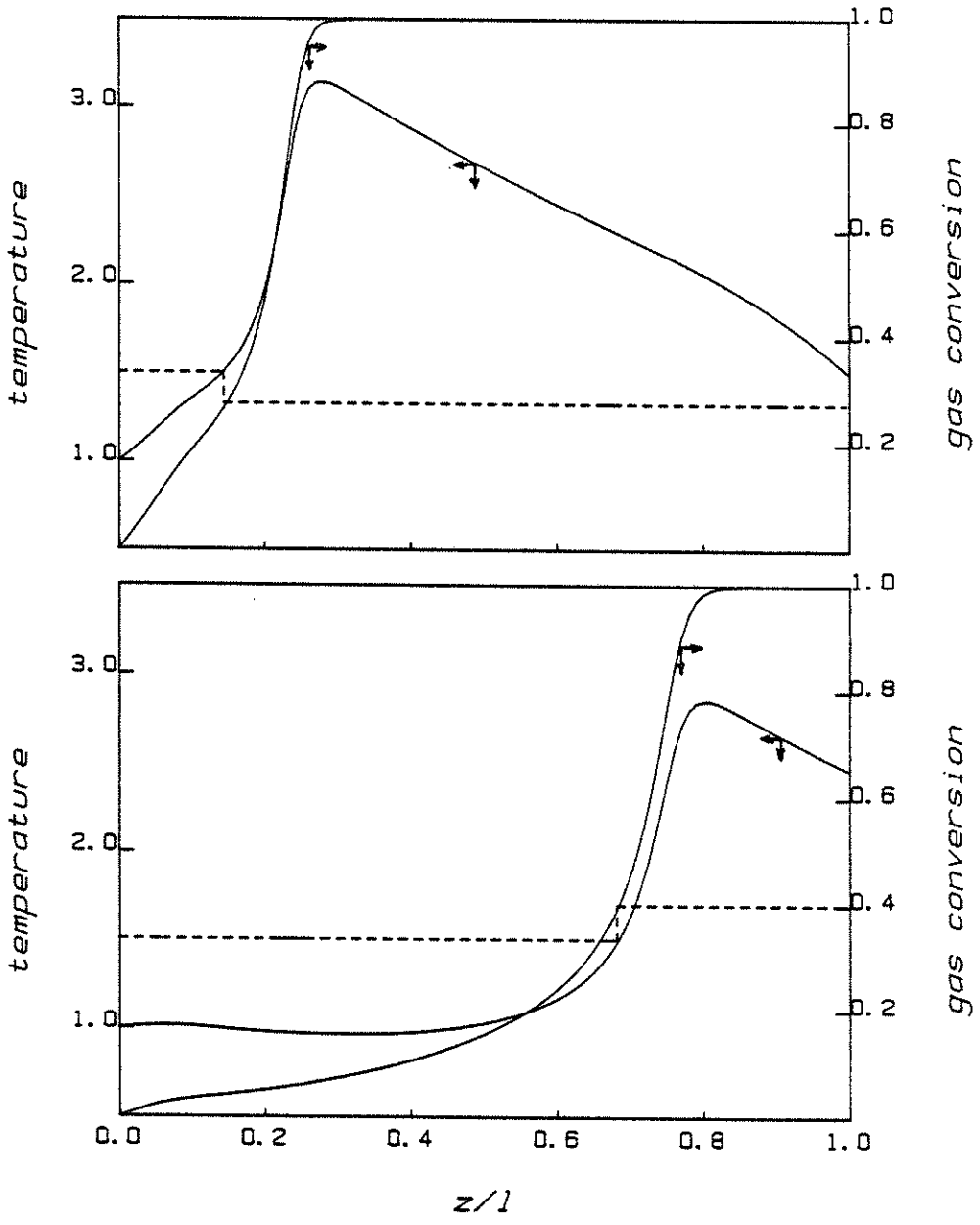

Figure 6.10 Comparison between two cases for system described in Table 6.2 (a) t = 1000 (b) t = 4000

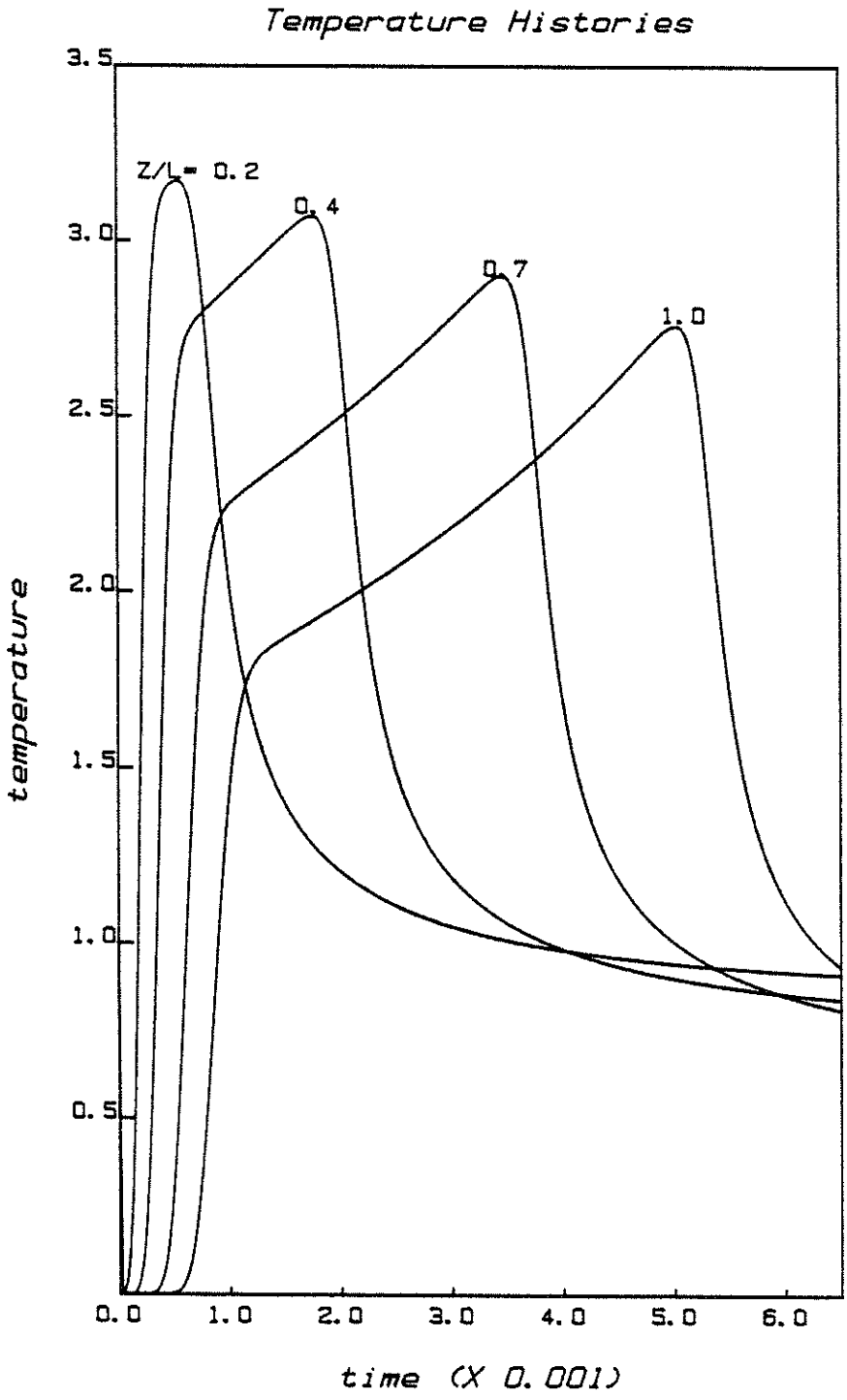

Figure 6.11 Temperature histories at various axial locations for system described in table 6.2

temperature maximums are lower with time is that at larger times, the gas reacts in a larger portion of the reactor with solid which has higher conversion (see Figure 6.8). When the gas eventually hits the reaction front, more of it has already been converted and less is available for reaction at the front, resulting in less heat being developed there (which ultimately determines the maximum temperature reached). This is apparent from Figure 6.10, which plots the temperature and gas conversion profiles at t = 1000 (Figure 6.10a) and at t = 4000 (Figure 6.10b). For any arbitrary θ (say 1.5), we can find the gas conversion corresponding to it. We see that for t = 4000, the value is much higher than the value for t = 1000 (0.4 vs 0.27).

Figure 6.11 plots the temperature profiles on a time scale,for 4 different axial locations in the reactor. Again, the decrease in the maximum temperatures is apparent. The sharp initial increase is because of the exothermicity of the reaction in the reactor, and indicates the rapid rise in temperature throughout the reactor when it starts from a cold state.

It can be argued that the heat transfer coefficient to the wall could affect the maximum reached. To see this effect by itself, it is necessary to have a larger reaction rate, so that there is complete solid conversion. The same system was now run with the k_o factor in the reaction rate expression multiplied by a factor of 5. The profiles for this system are shown in Figures 6.12 through 6.14. Note that at short times at least (Figure 6.13), the solid conversion profiles go to unity. The temperature profiles (Figure 6.12) do show a decrease in the maximums, but here they are caused by the initial decline as the gas enters the reactor (since solid conversion is complete, no reaction

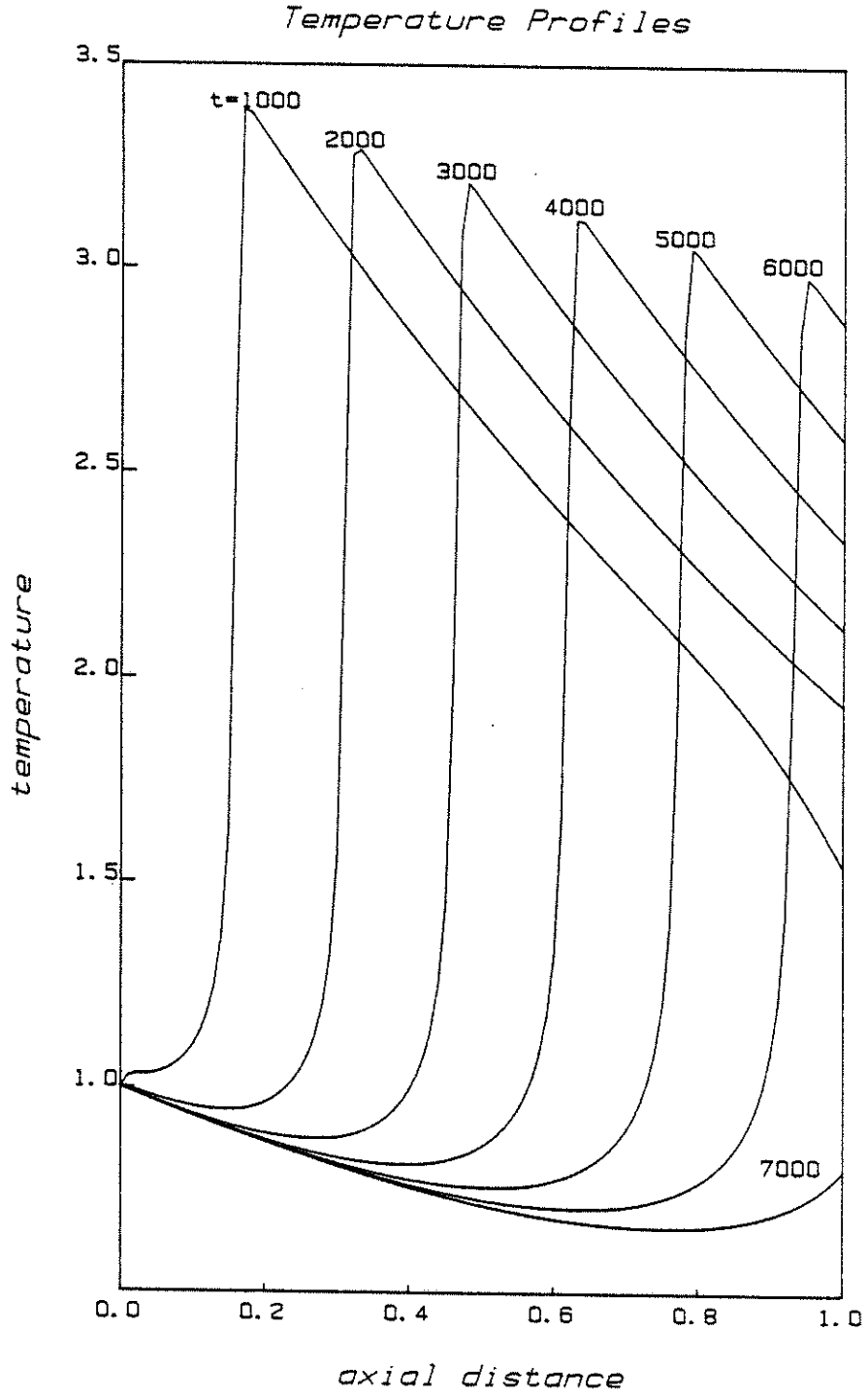

Figure 6.12 Temperature profiles at various times, larger reaction rate case.

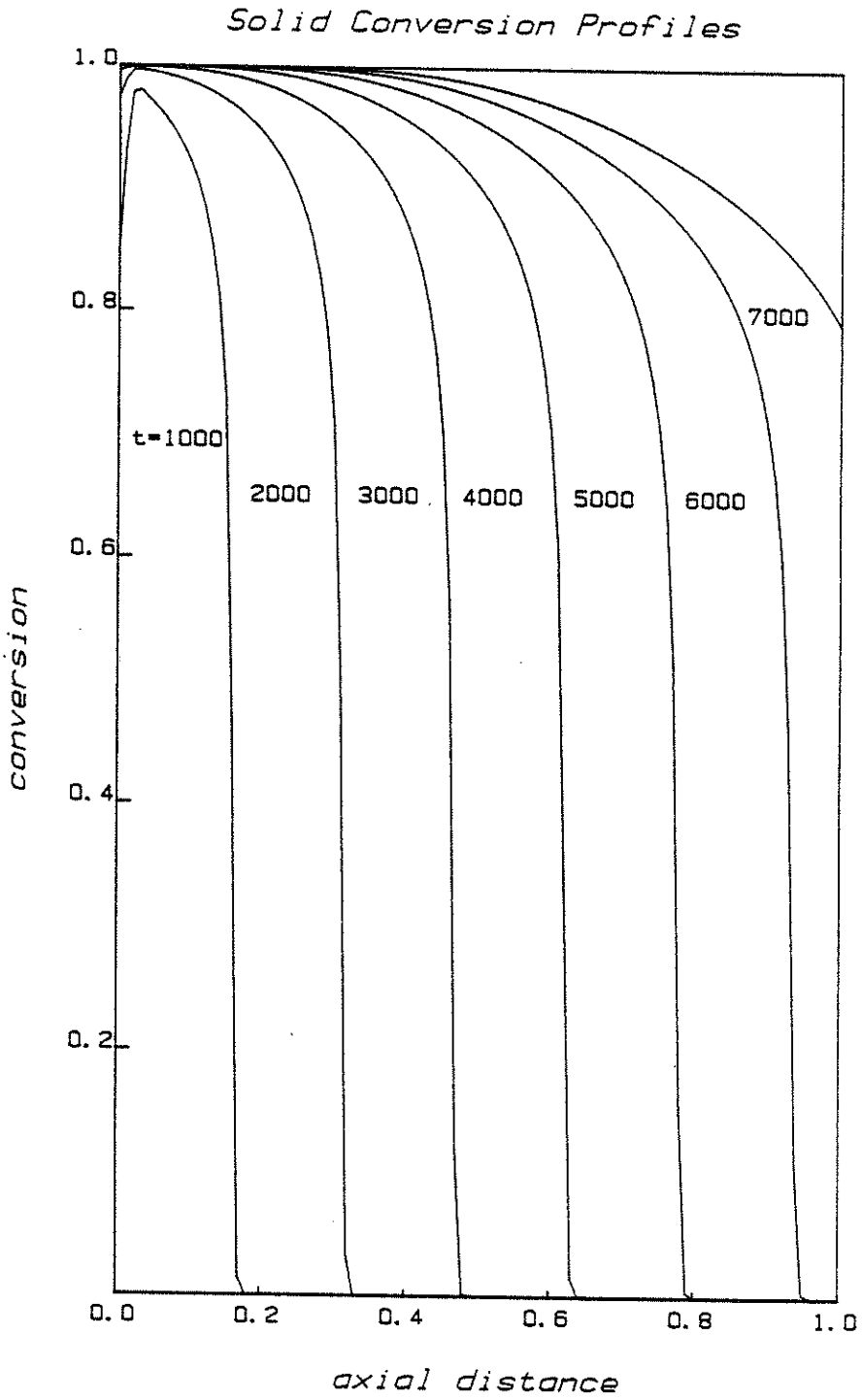

Figure 6.13 Solid conversion profiles at various times, larger reaction rate case.

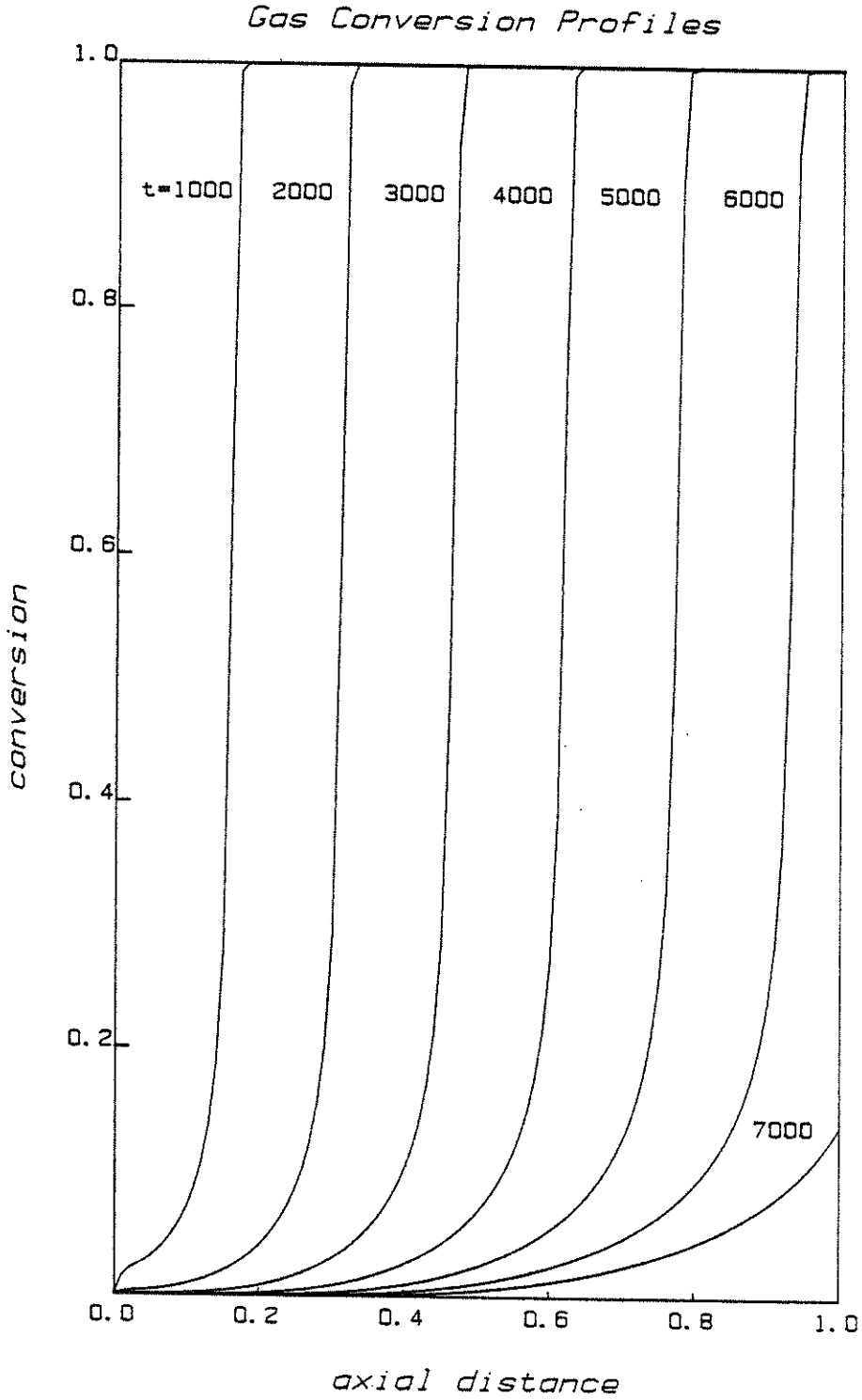

Figure 6.14 Gas conversion profiles at various times, larger reaction rate case

takes place , and there is a net heat loss to the wall). The difference between the two cases (Figures 6.7 - 6.9, and 6.12 - 6.14) is that in the former, the net increase in the temperatures decreases sharply (see Table 6.3) compared to the latter. The dominating cause therefore seems to be the solid conversion profile.

The decrease in the temperature maximums then, are affected by the solid conversion profiles to a very great extent. This effect increases as time passes because the solid conversion profiles themselves change increasingly with time.

TABLE 6.3

Comparison of Increase in Temperature

for Two Reaction Rates

	$k_o = 0.2$			$k_o = 1.0$		
t	T_{min}	T_{max}	ΔT	T_{min}	T_{max}	ΔT
1000	1.0	3.136	2.136	1.0	3.390	2.390
2000	1.0	3.037	2.037	0.946	3.292	2.346
3000	1.0	2.936	1.936	0.876	3.212	2.336
4000	0.959	2.842	1.883	0.813	3.123	2.310
5000	0.899*	2.764*	1.823*	0.757	3.054	2.297
6000	-	-	-	0.706	2.984	2.278

* at t = 4625, which is the final time at which a maximum was reached.

7. AXIAL DISPERSION OF ENERGY IN FIXED BED REACTORS

As mentioned in Chapter 2, some assumptions were made while formulating the material and energy balance equations. Some of these assumptions simplified the solution of the resulting equations considerably. For example, the assumption of homogenity reduced the number of PDEs by one and avoided the problem of quantifying the heat transfer between gas and solid phases when the solid phase is being consumed by reaction. Similarly, the assumption of absence of axial dispersion of energy makes the energy balance simpler to solve, because first order ODEs may be treated in a variety of ways whereas methods of handling second order split boundary value problems are relatively more difficult to apply. This Chapter investigates in greater detail this assumption made in Chapter 2, and examines the effect of removing it.

The six sections in this Chapter explores various aspects of the axial dispersion problem. In the first section, the reasons why axial dispersion of energy may be important is explored. In section 7.2, various methods used in the past to handle the resulting model equations are mentioned. Section 7.3 explores the feasibilty of applying orthogonal collocation to some stiff problems, whose solutions are the type expected from the axial dispersion problem. Section 7.4 examines the dynamic problem, and finally, the axial dispersion problem is investigated in Sections 7.5 and 7.6.

7.1 ASPECTS OF HEAT TRANSFER IN FIXED BEDS

Two dimensional models for heat transfer in fixed beds are generally written when pronounced heat effects are present in the reactor, so that temperature and conversion profiles are adequately

described for design or other purposes. The effective transport concept is generally used, in which an additional flux term is added to the convection term in the balance equation. This term is characterized by the effective radial thermal conductivity for heat transfer. Experimental observations indicate that this conductivity exhibits a sharp drop in value near the walls of such reactors and hence a second parameter (the effective heat transfer coefficient) is used to characterize the heat flux at the wall.

A number of papers have been published in the literature on estimation of these two parameters for different systems (eg. (37), (40), (44)). The estimates, however, show a dependence on bed length with the dependence being more pronounced at shorter lengths. Figure 7.1 (taken from (44)) shows this dependence clearly, as does Figure 7.2 (from Li and Finlayson (51)). Under the formulation given above, both parameters would have to depend on bed length (or more accurately, axial position in the bed) because each parameter would be affected by any change in the other. The general explanation for the behavior is that the dependence on axial location is because of the developing velocity and temperature profiles (44), and once these profiles have fully developed, the parameters exhibit a constant or asymptotic value. Most workers then, gear themselves towards ways and means of estimating these asymptotic values, and the dependance of these values on certain variables like Reynolds numbers and d_p/d_t ratios.

Some workers (52) noticed the length effect and observed that there was a statistically adequate fit between experimental and predicted temperatures when an axial dispersion term was included in the formulation, and also showed that the length dependence of the two

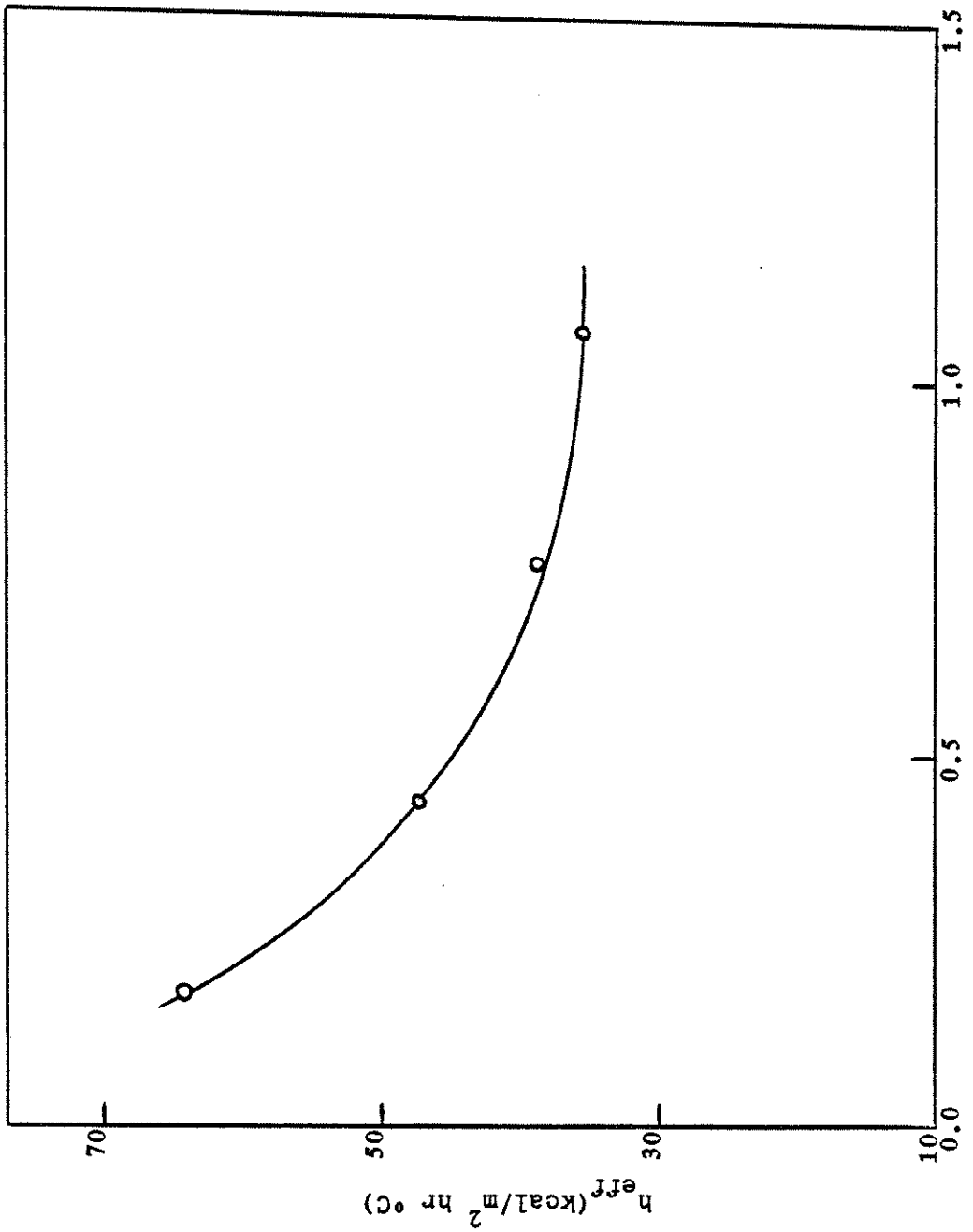

Figure 7.1 Positional dependence of heat transfer coefficient

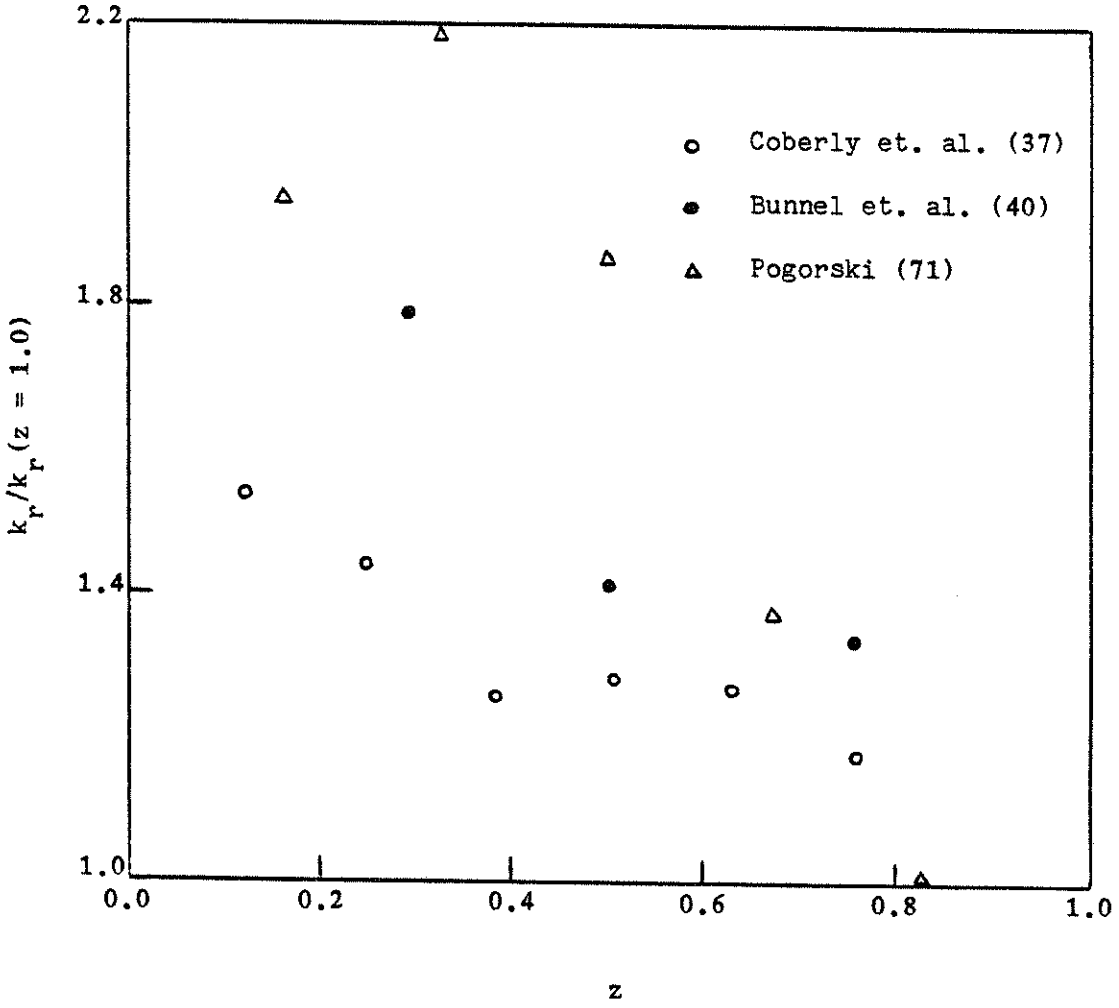

Figure 7.2 Positional dependence of effective radial conductivity

parameters disappeared.

Some workers studied the length dependence in detail, and made some recommendations as to when it is important (51). Paterson and Carberry (53) explain the failings (eg. overpredictions of hot spots) of the so-called 'conventional' model (a plug flow, two-dimensional model) partly because of the underestimation of the rate of heat removal from the bed which results when axial dispersion is neglected.

From these arguments, it would seem that axial dispersion should be included in the energy balance for the gasifier. Further reinforcement is given to the argument when one considers the fact that there is a dramatic decrease in the length of the bed, thereby further decreasing the values of the axial thermal Peclet numbers as time proceeds. Young, in a private communication to Li and Finlayson, presented a formula for the error in the estimates of the two parameters when axial dispersion was neglected:

$$\frac{\Delta k_e}{} = \frac{\Delta h_w}{} = - \frac{1}{e_h} \left[\frac{d_p}{R}\right]^2 \frac{3Bi}{Bi+3} + \frac{d_p}{2L}$$

where Δk_e and Δh_w are the errors in k_e and h_w due to the neglected axial dispersion effect. However, this formula is for the case when the parameters are constant, and therefore the estimated error is expected to be low. For the gasifier, $\Delta k_e/k_e$ works out to range between 0.5 and 1.0 percent, and the axial dispersion effect is therefore expected to be negligible for that part of the reactor where k_e is constant. The same authors present an approximate argument and state that whenever the product of Ld_p/R^2Pe_h and nondimensional z is greater than 0.2, the assumption of constant k_e and h_w is valid. Quick calculations show that for the gasifier, the assumption is valid for $z > 0.33$ at the beginning

of the run, and for $z > 2.5$ (meaning the entire reactor) at the end. This gives an estimate of the errors introduced: at the beginning of the run, the assumptions are adequate for the latter 67 percent of the bed; at the end, the assumptions are inadequate for the entire bed.

The question that remains to be answered is the magnitude of the errors introduced because of the assumption. As mentioned before, some authors have suggested that introduction of an axial dispersion term takes care of the anomaly. In the following sections the effect of axial dispersion terms on the temperature profiles are examined.

7.2 TREATMENT OF AXIAL DISPERSION

In general, the energy balance including axial dispersion (but without radial variation) in a fixed bed may be written as:

$$k_e \frac{\partial^2 T}{\partial z^2} - \rho v C_p \frac{\partial T}{\partial z} + (-\Delta H) r - \frac{4h}{d_t} (T - T_c) = \rho C_p \frac{\partial T}{\partial t}$$

with boundary conditions:

$$z = 0 \qquad -k_e \frac{\partial T}{\partial z} = \rho v C_p (T_o - T)$$

$$z = L \qquad \frac{\partial T}{\partial z} = 0$$

The solution of this system is complicated by the split boundary value specifications. On the one hand, marching techniques are difficult to use because the boundary conditions have to be satisfied at both ends. On the other hand, any differencing technique requires a large number of grid points if the axial profiles are expected (as they most often are in cases where axial dispersion is important) to be steep.

A review of some of the methods to solve the steady state version of the equation is given in the paper by Hlavacek and Van Rompay (54). The various methods include the following:

(1) A marching technique (Coste et al (55)) was used from Z=L to Z=0, using a Runge-Kutta-Gill algorithm. There is an inherent instability in going from Z=0 to Z=L; for their system, they showed that a change of a single unit in the sixth significant figure in the inlet gradient made the solution change from large positive to large negative values. For this method, initial estimates of the value of T at Z=L are required, and various authors (eg. Marek et al,(56)) have suggested guidelines for this. Of course, the method involves trial and error and iterations so that the slopes at the boundaries are matched.

(2) Linearization of the kinetic terms, and then solving by differencing or marching (Carberry et al,(57),or Lee (58)).

(3) Solution of the dynamic equations, and using the solution at $t-\infty$ (eg. Liu,(59)). There is some question as to how many steady state solutions one can get by this method.

(4) Collocation in both Z and r (for a 2-D model) was done ((16)). According to these authors, 6 interior points in both axial and radial directions are sufficient, with the resulting nonlinear equations being solved by a Newton-Raphson technique or by Picard iteration. Puszynski et al (60) used 2 interior points for radial collocation, and 3-point finite difference approximations (150 total axial points) for Z. A Newton Raphson method with band matrix structure was used to solve the nonlinear equations. They also used the backward shooting technique for the 1-D (axial) dispersion model (no radial terms) and reported serious problems for large Peclet numbers (they used as many as 900 mesh points as did Kubicek et al (61)).

(5) Variable grid methods, as by Eigenberger and Butt (62)

(6) Orthogonal Collocation on Finite Elements (OCFE) was used

by Carey and Finlayson (63) for some other problems, but can probably be applied here too.

Almost all the methods described above were applied to situations where the axial profiles were not very steep. Even so, several authors reported complications. Raymond and Amundsen (64) required 500 space increments, and time increments of 10^{-5} to 10^{-3} secs. Every calculation required the inversion of a square matrix of order 499, and computing times ran into several hours. Other authors reported problems when Peclet numbers were large. Flaherty and O'Malley (65) deal with this problem in detail. High values of Peclet numbers imply a singularly perturbed problem, in which the highest derivatives are multiplied by small parameters. These problems typically feature boundary layers (narrow regions where the solution changes rapidly), and their numerical solution is far from trivial.

Orthogonal Collocation would seem to compare favourably with the other techniques to handle this type of equation because of some obvious advantages: there is no iteration or trial-and-error involved, and the number of points at which the discretization is done is generally much less than that required by finite differencing. An improvement can be made to global collocation such that the number of collocation points are reduced. This improvement can be best illustrated by an example problem in the next section.

7.3 APPLICATION OF ORTHOGONAL COLLOCATION TO STEEP PROFILES

Consider the first order differential equation:

$$\frac{dy}{dx} = - C_2 y + (C_2 - C_1)\exp(-C_1 x)$$

$$y(0) = 0$$

whose solution is:

$$y(x) = \exp(-C_1 x) - \exp(-C_2 x)$$

The forms of the solution, depending on the choice of the constants C_1 and C_2 are shown in Figure 7.3. As can be seen, a choice of $C_2 \gg C_1$ makes the solution more steep and the ODE more stiff.

Direct applications of orthogonal collocation to this ODE would necessarily involve using a large number of collocation points, especially if the system were stiff. However, the form of the solution suggests a modification. The fact there is a maximum may be exploited as follows:

Define λ as the location in x where dy/dx = 0.

and $\xi = x/\lambda$

$\chi = (x-\lambda)/(1-\lambda)$

The ODE for $0 < \xi < 1$ is now:

$$\frac{1}{\lambda}\frac{dy}{d\xi} = - C_2 y + (C_2 - C_1)\exp(-C_1 \lambda \xi)$$

$$y(0) = 0$$

and for $0 < \chi < 1$ we have:

$$\frac{1}{1-\lambda}\frac{dY}{d\chi} = - C_2 Y + (C_2 - C_1)\exp[-C_1\{(1-\lambda)\chi + \lambda\}]$$

$$Y(0) = y(1)$$

For continuity, we need $$\left.\frac{1}{1-\lambda}\frac{dY}{d\chi}\right|_{\chi=0} = \left.\frac{1}{\lambda}\frac{dy}{d\xi}\right|_{\xi=1}$$

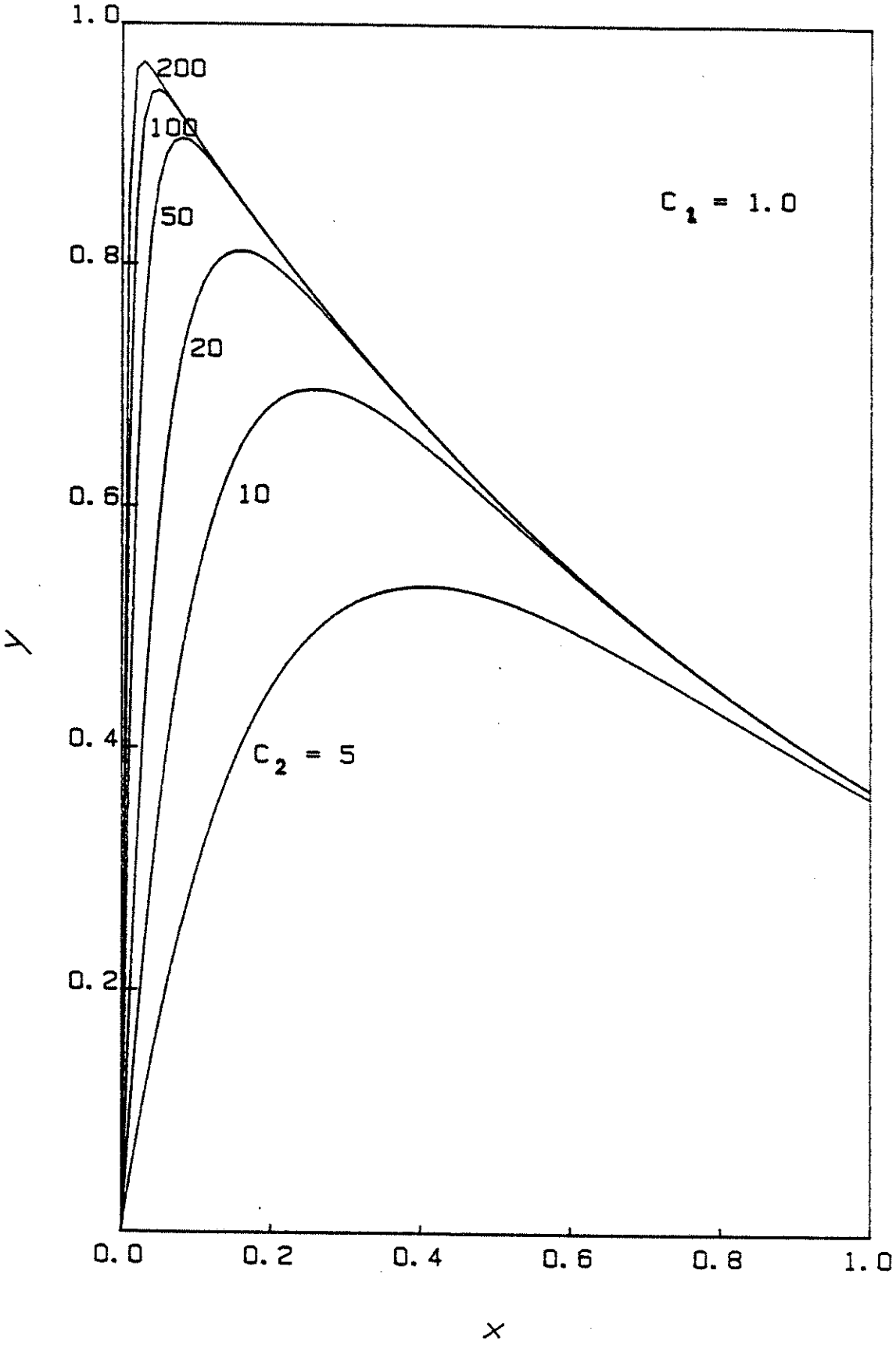

Figure 7.3 Profile variation with C_1 and C_2 for example problem

and the defining equation for λ is

$$\left.\frac{dy}{d\xi}\right|_{\xi=1} = 0$$

Now, N and M point collocation may be applied to ξ and χ respectively, yielding:

$$\frac{1}{\lambda}\sum_{1}^{N+2} A_{ij}y_j = -C_2y_i + (C_2 - C_1)\exp(-C_1\lambda\xi_i) \qquad i = 2,..,N+1$$

$$y_1 = 0$$

$$\frac{1}{(1-\lambda)}\sum_{1}^{M+2} \alpha_{ij}Y_j = -C_2Y_i + (C_2 - C_1)\exp[-C_1\{(1-\lambda)\chi_i+\lambda\}] \qquad i = 2,..,M+2$$

$$Y_1 = y_{N+2}$$

$$\sum_{1}^{N+2} A_{N+2,j}y_j = 0 = \sum_{1}^{M+2} \alpha_{1,j}Y_j$$

There are N+1+(M+1)+1+2 = N+M+5 equations to be solved for the (N+2)+(M+2)+1 = N+M+5 unknowns (y_i, Y_i and λ). In general a nonlinear equation solver would be required, but in cases like this simplifications are possible. If the value of λ is known, then this system of equations is simply a set of linear equations, and is easier to solve. Therefore, any one of the equations containing λ may be chosen as an equation to iterate on the value of λ: λ is first assumed, the remaining equations are solved, and the new value of λ is found from this equation. The process is carried on until the assumed and calculated values of λ satisfy a specified tolerance.

Figures 7.4 - 7.8 show some results. Figure 7.4 is for $C_1 = 1.0$, and $C_2 = 20.0$, resulting in a profile which is smooth. We can see that for this case, the solutions are as good with Global Collocation (GC) as with 'Adaptive Spline Collocation' (ASC), given a similar number of

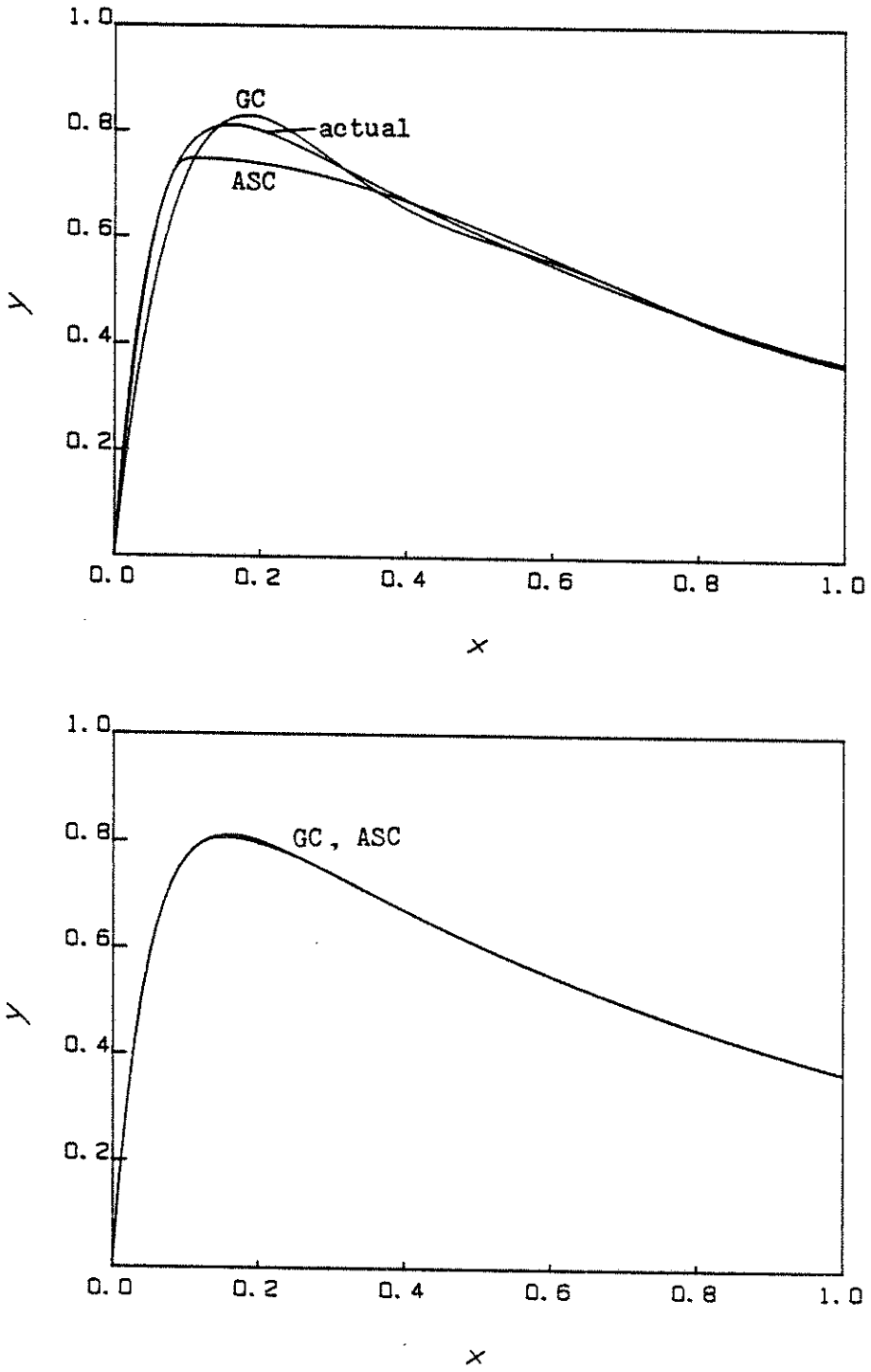

Figure 7.4 Solution comparison (C_1 = 1, C_2 = 20) (a) N = 5, N,M = 2,2 (b) N = 9, N,M = 3,5

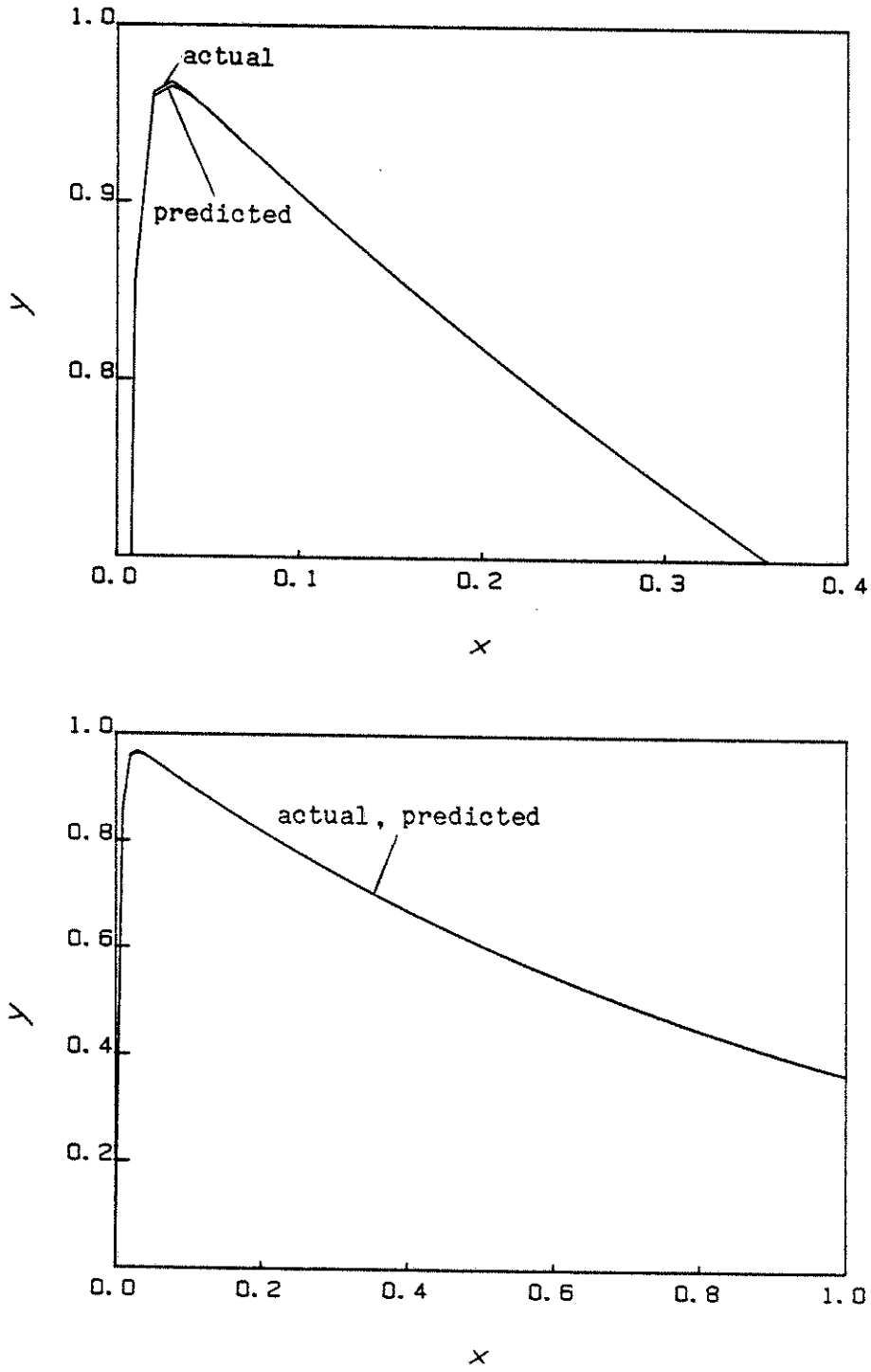

Figure 7.5 Solution comparison ($C_1 = 1$, $C_2 = 200$) with ASC method N,M = 3,14 (a) $0.0 < x < 0.4$ (b) $0.0 < x < 1.0$

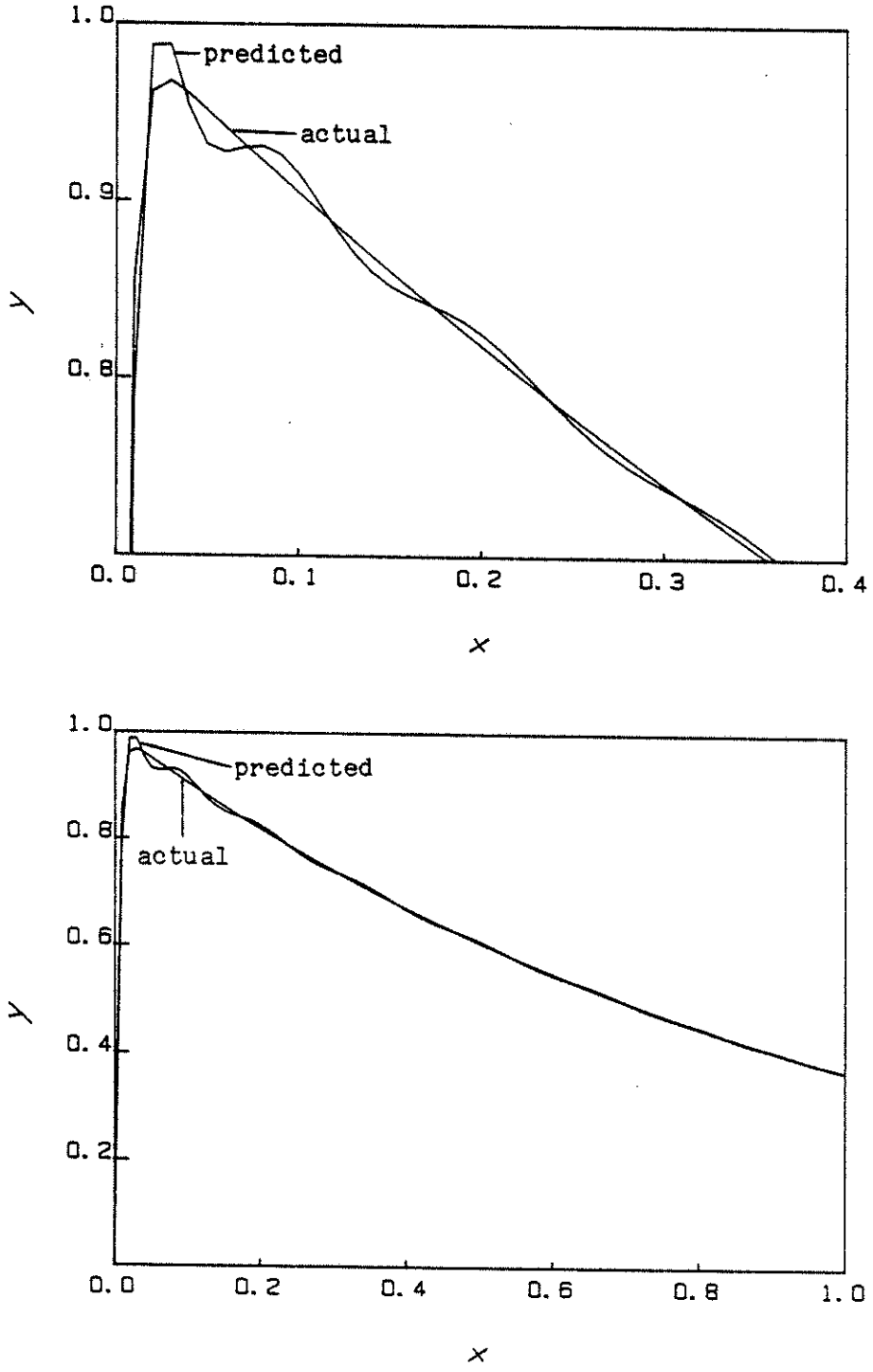

Figure 7.6 Solution comparison ($C_1 = 1$, $C_2 = 200$) with GC method N = 18 (a) $0.0 < x < 0.4$ (b) $0.0 < x < 1.0$

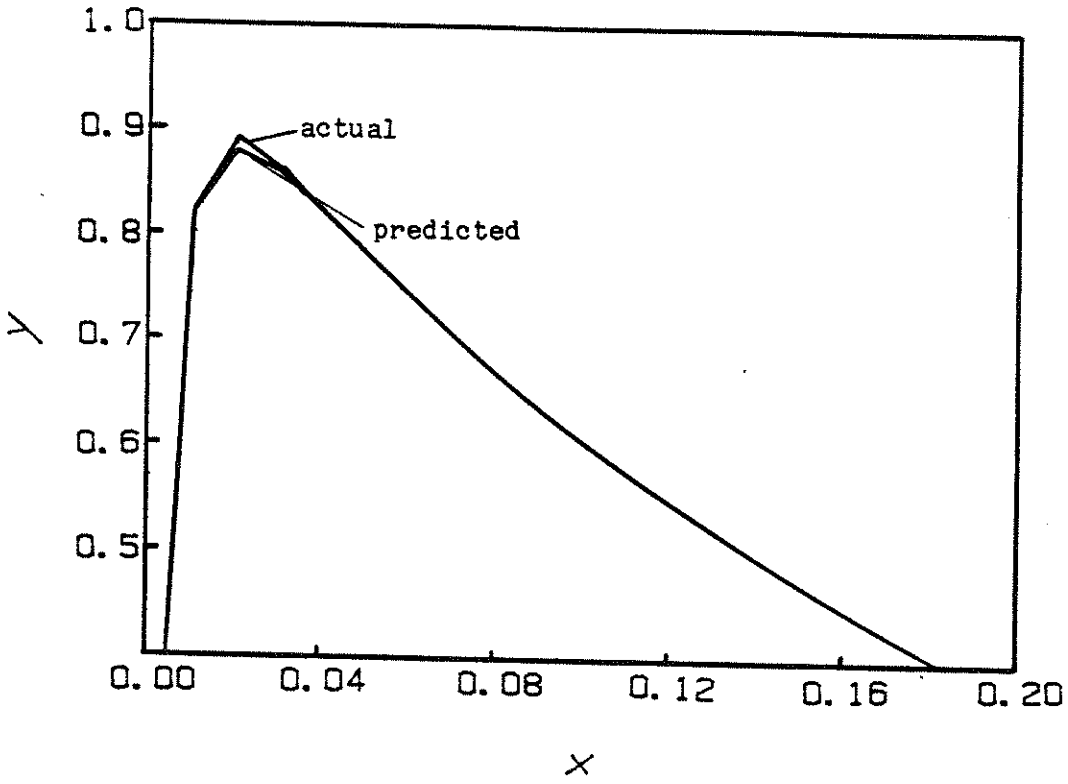

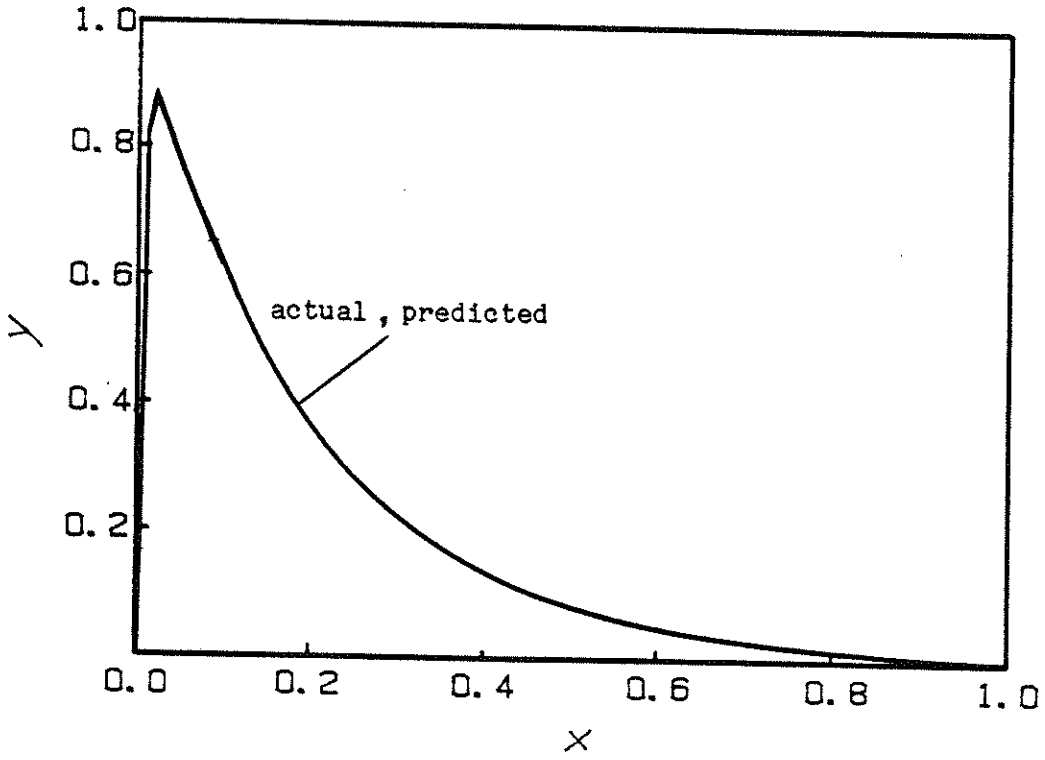

Figure 7.7 Solution comparison (C_1 = 5, C_2 = 200) with ASC method N,M = 3,14 (a) $0.0 < x < 0.2$ (b) $0.0 < x < 1.0$

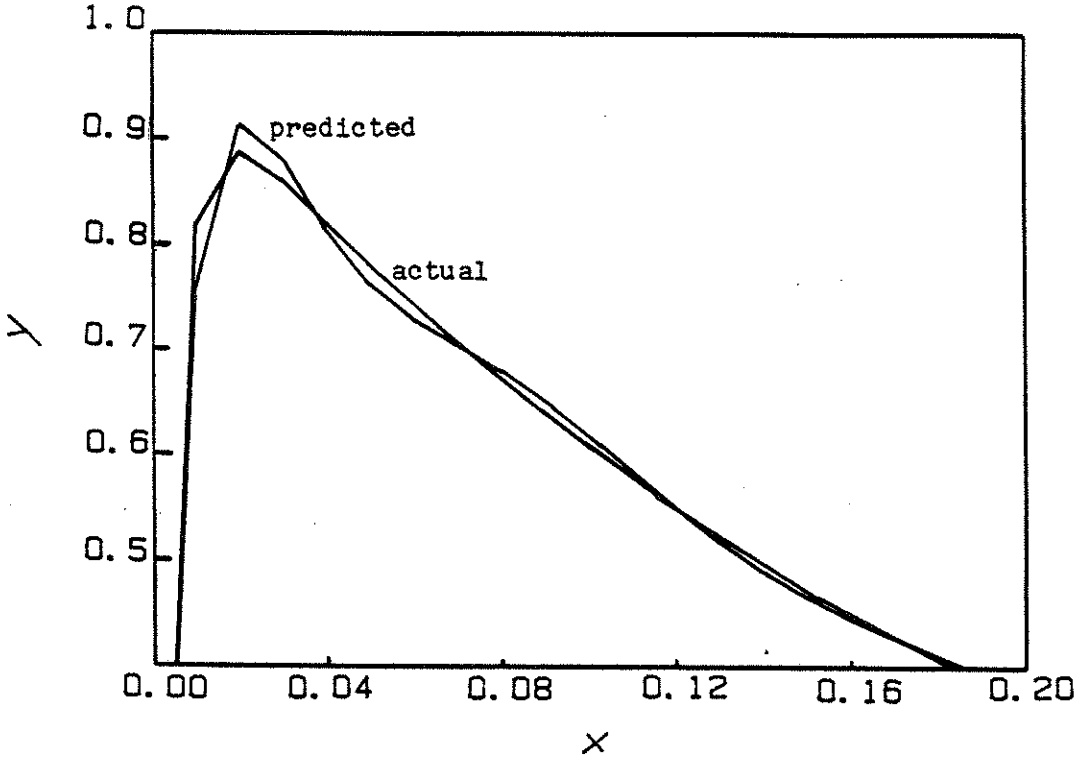

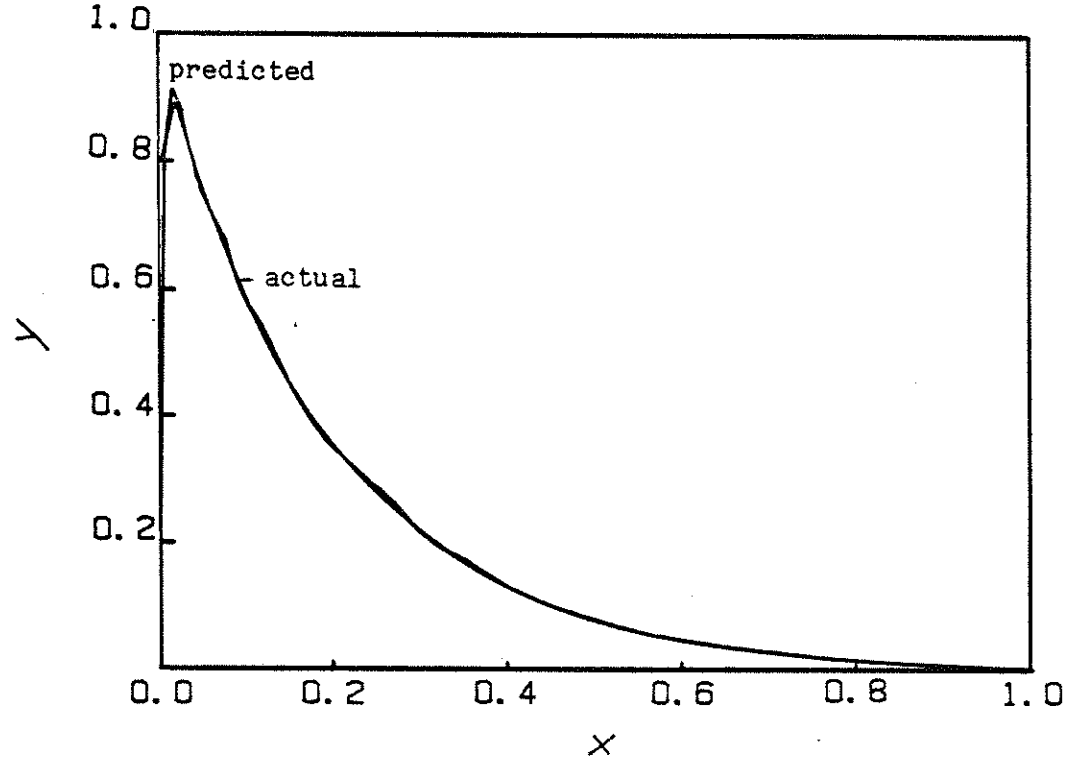

Figure 7.8 Solution comparison ($C_1 = 5$, $C_2 = 200$) with GC method N = 18 (a) $0.0 < x < 0.2$ (b) $0.0 < x < 1.0$

total collocation points. Figures 7.5 and 7.6 are for $C_1 = 1$, $C_2 = 200$, resulting in the steeper profiles. We see here that the performance of GC is not as good as ASC: with 19 internal collocation points the GC solution (Figure 7.6) shows considerable deviation from the actual solution, whereas the ASC solution is accurate. To get the level of accuracy with GC as in Figure 7.5, 27 collocation points were required, or an increase of 33 percent. Figures 7.7 and 7.8 show the same trend for a slightly different combination of C_1 and C_2 (equal to 5 and 200 respectively). In this case, 28 collocation points were required with GC to get the same level of accuracy as with 18 points with ASC.

If we consider a second order problem (having the same solution):

$$\frac{d^2y}{dx^2} = C_1^2\exp(-C_1x) - C_2^2\exp(-C_2x)$$

$$y(0) = 0$$

$$\left.\frac{dy}{dx}\right|_{x=1} = - C_1\exp(-C_1) + C_2\exp(-C_2)$$

and analysed by both methods, the improvement of ASC over GC becomes greater. Figure 7.9, plotted for $C_1 = 1$ and $C_2 = 200$, shows this effect. The level of accuracy obtained with 19 points (using ASC) can be matched with a minimum of 44 points using GC. One added advantage of ASC over GC is that the position and magnitude of the maximum is known without having to interpolate from the solution at the collocation points.

7.4 APPLICATION TO DYNAMIC PROBLEMS

We have seen that the ASC method works better for more difficult problems than the GC method. Though the solutions have not been compared with other integration methods, it would also likely be better than finite differencing methods or other marching techniques. This

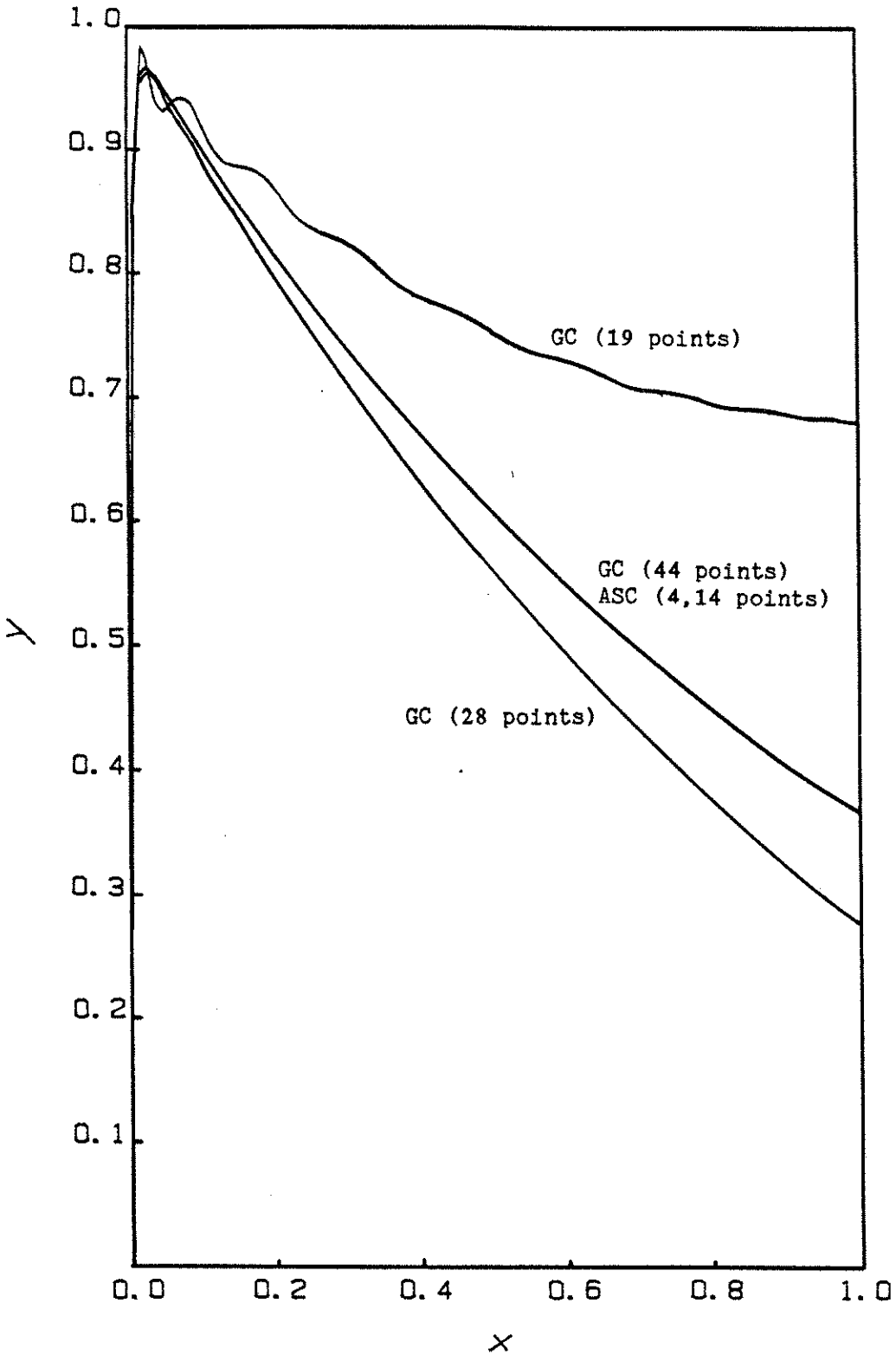

Figure 7.9 Solution comparison (C_1 = 1, C_2 = 200) for 2nd order ODE

would be especially so for the second order problem, for the same reasons that GC is better than these techniques (see Section 7.2). ASC then, seems to be a good candidate to apply to the axial dispersion problem. The difficulty, however, is the dynamic case. To solve the dynamic problem, one would have to solve a large nonlinear problem at each time step. One way to avoid this has been suggested by Ramachandran and Dudukovic (66), and is described next.

They considered the problem of transient heating of a packed bed with gas flowing in plug flow and with gas-film heat transfer as the only resistance. Assuming pseudo steady state in the gas phase, the energy balances are:

$$\frac{\partial \theta}{\partial z}_g = - St(\theta_g - \theta_s) \qquad (7.1)$$

$$\frac{\partial \theta}{\partial t}_s = \theta_g - \theta_s$$

with $z = 0, \ \theta_g = 1$

$t = 0, \ \theta_s = 0$

Defining λ as the position where $\theta_g = 0$, and the new coordinates $\xi = z/\lambda$ and $\tau = t$, the equations can be written as:

$$\frac{\partial \theta}{\partial \xi}_g = - St\lambda(\theta_g - \theta_s) \qquad (7.2)$$

$$\frac{\partial \theta}{\partial \tau}_s - \frac{z}{\lambda}\left(\frac{d\lambda}{d\tau}\right)\frac{\partial \theta}{\partial \xi}_s = \theta_g - \theta_s$$

with $\xi = 0, \ \theta_g = 1$

$\tau = 0, \ \theta_s = 0$

the equation for λ is $\partial \theta_g / \partial \xi \big|_{\xi=1} = 0$

Collocation in ξ can now be applied to equation 7.2, and the system of equations converted to a set of IVPs in τ. Therefore, no nonlinear solver is required.

Results for a similar situation, but for countercurrent moving bed

are shown in Figure 7.10. The equations are the same as equation 7.1, with the addition of a flux term ($-C\partial\Theta_s/\partial z$) to the left hand side of the solid energy balance. In this case, C was chosen as 0.1 and St as 20. The step change given was to the flow of solid, which was increased by 25 percent (resulting in C = 0.125). The temperature profiles move to a new steady state location consistent with the correct solution. In general, the method works well.

The method was also applied to a fixed bed catalytic reactor problem, whose governing equations are:

$$\frac{\partial X}{\partial \tau} = \gamma \frac{\partial^2 X}{\partial z^2} - \frac{\partial X}{\partial z} + \beta r$$

$$\frac{\partial T}{\partial \tau} = \gamma' \frac{\partial^2 T}{\partial z^2} - \frac{\partial T}{\partial z} + \beta' r - \alpha' T$$

$$z = 0, \quad \gamma \frac{\partial X}{\partial z} = X \quad \text{and} \quad \gamma' \frac{\partial T}{\partial z} = T - 1$$

$$z = 1, \quad \gamma \frac{\partial X}{\partial z} = 0 \quad \text{and} \quad \gamma' \frac{\partial T}{\partial z} = 0$$

Parameter values used for this system are given in Table 7.1. The reaction rate expression was assumed to be of a first order type. The condition for λ was now chosen to be $dx/dz = \varepsilon$ (= 0.005). This problem is more difficult to solve because the region $\lambda < z < 1$ has also to be considered, unlike the previous problem. The definition of λ however, makes it possible to neglect the material balance for $\lambda < z < 1$.

Figure 7.11 shows the movement of the two profiles when the inlet temperature is increased from 465 K to 475 K and then to 485 K. The method worked well for changes of reasonable magnitude. If temperatures were increased by 20 K, problems occurred because of the rapid shift in the position of λ. This shift caused the $d\lambda/dt$ term to be large,

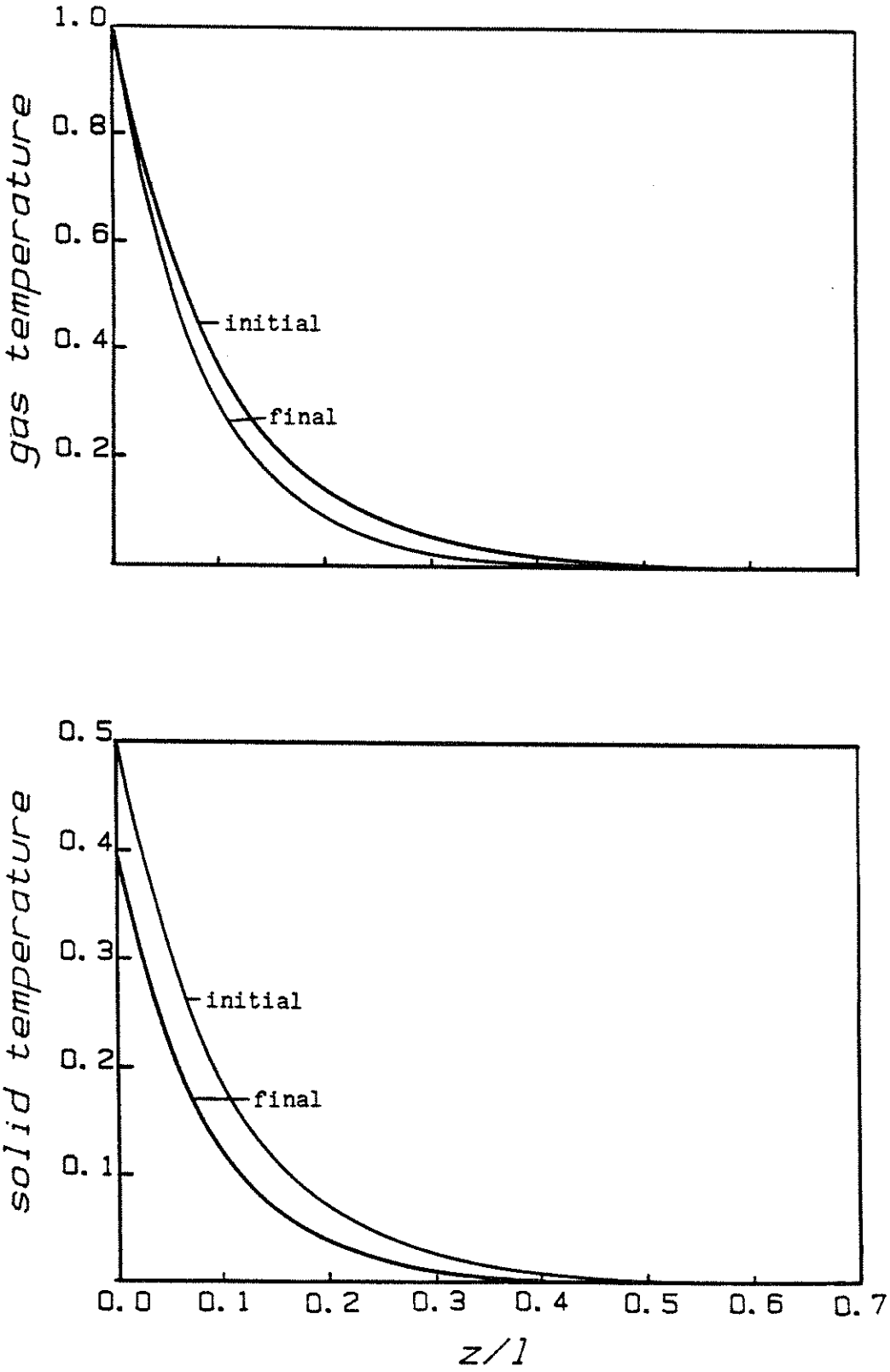

Figure 7.10 Transient heating of a moving bed (a) Gas temperature profiles (b) Solid temperature profiles

TABLE 7.1

Parameters for Catalytic Reactor Problem

α'	0.3
β	10.0
β'	$1000/(T_o - T_s)$
γ	0.001
γ'	0.001
T_s	300

$$r = 8.75\ 10^8 \exp(-10000/8314\ T)$$

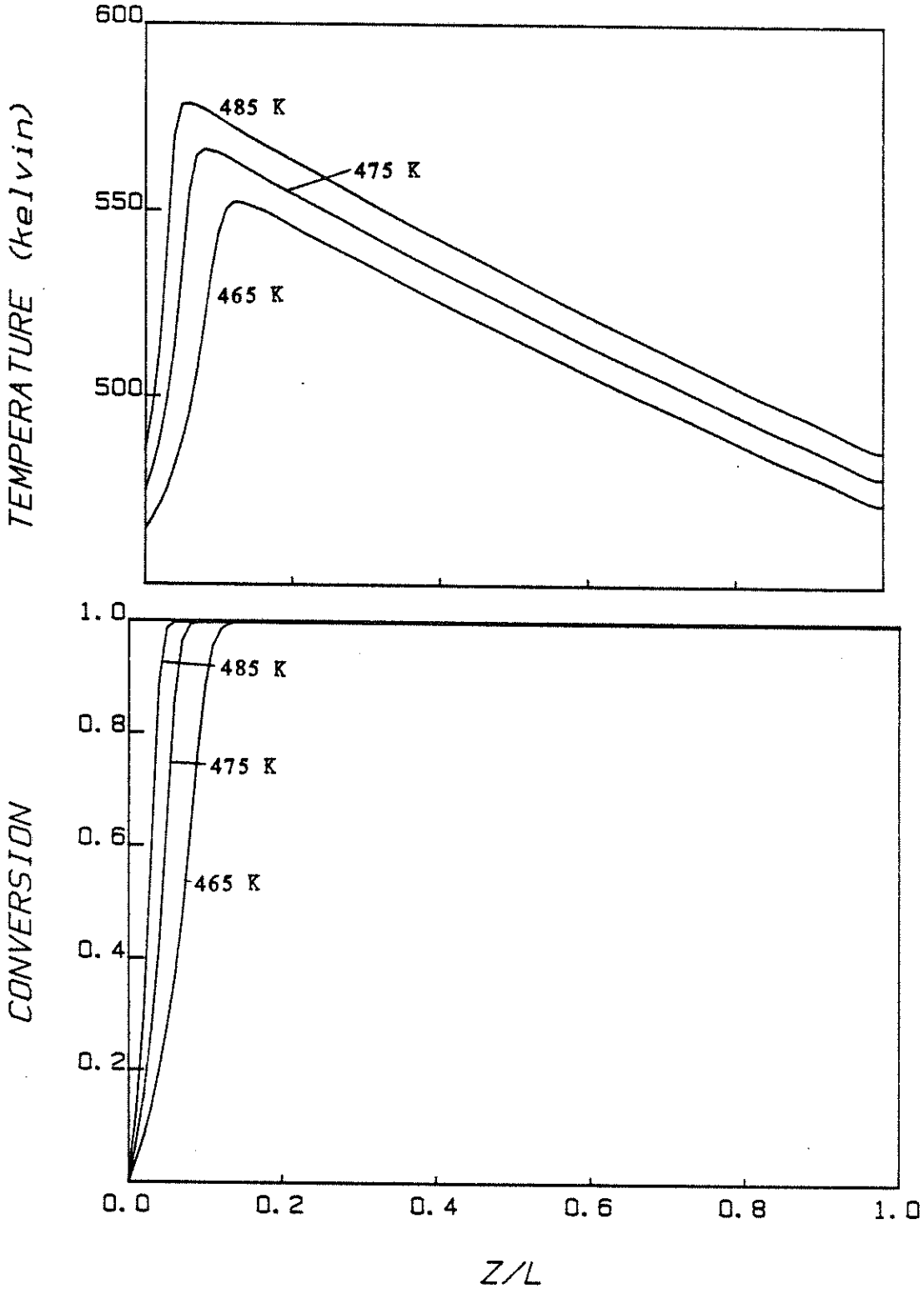

Figure 7.11 Dynamic profiles for fixed bed catalytic reactor problem (T = 465, 475 485 K) (a) Temperature (b) Conversion

resulting in instability.

7.5 EFFECT OF AXIAL DISPERSION ON THE TEMPERATURE PROFILE IN A GAS - SOLID REACTOR.

The method used in the previous section has been shown to be fairly versatile, and can presumably be applied toward solving the equations for a gas-solid reactor. The system chosen was the same as described in Chapter 6 (Section 6.3), but with the axial dispersion term added. The kind of creeping profiles expected (see Figure 6.6) can be handled by the ASC method. The intention in this Section is to see whether inclusion of the axial dispersion term affects the temperature profiles substantially.

The defining equation for λ was taken to be $dT/dz = 0$. 15 internal collocation points were used in the region $0 < z < \lambda$, and 10 in the region $\lambda < z < 1$. The energy balance equations now become:

$0 < Z < 1 \qquad (Z = z/l)$:

$$\frac{\partial\theta}{\partial\tau} - \frac{Z}{\lambda}\left(\frac{d\lambda}{d\tau}\right)\frac{\partial\theta}{\partial Z} = \frac{\alpha}{L^2\lambda^2}\frac{\partial^2\theta}{\partial Z^2} - \frac{\beta}{L\lambda}\frac{\partial\theta}{\partial Z} - \gamma\theta + \delta r$$

$$\frac{\partial x}{\partial\tau} - \frac{Z}{\lambda}\left(\frac{d\lambda}{d\tau}\right)\frac{\partial x}{\partial Z} = -\frac{v}{L\lambda}\frac{\partial x}{\partial Z} + \mu T_o r$$

$0 < Y < 1 \qquad (Y = (z-\lambda)/(1-\lambda))$:

$$\frac{\partial\theta}{\partial\tau} - \frac{(1-Y)}{(1-\lambda)}\left(\frac{d\lambda}{d\tau}\right)\frac{\partial\theta}{\partial Y} = \frac{\alpha}{L^2(1-\lambda)^2}\frac{\partial^2\theta}{\partial Y^2} - \frac{\beta}{L\lambda}\frac{\partial\theta}{\partial Y} - \gamma\theta + \delta r$$

$$\frac{\partial x}{\partial\tau} - \frac{(1-Y)}{(1-\lambda)}\left(\frac{d\lambda}{d\tau}\right)\frac{\partial x}{\partial Y} = -\frac{v}{L\lambda}\frac{\partial x}{\partial Y} + \mu T_o r$$

There are some minor problems associated with applying the ASC method with the condition $dT/dz = 0$. To use the ASC method, an initial solution is required. The only way to get this initial solution is for some other integration method to be applied for some time until a profile develops which has a significant numerical value for λ (this will be explained further later). One simplification may be made which

avoids the problem. In looking at the original problem (Section 6.3), we can see that the time derivatives of the energy balance and gas-phase material balance will both be much larger in magnitude than the solid material balance. Since the faster modes may be assumed to be in steady state when compared with the slower modes, these derivatives may be set to zero (the logic is the same as that used to make the PSSA for catalytic reactor problems). Therefore, a 'steady state' initial profile may be found corresponding to a solid conversion profile of zero over the entire length of the reactor.

The other problem arises because of the method of solution. If a simple problem is thought of :

$$\frac{dy}{dx}1 = g_1(\lambda)\ f_1(y_1,y_2), \qquad g_1(\lambda) \propto \frac{1}{\lambda^2}$$

$$\frac{dy}{dx}2 = g_2(\lambda)\ f_2(y_1,y_2), \qquad g_2(\lambda) \propto \frac{1}{(1-\lambda)^2}$$

$$\text{with } y_1(0) = y_{10};\ y_2(0) = y_{20}$$

then the eigenvalues of the system vary as $\lambda^2/(1-\lambda)^2$. The closer this ratio is to 1.0, the easier the system is to solve, and the further from 1.0, the stiffer the system becomes. The ratio then, is an indication of the stiffness of the problem, and both small and large values of λ causes difficulties. Since the ASC method introduces $1/\lambda^2$ and $1/(1-\lambda)^2$ terms, an artificial stiffness is introduced. At low or high λ, the system of ODEs becomes difficult to solve. For the system of Section 6.3, the initial value of λ was not too low, so cpu times were not exorbitant. It is suggested that if the situation does arise, then the PSSA argument may be used to convert that particular set of ODEs having the fastest modes into nonlinear algebraic equations (by setting the time derivatives equal to zero). So at small λ, equation 7.3a would

have its left hand side equal to zero, and at large λ equation 7.3c would have its left hand side equal to zero.

The results of the simulation are shown in Figures 7.12 and 7.13. Comparison of the temperature profiles (Figure 7.12) with the temperature profiles of Figure 6.6 show that the current maxima are indeed lower than the previous ones, though marginally so. The trend of lower maxima at larger times is also repeated, as is the trend of incomplete solid conversion. The major reason for the decreasing maxima remains the same as before: the changing solid conversion profile (Figure 7.13). The effect of the dispersion term is not major. Changing the axial thermal conductivity or other parameters of the problem may change this conclusion somewhat. It should be noted that all parameters were chosen such that the system was operating at similar conditions as in the gasifier.

7.6 AXIAL DISPERSION WITH CHANGE IN BED LENGTH

If a change in bed length is accounted for by linking the current length to the solid conversion by a linear relationship of the type

$$L_n = [a + b(1 - X_n)]L_{n-1}$$

the results turn out to be contrary to what is expected. Since the length decreases substantially with time, it is presumed that the relative magnitude of the dispersion term (which varies inversely with L^2) should increase, when compared with the other terms of the energy balance. This should therefore decrease the maximum temperature values reached at each time. However, another factor appears which opposes this. At every time step, the solid conversion profile has to be recalculated so that the collapse in the bed is confined to the area where the reaction is taking place (that is, at the reaction front). As

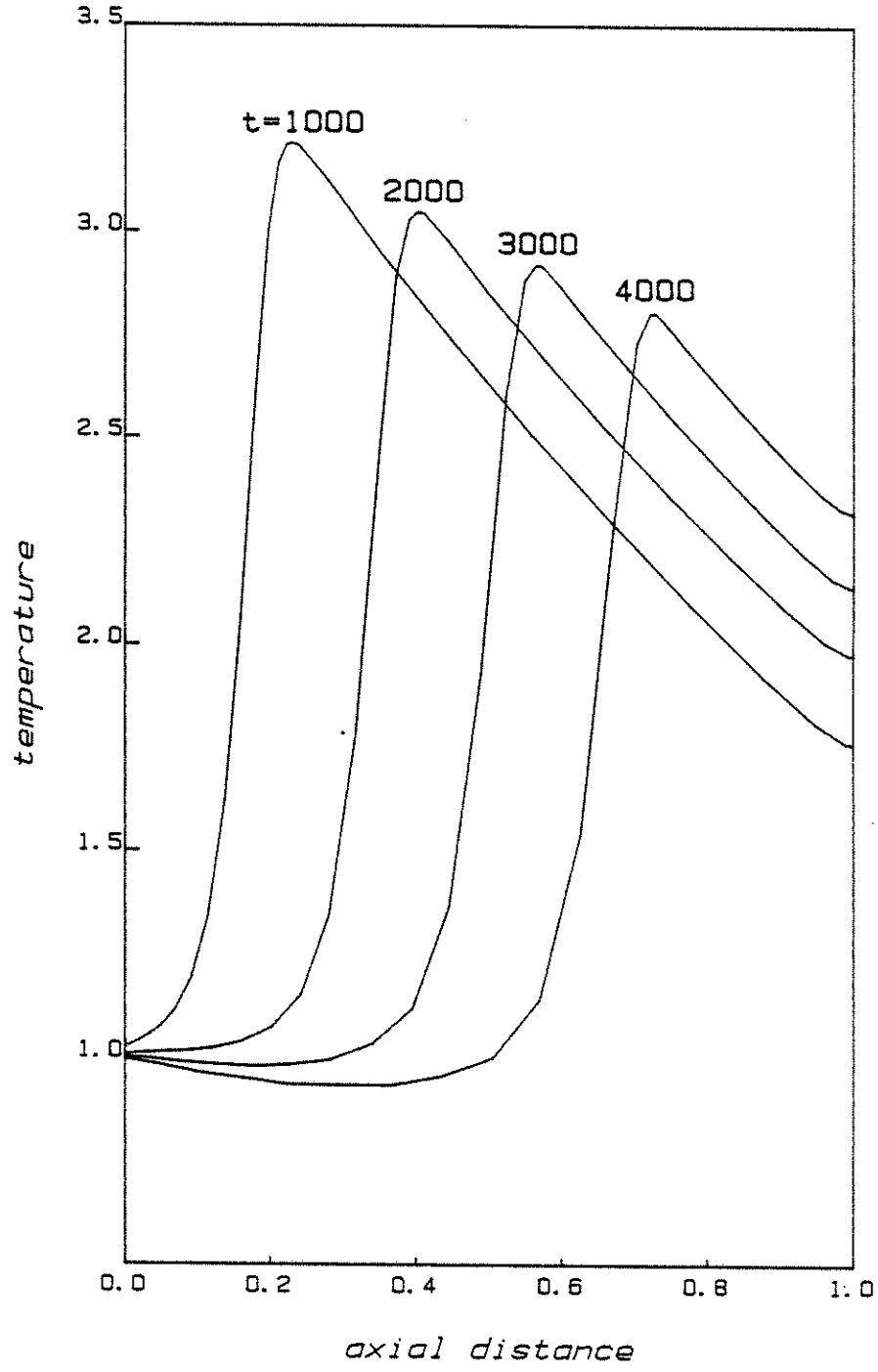

Figure 7.12 Temperature profiles at various times for dispersion problem

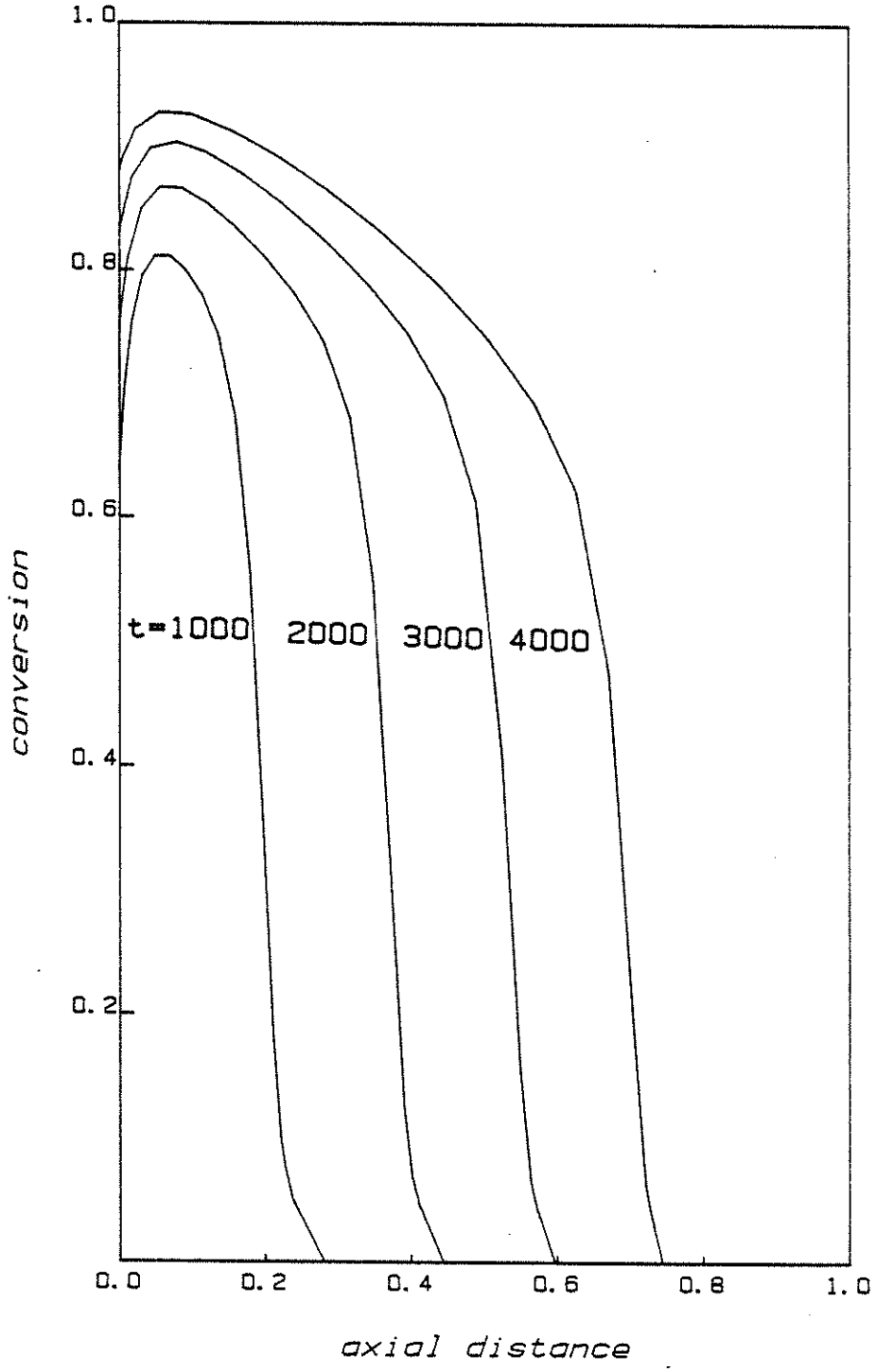

Figure 7.13 Solid conversion profiles for dispersion problem

a result, the entering gas now 'sees' a smaller region of comparably-converted solid as opposed to the case when the length did not change, resulting in lower gas conversions at the point of contact with the front. This results in higher temperature maxima than before (see Figure 7.14, and compare with Figure 7.12). We can see that in Figure 7.14 (the current case), the temperature maxima at the same times have greater magnitudes than those in Figure 7.12 (which is the plot for the case when no change in bed length is considered). Figure 7.15 shows the same profiles as in Figure 7.14, plotted on a scale which shows the change in bed length: that is, the exit of the reactor is kept fixed at a constant position, resulting in the inlet changing position with time.

These plots show that the lowering of the temperature maxima is mainly caused by the changing solid conversion profiles, which are actually controlled by the reaction rate expressions. Axial dispersion does not seem to play a major role. The decreasing bed length, instead of lowering the maxima as expected, tends to raise them. Again, the reason is the form of the solid conversion profile. In the gasifier too, these trends are expected to hold because the operating conditions in the example problem are similar to those in the gasifier.

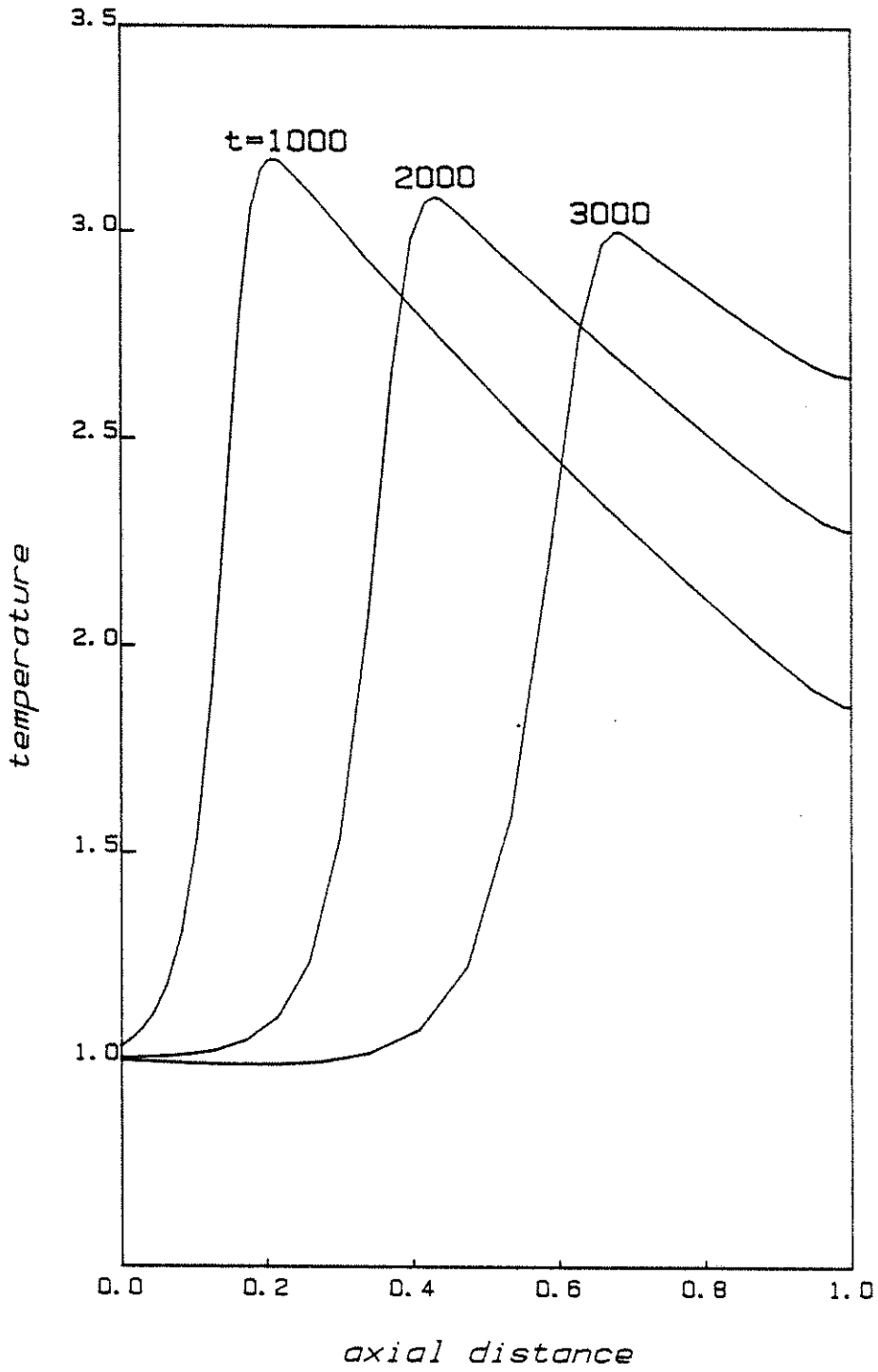

Figure 7.14 Temperature profiles at various times for changing bed length problem

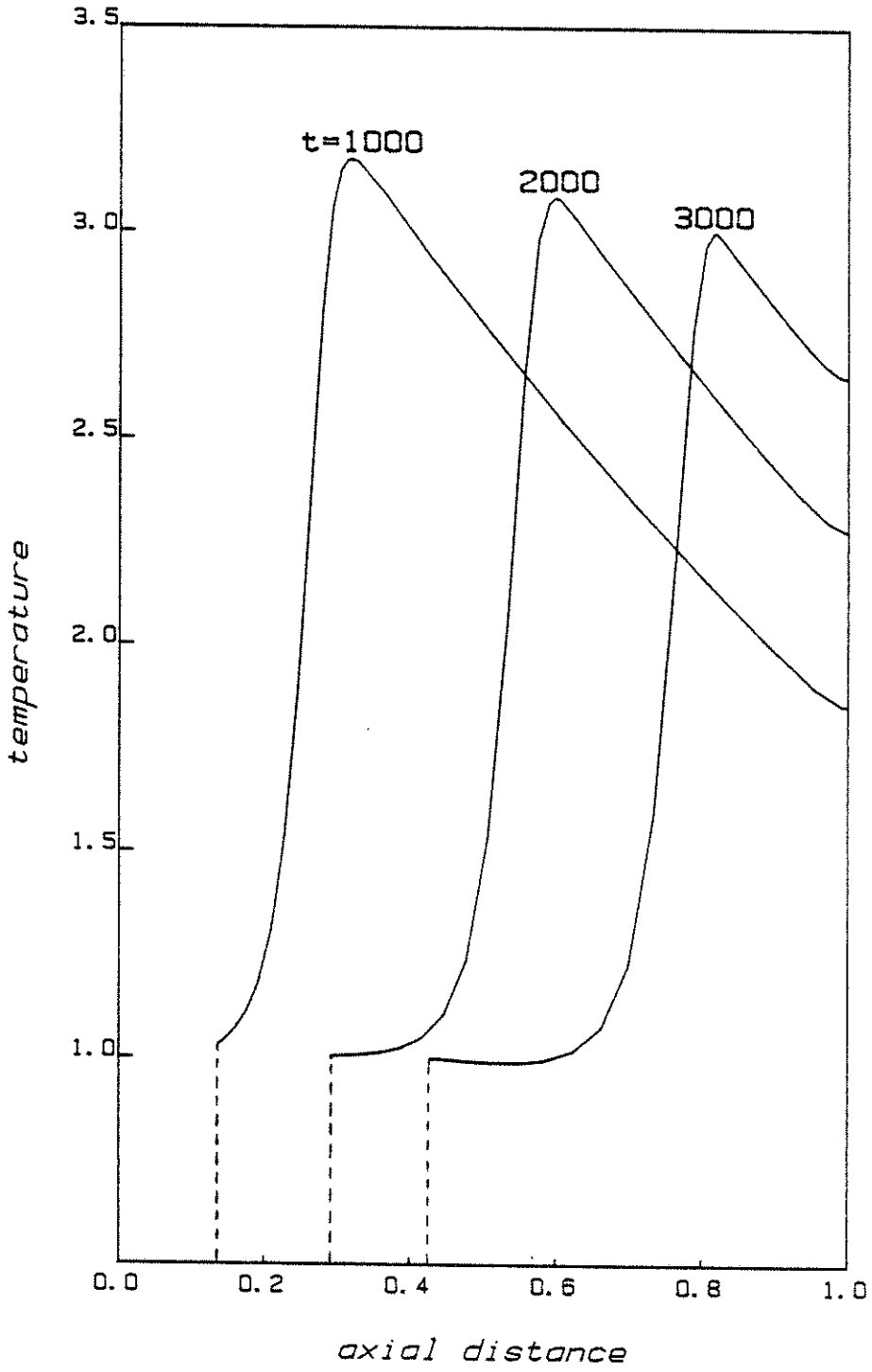

Figure 7.15 Temperature profiles at various times for changing bed length problem: axial coordinate reflects actual positions

8. APPLICATIONS TO MOVING BEDS

As mentioned elsewhere, the ultimate objective of the gasifier model is to have it applied to industrial situations. Since fixed bed models are inapplicable here, moving bed models have to be built. The model of a fixed bed gasifier with a char load is the same as that of a moving bed reactor with coal in which the coal feed has been abruptly turned off. Extension of the fixed bed model to the general moving bed case is therefore a simple matter.

The actual governing equations for a moving bed gasifier can be found elsewhere (eg., (7)). The difference between the two cases (fixed and moving beds) is that one more term is introduced into the solid material balance and the energy balance, corresponding to the solid flux terms. The method of solution of the PDEs remains the same. The char conversion profiles are updated with a slight amount of extra effort: since finite differencing is used on the $\partial F/\partial Z$ in the solid material balance, the THOMAS algorithm is used.

Some results have been obtained for the Lurgi gasifier. The operating conditions, reactor dimensions etc. are reported in Table 8.1. Two simulation studies were carried out: one for startup, and one for the change in steady states which resulted because of a disturbance in the inlet char feed rate. Other disturbances, like changes in inlet gas flow rates or composition can also be accommodated.

8.1 STARTUP OF A MOVING BED

Figures 8.1 through 8.6 show the dynamic profiles for startup, the eventual steady states being reached for the conditions of Table 8.1. The time taken to reach steady state is approximately 28 hours. Figures

TABLE 8.1

Operating Conditions and Feed Conditions
Used in Lurgi Gasifiers

System pressure	2533 KPa (25 atm)
Blast temperature	644 K
Temperature of cooling water	496 K
Wall heat transfer coefficient	340 kJ/m²-hr-K
Height of gasifier	3.0 m
Diameter of gasifier	3.7 m
Average particle diameter	0.01 m

Feed rates:

Steam	1275 kgmol/hr
Oxygen	187.5 kgmol/hr
Nitrogen	0 kgmol/hr
Char	725 kgmol/hr

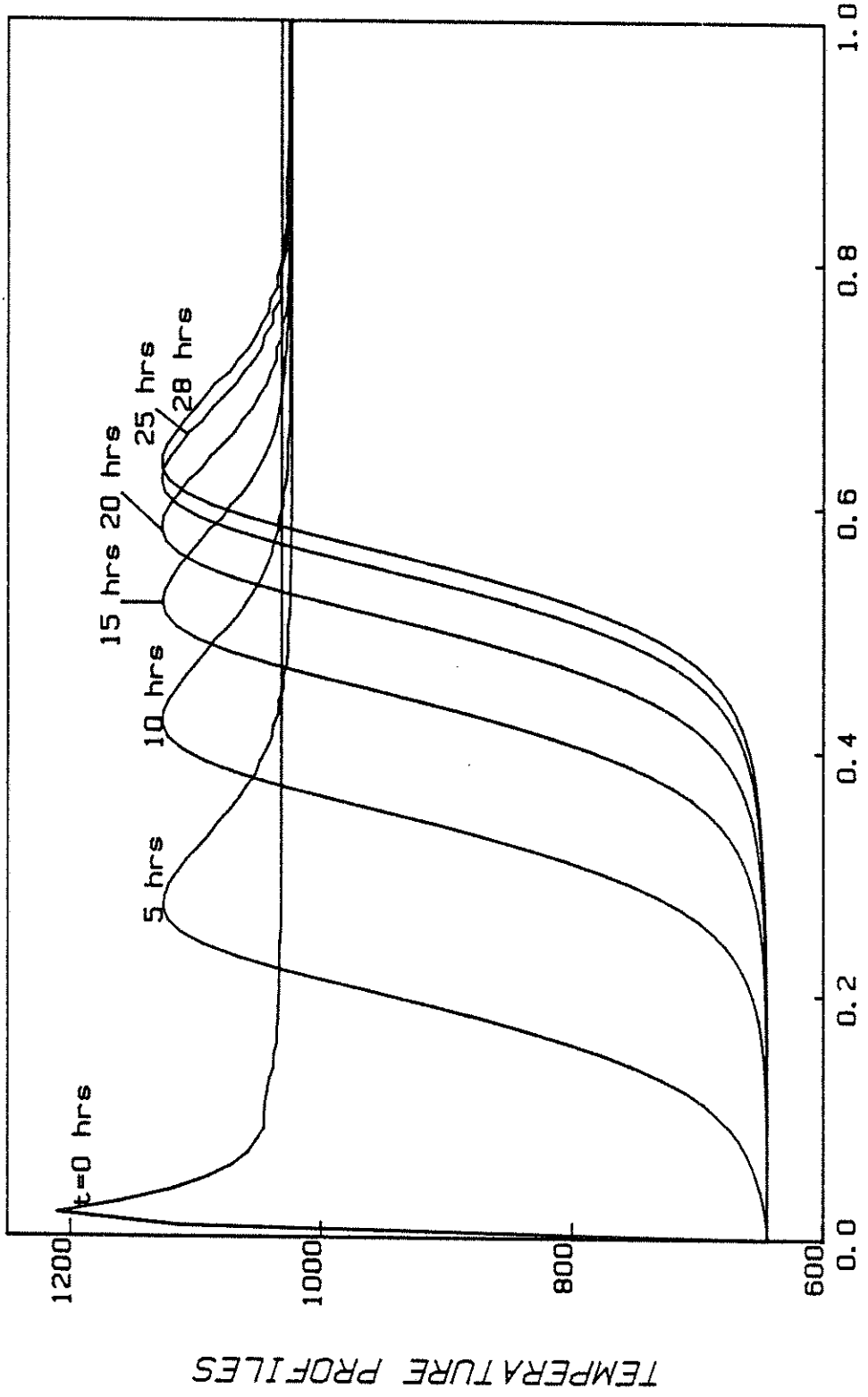

Figure 8.1 Dynamic temperature profiles for startup, inner coll. point

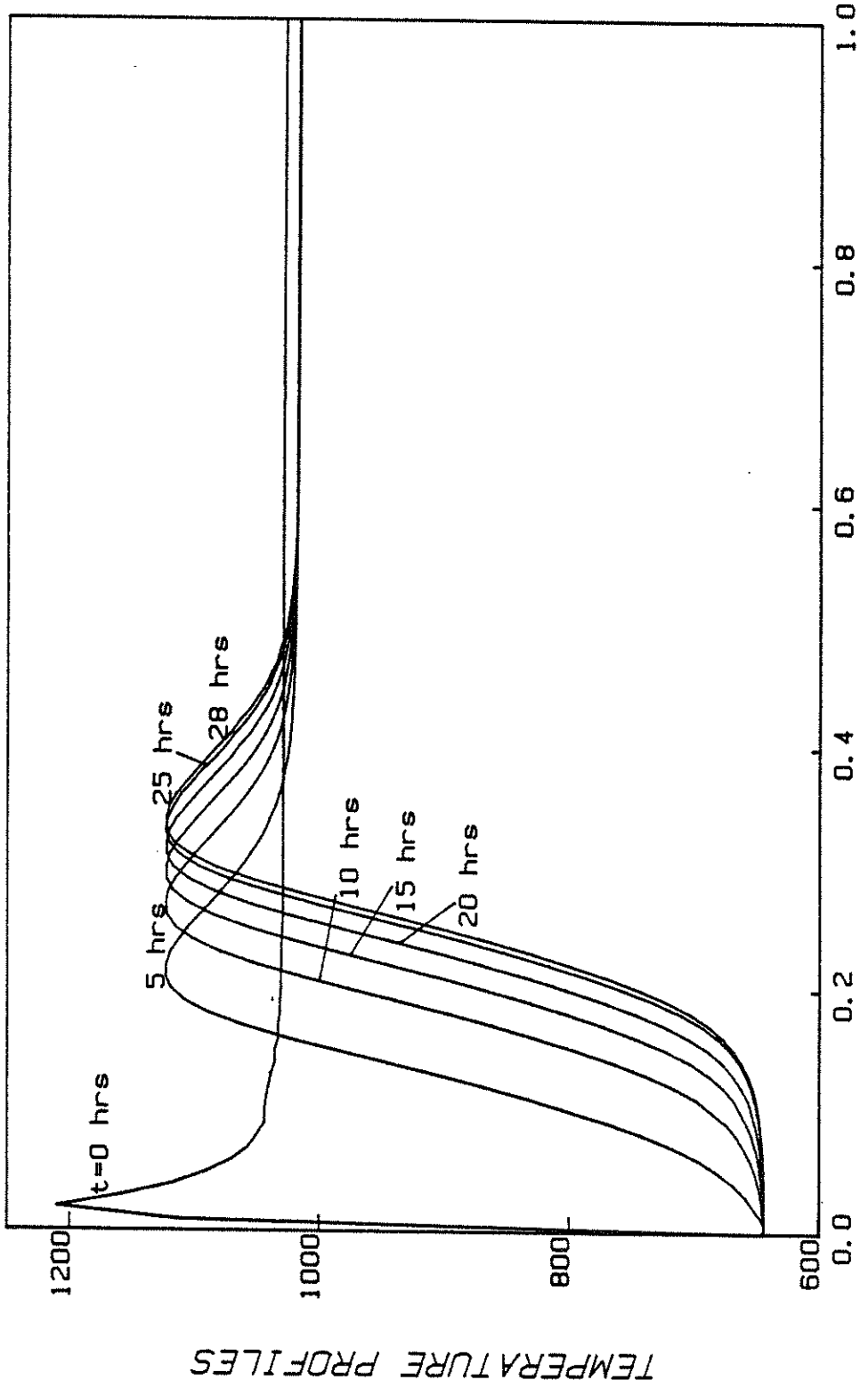

Figure 8.2 Dynamic temperature profiles for startup, outer coll. point

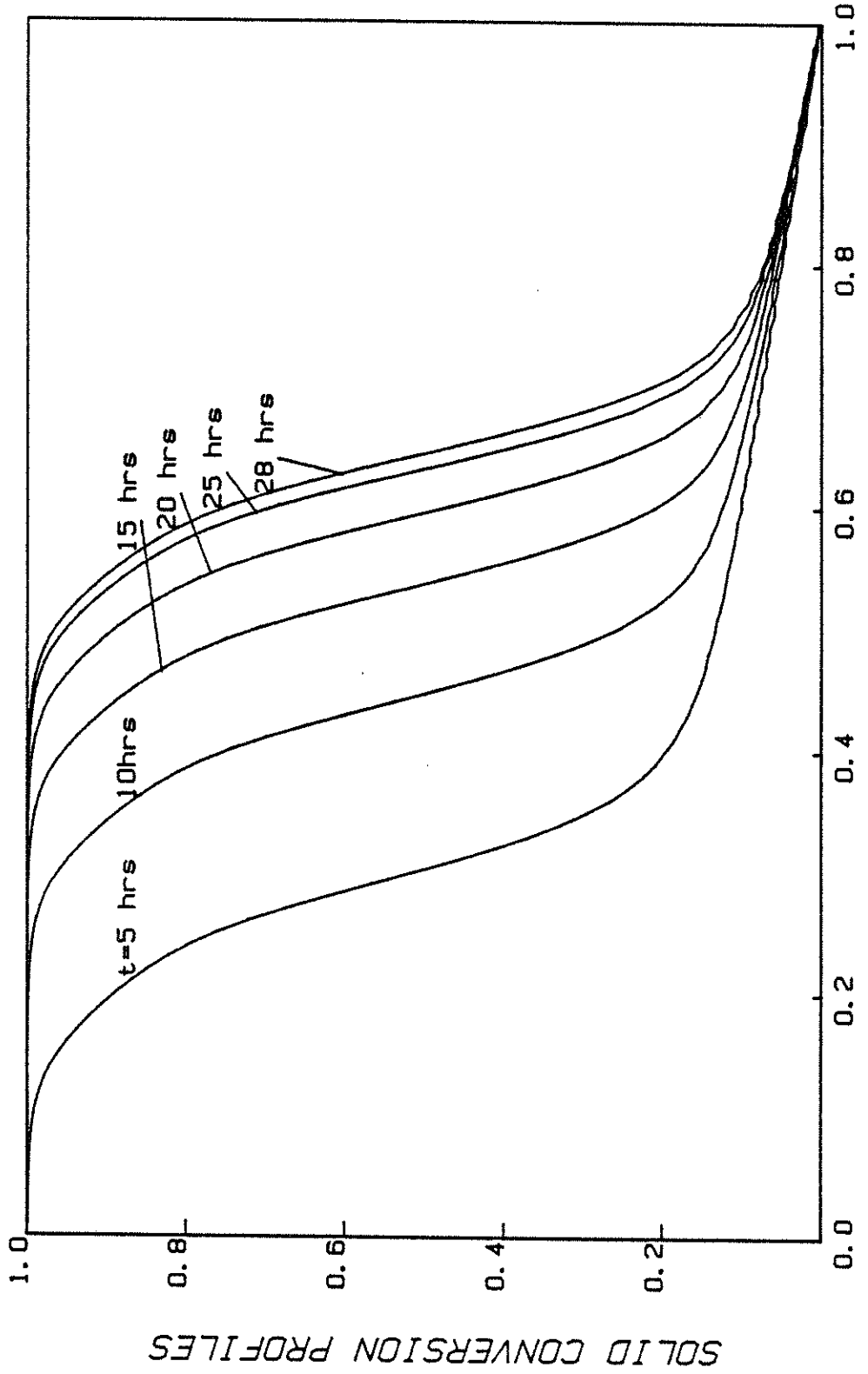

Figure 8.3 Dynamic solid conv. profiles for startup, inner coll. point

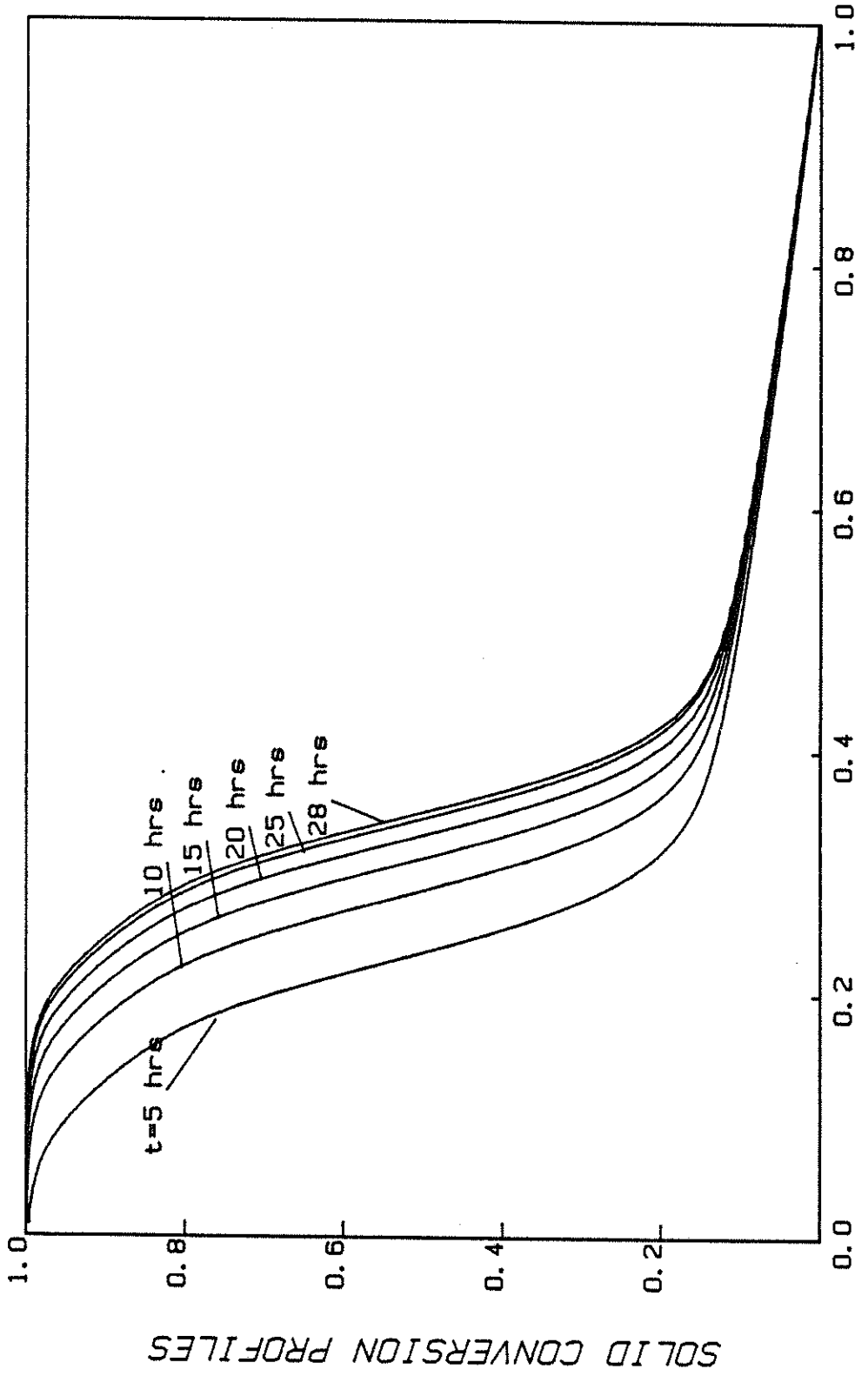

Figure 8.4 Dynamic solid conv. profiles for startup, outer coll. point

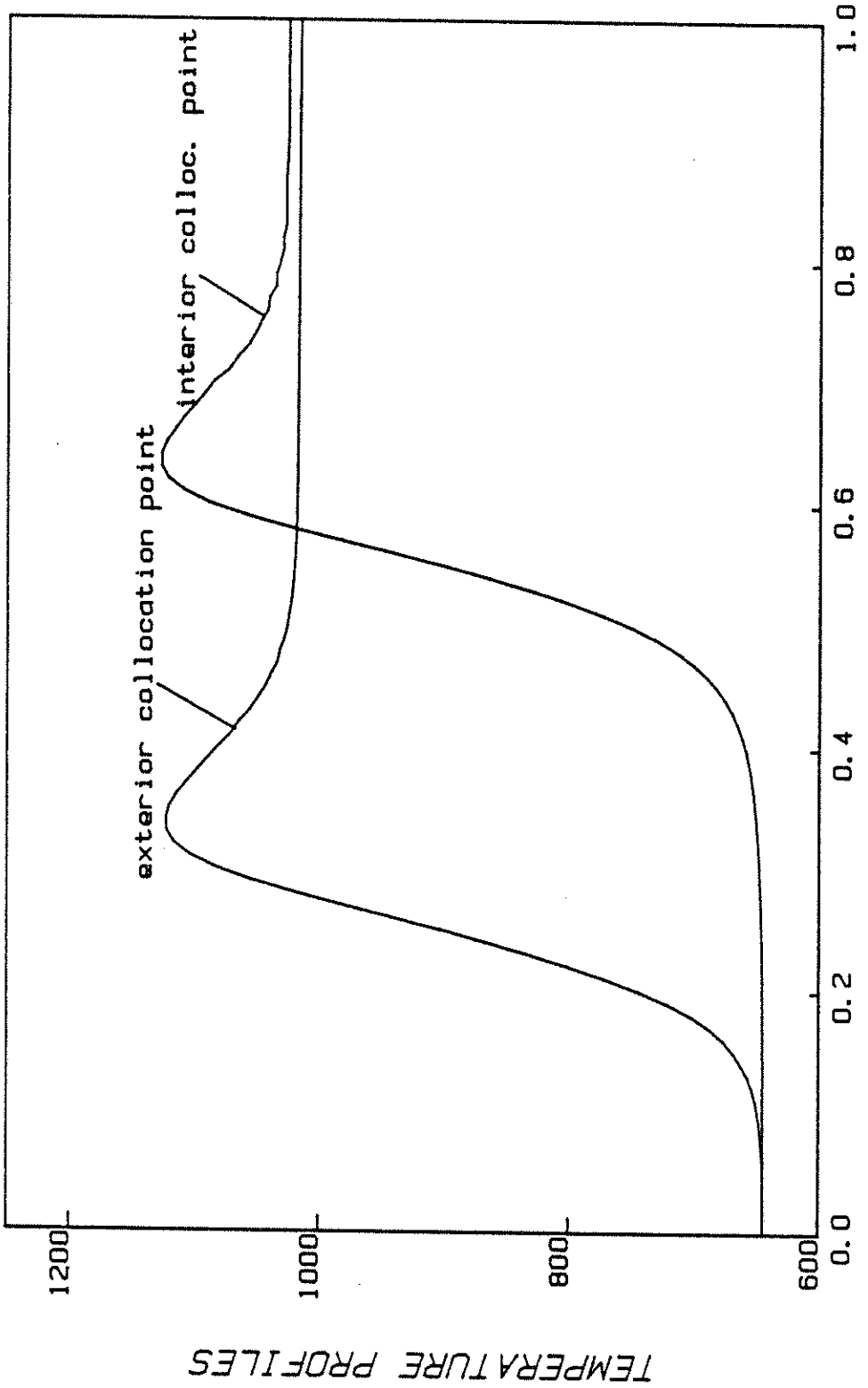

Figure 8.5 Final steady state temperature profiles, after startup

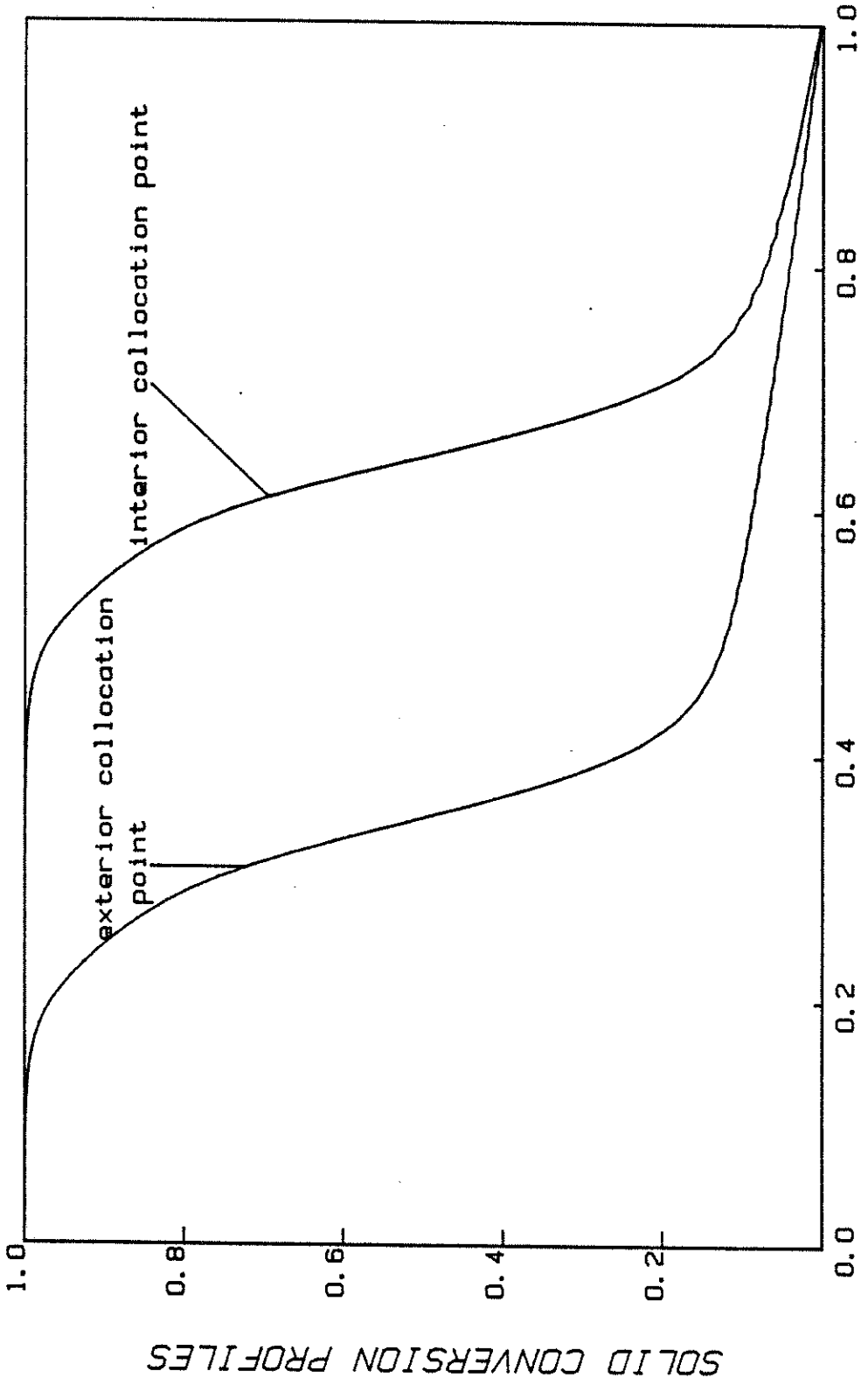

Figure 8.6 Final steady state solid conversion profiles, after startup

8.1 to 8.4 show the dynamic effects very well: the first two are the temperatures for the two radial collocation points, and the latter two are the corresponding solid conversion profiles. Figures 8.5 and 8.6 show the large radial effects on the final steady state. Figure 8.6 in particular, shows graphically the deterioration of gasifier performance with increasing radial position: the solid conversion profile is much lower near the wall.

8.2 STEP CHANGE TO CHAR FLOW

Figures 8.7 to 8.10 are some of the results of the simulation run for the case when a positive disturbance of 25 kgmol/hr was given to the steady state at 725 kgmol/hr. The time taken to reach the new steady state was roughly 15 hours in this case, and the three sets of lines for each radial collocation point in each of these figures show the profiles at the initial steady state, after 7.5 hours, and at the final steady state. The increase in the solid flow tends to push the profiles from right to left (since the solids enter from the right and the gases from the left), with the larger change being in the exterior location. Table 8.2 shows the outlet compositions of the product gas at the two steady states, and compares these results with the results of other workers. The major differences are in the figures for methane production in the first two cases, in which the numbers are somewhat low. However, this is explained by the fact that the devolatization process (in which a major portion of the methane is produced) has not been included in the current model. The last two rows give numbers for these same two cases in which estimates of the devolatization products have been added, and the methane values show much closer agreement. The other compositions are also reasonably close to the reported values.

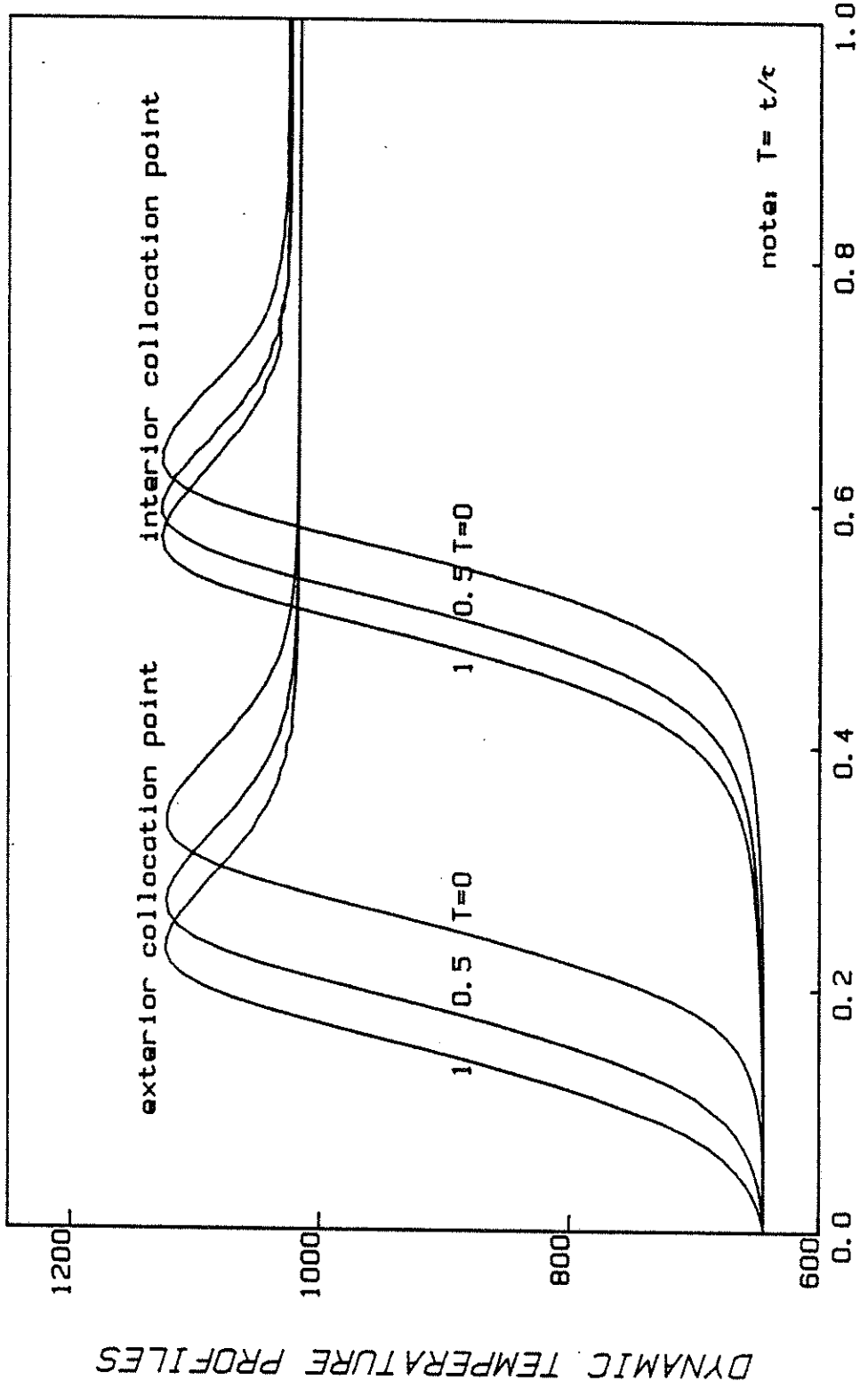

Figure 8.7 Dynamic temperature profiles for increase in char flow

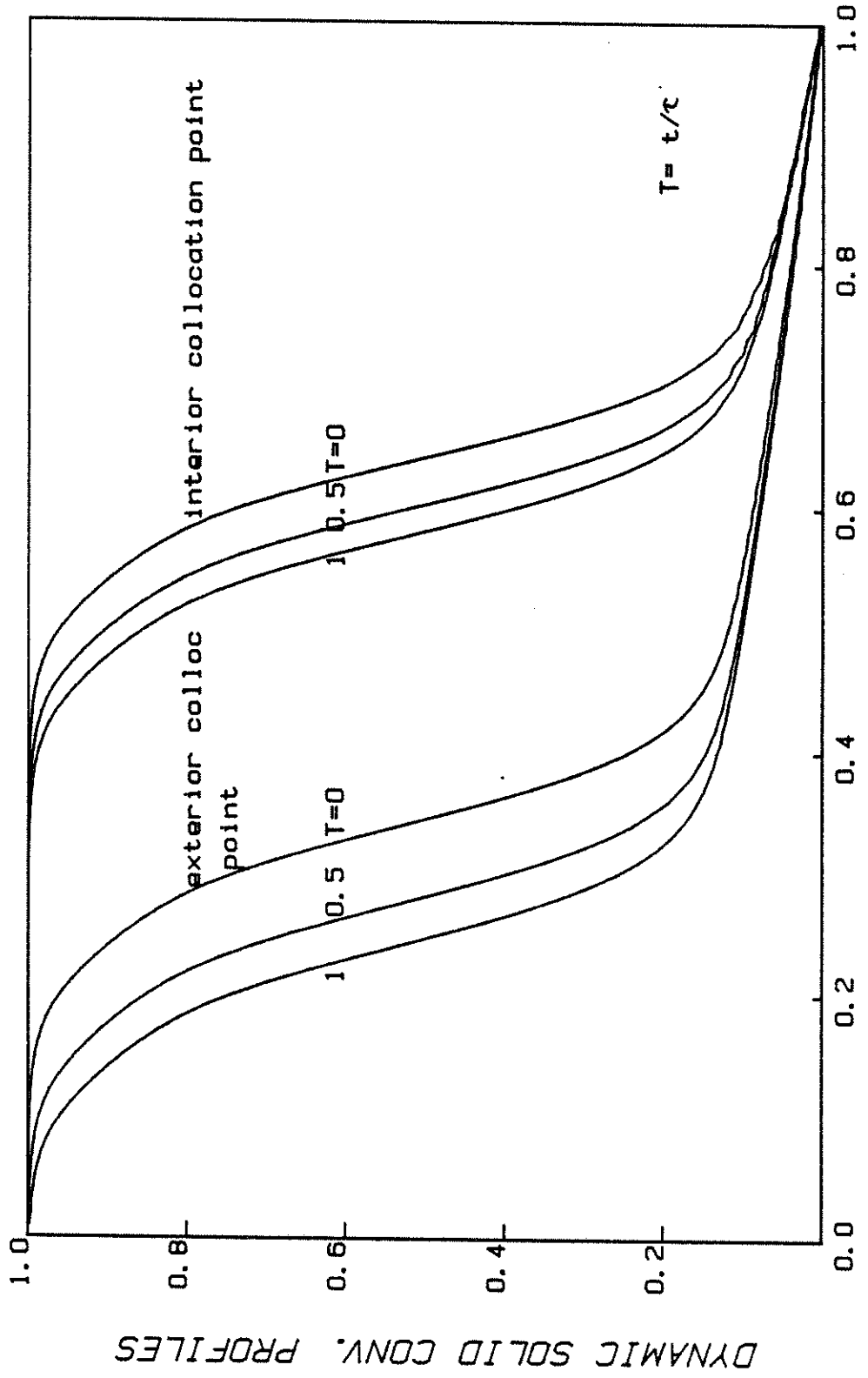

Figure 8.8 Dynamic solid conversion profiles for increase in char flow

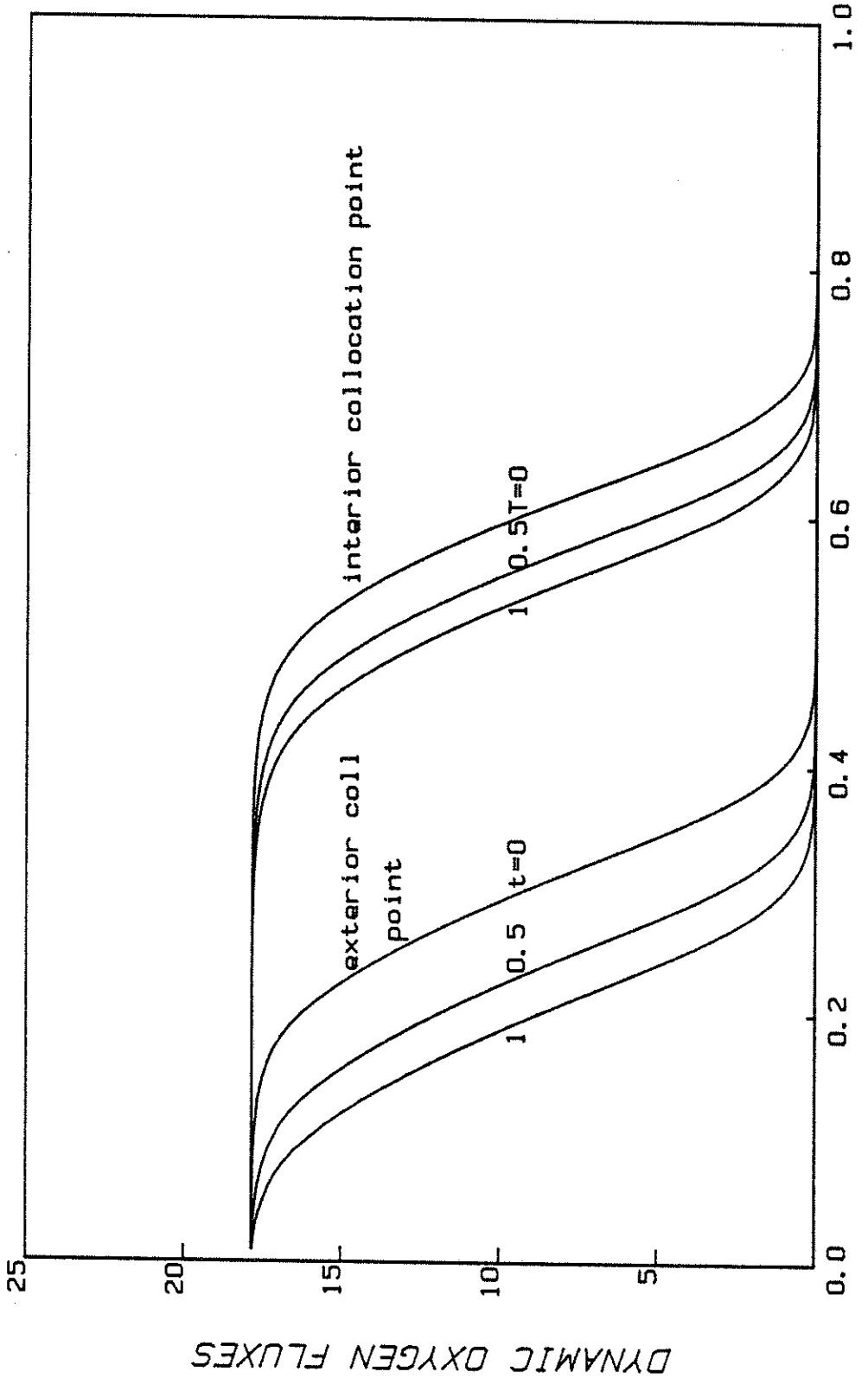

Figure 8.9 Dynamic oxygen flux (kgmol/m^2 hr) profiles for increase in char flow

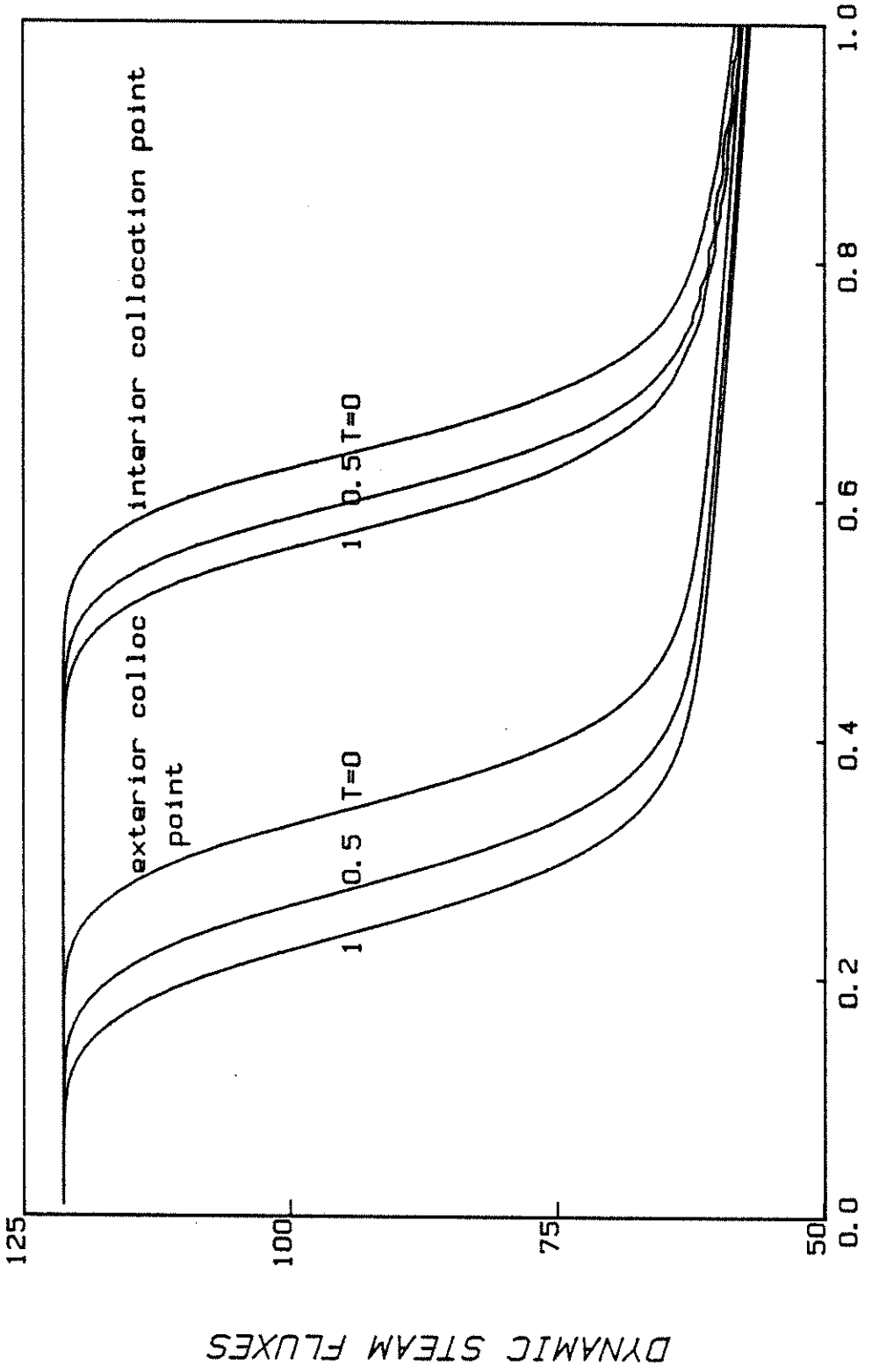

Figure 8.10 Dynamic steam flux (kgmol/m^2 hr) profiles for increase in char flow

TABLE 8.2

Outlet Composition of Product Gas

	Input rates (kgmol/hr)			Outlet composition, H_2O free			
Model	O_2	H_2O	C	CH_4	H_2	CO	CO_2
This work[1]	187.5	1275	750	5.5	42.2	21.6	30.6
This work[1]	187.5	1275	725	4.9	43.0	21.6	30.5
Yu (7)	187.5	1275	694	8.6	42.1	20.7	27.4
Yoon (3)	187.5	1275	694	8.3	46.1	20.0	24.5
This work[2]	187.5	1275	750	8.9	40.4	21.7	29.0
This work[2]	187.5	1275	725	8.3	41.2	21.6	29.0

[1] without devolatization products

[2] with devolatization products

From Figures 8.1 - 8.10 it is apparent that the radial terms tend to show that the gasifier 'performance' (measured in steam utilization (see Figure 8.10) or char conversion (Figure 8.8), etc.) deteriorates with increasing distance from the central axis of the reactor. Even though this effect is negligible because the outlet compositions are not affected to a major degree, it is conceivable that given other operating conditions or disturbances, the profiles may be greatly different. For example, if the char flow rate were increased to 775 kgmol/hr, then extrapolating on the trend seen in Figure 8.8, it is easy to see that the solid exiting the reactor at the outer radial location would not be completely converted, leading to underutilization. What this implies is there is a range of feed/operating conditions for which the gasifier may be said to be efficiently utilized, and that this model may be used to determine this range.

9. SUMMARY AND CONCLUSIONS

A homogeneous dynamic model of a fixed bed gasifier has been developed and tested against experimental results. Since radial variations in the temperature profiles were expected to be substantial, radial dispersion in the energy balance was included, giving rise to a two dimensional model. A computer program was written to simulate this model, and was also modified to handle moving beds. The program consists of about 1500 lines of Fortran code (excluding the Gear integrator). Execution times are typically 1.5 hrs. of CPU time on a DEC-20 computer for dynamic simulations of moving beds, and substantially more for fixed bed simulations.

There has been a fair amount of work done in the past in the area of gasifier modeling. However, verification of these models has been limited to matching flow rates and compositions of outlet gas. Since these variables are not very sensitive to the actual profiles inside the gasifier, the reliability of the models -- especially for purposes like transient analysis and control, where internal profiles may be important -- has not been proved. This work, by matching experimental internal temperature data from a bench-scale gasifier to simulation values, attempts to fill this gap.

Tests show that the predictions from the model are quite good for conditions for which the model is meant to be used. At short times, all assumptions are valid, and agreement is good. Deviations appear between the predicted and measured values of temperature at larger times, raising doubts as to the validity of some of the assumptions used in formulating the model. The causes for these deviations are explored,

and it is shown that the likely cause is an uncertainty in the effective reaction rates in the two major reactions occurring in the gasifier: the char + oxygen and the char + steam reactions. Axial dispersion of energy, also thought to be a cause of these deviations, is shown to have a minor effect on the temperature profiles of a similar system.

The uncertainty in the overall reaction rates is caused by the uncertainty in the values of the mass transfer coefficient through the gas film surrounding the coal particle. At the operating conditions of the gasifier, estimates of this coefficient from available correlations become unreliable. This unreliabilty increases after significant amounts of time have elapsed since the beginning of the run. The fact that the reacting particle changes shape and size also contributes to this uncertainty.

Axial dispersion of energy was investigated using a fairly recent numerical technique of solving differential equations. Though axial dispersion was not found to be important, the technique used to solve this difficult problem was studied in great detail. Certain advantages as well as disadvantages were encountered. The method was found to be versatile, and offered substantial advantages over some of the other standard methods (like global collocation, etc.). The disadvantage was that of an artificial stiffness that is introduced when this technique is applied.

The model was used for some moving bed simulations, and the results show agreement with the results of other workers. The program may be used for extensive simulations to determine optimum operating conditions for a given gasifier, and also for transient and control systems evaluations.

Though the model which has been developed is adequate, it is not exact. A number of gray areas exist, and some of them (like uncertainties in reaction rates of critical reactions and parameter values like mass transfer coefficients) have already been mentioned. Additional uncertainties exist in the heat transfer parameter values, which have a great influence on the temperature profiles. In building any model, some degree of compromise is necessary so that realistic assumptions may be balanced against realistic demands on model performance. Some of the assumptions may not be valid under different situations, and some may not be very realistic (eg., the assumption of homogenity). It is suggested that improvements in the current model look at two major aspects: that of removing the gray areas described above, and removing some of the assumptions made while formulating the model. Extensive work may be necessary to produce reliable correlations for k_g and the two heat transfer parameters h_{eff} and k_r. Removing some of the assumptions would introduce numerical complications like increasing the number of PDEs. These complications may be easier to handle in the future when better and faster computational techniques become available.

10. ACKNOWLEDGEMENTS

The author wishes to express his sincere gratitude to Dr. Babu Joseph for his invaluable guidance and encouragement during the pursuit of this work. The numerous helpful suggestions made at the Friday afternoon meetings by Drs. M. P. Dudukovic and P. A. Ramachandran as well as the graduate students of the CREL is also gratefully acknowledged.

Financial support provided by the Department of Chemical Engineering, Washington University, and the Department of Energy is sincerely appreciated.

11. APPENDICES

APPENDIX 11.1

Stability of Integrators

Some mathematically well behaved (stable) systems of ODE cannot be solved effectively with traditional algorithms (explicit RK or Adams predictor-corrrector linear multistep (LMS) methods) because the rather limited regions of absolute stability force the use of extremely small stepsizes, or, correspendingly, an impossibly large number of steps for integration over a reasonable interval in the independent variable. Usually such systems are characterized by solutions consisting of both rapidly snd slowly changing components, and equations exhibiting such behaviour are called 'stiff'. The transient components may be of importance only during a very short portion of the overall integration interval; however they may limit the maximum step-size that can be used over the entire integration interval.

Consider the example of Carnahan et. al. (67):

$$\frac{dy}{dx} = f(x,y) = -10^5 y + 10^5 \exp(-x) - \exp(-x)$$

$$y(0) = 0$$

The solution of the above is :

$$y(x) = \exp(-x) - \exp(-10^5 x)$$

and has been shown in Figure 11.1.1. Here, $-\exp(-10^5 x)$ is a rapidly decaying transient component superimposed on a slowly changing 'steady-state' component, $\exp(-x)$. For $x > 1.4*10^{-4}$, the transient component is smaller than 10^{-6} in magnitude, and has effectively no influence on the solution, as shown in the Figure.

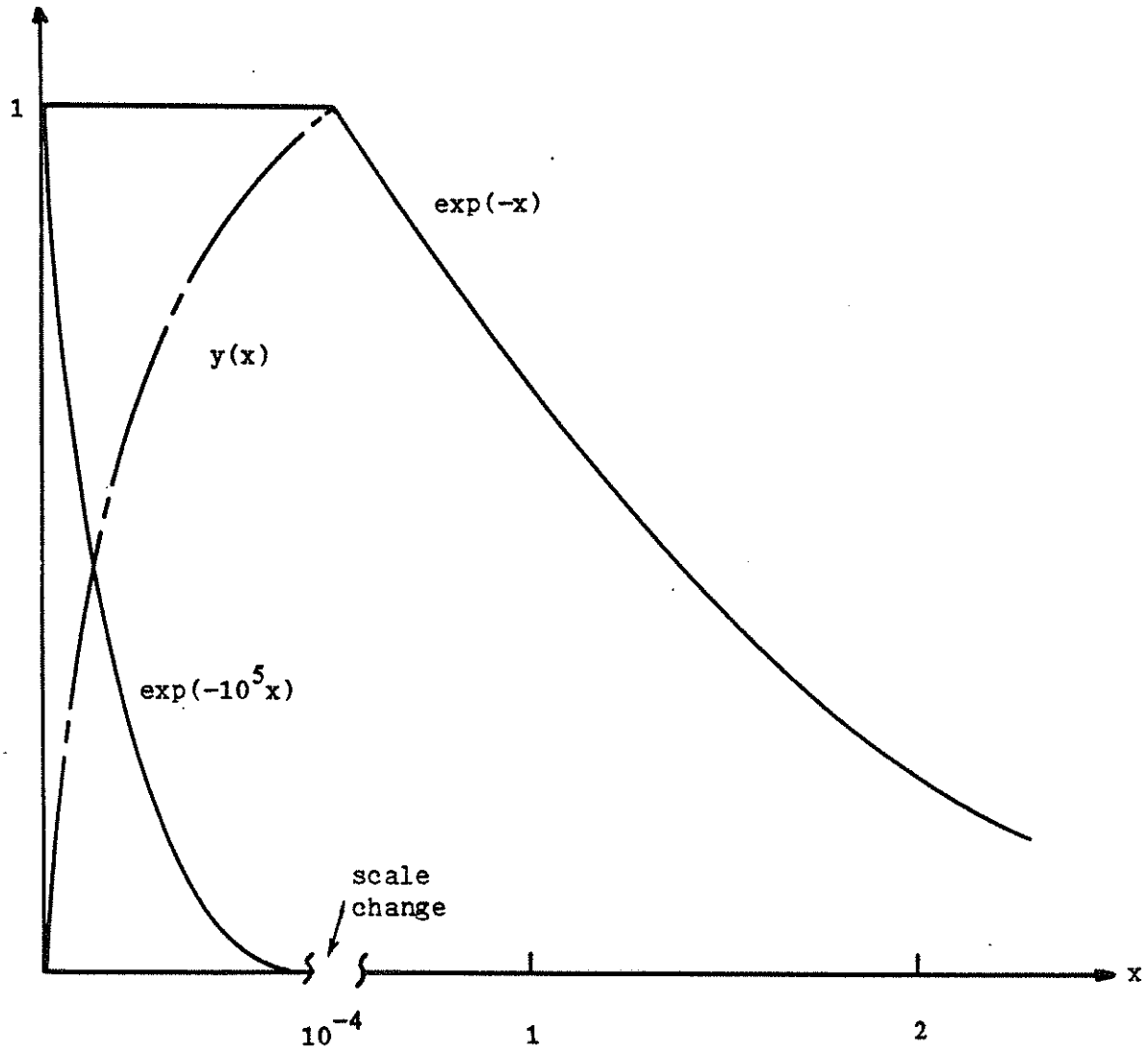

Figure 11.1.1 Solution of Carnahan's problem

If Euler's method were to be applied to this DE, the absolute stability criterion — derived from truncation error criteria — would give

$$| 1 + \lambda h | < 1$$

where λ is the eigenvalue of the system. For this case,

$$| 1 - 10^5 h | < 1, \text{ or } \quad h < 2*10^{-5}$$

This is true even after the transient has vanished : if larger stepsizes were used after $x=1.4*10^{-4}$, unstable propagation of error caused by the transient component will overwheln the true solution.

Stability criteria have been developed in the past for most of the common integrating schemes. Figure 11.1.2 shows the criteria (for some integrating schemes) for selecting h : to ensure stability, all h values for the system have to lie in the stable region for the method being used. We can see therefore, that for a system with a large value of $-\lambda$, the stepsize for the 4th order RK method would have to be very small.

Implicit or semi-implicit RK methods of high order having A stability (that is, the method is absolutely stable over the entire left-half of the complex ha plane) or strong A stability have been developed (Rosenbrock (68), Calahan (69), Caillaud and Padmanabhan (70), etc.). However, these methods involve Jacobian evaluation and matrix inversion.

We see therefore, that if the stiff problem is to be solved with reasonable computational effort, it is essential that the IV algorithm used possesses A stability, or a very close approximation of it. Several high-order LMS correctors having near A stability have been developed by Gear (36) and incorporated into widely available software

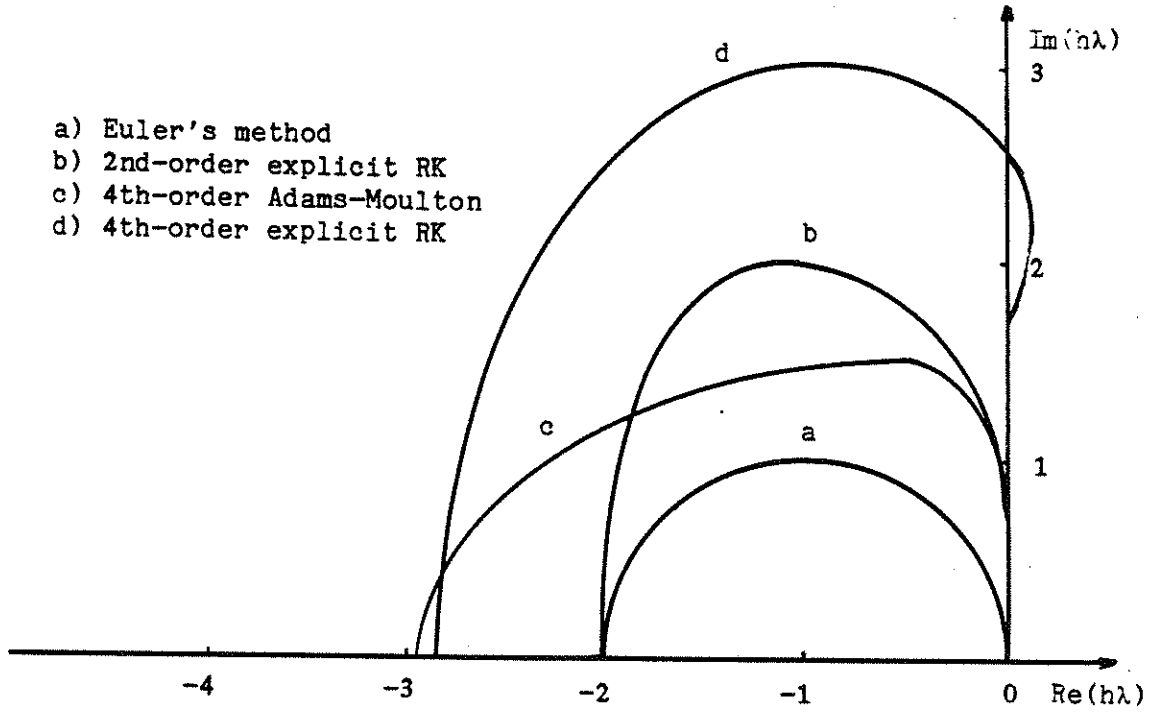

Figure 11.1.2 Regions of absolute stability for a sample problem, for complex hλ (symmetric about the real axis)

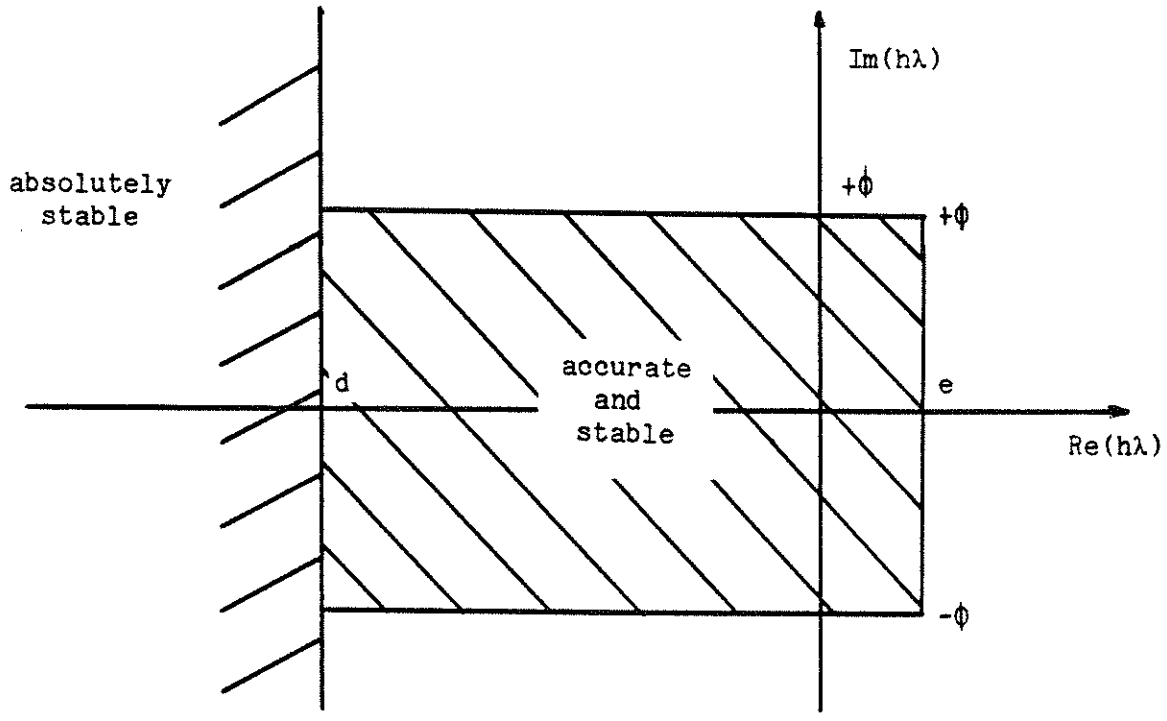

Figure 11.1.3 Stable and accurate regions for the stiffly-stable Gear BDF correctors

packages. Gear has shown that these correctors have a property that he calls stiff stability defined as follows :

A method is stiffly stable for the model problem if in the region ($Re(h\lambda) < d$), it is absolutely stable, and in the region ($d < Re(h\lambda) < e, |Im(h\lambda)| < \phi$) it is accurate.

Graphically, this stiffly stable region is shown in Figure 11.1.3. A component of a solution for which λ is large and negative (a rapid transient) can be computed accurately with sufficiently small h, and when no longer of significance will remain stable, even for very large h. The upper bound for the absolutely stable region varies from d = -6.1 to 0 for orders 6 through 2, and the minimum value for ϕ is about 0.5.

APPENDIX 11.2

Program Features

11.2.1 Program Description

The program simulates the dynamic behavior of a fixed bed gasifier. Basically the program does the following: Given

(i) char characteristics and feed rate

(ii) steam and air feed rate

(iii) characteristics of gasification reactor

(iv) initial operatin conditions of the gasifier

the program computes

(i) the temperature profiles (both axial and radial)

(ii) product gas compositions

(iii) char conversion profiles

The model is based on mass balances on each of the gaseous and solid species, and a heat balance equation. Radial dispersion of heat is incorporated. Collocation is used in the radial direction, and the resulting PDEs are solved by Gear's method of integration in the axial direction and Euler's method of integration in the time domain. The program consists of about 1500 lines of Fortran code and executes typically in about 1.5 hrs of CPU time (on a DEC-20 computer) for a dynamic simulation of moving beds.

11.2.2 Program Structure

The program structure is shown in Figure 11.2.1. MAIN is the main program, and calls a sequence of subroutines which perform various tasks:

(i) Reading of data, done by INPUT

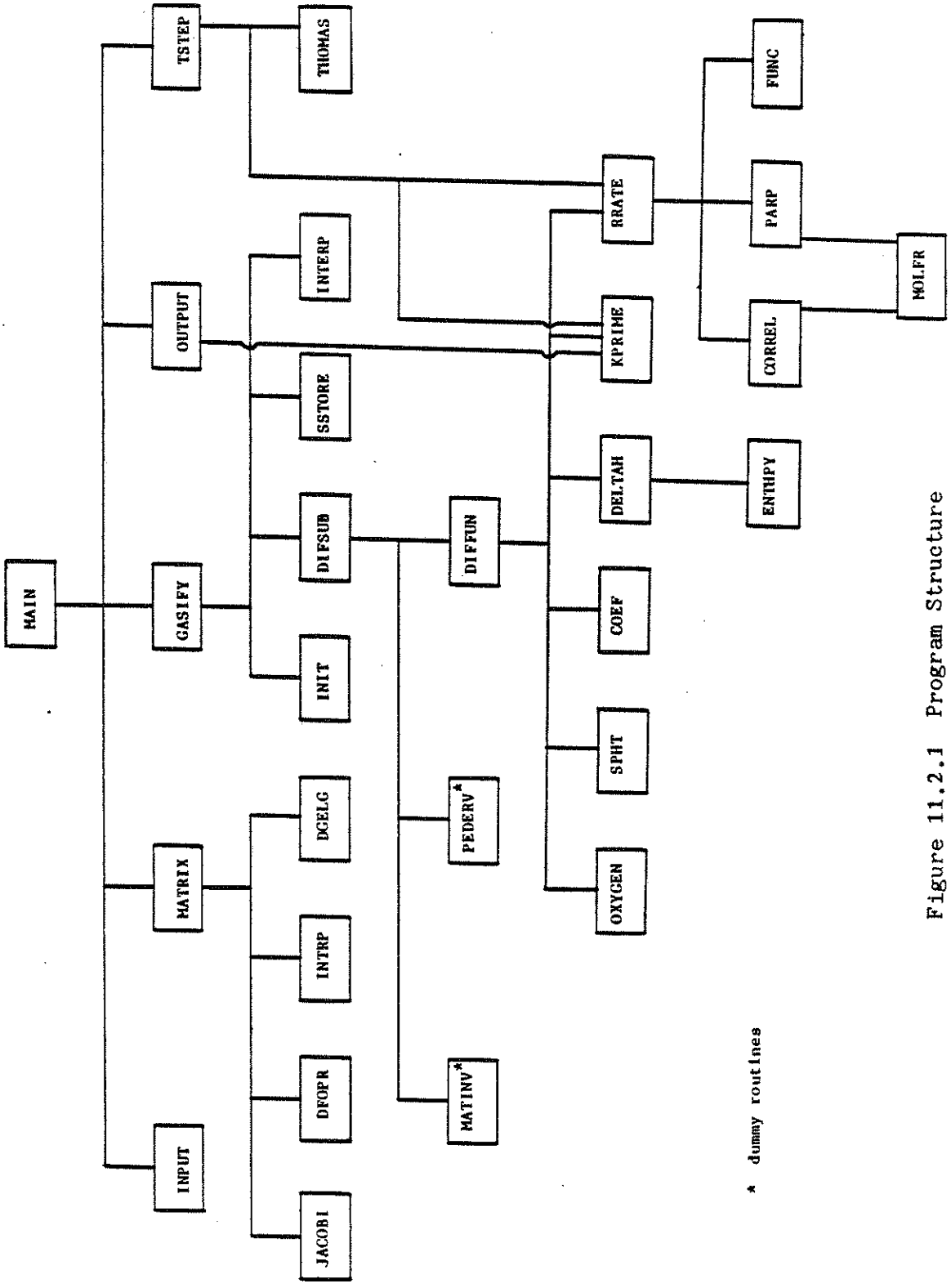

Figure 11.2.1 Program Structure

(ii) Calculation of collocation matrices and quadrature weights, done by MATRIX

(iii) Gasification, done by GASIFY

(iv) Calculation of output values, done by OUTPUT

(v) Taking a step in time, done by TSTEP

(iii), (iv) and (v) are repeated in sequence until conversion is complete. The individual subroutines are described later.

The logical unit numbers and the corresponding file names are given in Table 11.2.1. Unit numbers 20-22 correspond to sequential files, whereas 25-27 correspond to direct access files. INDAT.DAT is the only input data file, and a sample is described elsewhere. OUTDAT.DAT contains overall dynamic information at certain z locations for the run, and is also described later. PROF.DAT contains the solid conversion-, the bed temperature- and the wall temperature-profiles (at all collocation points) at each of one hundred equidistant z locations. This file therefore, can be used to re-start the program.

PLOT1.DAT, PLOT2.DAT and PLOT3.DAT are direct access files which may be used for plotting purposes. PLOT1 contains the profiles of each independent variable at each collocation point at specified times. PLOT2 contains the outlet flow rates of each gaseous species at each time step. PLOT3 contains the extrapolated temperature profiles at $r = 0$ and $r = R$ at specified times.

Restarting the program can be done with the help of PROF.DAT. Simply changing lines 33 to 242 of INDAT.DAT with lines 1-210 of PROF.DAT will usually be enough, unless the heat terms (the 4th and 5th numbers on the CALCulation control line) are non-zero. If they were non-zero (i.e. startup was being simulated), they should be set to zero.

TABLE 11.2.1

File Description

LOGICAL UNIT #	I/O	FILE NAME
20	I	INDAT.DAT
21	O	OUTDAT.DAT
22	O	PROF.DAT
25	O	PLOT1.DAT
26	O	PLOT2.DAT
27	O	PLOT3.DAT

11.2.3 Description of Subroutines

INPUT	Reads input data
MATRIX	Sets up the calculation of weight matrices for collocation and
JACOBI	calculates the weight matrices and quadrature weights for
DFOPR	collocation
INTRP	Calculates quadrature weights
DGELG	Simultaneous linear equation solver
GASIFY	Performs the gasification
INIT	Initializes all variables
DIFSUB	Gear's program to integrate a set of first order ODEs
MATINV	
PEDERV	Dummy routines required for DIFSUB
DIFFUN	Evaluates the values of the derivatives
OXYGEN	Evaluates the coefficient for O_2 in the combustion reaction
SPHT	Evaluates the specific heats of gaseous species
COEF	Supplies the stoichiometric coefficients af all species
DELTAH	Supplies the heats of reaction
ENTHPY	Calculates the enthalpy of each species
KPRIME	Supplies the two heat transfer parameters
RRATE	Calculates the reaction rates
CORREL	Calculates the values of physical parameters like k_g, D_{ij} etc.
PARP	Calculates the partial pressures of each gaseous species
MOLFR	Evaluates the mole fractions of each gaseous species
FUNC	Does a calculation in the evaluation of effectiveness factor
SSTORE	Stores all profiles at specified grid points
INTERP	Interpolates to find values of the variables at grid points
OUTPUT	Creates output files

TSTEP Performs the time-step

THOMAS Solves a set of tridiagonal simultaneous linear equations

11.2.4 Sample Input File and Description

The input data file need not be written in any particular order (except the ESSE segment, which has to come first) since segments are identified by keywords. Their description is as follows:

ESSENTIAL PARAMETERS

Number of components, number of reactions

TITLE

Title of run

REACTOR PARAMETERS

Length,inner diameter of wall, outer diameter of wall, temperature of surroundings,effective wall heat transfer coefficient,entering gas temperature,solid temperature,pressure in reactor,thermal conductivity of wall

CALCULATION CONTROL

Time of run, time-step size,number of iterations after which output is to be recorded,heat required for startup,heat added to wall at startup,z-location where heat is added,number of time steps for which heat is added (minus one)

KINETIC CONSTANTS

First line: k_0 for reactions 1 through 6

Second line: E for reactions 1 through 6

PROXIMATE ANALYSIS OF COAL

Water, volatile material, ash

ULTIMATE ANALYSIS OF COAL

C, H, O, S, N

FLOW RATES

Steam, oxygen, nitrogen and coal flow rates

ENTHALPY COEFFICIENTS

Heat of formation and specific heat coefficients in the formula $C_p = a + bT + cT^2$ (T in Kelvin) for each of the eight species: coal, H_2O, CH_4, O_2, CO, CO_2, N_2

COAL PARAMETERS

Particle size, heating value, density, specific heat, weight of coal in the gasifier

EQUILIBRIUM DATA

First line: k_0 for equilibrium constants of reactions

Second line: E for the same

PROFILES

First 100 lines: char conversion profiles for each coll. point

Second 100 lines: Temperature profiles for each coll. point

next 10 lines: wall temperature profile (10 successive z-locations on each line

Note: (a) All units are SI

(b) Some of the segments are unnecessary now, but have been put in in case some means of devolatization can be incorporated.

Interactive parameters required:

N Number of radial collocation points (maximum: 10)

FACTOR1 Factor to be put on mass transfer resistance for oxygen reaction

FACTOR2 Factor to be put on intrinsic resistance for steam reaction

TRIAL Temperature after which heat for startup is to be shut off

EFFCON Effective conductivity of the bed

EFCOEFF Effective wall heat transfer coefficient

EPS Tolerance criterion for the integrating routine

ALPHA
BETA α and β in $CH_\alpha O_\beta$

11.2.5 Sample Output File and Description

There are seven columns in the profile section that need to be explained. They are in order of appearance: Temperature, Steam flux, Methane flux, Oxygen flux, Hydrogen flux, Carbon Monoxide flux and Carbon Dioxide flux.

Lines are to be read in sets of N+1 (where N is the number of interior radial collocation points). The first line is for the innermost collocation point; the others come in order.

The line describing the outlet flow rates have the following order: H_2O, CH_4, O_2, H_2, CO, CO_2, N_2.

The 11 lines following the flow rates are the coal conversion profiles for the N collocation points.

TABLE 11.3.1

Sample Input File

```
ESSENTIAL PARAMETERS FIRST:NO. OF COMPONENTS, NO. OF RXNS
  8,6
TITLE:
  TRIAL RUN: FIXED BED GASIFIER
REACTOR PARAMETERS:L,D1,D2,TA,U,TG,TS,P,COND
  3.048,3.658,3.8,496.0,340.0,644.0,644.0,2533.0,19.0
CALCULATION CONTROL:T,DT,IFORTN,Q,htadi,POSN,NO. OF T-STEPS
  15.0,0.10,5,0.0d+10,0.0D+08,1,0
KINETIC CONSTANTS:KO & AE FOR RXNS 1 THROUGH NRCTN
  .1464D+05, .8784D+04, .2931D-03, .2931D-03, .6360D+08, .01543
  .1465D+09, .1465D+09, .6716D+08, .6716D+08, .1130D+09, .4070D+08
PROX. ANALYSIS OF COAL(AFTER DEV. AT 900 F): WATER, VOL. MAT., ASH
  0.1272,0.1881,0.1331
ULTIMATE ANALYSIS OF THE COAL: C,H,O,S,N
  0.7147,0.0483,0.0902,0.0313,0.0135
FLOW RATES: STEAM, OXYGEN, NITROGEN, COAL (MOLAR FLOWS)
1274.93,187.5,0.0,750.0
ENTHALPY COEFFICIENTS: HOF, CPA, CPB, CPC FOR COMPONENTS
  0.5000D+03,  0.1000D+02,  0.1000D-01,  0.1000D-06
 -0.2419D+06,  0.2986D+02,  0.1105D-01,  0.1921D-06
 -0.7485D+05,  0.1341D+02,  0.7703D-01, -0.1875D-04
  0.0D+00   ,  0.2560D+02,  0.1325D-01, -0.4295D-05
  0.0D+00   ,  0.2907D+02, -0.8201D-03,  0.1991D-05
 -0.1105D+06,  0.2657D+02,  0.7578D-02, -0.1119D-05
 -0.3936D+06,  0.2653D+02,  0.4243D-01, -0.1429D-04
  0.0D+00   ,  0.2702D+02,  0.5812D-02, -0.2887D-06
COAL PARAMETERS: DF,HV,DENSITY,SPHT,WT
  0.01,-27780.,1.0,1.0,27000.0
EQUILIBRIUM DATA: (INCLUDING CO/CO2 RATIO)
  0.3139D+10,  0.1238D+12,  0.1453D-07,  0.2650D-01,  0.2512D+04
  0.1358D+09,  0.1686D+09, -0.9144D+08, -0.3289D+08,  0.4190D+08
PROFILES:CHAR CONVERSION,TEMPERATURE & WALL TEMPERATURE
   0.1000D+01  0.9999D+00
   0.1000D+01  0.9998D+00
   0.1000D+01  0.9998D+00
   0.1000D+01  0.9997D+00
   0.1000D+01  0.9996D+00
   0.1000D+01  0.9995D+00
   0.1000D+01  0.9993D+00
   0.1000D+01  0.9991D+00
   0.1000D+01  0.9988D+00
   0.1000D+01  0.9984D+00
   0.1000D+01  0.9978D+00
   0.1000D+01  0.9970D+00
   0.1000D+01  0.9959D+00
   0.1000D+01  0.9945D+00
   0.1000D+01  0.9925D+00
   0.1000D+01  0.9898D+00
   0.1000D+01  0.9862D+00
   0.1000D+01  0.9813D+00
   0.1000D+01  0.9746D+00
   0.1000D+01  0.9655D+00
   0.1000D+01  0.9536D+00
   0.1000D+01  0.9408D+00
   0.1000D+01  0.9256D+00
   0.1000D+01  0.9093D+00
   0.1000D+01  0.8908D+00
   0.1000D+01  0.8709D+00
   0.1000D+01  0.8484D+00
   0.9999D+00  0.8233D+00
   0.9999D+00  0.7934D+00
   0.9999D+00  0.7579D+00
   0.9999D+00  0.7152D+00
```

TABLE 11.3.2

Sample Output File

```
 TIME =  0.0

 MAX. TEMP. FOR 2TH COLL. PT. OCCURRED AT Z= 0.0165 . PROFILES HERE ARE:

  0.1245D+04 0.1191D+01 0.7398D-05 0.8905D+00 0.6676D+00 0.1510D+01 0.4119D+00
  0.1125D+04 0.1446D+01 0.1493D-05 0.8937D+00 0.4119D+00 0.1240D+01 0.4160D+00

 MAX. TEMP. FOR 1TH COLL. PT. OCCURRED AT Z= 0.0355 . PROFILES HERE ARE:

  0.1283D+04 0.4370D+00 0.1309D-03 0.4144D+00 0.1421D+01 0.2852D+01 0.5939D+00
  0.1061D+04 0.9501D+00 0.2058D-04 0.4086D+00 0.9080D+00 0.2232D+01 0.6532D+00

  0.1049D+04 0.4669D-01 0.6657D-03 0.4291D-01 0.1810D+01 0.3839D+01 0.6672D+00
  0.7583D+03 0.7806D+00 0.5570D-04 0.5611D-01 0.1077D+01 0.2756D+01 0.8283D+00
  0.5689D+03 0.9380D+00 0.0000D+00 0.5895D-01 0.9203D+00 0.2524D+01 0.8628D+00
  0.6515D+03 0.4413D-01 0.7329D-03 0.3817D-02 0.1813D+01 0.3882D+01 0.6858D+00
  0.5117D+03 0.7804D+00 0.5666D-04 0.4363D-01 0.1078D+01 0.2766D+01 0.8360D+00
  0.4334D+03 0.9382D+00 0.0000D+00 0.5216D-01 0.9201D+00 0.2526D+01 0.8682D+00
  0.4613D+03 0.4413D-01 0.7335D-03 0.3208D-02 0.1813D+01 0.3882D+01 0.6863D+00
  0.4097D+03 0.7803D+00 0.5678D-04 0.4358D-01 0.1078D+01 0.2766D+01 0.8361D+00
  0.3808D+03 0.9382D+00 0.0000D+00 0.5223D-01 0.9201D+00 0.2526D+01 0.8682D+00
  0.3900D+03 0.4413D-01 0.7338D-03 0.3208D-02 0.1813D+01 0.3882D+01 0.6863D+00
  0.3715D+03 0.7803D+00 0.5690D-04 0.4358D-01 0.1078D+01 0.2766D+01 0.8361D+00
  0.3611D+03 0.9382D+00 0.0000D+00 0.5223D-01 0.9201D+00 0.2526D+01 0.8682D+00
  0.3651D+03 0.4413D-01 0.7341D-03 0.3208D-02 0.1813D+01 0.3882D+01 0.6863D+00
  0.3581D+03 0.7803D+00 0.5701D-04 0.4358D-01 0.1078D+01 0.2766D+01 0.8361D+00
  0.3542D+03 0.9382D+00 0.0000D+00 0.5223D-01 0.9201D+00 0.2526D+01 0.8682D+00
  0.3557D+03 0.4413D-01 0.7344D-03 0.3208D-02 0.1813D+01 0.3882D+01 0.6863D+00
  0.3531D+03 0.7803D+00 0.5713D-04 0.4358D-01 0.1078D+01 0.2766D+01 0.8361D+00
  0.3516D+03 0.9382D+00 0.0000D+00 0.5223D-01 0.9201D+00 0.2526D+01 0.8682D+00
  0.3521D+03 0.4413D-01 0.7347D-03 0.3208D-02 0.1813D+01 0.3882D+01 0.6863D+00
  0.3511D+03 0.7803D+00 0.5725D-04 0.4358D-01 0.1078D+01 0.2766D+01 0.8361D+00
  0.3506D+03 0.9382D+00 0.0000D+00 0.5223D-01 0.9201D+00 0.2526D+01 0.8682D+00
  0.3508D+03 0.4413D-01 0.7350D-03 0.3208D-02 0.1813D+01 0.3882D+01 0.6863D+00
  0.3504D+03 0.7803D+00 0.5737D-04 0.4358D-01 0.1078D+01 0.2766D+01 0.8361D+00
  0.3502D+03 0.9382D+00 0.0000D+00 0.5223D-01 0.9201D+00 0.2526D+01 0.8682D+00
  0.3503D+03 0.4413D-01 0.7352D-03 0.3208D-02 0.1813D+01 0.3882D+01 0.6863D+00
  0.3502D+03 0.7803D+00 0.5748D-04 0.4358D-01 0.1078D+01 0.2766D+01 0.8361D+00
  0.3501D+03 0.9382D+00 0.0000D+00 0.5223D-01 0.9201D+00 0.2526D+01 0.8682D+00
  0.3501D+03 0.4413D-01 0.7355D-03 0.3208D-02 0.1813D+01 0.3882D+01 0.6863D+00
  0.3501D+03 0.7803D+00 0.5760D-04 0.4358D-01 0.1078D+01 0.2766D+01 0.8361D+00
  0.3500D+03 0.9382D+00 0.0000D+00 0.5223D-01 0.9201D+00 0.2526D+01 0.8682D+00

 OUTLET FLOW RATES(KGMOL/HR) ARE:

  0.3251D-02 0.1913D-05 0.1832D-03 0.8345D-02 0.1972D-01 0.4890D-02 0.4304D-01

 NEW LENGTH OF BED= 0.8565339525795501D+00

    1 0.159D+00 0.133D+00
   10 0.309D-02 0.337D-02
   20 0.763D-04 0.523D-05
   30 0.229D-07 0.906D-08
   40 0.353D-08 0.177D-08
   50 0.344D-08 0.157D-08
   60 0.343D-08 0.154D-08
   70 0.343D-08 0.154D-08
   80 0.343D-08 0.153D-08
   90 0.343D-08 0.153D-08
```

APPENDIX 11.3

Additional Simulation Results

This appendix presents the results of the simulation run in which the reaction rate expression (for the char + oxygen and char + steam reactions) was altered such that the resistance due to the ash layer was absent. Some figures have been presented in Chapter 6 (see Figures 6.4-6.6). Here, the wall temperature profiles (Figure 11.3.1), the char conversion profiles (Figure 11.3.2) and the various gas flux profiles (Figures 11.3.3- 11.3.7) are presented. In addition, comparisons between experimental and measured temperatures at the two thermowell locations after one hour of operation are also presented (see Figures 11.3.8 and 11.3.9).

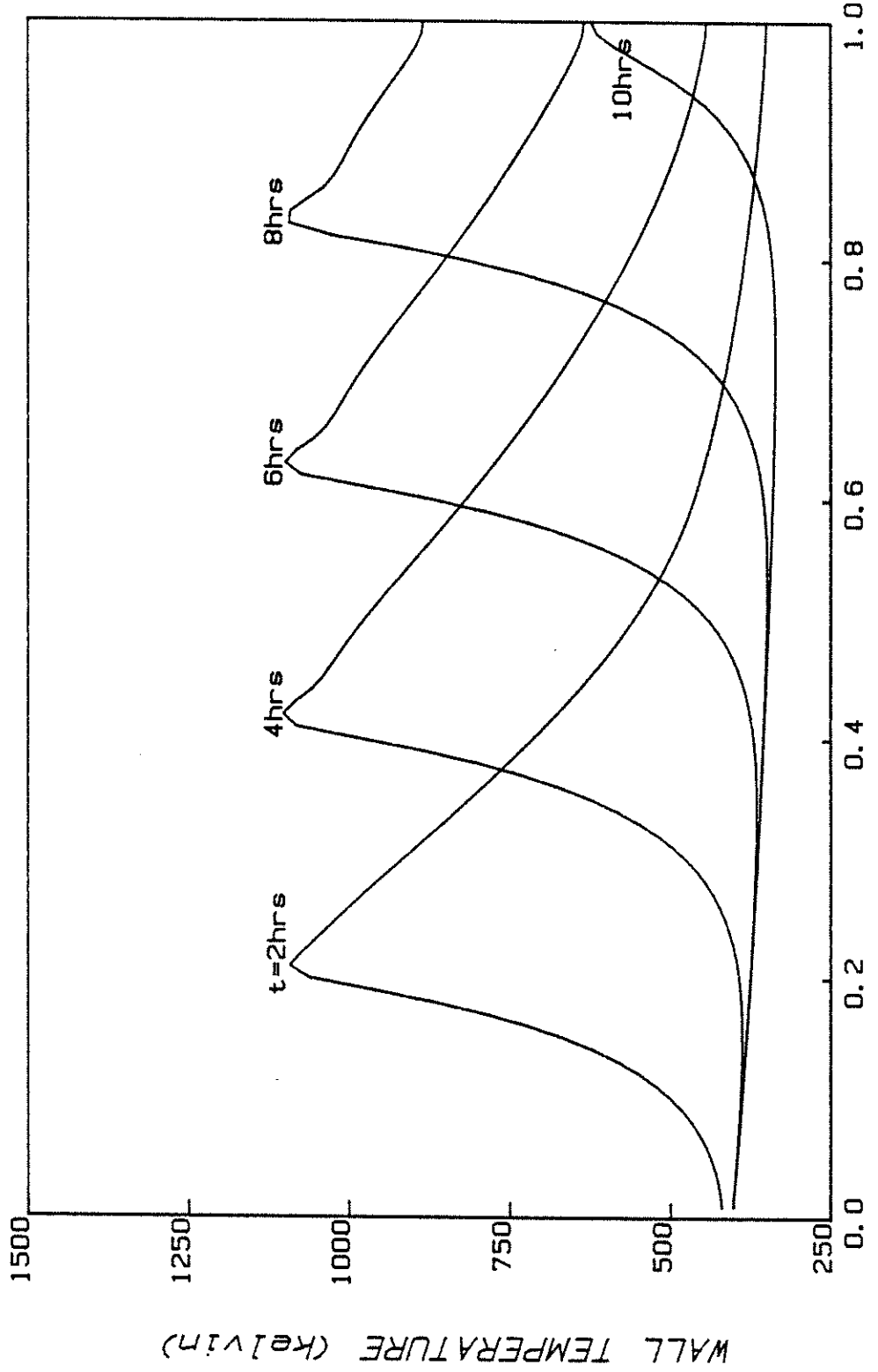

Figure 11.3.1 Temperature profiles at various times at the wall

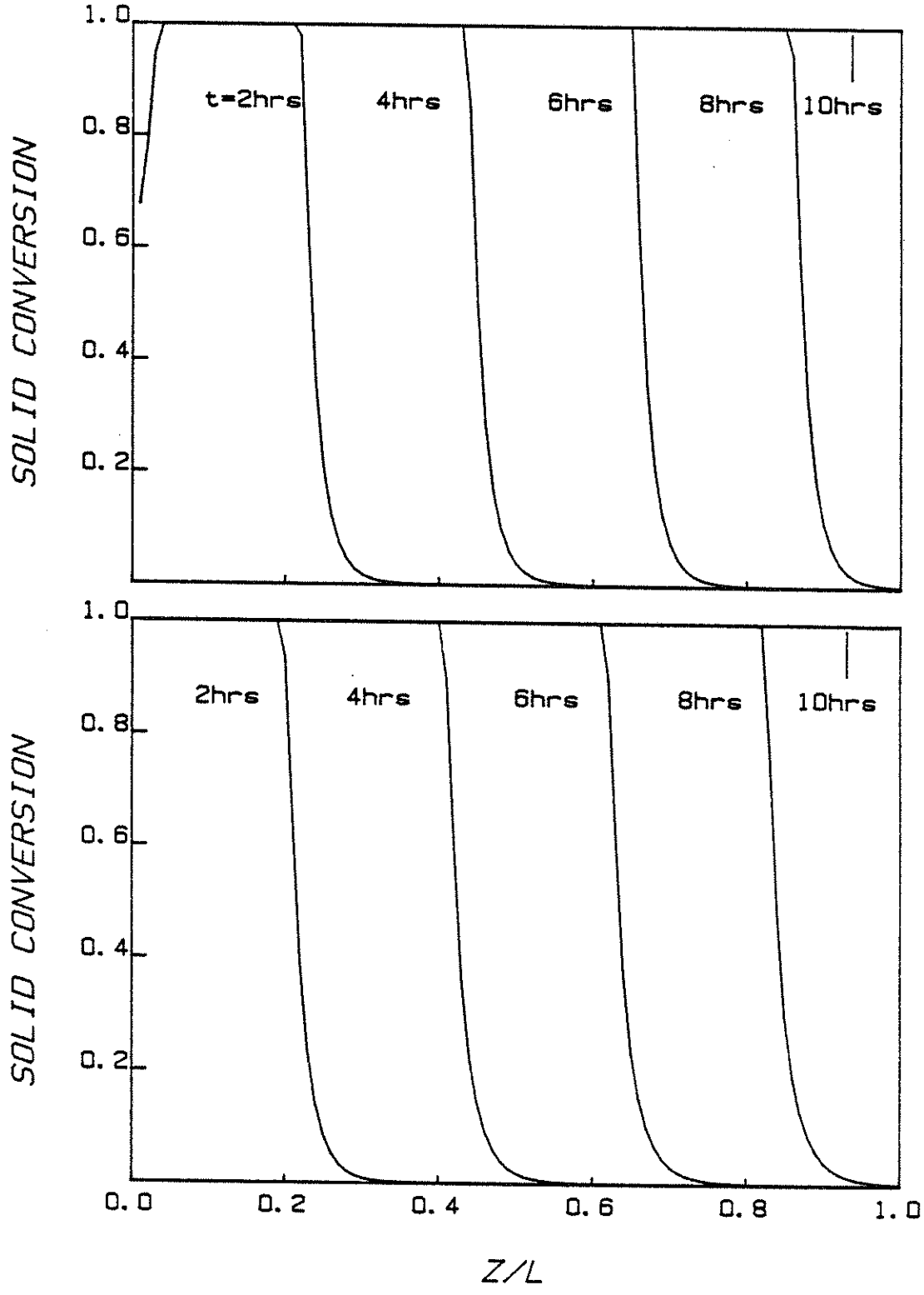

Figure 11.3.2 Axial profiles of solid conversion at various times (a) inner collocation point (b) outer collocation point

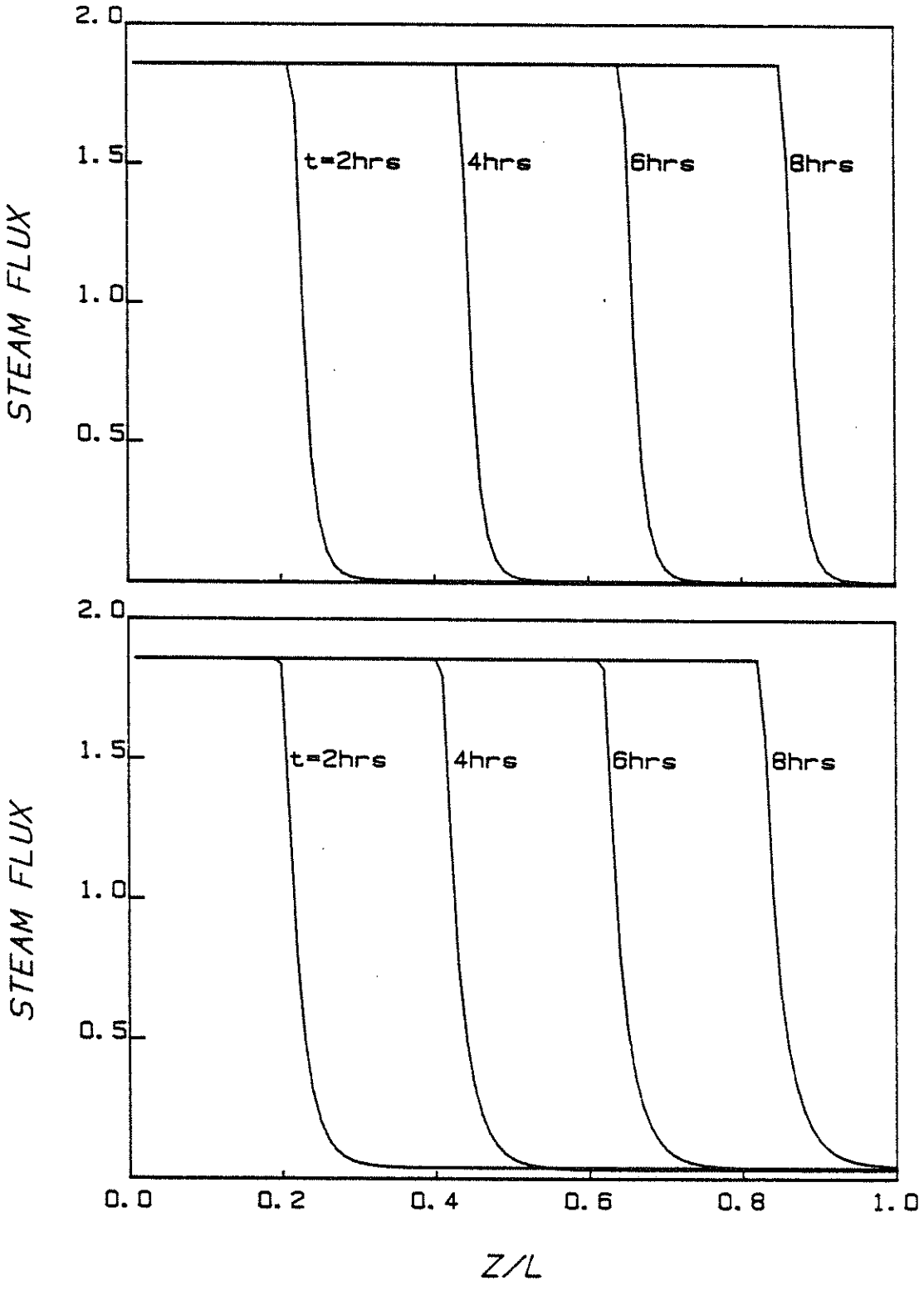

Figure 11.3.3 Axial steam flux (kgmol/m^2 hr) profiles at various times (a) inner collocation point (b) outer collocation point

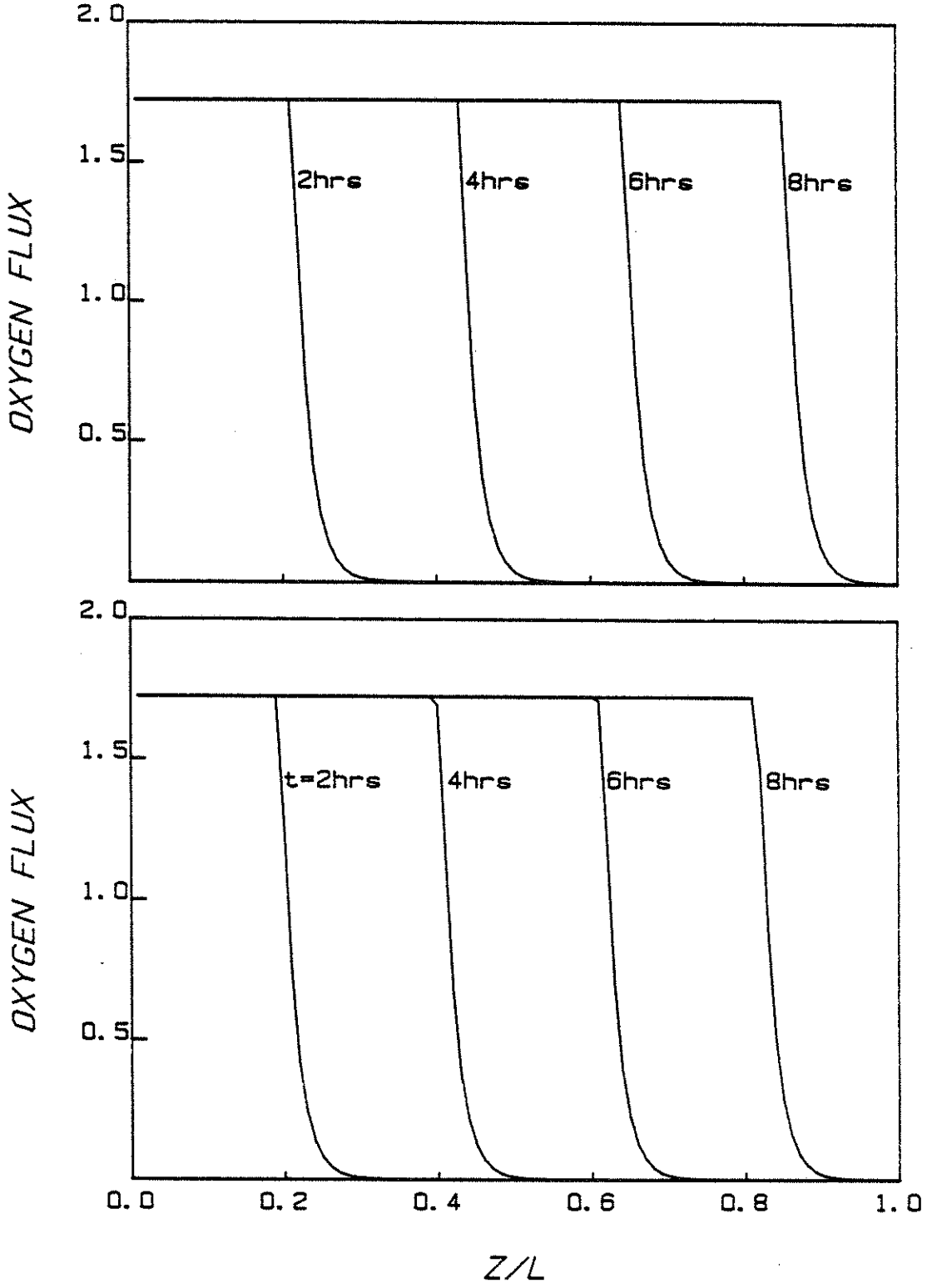

Figure 11.3.4 Axial oxygen flux (kgmol/m^2 hr) profiles at various times (a) inner collocation point (b) outer collocation point

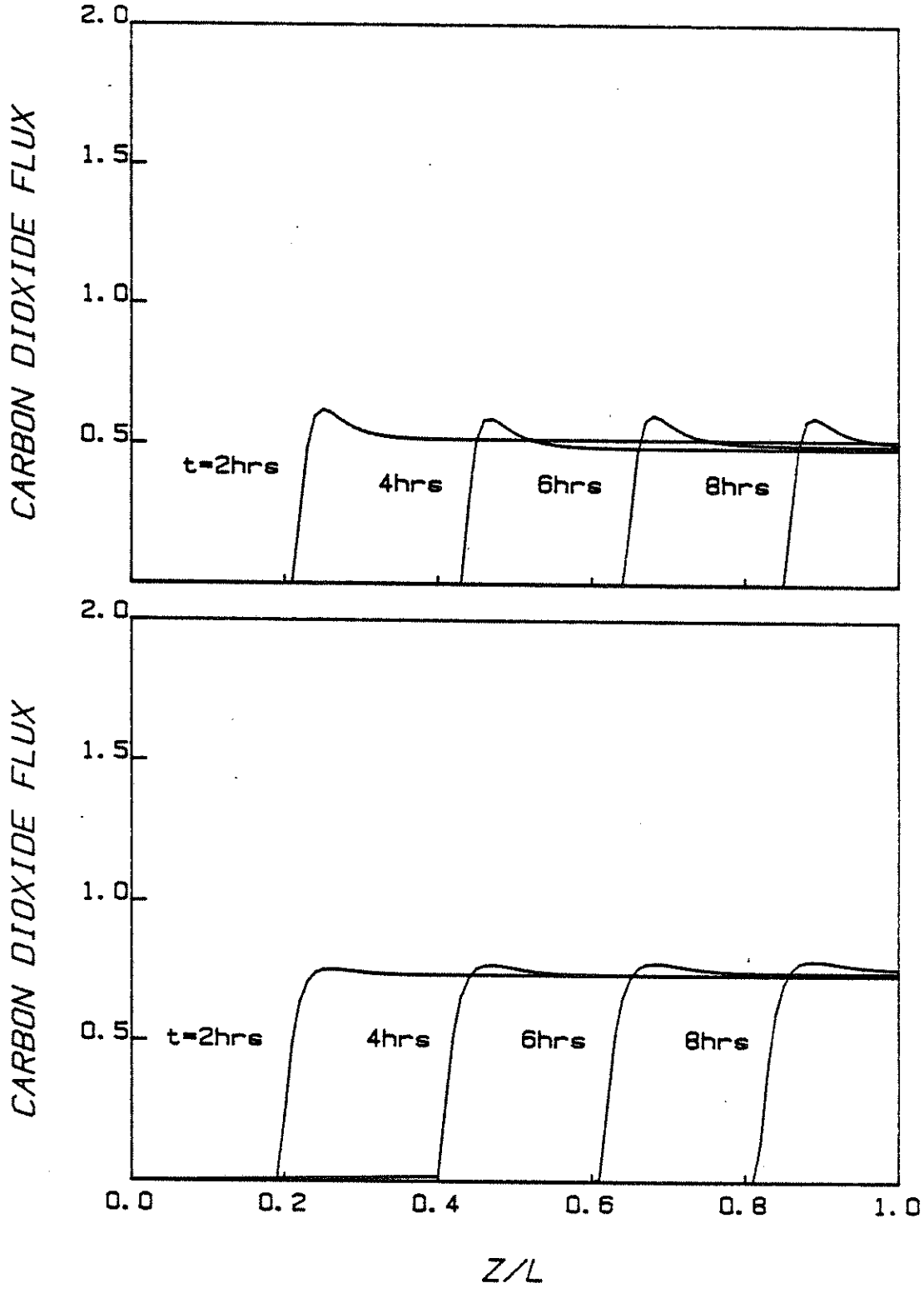

Figure 11.3.5 Axial CO_2 flux (kgmol/m^2 hr) profiles at various times (a) inner collocation point (b) outer collocation point

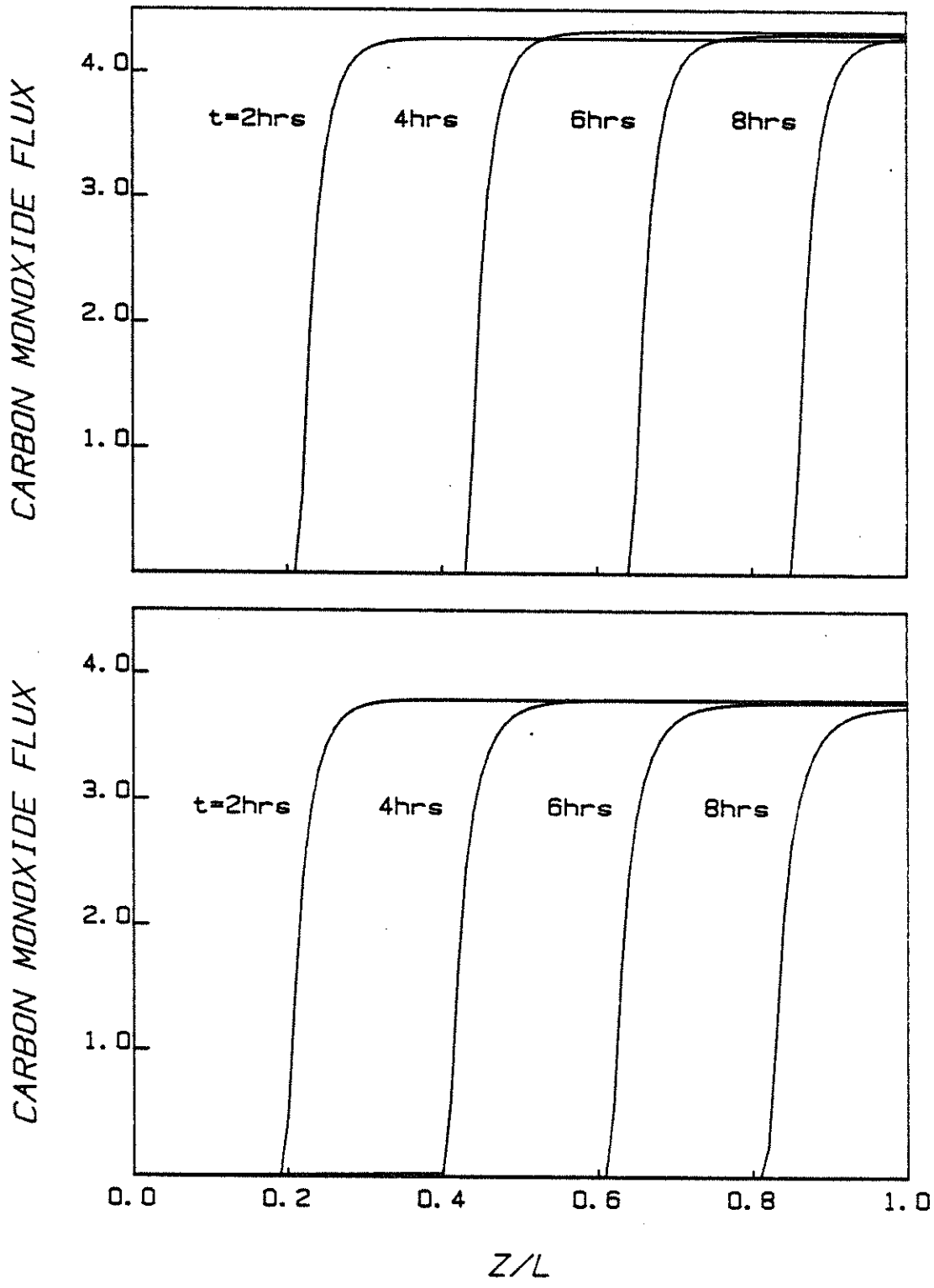

Figure 11.3.6 Axial CO flux (kgmol/m^2 hr) profiles at various times (a) inner collocation point (b) outer collocation point

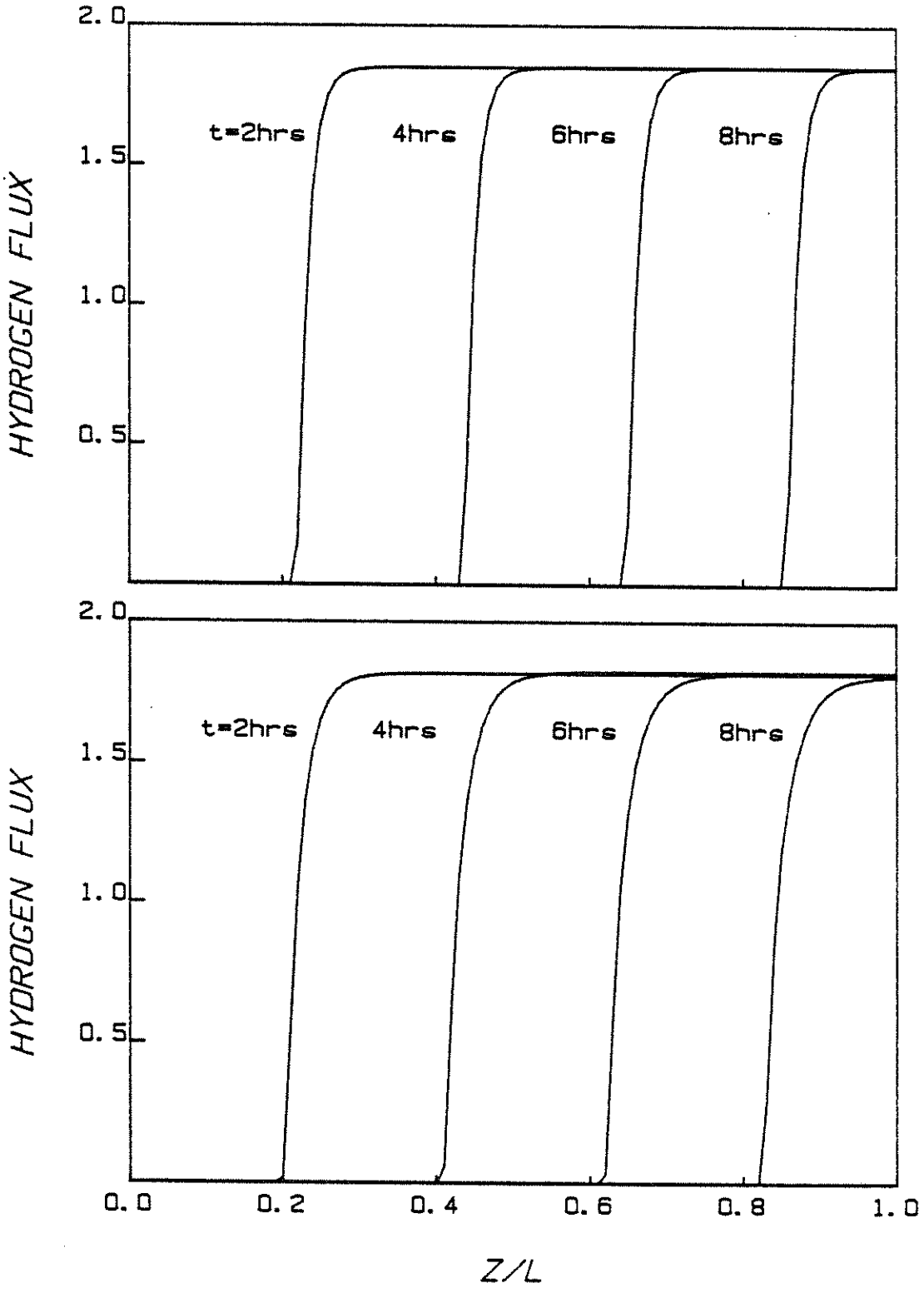

Figure 11.3.7 Axial H_2 flux (kgmol/m^2 hr) profiles at various times (a) inner collocation point (b) outer collocation point

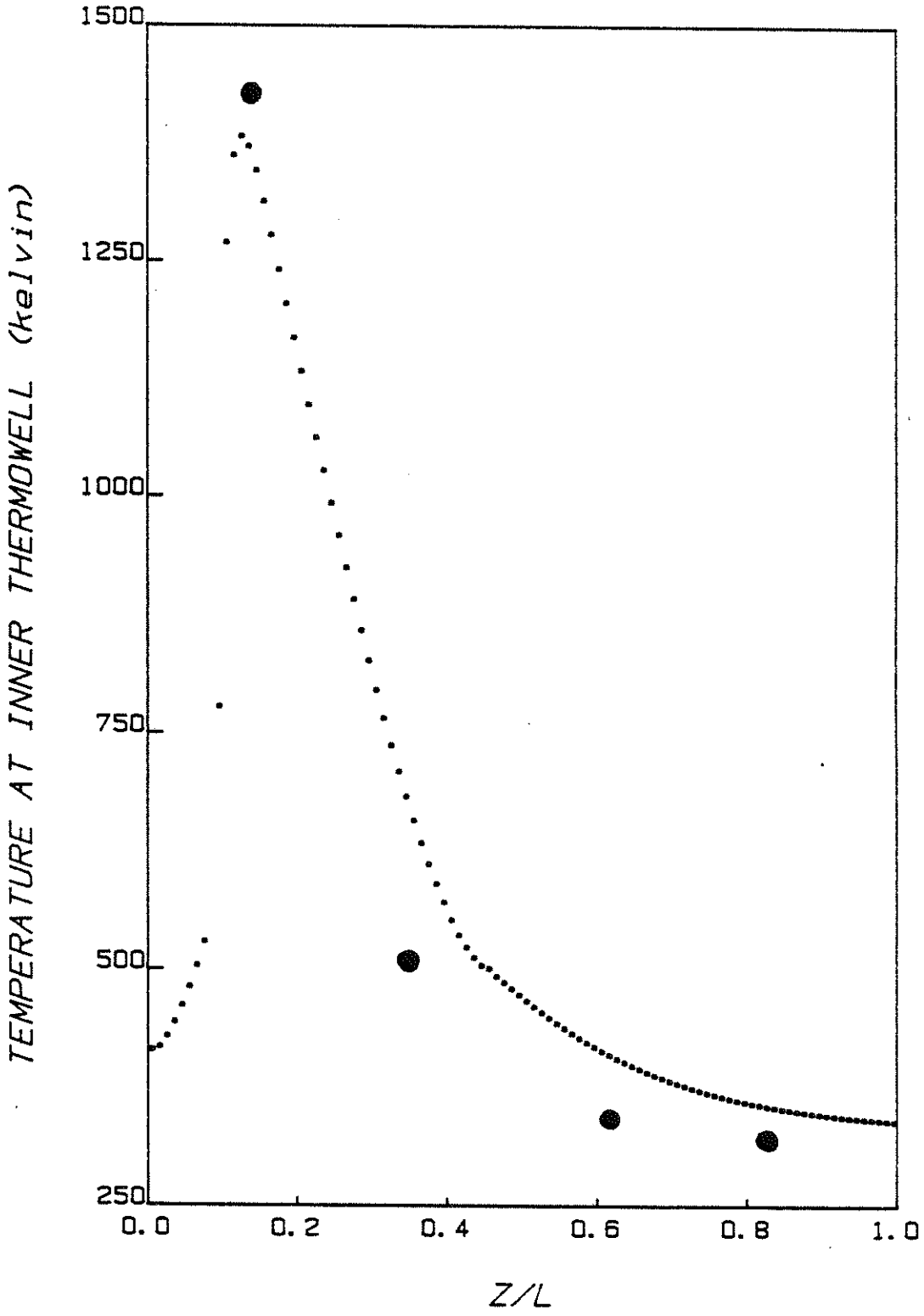

Figure 11.3.8 Comparison of axial temperature profiles after one hour of operation, inner thermowell location. ▪ predicted, ● measured

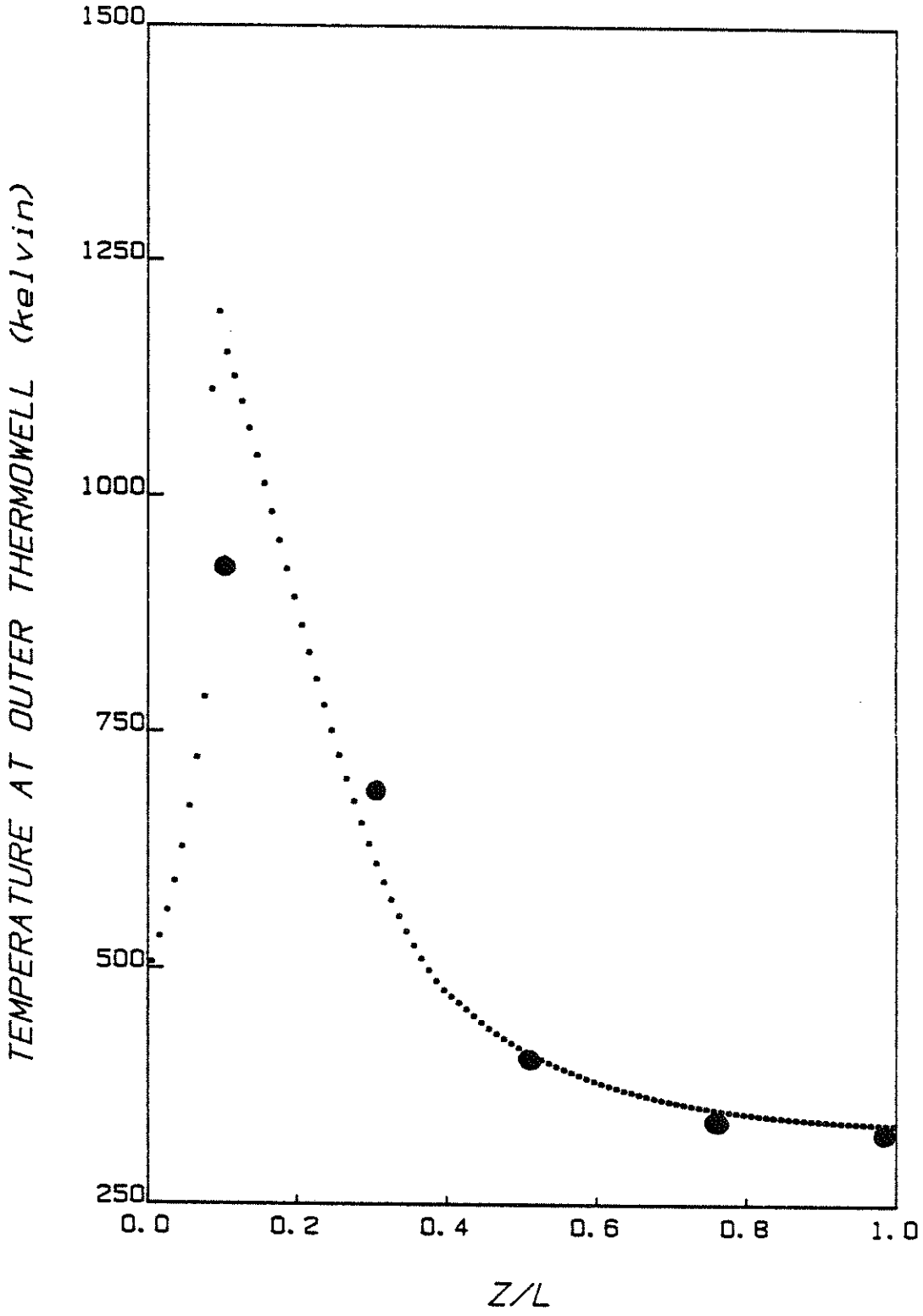

Figure 11.3.9 Comparison of axial temperature profiles after one hour of operation, outer thermowell location. • predicted, ● measured

APPENDIX 11.4

Nomenclature

A_{ij} collocation matrix

B_{ij} collocation matrix

Bi Biot number

C_c^o initial carbon concentration in char

C_{pi} specific heat of species i

C_w specific heat of wall

D_i bulk diffusivity of species i

$D_{e,i}$ effective diffusivity of species i in core

D_{ij} binary diffusion coefficient, species i and j

$D_{M,i}$ effective diffusivity of species i in ash layer

d_p particle diameter

d_t tube diameter

E_i activation energy of reaction i

F_G total molar flux of gas phase

F_i molar flux of species i

F_{io} inlet molar flux of species i

f friction factor in Ergun pressure drop equation

G flow rate of gas

g_c gravitational constant

H_i enthalpy of species i

h step size for integration

h_{eff} effective wall heat transfer coefficient

h_o heat transfer coefficient (wall-surroundings)

h_{wf} heat transfer coefficient (gas-wall)

h_{ws} heat transfer coefficient (solid-wall)

k^{o} pre-exponential factor in expression for CO/CO_2 ratio

k_a axial conductivity of homogeneous phase

k_{af} axial conductivity of gas phase

k_{ax} axial conductivity of solid phase

$k_{g,i}$ mass transfer coefficient of species i through gas film

k_r effective radial thermal conductivity of coal bed

k_{rf} radial conductivity of gas phase

k_{rs} radial conductivity of solid phase

$k_{r,i}$ reaction rate coefficient for reaction i

M_i molecular weight of species i

N number of collocation points

P total pressure in the gasifier

Pe Peclet number

P_i^* equilibrium partial pressure of species i

R radius of bed, gas constant

R_o outer radius of wall

r distance from central axis of gasifier

r_i reaction rate of reaction i

Sc Schmidt number

Sh Sherwood number

St Stanton number

T_c temperature of surroundings

T_g gas phase temperature

T_o inlet temperature of gas

T_w temperature of wall

t time

V_i bulk phase velocity of species i

v gas phase velocity

X gas phase conversion

X_c char conversion

y_i mole fraction of species in gas phase

z distance from gas inlet

Greek symbols

α subscript of H in char molecular formula

β subscript of O in char molecular formula

γ stoichiometric constant in oxidation reaction

δ_i stoichiometric factor

ε void fraction of bed

η_i effectiveness factor for reaction i

λ eigenvalue, axial location where maximum temperature occurs

λ_w thermal conductivity of wall

μ gas viscosity

ξ dimensionless Z coordinate

ρ fractional radius of unreacted core, dimensionless r-coordinate

ρ_w density of wall

τ nondimensional temperature, time

θ_a void fraction in shell

θ_c void fraction in core

θ_g temperature of gas phase

θ_s temperature of solid phase

Φ_i Thiele modulus

12. BIBLIOGRAPHY

1. Wilson, C. S., 'Coal -- Bridge to the Future. Report of the World Coal Study', Ballinger Publishing Co. (1980).

2. Hebden, D. and H. J. F. Stroud, 'Coal Gasification Processes',Chap. 24 of 'Chemistry of Coal Utilization', 2nd Suppl. Vol., edited by M. A. Elliott. Wiley Interscience (1981).

3. Yoon, H., J. Wei and M. M. Denn, 'A Model for Moving-Bed Coal Gasification Reactors', AIChE Journal, 24, 885 (1978).

4. Cho, Y. S., 'Modeling and Simulation of Lurgi-Type Gasifiers', M.S. Thesis, Washington University in St. Louis (1980).

5. Desai, P. R., 'Comparison of Processes Generating Electricity From Coal Via Low BTU Gas Production', MSChE Thesis, West Virginia Univ. Morgantown, WV (1975).

6. Kim, M. H., 'The Dynamic Behaviour of Moving-Bed Gasifiers', M. S. Thesis, Washington University in St. Louis (1981).

7. Yu, W. C., 'Dynamic Simulation of Moving-Bed Coal Gasifiers', PhD Thesis, University of Delaware (1981).

8. Anthony, D. B. and J. B. Howard, ' Coal Devolatilization and Hydrogasification', AIChE Journal, 22, 625 (1976).

9. Arthur, J. A., 'Reactions Between Carbon and Oxygen', Trans. Far. Soc., 47, 164 (1951).

10. Rossberg, M., 'Experimental Results Concerning the Primary Reactions in the Combustion of Carbon', Z. Eleckrochem, 60, 952 (1956).

11. Aris, R., and N. R. Amundson, 'Mathematical Methods in Chemical Engineering', Vol 2, 316. Prentice-Hall (1973).

12. SenGupta, A. and G. Thodos, 'Direct Analogy Between Mass and Heat Transfer to Beds of Spheres', AIChE Journal, 9, 751 (1963).

13. Wheeler, A., 'Reaction Rates and Selectivity in Catalyst Pores', Adv. in Catalysis, 3, 249 (1951).

14. Geankoplis, C. J., 'Mass Transfer Phenomena', Holt, Rhinehart and Winston (1972).

15. Fuller, E. N., P.D. Schettler and J. C. Giddings, 'New Method for Prediction of Binary Gas-Phase Diffusion Coefficients', Ind. Eng. Chem., 58, No. 5, 18 (1966).

16. Young, L. C. and B. A. Finlayson,'Axial Dispersion in Nonisothermal Packed Bed Chemical Reactors', Ind. Eng. Chem. Fund, 12, 412 (1973)

17. Eigenberger, G., 'Influence of the Wall on the Dynamic Behaviour of Homogeneous Tubular Reactors with a Highly Exothermic Reaction', ACS Symposium Series, Chemical Reaction Engineering-II, Houston.

18. Klein, H. H., 'Computer Modeling of Chemical Process Reactors', JAYCOR report (1983).

19. Amundson, N. R., 'Solid-Fluid Interactions in Fixed and Moving Beds', Ind. Eng. Chem., 48, 26 (1956).

20. Munro, W. D. and N. R. Amundson, 'Solid-Fluid Heat Exchange in Moving Beds', Ind. Eng. Chem., 42, 1481 (1950).

21. Siegmund, C. W., W. D. Munro and N. R. Amundson, 'Two Problems on Moving Beds', Ind. Eng. Chem., 48, 43 (1956).

22. Ishida, M. and C. Y. Wen, 'Analysis of Nonisothermal Moving Bed for Noncatalytic Solid-Gas Reactions', Ind. Eng. Chem. Proc. Des. Dev., 10, 164 (1971).

23. Amundson, N. R. and L. E. Arri, 'Char Gasification in a Countercurrent Gasifier', AIChe Journal, 24, 87 (1978).

24. Pirkle, J. C., I. E. Wachs and J. E. Sobel, 'Numerical Methods for Simulation of Fixed Bed Reactors for Complex Exothermic Reactions' p 401 of 'Foundations of Computer-Aided Chemical Process Design', Vol-II, edited by R. S. H. Mah and W. D. Seider. Engineering Foundation, NY (1981).

25. Villadsen, J. V. and W. E. Stewart, 'Solution of Boundary Value Problems by Orthogonal Collocation', Chem. Eng. Sci., 22, 1483 (1967).

26. Finlayson, B. A., 'Nonlinear Analysis in Chemical Engineering', p 73, McGraw Hill (1980).

27. Michael, R. and C. Iordache, 'Performance of Some Numerical Techniques Used for Simulation of Fixed Bed Catalytic Reactors', Chem. Eng. Sci., 31, 83 (1976).

28. Hopkins, T. R. and R. Wait, 'A Comparison of Galerkin Collocation and the Method of Lines for Partial Differential Equations', Int. J. Num. Method Eng., 12, 1081 (1978).

29. Birnbaum, I. and L. Lapidus, 'Studies in Approximation Methods'
(a) 'II. Initial Value Ordinary Differential Equations', Chem. Eng. Sc., 33, 427 (1978).
(b) 'III. Boundary Value Differential Equations', Chem. Eng. Sc., 33, 443 (1978).

30. Villadsen, J. V. and J. P. Sorensen, 'Simulation of Parabolic Partial Differential Equations by Double Collocation Methods', Chem. Eng. Sci., 24, 1337 (1969).

31. Young, L. C. and B. A. Finlayson, 'Mathematical Methods of Monolithic Catalytic Converters. Part I. Development of Model and Application of Orthogonal Collocation', AIChE J., 22, 331 (1976).

32. Dixon, A. and D. C. Cresswell, 'Theoretical Prediction of Effective Heat Transfer Parameters in Packed Beds', AIChe J., 19, 969 (1973).

33. Sorensen J. P., E. W. Guertin and W. E. Stewart, 'Computational Models for Cylindrical Catalyst Particles', AIChE Journal, 19, 969 (1973).

34. Finlayson, B. A., 'Packed Bed Reactor Analysis by Orthogonal Collocation', Chem. Eng. Sci., 26, 1081 (1971).

35. Finlayson, B. A., 'Orthogonal Collocation in Chemical Reaction Engineering', Cat. Rev. Sci. Eng., 10, 69 (1974).

36. Gear, C. W., 'The Automatic Integration of Ordinary Differential Equations', Comm. of the ACM, 14, 176 (1971).

37. Coberly, C. A. and W. R. Marshall, 'Temperature Gradients in Gas Streams Flowing Through Fixed Granular Beds', Chem. Eng. Prog., 47, 141 (1951).

38. Kwong, S. S. and J. M. Smith, 'Radial Heat Transfer in Packed Beds' Ind. Eng. Chem., 49, 894 (1957).

39. Plantz, D. A. and H. F. Johnstone, 'Heat and Mass Transfer in Packed Beds', AIChE Journal, 1, 193 (1955).

40. Burnell, D. G., H. B. Irvin, R. W. Olson and J. M. Smith,'Effective Thermal Conductivities in Gas-Solid Systems', Ind. Eng. Chem., 41, 1977 (1949).

41. Yagii, S. and D. Kunii, 'Studies on Heat Transfer Near Wall Surface in Packed Beds', AIChE Journal, 6, 97 (1960).

42. Froment, G. F. and K. B. Bischoff, 'Chemical Reactor Analysis and Design', p 533, John Wiley (1979).

43. Merrick, D., 'Mathematical Models of the Thermal Decomposition of Coal. Heat Transfer and Temperature Profiles in a Coke-Oven Charge,' Fuel, 62, 553 (1983).

44. De Wasch, A. P. and G. F. Froment, 'Heat Transfer in Packed Beds', Chem. Eng. Sci., 27, 567 (1972).

45. Salam, L., 'An Experimental Investigation of Fixed-bed Coal Gasification', M. S. Thesis, Washington University in St. Louis (1983).

46. Ergun, S., 'Fluid Flow Through Packed Columns', Chem. Eng. Prog., 48, 89 (1952).

47. Mehta, D. and M. C. Hawley, 'Wall Effect in Packed Columns', Ind. Eng. Chem. Proc. Des. Dev., 8, 280 (1969).

48. Schertz, W. W., and K. B. Bischoff, 'Thermal and Material Transport in Nonisothermal Packed Beds', AIChEJ, 15, 597 (1969).

49. Morales, M., C. W. Spinn and J. M. Smith, 'Velocities and Effective Thermal Conductivities in Packed Beds', Ind. Eng. Chem., 43, 225

50. Kato, K., H.Kubota and C. Y. Wen,'Mass Transfer in Fixed and Fluidized Beds', CEP Symposium Series (ed. H. Littman), 87, Volume 66 No. 105 (1970).

51. Li, H-S and B. A. Finlayson, 'Heat Transfer in Packed Beds - A Re-Evaluation', Chem. Eng. Sci., 32, 1055 (1977).

52. Dixon, A. G., W. R. Paterson and D. L. Cresswell, 'Heat Transfer in Packed Beds of Low Tube/Particle Diameter Ratio', ACS Symposium Series, Chemical Reaction Engineering-II, Evanston, 477 (1974).

53. Paterson, W. R. and J. J. Carberry, 'Fixed Bed Catalytic Reactor Modeling', Chem. Eng. Sci., 38, 175 (1983).

54. Hlavacek, V. and P. Van Rompay, 'Current Problems of Multiplicity, Stability and Sensitivity of States in Chemically Reacting Systems' Chem. Eng. Sci., 36, 1587 (1981).

55. Coste, J., D. Rudd and N. R. Amundsen, 'Taylor Diffusion in Tubular Reactors', Can. J. Chem. Eng., 39, 149 (1961).

56. Marek, M. and V. Hlavacek,'Axialer Stoff- und Warmetransport im adiabatischen Rohrreaktor - I. Gleichungen und Losungsmethoden', Chem. Eng. Sci., 21, 493 (1966).

57. Carberry, J. J. and M. M. Wendel, 'A Computer Model of the Fixed Bed Chemical Reactor: The Adiabatic and Quasi-adiabatic Cases', AIChEJ, 9, 129 (1963).

58. Lee, E. S., 'A Generalized Newton-Raphson Method for Nonlinear Partial Differential Equations- Packed Bed Reactors with Axial Mixing' Chem. Eng. Sci., 21, 143 (1966).

59. Liu, Shean-Lin, 'Numerical Solution of Two-point Boundary Value Problems in Simultaneous Second-order Nonlinear Ordinary Differential Equations', Chem. Eng. Sci., 22, 871 (1967).

60. Puszynski, J., D. Snita, V. Hlavacek and H. Hofmann, 'A Revision of Multiplicity and Parametric Sensitivity Concepts in Nonisothermal Nonadiabatic Packed Bed Chemical Reactors', Chem. Eng. Sci., 36, 1605 (1981).

61. Kubicek, M., H. Hofmann and V. Hlavacek 'Modeling of Chemical Reactors - XXII. Nonisothermal Nonadiabatic Tubular Reactor. One Dimensional Model - Detailed Analysis', Chem. Eng. Sci.,34, 593 (1979)

62. Eigenberger, G. and J. B. Butt, 'A Modified Crank-Nicholson Technique with Non-equidistant Space Steps', Chem.Eng.Sci.,31,681(1976)

63. Carey, G. F. and B. A. Finlayson, 'Orthogonal Collocation on Finite Elements', Chem. Eng. Sci., 30, 587 (1975).

64. Raymond, L. R. and N. R. Amundsen, 'Some Observations on Tubular Reactor Stability', Can. J. Chem. Eng., 42, 173 (1964).

65. Flaherty, J. E. and R. E. O'Malley Jr., 'The Numerical Solution of Boundary Value Problems for Stiff Differential Equations', Math. of Comput., 31, 66 (1977).

66. Ramachandran, P.A., and M. P. Dudukovic, 'A Moving Finite Element Collocation Method for Transient Problems with Steep Gradients', Chem. Eng. Sci., 39, 1321 (1984).

67. Carnahan, B. and J. O. Wilkes, 'Numerical Solution of Differential Equations -- An Overview', in 'Foundations of Computer-aided Chemical Process Design', Edited by R. S. H. Mah and W. D. Seider, Engineering Foundation, NY (1981).

68. Rosenbrock, H. H., 'Some General Implicit Processes for the Numerical Solution of Differential Equations', Comp. J., 5, 329 (1963)

69. Calahan, D. A., 'A Stable Accurate Method of Numerical Integration for Nonlinear Systems', Proc. IEEE, 56, 744 (1968).

70. Caillaud, J. B. and L. Padmanabhan, 'An Improved Semi-Implicit Runge-Kutta Method for Stiff Systems', Chem. Eng. J., 2, 227 (1971)

71. Pogorski, L. A., Ph.D. Thesis, University of Toronto (1957).

13. VITA

Biographical items on the author of the thesis, Mr. Amitava Bhattacharya

1) Born May 5, 1958

2) Attended the Indian Institute of Technology, Kanpur (India) from August, 1975 to May, 1980. Received the degree of Bachelor of Technology in Chemical Engineering in May, 1980.

3) Attended Washington University from August, 1980 to the present date. Awarded a Teaching Assistantship for the academic year 1980-1981, and a Research Assistantship for the years 1981-1985.

4) Membership in Professional Societies: A.I.Ch.E.

May, 1985